KATHOLIEKE UNIVERSITEIT LEUVEN
FACULTEIT DER TOEGEPASTE WETENSCHAPPEN
DEPARTEMENT ELEKTROTECHNIEK
Kardinaal Mercierlaan 94, 3001 Leuven (Heverlee)

EQUALIZATION AND ECHO CANCELLATION FOR DMT-BASED DSL MODEMS

Promotor:
Prof. dr. ir. M. Moonen

Proefschrift voorgedragen tot
het behalen van het doctoraat
in de toegepaste wetenschappen

door

Katleen VAN ACKER

Januari 2001

KATHOLIEKE UNIVERSITEIT LEUVEN
FACULTEIT DER TOEGEPASTE WETENSCHAPPEN
DEPARTEMENT ELEKTROTECHNIEK
Kardinaal Mercierlaan 94, 3001 Leuven (Heverlee)

EQUALIZATION AND ECHO CANCELLATION FOR DMT-BASED DSL MODEMS

Jury:
Prof. dr. ir. E. Aernoudt, voorzitter
Prof. dr. ir. M. Moonen, promotor
Prof. dr. ir. B. De Moor
Prof. dr. ir. J. Vandewalle
Prof. dr. ir. L. Vandendorpe (U.C.L.)
Prof. dr. ir. G. Gielen
Prof. dr. ir. B. Preneel
Prof. dr. ir. M. Moeneclaey (U. Gent)
Ir. P. Spruyt (Alcatel)

Proefschrift voorgedragen tot
het behalen van het doctoraat
in de toegepaste wetenschappen

door

Katleen VAN ACKER

U.D.C. 621.376

Januari 2001

D/2000/7515/55

ISBN 80-5682-286-1

Voorwoord

Bij het beëindigen van vier jaar doctoraatswerk, wil ik graag enkele mensen vernoemen die een belangrijke rol hebben vervuld. In de eerste plaats dank ik mijn promotor Prof. Marc Moonen voor het voorgestelde thesisonderwerp en de goede begeleiding. Het onderwerp bevatte voor mij de ideale combinatie van wiskundige diepgang en praktische toepasbaarheid. Marc bewandelde de gulden middenweg tussen voldoende begeleiding en vrijheid in het onderzoekswerk.

Verder gaat mijn dank uit naar de leden van het leescomité. Ik dank Prof. Bart De Moor en Prof. Joos Vandewalle voor het zorgvuldig nalezen van de tekst en hun constructieve opmerkingen. I also thank Prof. Luc Vandendorpe (Université Catholique de Louvain) for carefully proofreading this thesis and his interest in my research.

Ik bedank ook graag Prof. Georges Gielen, Prof. Bart Preneel, Prof. Marc Moeneclaey (Universiteit Gent) en Ir. Paul Spruyt (Alcatel) voor hun onmiddellijke bereidheid in de jury te zetelen, ondanks een drukke agenda. Verder dank ik Prof. Etienne Aernoudt voor het waarnemen van het voorzitterschap van de jury.

Ook wil ik een welgemeend woordje van dank richten tot iedereen van de onderzoeksgroep SISTA voor de interesse in dit werk en de aangename sfeer. In het bijzonder dank ik Geert Leus voor de vele nuttige, verhelderende discussies. Ik bedank ook mijn andere bureaugenoten van het eerste en tweede uur, met name Katrien De Cock, Johan Cambré, Geert Ysebaert, Gert Cuypers en Koen Vanbleu. Voor hun raad bij computerproblemen dank ik graag Bart De Schutter en Geert Rombouts. SISTA bood me de mogelijkheden om internationale conferenties bij te wonen. Het was een verrijkende ervaring.

Dit doctoraat behelst een intensieve samenwerking met Alcatel. Ik wens een aantal werknemers te bedanken voor de interessante wisselwerking tijdens de voorbije jaren. Ik denk hierbij aan Thierry Pollet, Olivier van de Wiel (nu werkzaam bij ETSI), Stan Claes, Marc Van Bladel, Luc de Clercq, Danny Sallaerts en Vincent Migeotte.

Tenslotte gaat mijn oprechte dank uit naar de families Van Acker en Breesch voor hun steun en interesse. Ook de schouderklopjes van vrienden betekenden een welgekomen aanmoediging. Dank aan Els, Kristof, Bie, Lieven, Isabel, Janneck, An, Zeger, Ilse, Frode, Julien, Laura en alle anderen. Ik dank mijn echtgenoot Jo in het bijzonder voor zijn engelengeduld en vertrouwen om dit werk tot een goed einde te brengen.

Katleen Van Acker

December 2000

Abstract

Broadband communications over the local telephone loop has become feasible nowadays by means of Digital Subscriber Line (DSL) technologies. Asymmetric DSL and one proposal for Very high bit rate DSL adopt Discrete Multitone (DMT) as modulation scheme. In this thesis we develop new equalization and echo cancellation structures for DMT-based receivers. Our main motivation is the application to DMT-based DSL-modems.

In literature, a DMT-based receiver containing a multitap time domain equalizer (TEQ) and a 1-taps frequency domain equalizer per tone, has been presented. The TEQ is usually initialized by means of the so-called channel shortening algorithm. This does however not correspond to bit rate optimization, which is a major disadvantage. In part I, we aim at improving upon the channel shortening algorithm. In a first attempt, we maintain the receiver structure and only change the TEQ-initialization algorithm. In a second attempt, we change the receiver structure such that each tone has its own multitap equalizer (per tone equalization). The latter structure is shown to enable bit rate optimization.

In part II, we study echo cancellation. With (partly) overlapping up- and downstream bands, echo cancellation may allow to achieve a higher overall bit rate. Echo cancellation may also be employed in a frequency division duplexing set-up as an alternative to highly selective filters. We investigate the combination of an echo canceller presented in literature, with TEQ and per tone equalization. We further propose a new echo cancellation structure based on an echo filter for each tone separately (per tone echo cancellation).

Korte inhoud

Breedbandcommunicatie over de lokale telefoonlijn wordt verwezenlijkt door digitale lijnen naar de abonnee (*Digital Subscriber Lines* of xDSL). Asymmetrische DSL en één voorstel voor zeer-hoge-snelheids DSL passen discrete multitoon-modulatie (*Discrete Multitone* of DMT) toe. In dit proefschrift ontwikkelen we nieuwe egalisatie- en echo-onderdrukkingstechnieken voor ontvangers gebaseerd op DMT, waarbij de toepassing in DSL-modems onze voornaamste doelstelling is.

Een op DMT gebaseerde ontvanger met multitap tijdsdomein egalisator en 1-taps frequentiedomein egalisator per toon, is beschreven in de literatuur. De tijdsdomein egalisator wordt meestal geïnitialiseerd door middel van het zogenaamde kanaalverkortingsalgoritme. Dit komt echter niet overeen met bitsnelheidsoptimalisatie, wat een belangrijk nadeel is. In deel I ontwikkelen we een egalisatietechniek die beter is dan TEQ-ontwerp gebaseerd op kanaalverkorting. In eerste instantie behouden we de ontvangerstructuur en veranderen we enkel het TEQ-initialisatie-algoritme. In tweede instantie, veranderen we ook de ontvangerstructuur. Elke toon heeft dan zijn eigen multitap egalisator (egalisatie per toon), wat bitsnelheidsoptimalisatie mogelijk maakt.

In deel II behandelen we echo-onderdrukking. Bij (gedeeltelijk) overlappende up- en downstream frequentiebanden kan echo-onderdrukking een hogere bitsnelheid mogelijk maken. Echo-onderdrukking kan ook aangewend worden in een structuur met frequentiegebaseerde tweevoudige toegang (*Frequency Division Duplexing* of FDD) als alternatief voor zeer selectieve filters. We bestuderen de combinatie van een in de literatuur voorgestelde echo-onderdrukker met TEQ en egalisatie per toon. Verder stellen we een nieuwe echo-onderdrukker voor gebaseerd op een echofilter voor elke gebruikte toon afzonderlijk (echo-onderdrukking per toon).

Glossary

Mathematical notation

$\mathbf{a}$	vector $\mathbf{a}$
$\bar{\mathbf{a}}$	vector $\mathbf{a}$ with its elements in reverse order
$\|\|\mathbf{a}\|\|_2$	2-norm of vector $\mathbf{a}$
$\mathbf{A}$	matrix $\mathbf{A}$
$\mathbf{A}^{\mathrm{T}}$	transpose of matrix $\mathbf{A}$
$\mathbf{A}^{\mathrm{H}}$	Hermitian transpose of matrix $\mathbf{A}$
$\mathbf{A}^{*}$	complex conjugate of matrix $\mathbf{A}$
$\mathbf{A}^{-1}$	inverse of matrix $\mathbf{A}$
$\mathbf{A}^{1/2}$	Cholesky factor of matrix $\mathbf{A}$
$\mathrm{diag}(\mathbf{a})$	square matrix with the elements of vector $\mathbf{a}$ on the main diagonal
$\mathrm{diag}(\mathbf{A})$	row vector formed from the diagonal elements of matrix $\mathbf{A}$
$\mathrm{diag}(\mathbf{A}, \mathbf{B}, \mathbf{C})$	block diagonal matrix with matrices $\mathbf{A}, \mathbf{B}$ and $\mathbf{C}$ on the main diagonal
$\mathbf{A}(m, n)$	element on the mth row and the nth column of matrix $\mathbf{A}$
$\mathbf{A}(:, m : n)$	columns m up to n of matrix $\mathbf{A}$
$\mathbf{A}(m : n, :)$	rows m up to n of matrix $\mathbf{A}$
$\mathbf{A}(m : l : n, :)$	rows $m, m + l, \ldots m + x.l$ of matrix $\mathbf{A}$ with $x = \lfloor \frac{n-m}{l} \rfloor$
$\mathbf{A} \odot \mathbf{B}$	componentwise multiplication of matrices $\mathbf{A}$ and $\mathbf{B}$ (also known as the Hadamard or Schur product)
$\mathbf{0}$	zero vector
$\mathbf{0}_{1 \times n}$	zero row vector of length n
$\mathbf{O}$	zero matrix
$\mathbf{O}_{m \times n}$	$m \times n$ zero matrix
$\mathbf{I}_N$	$N \times N$ identity matrix
$\mathcal{F}_N$	$N \times N$ DFT matrix
$\mathcal{I}_N$	$N \times N$ IDFT matrix
$\mathcal{E}\{a\}$	expectation of random variable a
$\|a\|$	absolute value of $a \in \mathbb{R}$; modulus of $a \in \mathbb{C}$

$\lfloor a \rfloor$	largest integer smaller than or equal to $a \in \mathbb{R}$
$\lceil a \rceil$	smallest integer larger than or equal to $a \in \mathbb{R}$
$\mathrm{mod}(a/b)$	remainder after division of a by b with $a, b \in \mathbb{R}$
$\mathbb{R}$	set of real numbers
$\mathbb{C}$	set of complex numbers
$X_i^{(k)}$	complex DMT subsymbol for tone i at symbol period k

Abbreviations

ADSL	Asymmetric Digital Subscriber Line
AM	Amplitude Modulation
ANSI	American National Standards Institute
AWG	American Wire Gauge
CAP	Carrierless Amplitude/Phase modulation
CIR	Channel Impulse Response
CO	Central Office
CP	Cyclic Prefix
CS	Cyclic Suffix
DFT	Discrete Fourier Transform
DMT	Discrete MultiTone
DWMT	Discrete Wavelet MultiTone
EC	Echo Cancellation
ETSI	European Telecommunications Standards Institute
FBLMS	Frequency domain Blocked Least Mean Squares
FDD	Frequency Division Duplexing
FDI	Feeder Distribution Interface
FEQ	Frequency domain EQualization
FEXT	Far End Crosstalk
FFT	Fast Fourier Transform
FIR	Finite Impulse Response
FMT	Filtered MultiTone
HDSL	High bit rate Digital Subscriber Line
HIPERLAN	HIgh PErformance Radio Local Area Network
HPNA	Home Phoneline Networking Alliance
ICI	InterCarrier Interference
IDFT	Inverse Discrete Fourier Transform
IFFT	Inverse Fast Fourier Transform
ISDN	Integrated Services Digital Network
ISI	InterSymbol Interference
LMS	Least Mean Squares
LS	Least Squares
MIMO	Multiple-Input/Multiple-Output
MMSE	Minimum Mean Square Error
NEXT	Near End Crosstalk

OFDM	Orthogonal Frequency Division Multiplexing
POTS	Plain Old Telephone Service
PSD	Power Spectral Density
PT-EC	Per Tone Echo Cancellation
PT-EQ	Per Tone EQualization
PTF	Per Tone Filter
QAM	Quadrature Amplitude Modulation
RFI	Radio Frequency Interference
RLS	Recursive Least Squares
RT	Remote Terminal
SFG	Signal Flow Graph
SIMO	Single-Input/Multiple-Output
SISO	Single-Input/Single-Output
SNR	Signal-to-Noise Ratio
SRC-RLS	Square-Root Covariance Recursive Least Squares
SSNR	Shortening Signal-to-Noise Ratio
SVD	Singular Value Decomposition
TDD	Time Division Duplexing
TEC	Time domain Echo Cancellation
TEQ	Time domain EQualization
TIR	Target Impulse Response
TLS	Total Least Squares
VDSL	Very high bit rate Digital Subscriber Line
WLAN	Wireless Local Area Network
xDSL	generic name for Digital Subscriber Line techniques

Contents

Egalisatie en echo-onderdrukking voor DMT-gebaseerde DSL-modems

Nederlandse samenvatting

Hoofdstuk 1. Inleiding

Sinds de uitvinding van de telefoon ontstond een wereldwijd telefoonnetwerk. Dit netwerk, dat oorspronkelijk ontworpen werd voor traditionele telefoondiensten (*Plain Old Telephone Services* of POTS), wordt nu meer en meer gebruikt voor breedbandcommunicatie. Deze evolutie wordt verklaard door de zoektocht naar economische oplossingen voor het aanbieden van breedbanddiensten. Hierbij gaat men bestaande media, zoals de telefoonlijn als ook de kabel, hergebruiken.

De recent ontwikkelde digitale technieken voor hoge-snelheidscommunicatie over de telefoonlijn worden digitale lijnen naar de abonnee (*Digital Subscriber Lines* of xDSL) genoemd. Twee van deze technieken zijn van bijzonder belang in dit proefschrift, meer bepaald asymmetrische DSL (*Asymmetric Digital Subscriber Line* of ADSL) en zeer-hoge-snelheids DSL (*Very high bit rate Digital Subscriber Line* of VDSL), omwille van het toegepaste modulatieschema. Het standaard modulatieschema voor ADSL is discrete multitoon-modulatie (*Discrete Multitone* of DMT). DMT verdeelt de bandbreedte in meerdere smalle banden en moduleert een drager in elke band: de modulatie is dus gebaseerd op meerdere dragers (*multicarrier*). Voor VDSL is er nog geen standaard modulatieschema bepaald. Er zijn momenteel twee kandidaten, enerzijds DMT en anderzijds modulatieschema's gebaseerd op één drager (*single carrier*). In dit proefschrift ontwerpen we egalisatie- en echo-onderdrukkingstechnieken voor DMT-gebaseerde systemen, waarbij de toepassing op DSL-modems de voornaamste doelstelling is.

Multidrager-modulatie

De eerste multidrager-modulatieschema's hadden filters en oscillatoren nodig om de verschillende dragers te moduleren. In de jaren '70, ontdekte men echter dat de Discrete Fourier Transformatie (DFT) kan aangewend worden om deze modulatie digitaal uit te voeren [137]. Het grote voordeel van de DFT is de bijhorende efficiënte implementatie door middel van de Fast Fourier Transformatie (FFT). Een DFT verdeelt de frequentieband in overlappende, maar wiskundig orthogonale, deelbanden met sinc-vorm.

Multidrager-modulatie wordt zowel toegepast in bedrade als in draadloze communicatiesystemen. Een populair DFT-gebaseerde modulatieschema met vele draadloze toepassingen, is orthogonale frequentiegebaseerde meervoudige modulatie (*Orthogonal Frequency Division Multiplexing* of OFDM) [16, 41]. OFDM is de Europese standaard voor digitale audio en video uitzending. Bovendien is OFDM opgenomen in het ontwerp voor de standaard van draadloze lokale netwerken (*Wireless Local Area Networks* of WLAN) [43, 126, 127]. De capaciteit van multidrager-modulatie kan worden vergroot door zogenaamde adaptieve bit-toekenning (*adaptive bit loading*) [29, 32, 77, 78]. Elke deelband krijgt dan een hoeveelheid energie en een aantal bits toegekend afhankelijk van zijn signaal-ruis-verhouding. Dit principe wordt getoond in figuur 1.1. Merk op dat adaptieve bit-toekenning alleen mogelijk is bij teruggekoppeling van de ontvanger naar de zender. Wanneer OFDM gecombineerd wordt met adaptieve bit-toekenning, spreekt men, in het domein van de DSL-modems, over DMT.

Tweevoudige toegang

In een DSL-systeem zijn er twee communicatierichtingen mogelijk: van de centrale (*Central Office* of CO) naar de afgelegen modem bij de abonnee (*Remote Terminal* of RT) wordt stroomafwaarts (*downstream*) genoemd en de omgekeerde richting, van RT naar CO, is stroomopwaarts (*upstream*). Wanneer de communicatie in beide richtingen verloopt over dezelfde telefoonlijn, worden zender en ontvanger aan elk uiteinde gekoppeld aan de lijn door middel van een hybride [21, 74]. Een perfect uitgebalanceerd hybride verhindert dat het verzonden signaal echo veroorzaakt in het ontvangen signaal. Omwille van de grote verscheidenheid in lijnkarakteristieken, zal een vast hybride niet perfect gebalanceerd kunnen zijn voor alle lijnen en zal echo ontstaan.

Om up- en downstream signalen van elkaar te scheiden, maakt men gebruik van een techniek om tweevoudige toegang te bieden (*duplexing*) [74], zie figuur 1.2. In tijds- en frequentiegebaseerde tweevoudige toegang (*Time* resp. *Frequency Division Duplexing* of TDD en FDD) kent men aan elke communicatierichting respectievelijk gescheiden tijds- en frequentiekanalen toe. Indien dezelfde frequentieband gelijktijdig in beide richtingen gebruikt wordt, zal een echo-onderdrukker toegevoegd worden aan de modem om de echo te verminderen die het hybride niet kan tegenhouden.

Digitale lijnen naar de abonnee

xDSL-modems kunnen veel hogere bitsnelheden bieden dan traditionele spraakband modems (*voice band* modems) [89], omdat ze een grotere bandbreedte van de lokale telefoonlijn benutten. Traditionele modems maken een verbinding over het volledige telefoonnetwerk dat ontworpen is voor spraaksignalen met 4kHz bandbreedte, en gebruiken enkel de POTS-band (300 tot 3400Hz). xDSL maakt gebruik van speciaal ontworpen modems aan beide uiteinden van de lokale lijn en kan op die manier een veel grotere bandbreedte benutten. In hoofdstuk 1 wordt een overzicht van xDSL technologieën gegeven [16, 21, 91]. Opeenvolgende systemen bieden een steeds hogere bitsnelheid aan over een groeiende bandbreedte.

ADSL [10, 22, 66, 72, 79] kan, afhankelijk van de ruis- en kanaalkarakteristieken, een up- en downstream bitsnelheid aanbieden tot respectievelijk 640kbit/s en 6Mbit/s in 1.104MHz bandbreedte over een 4km lange lijn. Deze bandbreedte wordt door het DMT-schema opgedeeld in 256 tonen. De verdeling van de tonen over up- and downstream is weergegeven in figuur 1.3. De hoogste tonen worden volgens de standaard aan downstream toegekend. De laagste tonen worden aan upstream toegekend of kunnen in beide richtingen gebruikt worden. In het eerste geval kunnen beide communicatierichtingen gescheiden worden door filters (FDD) en in het tweede geval is een echo-onderdrukker noodzakelijk. De asymmetrie van ADSL is bijzonder geschikt voor toepassingen als internettoegang en video-op-aanvraag (*video-on-demand*). ADSL en POTS moeten tegelijkertijd over dezelfde telefoonlijn beschikbaar zijn. Daarom zal ADSL geen data verzenden over de laagste tonen, zie ook figuur 1.3, en wordt er een zo genaamde *POTS-splitter* toegevoegd aan beide lijnuiteinden, zie figuur 1.4.

De opvolger van ADSL is VDSL [11, 35, 42, 103]. De benutte bandbreedte is tien keer hoger dan voor ADSL. VDSL is bedoeld om zeer hoge bitsnelheden te bieden over korte lijnen. De downstream bitsnelheid kan bijvoorbeeld tot 52Mbit/s reiken over 300m. Zowel symmetrische als asymmetrische verdelingen van de bitsnelheid over up- and downstream worden in de standaard voorzien. Omwille van het zeer korte bereik van VDSL, zal deze technologie gebruikt worden in een gemengde configuratie van glasvezel en koperdraad. VDSL verbindt dan de abonnee via zijn telefoonlijn met het kastje in de straat. Van daaruit loopt de aansluiting verder over glasvezel naar de CO, ook wel *fiber-to-the-cabinet* genoemd. Op dit moment zijn er twee kandidaat-modulatie schema's voor VDSL, namelijk DMT en modulatieschema's gebaseerd op één drager. Voor DMT-gebaseerde VDSL is *Zipper* recent voorgesteld als nieuwe duplexing-techniek [61, 62, 81, 104, 107]. Zipper beschouwt elke toon als een onafhankelijk frequentiekanaal dat aan up- of downstream kan toegekend worden, zoals getoond in figuur 1.5. In tegenstelling tot klassieke FFD schema's, waar frequentiekanalen volledig gescheiden zijn in frequentie, overlappen de tonen omwille van hun sinc-vorm. De tonen worden echter wiskundig orthogonaal gehouden zonder de invoering van vaste FDD-filters. Dit resulteert in een zeer flexibel systeem, waarbij de tonen op enorm veel manieren kunnen verdeeld worden tussen up- en downstream, zelfs tijdens modem-gebruik.

Stoorbronnen in het telefoonnetwerk

Vervolgens geven we in hoofdstuk 1 een overzicht van de opbouw van het telefoonnetwerk met zijn voornaamste stoorbronnen [35, 37, 49, 99, 138] die de performantie van xDSL beïnvloeden [13, 30, 69, 70, 101]. Een telefoonlijn bestaat uit koperparen: namelijk twee rond elkaar gedraaide koperdraden (*twisted pair*). Deze paren zijn gegroepeerd in kabels en het aantal paren in een kabel neemt af van CO naar RT, zie figuur 1.6. De lengte, de diameter en het type draaiing van de koperdraden beïnvloeden de capaciteit. Verder kunnen er ook vertakkingen (*bridged taps*) [134] voorkomen. Dit zijn ongebruikte stukken koperpaar, verbonden in parallel met de telefoonlijn. Ter hoogte van een vertakking wordt het signaal in twee gesplitst. Het ene deel wordt aan het open einde van de vertakking weerkaatst en voegt zich dan opnieuw bij het andere deel. Als tweemaal de lengte van de vertakking gelijk is aan een oneven aantal keer de golflengte, interfereren beide componenten destructief. Dit betekent dat de overdrachtsfunctie een grote verzwakking vertoond op de overeenkomstige frequenties. Standaardisatieverenigingen, zoals ETSI en ANSI, hebben testlijnen gedefinieerd die bestaan uit secties van verschillende lengte en diameter met en zonder vertakkingen om de performantie van ADSL en VDSL te evalueren.

Omdat de koperparen gebundeld zijn, zal ongewenste electromagnetische koppeling tussen verschillende paren voorkomen. Deze koppeling is gekend als overspraak (*crosstalk*), zie figuur 1.8. Er wordt een onderscheid gemaakt tussen overspraak veroorzaakt door een nabije zender, dit is aan dezelfde zijde van de lijn als de beschouwde modem, (*Near End Crosstalk* of NEXT), en overspraak veroorzaakt door een zender aan de andere kant van de lijn (*Far End Crosstalk* of FEXT). Beide types overspraak vergroten in functie van de frequentie. Overspraak wordt soms ook ingedeeld in zelf-overspraak (*self-crosstalk*), afkomstig van een zelfde type xDSL dienst, en vreemde overspraak (*alien crosstalk*), afkomstig van een verschillend type. Een zelfde type xDSL kan enkel NEXT en echo veroorzaken als up- en downstream tegelijkertijd verzonden worden in dezelfde frequentieband. FEXT komt altijd voor tussen diensten van hetzelfde type in dezelfde bundel. Een andere stoorbron is radio frequentie interferentie (RFI) [12, 105, 106, 109], afkomstig van AM en amateurradio. RFI is vooral belangrijk voor VDSL. De gespecifieerde amateurradiobanden liggen boven 1.8MHz en vallen dus enkel samen met de VDSL frequentieband. De AM banden vallen ook gedeeltelijk samen met de ADSL band. Zowel de interferentie veroorzaakt door een radiozender in xDSL (*ingress*) als de interferentie door xDSL in een radio-ontvanger (*egress*) zijn belangrijk. Verder wordt de performantie beïnvloed door thermische ruis en impulsruis [86].

Probleemformulering en bijdragen

Tenslotte formuleren we de problemen die in dit proefschrift aan bod komen en geven we een overzicht van de bijdragen. Het proefschrift omvat twee delen. In **deel I** behandelen we **egalisatie**. DMT-gebaseerde systemen verdelen de bandbreedte in parallelle tonen. De inkomende seriële bitstroom wordt dan verdeeld in parallelle bitstromen die de verschillende tonen QAM-moduleren (*Quadrature Amplitude Modulation*) door middel van een inverse FFT. Na modulatie wordt een zogenaamde cyclische prefix aan elk symbool toegevoegd. Indien de impulsresponsie kort genoeg is -dit is korter dan de cyclische prefix lengte plus één- kan de ontvanger eenvoudig opgebouwd worden uit een demodulerende FFT-operatie en een 1-taps frequentiedomein egalisator (FEQ) voor elke gebruikte toon. In ADSL is de impulsresponsie echter veel langer dan de cyclische prefix (bijvoorbeeld 250 versus 32 taps aan 2.208MHz) en bijgevolg zullen interferenties ontstaan tussen verschillende symbolen en tonen die de performantie negatief beïnvloeden. Een bestaande oplossing hiervoor is het invoegen van een tijdsdomein egalisator (TEQ) in de ontvanger vóór de demodulatie, om de impulsresponsie van het kanaal te verkorten. In de literatuur zijn verscheidene initialisatie-algoritmen voor de TEQ gepresenteerd die gebaseerd zijn op dit principe. Ze hebben echter een aantal duidelijke nadelen. Ten eerste heeft de resulterende kwadratische kostfunctie geen direct verband met de bitsnelheid. Ten tweede kan de bitsnelheid vrij sterk variëren in functie van de beslissingsvertraging (*decision delay*), zodat het beslissingsogenblik kritisch is. In hoofdstuk 3 bekijken we deze algoritmen in detail.

Ons doel is een egalisatietechniek te ontwikkelen die beter is dan TEQ-ontwerp gebaseerd op kanaalverkorting. In een eerste poging behouden we de ontvangerstructuur en veranderen we enkel de TEQ-initialisatie procedure. *Het TEQ-initialisatie algoritme is een eigen bijdrage en wordt beschreven in hoofdstuk 3.* In een tweede poging veranderen we ook de ontvangerstructuur zodat elke toon zijn eigen optimale en complexe TEQ heeft, echter na demodulatie en dus in het frequentiedomein. Deze egalisatie per toon is optimaal in de zin dat we de signaal-ruis-verhouding (*Signal-to-Noise Ratio* of SNR) per toon kunnen maximaliseren. *Deze nieuwe egalisatiestructuur en bijhorende initialisatie is een eigen bijdrage die wordt beschreven in de hoofdstukken 4 en 5.*

In **deel II** bestuderen we **echo-onderdrukking**. Echo-onderdrukking is noodzakelijk wanneer up- en downstream (gedeeltelijk) overlappende frequentiebanden toegewezen krijgen om zo hogere bitsnelheden mogelijk te maken. Echo-onderdrukking kan ook gebruikt worden in een FDD structuur als alternatief voor hoge filterordes van zeer selectieve filters. We bekijken eerst een bestaande echo-onderdrukking, meer bepaald tijds- en frequentiedomein echo-onderdrukking, en beschrijven hoe deze met egalisatie per toon kan gecombineerd worden. *De combinatie van tijds- en frequentie domein echo-onderdrukking en egalisatie per toon is een eigen bijdrage en wordt beschreven in hoofdstuk 6.* Vervolgens ontwikkelen we een nieuwe echo-onderdrukking gebaseerd op het per-toon-principe dat we ook in deel I toegepast hebben. Met echo-onderdrukking per toon zijn we in staat om, voor gegeven egalisatie- en echofilterlengtes, de SNR per toon te maximaliseren. *Echo-onderdrukking per toon is een eigen bijdrage die wordt beschreven in hoofdstuk 7.*

Hoofdstuk 2. Concepten

Multitoon-modulatie

De DMT-gebaseerde zender en ontvanger worden voorgesteld in de figuren 2.1 en 2.2 [15, 28]. We beschrijven op een wiskundige manier het principe van de DMT-modulatie. Indien de lengte van de impulsresponsie van het kanaal korter is dan (of gelijk aan) de cyclische prefixlengte plus één, dan is de lineaire convolutie van de ingangssequentie met de impulsresponsie equivalent met een circulaire convolutie. Of, uitgedrukt in het frequentiedomein, een subsymbool voor toon i ($i = 1 \dots N$), X_i, wordt vermenigvuldigd met de i-de component van de N-punts FFT van de impulsresponsie, H_i. Bijgevolg verdeelt DMT het kanaal in N parallelle, onafhankelijke subkanalen en is een 1-taps FEQ voldoende om de amplitude en de fase van het kanaal te compenseren.

Wanneer de impulsresponsie echter langer is, interfereren andere subsymbolen met het beschouwde subsymbool [94, 102]. De verschillende interferenties worden voorgesteld in figuur 2.4. Een subsymbool verzonden tijdens de symboolperiode k, maar op een andere toon i_2, $X_{i_2}^{(k)}$, veroorzaakt *Intercarrier Interferentie* van type 1 (ICI1) in subsymbool $X_{i_1}^{(k)}$. Een subsymbool verzonden tijdens een andere (vorige of volgende) symboolperiode, op dezelfde toon, $X_{i_1}^{(k')}$ veroorzaakt *Intersymbool Interferentie* (ISI) in subsymbool $X_{i_1}^{(k)}$. Een subsymbool verzonden tijdens een andere symboolperiode, op een andere toon, $X_{i_2}^{(k')}$, veroorzaakt *Intercarrier Interferentie* van type 2 (ICI2) in subsymbool $X_{i_1}^{(k)}$. In ADSL wordt dan een T-taps TEQ ingevoegd om het kanaal te verkorten en zo de interferenties te onderdrukken. Het TEQ-initialisatie-algoritme gebaseerd op kanaalverkorting, heeft enkele belangrijke nadelen: de resulterende kwadratische kostfunctie heeft geen rechtstreeks verband met de bitsnelheid en de bitsnelheid kan sterk variëren in functie van de beslissingsvertraging. Hiernaast heeft de TEQ-structuur op zich nog een bijkomend nadeel: alle tonen worden geëgaliseerd met hetzelfde filter en op die manier beperkt de TEQ de capaciteit van het systeem.

Naast de TEQ zijn er in de literatuur ook egalisatiestructuren in het frequentiedomein voorgesteld zoals multiple-input/multiple-output (MIMO) en single-input/multiple-output (SIMO) [93]. In hoofdstuk 4 stellen we egalisatie per toon voor als een nieuwe alternatieve egalisatiestructuur in het frequentiedomein.

Capaciteit

Vervolgens worden de formules van Shannon voor de theoretische capaciteit en voor de werkelijk bitsnelheid besproken. De tweede formule wordt gebruikt in simulaties.

DMT-gebaseerde VDSL

De DMT-gebaseerde zender en ontvanger voor VDSL, met Zipper als duplexingtechniek, worden voorgesteld in de figuren 2.8 en 2.11. In tegenstelling tot ADSL, maakt VDSL ook gebruik van een cyclische suffix: een bijkomende cyclische extensie op het einde van een symbool [104]. Verder is er een pulsvormingsoperatie (*pulse shaping*) in de zender en een vensterfunctie (*windowing*) in de ontvanger, zie figuur 2.9 [64]. De VDSL-ontvanger bevat geen TEQ. De orthogonaliteit tussen de tonen wordt bewaard door beide cyclische extensies. De suffixlengte is in het ideale geval gelijk aan de grootste vertraging die voorkomt in de beschouwde bundel van telefoonlijnen. De bedoeling is dat de FFT (in de ontvanger) werkt op N monsters (*samples*) van hetzelfde symbool, en dit geldt zowel voor het nuttig signaal als voor het echosignaal (en alle andere DMT-signalen die in de ontvanger terechtkomen). Indien de modems aan beide uiteinden van alle lijnen in één bundel gesynchroniseerd zijn, worden echo en NEXT vermeden. De orthogonaliteit tussen up- en downstream tonen is in dat geval immers gegarandeerd. In realiteit echter, zal een hoeveelheid echo en NEXT voorkomen omdat de cyclische extensies niet voldoende lang zijn en omdat de synchronisatie niet perfect is. Om deze residuele echo en NEXT te beperken, is de pulsvormingsoperatie toegevoegd aan de zender. Voor verzending worden symbolen vermenigvuldigd met een niet-rechthoekig venster (meestal met cosinus-vorm aan begin en einde, de zogenaamde *raised cosine shape*) zodat de zijlobben van de sinc-vormige tonen (in het frequentiedomein) verlagen, zie figuur 2.10. Daarna laat men opeenvolgende symbolen overlappen in het interval met cosinus-vorm (*roll-off region*).

In de DMT-gebaseerde VDSL-ontvanger, wordt slechts een gedeelte van de cyclische extensies verwaarloosd. De overblijvende delen worden gebruikt in de vensterfunctie [109]. Een vensterfunctie verhindert dat Radio Frequentie Interferentie (RFI) te veel buurtonen aantast door de zijlobben in de ontvanger te verlagen. Na vermenigvuldiging met een niet-rechthoekig venster wordt het overblijvende gedeelte van de cyclische prefix teruggeplooid op het einde van het symbool en het overblijvende gedeelte van de cyclische suffix op het begin van het symbool, zie figuur 2.12, om ISI- en ICI-introductie te vermijden. Het resulterende symbool wordt gedemoduleerd.

Datamodellen

In het tweede deel van dit hoofdstuk beschrijven we een aantal datamodellen voor het ontvangen signaal. We beginnen met het basismodel waarbij we de IFFT (in de zender) en de FFT (in de ontvanger) van dezelfde grootte veronderstellen. In het tweede datamodel wordt het echosignaal expliciet als een

DMT-signaal beschreven in plaats van een gedeelte van de additieve ruis. Dit heeft als voordeel dat fase-informatie over het echosignaal aanwezig is in het datamodel. Het basisdatamodel wordt vervolgens uitgebreid voor een tweemaal hogere bemonsterfrequentie in de ontvanger, een gedecimeerd en een geïnterpoleerd DMT-signaal. Al deze datamodellen zijn geschikt om ADSL signalen te modelleren. Als laatste, geven we nog een VDSL datamodel dat naast een cyclische prefix ook een suffix, een pulsvormingsoperatie en een vensterfunctie bevat.

Deel I. Egalisatie

Hoofdstuk 3. Tijdsdomein egalisatie

Kanaalverkorting

In dit hoofdstuk bestuderen we grondig een aantal initialisatieprocedures voor de TEQ. De kanaalverkorting is een welgekende en in de literatuur veelbesproken procedure [4, 7, 28, 75, 80, 84, 123]. Het principe is weergegeven in figuur 3.1. Voor een gegeven impulsresponsie van het kanaal $\mathbf{h}$ met additieve ruis n_l, TEQ-lengte T en cyclische prefixlengte ν, zoeken we een T-taps TEQ $\mathbf{w}$, een $(\nu+1)$-taps doelimpulsresponsie $\mathbf{b}$ (*target impulse response* of TIR) en een waarde voor de beslissingsvertraging δ_{tot} zodat de verwachte waarde van de kwadratische fout minimaal is (*Minimum Mean Square Error* of MMSE). Dit wordt uitgedrukt in vergelijking (3.1). Het resultaat is een kwadratische kostfunctie met uniek globaal minimum, wat leidt tot eenvoudige algoritmen, echter zonder rechtstreeks verband met de resulterende bitsnelheid. Om de triviale nuloplossing te vermijden, legt men een beperking op. Dit kan een eenheidscoëfficiënt-, een eenheidsnorm- of een eenheidsenergiebeperking zijn op de TIR $\mathbf{b}$ of op de TEQ $\mathbf{w}$. De eenheidsenergiebeperkingen komen respectievelijk overeen met constante energie in het ontvangen nuttig signaal, $\mathbf{b}^{\mathrm{T}}\mathbf{R}_{xx}\mathbf{b} = 1$, en in het totaal ontvangen signaal, $\mathbf{w}^{\mathrm{T}}\mathbf{R}_{yy}\mathbf{w} = 1$. De beperkingen hebben eveneens geen verband met de bitsnelheid, en daarom is het moeilijk de 'juiste' beperking te kiezen.

Verder tonen we aan dat de oplossing voor eenheidsenergiebeperking op de TIR $\mathbf{b}$ en/of op de TEQ $\mathbf{w}$ gerelateerd zijn. De oplossingen voor de TIR en de TEQ bepalen (in de drie gevallen) de principale vectoren in de deelruimten respectievelijk van het verzonden signaal x en het ontvangen signaal y, die overeenstemmen met de minimale principale hoek tussen beide deelruimten. De cosinussen van de principale hoeken tussen beide deelruimten worden gevonden als de veralgemeende eigenwaarden van een bepaalde matrix, of de singuliere waarden van een bijhorende matrix, zie vergelijkingen (3.23) en (3.84). Indien de grootste singuliere waarde strict groter is dan de daaropvolgende singuliere waarden, zijn de oplossingen voor de TEQ en de TIR in de drie beschouwde gevallen op een schaalfactor na gelijk.

De frequentiedomein-aanpak [27, 135] van MMSE-gebaseerde kanaalverkorting wordt kort besproken. Deze benadering geeft een verklaring voor de vreemde TEQ-oplossingen van MMSE-gebaseerde kanaalverkorting in een FDD-structuur, indien de eenheidsnorm op de TEQ opgelegd wordt [125]. De TEQ krijgt dan een grote versterking in de stopband en een zeer kleine versterking in de doorlaatband. Ruis in de stopband zal dus versterkt worden door de TEQ. Omdat de demodulerende FFT zich gedraagd als een filterbank van sinc-filters met aanzienlijke zijlobben, lekt de versterkte stopbandruis in de doorlaatband en daalt de SNR van de gebruikte tonen. Een controle van de TEQ-overdrachtsfunctie is dan ook belangrijk. In [125] is virtuele ruis voorgesteld om een grote stopbandversterking voor de TEQ te vermijden. De methode komt neer op het toevoegen van wiskundige (niet werkelijk aanwezige) ruis in de stopband in het initialisatie-algoritme.

Gewogen kanaalverkorting

Om de performantie van de MMSE-gebaseerde kanaalverkorting te verbeteren, hebben we zowel de kostfunctie als de beperking veranderd. In tegenstelling tot de voorgaande algoritmen, negeert ons algoritme expliciet de niet-gebruikte tonen in kostfunctie en beperking, door middel van gewichtsmatrices, om triviale oplossingen in de doorlaatband te vermijden. In de berekening van de correlatiematrix van het verzonden signaal, maken we echter een aantal vereenvoudigingen om de complexiteit van het algoritme te verlagen. Uiteindelijk veronderstellen we dat het verzonden signaal wit is, maar optimaliseren we alleen over de gebruikte tonen. Simulaties tonen aan dat het algoritme resulteert in een significante perfomantieverbetering in upstream in vergelijking met de oorspronkelijk MMSE-gebaseerde kanaalverkorting. We merken echter op dat de gewogen kostfunctie nog steeds niet equivalent is met bitsnelheidsoptimalisatie.

Andere TEQ-initialisatie-algoritmen

Naast MMSE-gebaseerde kanaalverkorting zijn er in de literatuur nog andere TEQ-initialisatie-algoritmen voorgesteld. De geometrische SNR [8] optimaliseert de bitsnelheid wat leidt tot een niet-lineair optimalisatieprobleem met beperkingen. De verkortings-SNR [80] geeft de verhouding weer van de grootste energie in $\nu + 1$ opeenvolgende monsters in de verkorte impulsresponsie tot de energie in de overige monsters. De TEQ-oplossing wordt dan gegeven door een eigenwaardeprobleem. De verkortings-SNR houdt geen rekening met de kanaalruis en is niet equivalent met bitsnelheidsoptimalisatie.

Hoofdstuk 4. Egalisatie per toon

De belangrijkste bijdrage in dit proefschrift is het per-toon-concept voor DMT-gebaseerde DSL-modems. In hoofdstuk 4, introduceren we egalisatie per toon van DMT-signalen. Hiervoor passen we de gekende DMT-ontvanger (met TEQ) aan zodat elke gebruikte toon een eigen T-taps egalisator heeft. De opeenvolging van TEQ en FFT kan immers, voor elke toon, beschouwd worden als een convolutie van twee filters. Het eerste filter, nl. de TEQ, is hetzelfde voor alle tonen vermits de TEQ-operatie vóór demodulatie uitgevoerd wordt. Het tweede filter is afhankelijk van de toonindex i en komt overeen met de i-de rij van de DFT-matrix. Omdat beide filters mogen omgewisseld worden (de convolutie is commutatief), stellen we voor om eerst de FFT-operatie uit te voeren en dan pas de TEQ. Dit betekent dat elke toon nu zijn eigen TEQ heeft, geplaatst na demodulatie. Het product van de TEQ met de 1-taps FEQ (uit de oorspronkelijke DMT-ontvanger) wordt vervolgens beschouwd als een complexe T-taps *Egalisator Per Toon* (*Per Tone EQualizer* of PT-EQ) $\mathbf{w}_i$, die kan geoptimaliseerd worden voor elke toon afzonderlijk. De overeenkomstige DMT-ontvanger is weergegeven in figuur 4.1.

Complexiteit tijdens datatransmissie

Op het eerste zicht, lijkt de PT-EQ duurder dan de TEQ. De ontvanger met TEQ heeft slechts één FFT-operatie nodig per DMT-symbool omdat de frequentiedomeinegalisatie bestaat uit 1-taps filters. De ontvanger met PT-EQ daarentegen heeft T-taps filters in het frequentiedomein en heeft dus T opeenvolgende FFT-operaties per DMT-symbool nodig. We kunnen echter handig gebruik maken van een eigenschap van opeenvolgende FFT's (*sliding FFT*). Voor elke toon i, kunnen de nodige FFT-uitgangen ook berekend worden als (complexe) lineaire combinaties van één FFT-uitgang en $T-1$ reële verschiltermen, zoals weergegeven in vergelijking (4.4). Deze lineaire combinaties kunnen opgenomen worden in de PT-EQ $\mathbf{w}_i$ zodat de uiteindelijke PT-EQ $\mathbf{v}_i$ als ingangen één FFT en $T-1$ verschiltermen heeft. Deze DMT-ontvanger is voorgesteld in figuur 4.2. We hebben aangetoond dat ontvangers met respectievelijk T-taps PT-EQ (geïmplementeerd d.m.v. $\mathbf{v}_i$) of met T-taps TEQ een vergelijkbare complexiteit hebben tijdens datatransmissie. Een bijkomende complexiteitswinst kan bekomen worden door het aantal filtercoëfficiënten per toon te optimaliseren. Het nadeel van PT-EQ ten opzichte van TEQ, is het grotere geheugen nodig om alle filtercoëfficiënten te bewaren.

Optimale PT-EQ coëfficiënten

Het grote voordeel van de nieuwe structuur is dat de SNR, en dus de bitsnelheid, kan geoptimaliseerd worden door de verwachte waarde van de kwadratische fout voor elke toon te minimaliseren (MMSE per toon), zie vergelijking (4.8). Indien de impulsresponsie van het kanaal en de signaal- en ruiscovariantiematrices gekend zijn, kunnen de optimale PT-EQ's rechtstreeks berekend worden als de oplossing van een kleinste kwadraten probleem per toon. Omdat de PT-EQ kan beschouwd worden als een complexe TEQ per toon, vormt de bitsnelheid van de optimale T-taps PT-EQ een bovengrens voor de bitsnelheid van de T-taps TEQ, wat bevestigd wordt in de simulatieresultaten. Verder besluiten we uit de simulaties dat de grootste capaciteitswinst wordt bekomen in upstream en dat de bitsnelheid, in beide communicatierichtingen, een zeer vlakke functie is van de beslissingsvertraging.

Combinatie van PT-EQ en vensterfunctie

Vervolgens bestuderen we de combinatie van PT-EQ en een vensterfunctie (geïmplementeerd in het tijdsdomein). Na een vensterfunctie kunnen opeenvolgende FFT's niet meer op een eenvoudige wijze geschreven worden als een (complexe) lineaire combinatie van één FFT en $T-1$ verschiltermen. Dus, als we PT-EQ willen combineren met een (tijdsdomein-) vensterfunctie, moeten we de T opeenvolgende FFT's expliciet berekenen, wat duur is. We tonen echter aan dat een vensterfunctie over $N+\mu$ elementen in het tijdsdomein, equivalent is met een bepaalde set van $(\mu+1)$-taps PT-EQ's $\mathbf{g}_i$. Deze PT-EQ's $\mathbf{g}_i$ kunnen dan gecombineerd worden met de oorspronkelijke T-taps PT-EQ's $\mathbf{w}_i$. Het resultaat is een set van $(T+\mu)$-taps PT-EQ's die wel met behulp van één FFT en $T+\mu-1$ verschiltermen geïmplementeerd kunnen worden. Door de totale PT-EQ te optimaliseren, zijn we dan in staat om impliciet de vensterfunctie per toon te optimaliseren. De resulterende SNR vormt een bovengrens voor de SNR bekomen met T-taps PT-EQ's en een vaste (tijdsdomein-) vensterfunctie.

SIMO-egalisatie

Daarna vergelijken we de performantie van PT-EQ en SIMO-egalisatie (*Single Input Multiple Output* of een systeem met één ingang en meerdere uitgangen) [93]. In SIMO-egalisatie wordt de convolutie van de demodulerende FFT en de PT-EQ beschouwd als één filter (voor elke gebruikte toon), dat kan geoptimaliseerd worden voor elke toon afzonderlijk. Het ontvangen signaal is dan rechtstreeks de ingang van deze SIMO-egalisatoren. De simulatieresultaten tonen slechts een geringe perfomantieverbetering voor SIMO-egalisatie. De complexiteit van SIMO-egalisatie is echter beduidend hoger.

Hoofdstuk 5. Initialisatie van egalisatoren per toon

De optimale PT-EQ's kunnen berekend worden door, per toon, een MMSE-probleem op te lossen, zoals uitgelegd in het vorige hoofdstuk. Het nadeel van deze rechtstreekse initialisatie is de hoge complexiteit. In dit hoofdstuk, ontwikkelen we een efficiënt recursief initialisatieschema, *i.e.* gebaseerd op trainingssymbolen.

Recursieve initialisatie

De kostfunctie is weergeven in vergelijking (5.1). In plaats van de verwachte waarde van de kwadratische fout te minimaliseren, zoals in het vorige hoofdstuk, zoeken we het minimum van de som van kwadratische fouten over de trainingssequentie. Dit kleinste kwadraten probleem kan recursief opgelost worden: voor elk ontvangen trainingsymbool worden de filtercoëfficiënten opnieuw aangepast.

LMS-gebaseerde schema's (*Least Mean Squares* [50]) hebben een lage complexiteit per trainingssymbool ($\mathcal{O}(T)$ met T de filterlengte). Hun convergentiesnelheid wordt bepaald door de eigenwaardenspreiding van de autocorrelatiematrix van het ingangssignaal. Deze spreiding is enorm groot voor het ingangssignaal van de PT-EQ's. De convergentie is dan ook zeer traag.

Omwille van het slechte convergentiegedrag van LMS-gebaseerde initialisatie, schakelen we over op RLS-gebaseerde schema's (*Recursive Least Squares* [50]). De complexiteit per trainingssymbool voor RLS ($\mathcal{O}(T^2)$) is hoger dan voor LMS maar de convergentie-eigenschappen zijn optimaal. In plaats van de ingangsvector direct te gebruiken om de filtercoëfficiënten aan te passen (zoals bij LMS), wordt deze vector eerst getransformeerd met de inverse van de autocorrelatiematrix. De resulterende zogenaamde kalmanvector wordt dan gebruikt in de filteraanpassing. De matrix die de convergentie van RLS bepaalt heeft T dezelfde eigenwaarden, de eigenwaardenspreiding is dus gelijk aan nul en daarom is de convergentie optimaal.

RLS-algoritme met inverse updating

We passen het RLS-algoritme met inverse updating [90] toe op de PT-EQ's. Dit algoritme wordt voorgesteld in figuur 5.2. In het benedendriehoekig gedeelte van de schematische voorstelling van het algoritme, worden operaties op de ingangsvector uitgevoerd. De $T \times T$ benedendriehoeksmatrix $\mathbf{L}$ staat in verband met de autocorrelatiematrix van de ingangsvector. Wanneer we RLS met inverse updating combineren met PT-EQ, bekomen we figuur 5.3. Hoewel de complexiteit van RLS kwadratisch is in het aantal filtercoëfficiënten, kan de complexiteit beperkt blijven. We kiezen de volgorde van de filteringangen namelijk zodanig dat de (reële) verschiltermen eerst worden verwerkt en dan pas de (complexe) FFT-uitgang. Op deze manier heeft het resulterende initialisatie-algoritme slechts één $(T-1) \times (T-1)$ driehoekig (reëel) gedeelte dat gemeenschappelijk is voor alle gebruikte tonen. Elke gebruikte toon heeft daarnaast nog een individueel (complex) gedeelte dat bestaat uit de laatste, *i.e.* de T-de, rij van $\mathbf{L}$ en de filteraanpassing zelf. Bijgevolg heeft het (complex) gedeelte per toon een lineaire complexiteit.

Toongroepering

Om de initialisatiecomplexiteit verder te verlagen, introduceren we toongroepering. We verdelen de tonen in groepen en berekenen de optimale PT-EQ alleen voor de middelste toon van elke groep met directe of recursieve initialisatie.

Daarna hergebruiken we deze PT-EQ voor de andere tonen in dezelfde groep. Men moet echter rekening houden met het volgende.

Ten eerste egaliseert een egalisator van het type $\mathbf{v}_i$ niet alleen het kanaal, maar bevat die egalisator ook de sliding FFT voor toon i. Daarom kan men een egalisator $\mathbf{v}_i$ als zodanig, niet gebruiken voor een andere toon in dezelfde groep. Met behulp van het verband tussen $\mathbf{w}_i$ en $\mathbf{v}_i$, gegeven in formule (4.6), berekenen we dan eerst de overeenkomstige egalisator van het type $\mathbf{w}_i$ die enkel de egalisatie van het kanaal bevat, en hergebruiken deze voor de andere tonen i' in dezelfde groep, *i.e.* $\mathbf{w}_{i'} = \mathbf{w}_i$. Daarna berekenen we $\mathbf{v}_{i'}$ voor toon i' uitgaande van $\mathbf{w}_{i'}$.

Ten tweede heeft de impulsresponsie van het kanaal een toonafhankelijke amplitude en fase. De optimale PT-EQ $\mathbf{v}_i$, en dus ook $\mathbf{w}_i$, bevat een schaalfactor en rotatie overeenkomstig de amplitude en fase van toon i. Deze is niet noodzakelijk optimaal voor de andere tonen i' in dezelfde groep. We voegen daarom een extra 1-taps FEQ toe aan elke toon die geen middelste toon van een groep is. Als besluit kunnen we stellen dat toongroepering tussenliggende oplossingen biedt met de TEQ en de PT-EQ als bijzondere gevallen.

Initialisatie-complexiteit

Vervolgens berekenen we de complexiteit van het RLS-algoritme met inverse updating, toegepast op PT-EQ. We besluiten dat, wanneer het aantal filtercoëfficiënten kleiner is dan het aantal gebruikte tonen (zoals in downstream ADSL), de complexiteit van het kwadratische gedeelte slecht een kleine fractie is van de complexiteit van het lineaire gedeelte. Wanneer we bovendien toongroepering toepassen, wordt de initialisatie-complexiteit vergelijkbaar met de complexiteit tijdens datatransmissie voor downstream ADSL. In upstream ADSL daarentegen, is de complexiteit van het kwadratische gedeelte belangrijker omwille van het kleiner aantal gebruikte tonen en het groter aantal filtercoëfficiënten.

Performantie

Uit de simulaties volgt dat het groeperen van tonen in groepen van 11 geen significante invloed heeft op de performantie in downstream ADSL. In upstream ADSL heeft toongroepering een iets grotere invloed maar de bitsnelheid blijft nog steeds veel hoger dan de TEQ-bitsnelheid, bijvoorbeeld voor groepgrootte 5 en 7. Daarnaast simuleren we het RLS-algoritme met inverse updating met en zonder toongroepering. We besluiten dat RLS een goed performantie bereikt voor een aanvaardbaar aantal trainingssymbolen.

Deel II. Echo-onderdrukking

Hoofdstuk 6. Tijds- en frequentiedomein echo-onderdrukking en egalisatie

In dit hoofdstuk bestuderen we de combinatie van tijds- en frequentiedomein echo-onderdrukking (t/f domein echo-onderdrukking) met tijdsdomein egalisatie (TEQ) en vervolgens met egalisatie per toon (PT-EQ). Als vertrekpunt geven we eerst een overzicht van t/f domein echo-onderdrukking.

Tijds- en frequentiedomein echo-onderdrukking

T/f domein echo-onderdrukking wordt in de literatuur voorgesteld als een efficiënt algoritme om de echo in DMT-gebaseerde systemen te onderdrukken [54, 55]. De echo-onderdrukker is weergegeven in figuur 6.1 voor de vereenvoudigde architectuur van een symmetrische modem (IFFT en FFT hebben dezelfde grootte) met gesynchroniseerde verzonden en ontvangen symbolen. De echo wordt gedeeltelijk in tijds- en frequentiedomein gemodelleerd en weggefilterd. Het tijdsdomein gedeelte maakt de nodige correctie op de ontvangen echo zodat de residuele echo periodisch lijkt en een (complex) 1-taps echofilter per toon voldoende is in het frequentiedomein gedeelte van de echo-onderdrukker. De aanpassing van de filtercoëfficiënten gebeurt in het frequentiedomein met een 1-taps LMS algoritme per toon en heeft een zeer lage complexiteit. De totale complexiteit wordt gedomineerd door het tijdsdomein gedeelte van de echo-modellering. In vergelijking met een volledige tijdsdomein echo-modellering, wint men een factor twee in complexiteit. Uitbreidingen naar asymmetrische modems (met factor γ tussen IFFT- en FFT- grootte) worden afgeleid in [54, 55] en resulteren in een extra complexiteitswinst met factor γ in de tijdsdomein echo-modellering. Door het toepassen van een alternatief alignement van verzonden en ontvangen symbolen kan een extra factor twee gewonnen worden [67, 140]. Omwille van de propagatievertraging van het kanaal kan het alignement van de symbolen slechts aan één zijde van de telefoonlijn gekozen worden. Het alignement aan de andere zijde ligt dan automatisch vast en zal in het algemeen asynchroon zijn. In [54, 55] worden aanpassingen aan het oorspronkelijke schema voorgesteld voor een asynchrone werkingsmode.

Volgorde van TEQ en t/f domein echo-onderdrukking

Vervolgens bestuderen we de combinatie van t/f domein echo-onderdrukking en TEQ. Meestal wordt de TEQ uitgevoerd vóór de echo-onderdrukking, *i.e.* *'eerst-TEQ-daarna-echo'*, om de zogenaamde *gezamelijke verkorting* van de kanaalimpulsresponsie en de echo-impulsresponsie [3, 80] mogelijk te maken zodat men een korter echofilter kan gebruiken. De MMSE-gebaseerde, gezamelijke verkorting, voorgesteld in figuur 6.11, heeft echter geen verband met de resulterende bitsnelheid, analoog aan de MMSE-gebaseerde kanaalverkorting in hoofdstuk 3. De combinatie van kanaal- en echo-impulsresponsieverkorting kan dan ook aanleiding geven tot een slechtere kanaalimpulsresponsieverkorting wat de bitsnelheid kan verlagen. Anderzijds zal de TEQ de echo-impulsresponsie in het algemeen verlengen wanneer de TEQ ontworpen wordt om alleen de kanaalimpulsresponsie te verkorten. We tonen aan dat de volgorde van de TEQ en de t/f domein echo-onderdrukking veranderd kan worden om de verlenging van de echo-impulsresponsie te vermijden, *i.e. 'eerst-echo-daarna-TEQ'*, weergegeven in figuur 6.12. Dit veroorzaakt echter een complexiteitsstijging in de tijdsdomein echomodellering. Complexiteitsberekeningen tonen aan dat de configuraties 'eerst-TEQ-daarna-echo' en 'eerst-echo-daarna-TEQ' een vergelijkbare complexiteit hebben indien de verlenging van de echo-impulsresponsie in de eerste configuratie in rekening gebracht wordt. De convergentie van de filteradaptatie in de 'eerst-echo-daarna-TEQ' configuratie is niet eenvoudig te bewijzen. Ons doel is echter aan te tonen hoe de volgorde van TEQ en echo-onderdrukking veranderd kan worden om uiteindelijk PT-EQ te kunnen toepassen in plaats van TEQ. We beschouwen de 'eerst-echo-daarna-TEQ' configuratie dan ook eerder als een tussenresultaat.

Combinatie van t/f domein echo-onderdrukking en PT-EQ

Het voordeel van de toepassing van PT-EQ na t/f domein echo-onderdrukking is dat PT-EQ de bitsnelheid per toon optimaliseert voor een gegeven echo-onderdrukker. De *combinatie van t/f domein echo-onderdrukking en PT-EQ* is voorgesteld in figuur 6.14. Uit hoofdstuk 4 weten we dat de ingang van de PT-EQ bestaat uit één FFT-uitgang en $T-1$ (reële) verschiltermen van het ontvangen signaal. Na het tijdsdomein gedeelte van de echo-onderdrukker, is de residuele echo periodisch met de symboolperiode. Wanneer we dus na de tijdsdomein echo-onderdrukking, verschiltermen maken van ontvangen signaalmonsters die precies één symboolperiode verschillen in tijdsindex, zullen de verschiltermen zelf geen residuele echo meer bevatten. Bijgevolg zal het frequentiedomein gedeelte van de echo-onderdrukker geen echo-onderdrukking meer uitvoeren op de verschiltermen. De FFT-uitgang zelf bevat echter wel nog residuele echo die door de frequentiedomein echo-onderdrukker wordt onderdrukt. We tonen aan dat de bijhorende echofilteraanpassing kan herleid worden tot de oorspronkelijke filteraanpassing waarvoor convergentie bewezen werd in [54, 55]. Het is verder eenvoudig in te zien dat de 'eerst-TEQ-daarna-echo' en de 'eerst-echo-daarna-PT-EQ' configuraties een vergelijkbare complexiteit hebben indien de verlenging van de echo-impulsresponsie in rekening wordt gebracht in de eerste configuratie.

Hoofdstuk 7. Echo-onderdrukking per toon

We passen het per-toon-concept, dat geïntroduceerd werd in hoofdstuk 4 voor de egalisatie van DMT-signalen, toe op echo-onderdrukking. Het resultaat is *een DMT-modem die volledig per toon georganiseerd is met zowel egalisatie per toon (PT-EQ) als echo-onderdrukking per toon (PT-EC).* In tegenstelling tot t/f domein echo-onderdrukking, laat de nieuwe structuur toe de SNR voor elke toon afzonderlijk te maximaliseren voor gegeven filterlengtes van de PT-EQ en PT-EC door middel van een kwadratische kostfunctie per toon.

Egalisatie en 1-taps echo-onderdrukking per toon

Als vertrekpunt bespreken we het vereenvoudigde schema, weergegeven in figuur 7.1, met T-taps PT-EQ en 1-taps PT-EC. Er is nu geen tijdsdomein gedeelte in de echo-onderdrukking aanwezig. De PT-EQ wordt echter uitgevoerd vóór de 1-taps PT-EC. Dit betekent dat de PT-EQ de kanaal- en echo-impulsresponsie gezamelijk kan egaliseren of 'verkorten'. Een 1-taps PT-EC is dan voldoende om de residuele echo te onderdrukken indien de lengte van de 'verkorte' echo-impulsresponsie kleiner is of gelijk aan de cyclische prefixlengte vermeerderd met 1 en indien de verzonden en ontvangen symbolen gesynchroniseerd zijn. Wanneer aan deze voorwaarden voldaan wordt, ondervinden enkel de tonen die in beide communicatierichtingen gebruikt worden, echo van het overeenkomstig verzonden subsymbool, *i.e.* het ontvangen en geëgaliseerde subsymbool $Z_i^{(k)}$ bevat echo van het verzonden subsymbool $U_i^{(k)}$. Een toon die slechts aan één communicatierichting toegewezen wordt, ondervindt geen echo omdat het overeenkomstige subsymbool $U_i^{(k)}$ nul is. De optimale T-taps PT-EQ en 1-taps PT-EC zijn de oplossing van een (uitgebreid) MMSE probleem per toon, zie formule (7.6). Deze kostfunctie maximaliseert de SNR per toon en omvat dus *optimale gezamelijke verkorting per toon.*

Egalisatie en echo-onderdrukking per toon

Indien de 'verkorte' echo-impulsresponsie langer is dan de prefixlengte plus 1 of indien verzonden en ontvangen symbolen niet gesynchroniseerd zijn, ontstaan er interferenties in het echosignaal, gelijkaardig aan de interferenties in het nuttig signaal wanneer de kanaalimpulsresponsie langer is dan de prefixlengte plus 1, *i.e.* ICI1, ICI2 en ISI. Een ontvangen en geëgaliseerd subsymbool $Z_i^{(k)}$ bevat dus niet alleen echo afkomstig van $U_i^{(k)}$ maar ook van $U_{i'}^{(k')}$. Om deze echo te onderdrukken, introduceren we een PT-EC met meerdere taps. De volledig per toon gebaseerde structuur wordt afgeleid van de structuur met T-taps TEQ en T_E-taps tijdsdomein echo-onderdrukking (TEC), weergegeven in figuur 7.2. De volgorde van TEC en FFT mag veranderd worden op dezelfde wijze als de volgorde van TEQ en FFT. Het product van de TEQ en de TEC met de oorspronkelijke 1-taps FEQ resulteert dan respectievelijk in een T-taps PT-EQ en een T_E-taps PT-EC, die kunnen geoptimaliseerd worden voor elke toon afzonderlijk. De per-toon-structuur is voorgesteld in figuur 7.4 en bestaat uit twee zogenaamde per-toon-filterblokken (PTF) die elk één FFT en respectievelijk T- en T_E-taps filters per toon bevatten. Naast de FFT-uitgang hebben de filters per toon respectievelijk $T-1$ en T_E-1 (reële) verschiltermen als ingang.

Indien verzonden en ontvangen symbolen synchroon zijn, zal de FFT in de echotak het verzonden echosymbool reproduceren. Bijgevolg wordt de FFT in de echotak dan overbodig. Bovendien tonen we ook aan dat de eerste ν verschiltermen (met ν de prefixlengte) in dat geval nul zijn.

Daarnaast bestuderen we de performantie van een ontvanger met tweemaal hogere bemonsterfrequentie. De TEQ en dus ook de PT-EQ kan dan herschreven worden met behulp van de polyfase componenten, resulterend in een even en en oneven filter aan de originele bemonsterfrequentie zoals in figuur 7.5.

Om de even en oneven PT-EQ en de PT-EC gezamelijk te initialiseren, lossen we een (uitgebreid) MMSE-probleem op, gegeven in formule (7.13). Deze kostfunctie bevat *optimale gezamelijke verkorting per toon voor de algemene structuur met T-taps PT-EQ en T_E-taps PT-EC*. De gezamelijke verkorting per toon is beter dan de oorspronkelijk gezamelijke verkorting door een TEQ [3, 80], omdat met de nieuwe kostfunctie de SNR per toon wordt gemaximaliseerd.

Vervolgens leiden we aangepaste PT-EC structuren af voor asymmetrische modems (met factor γ tussen IFFT- en FFT-grootte). Deze resulteren in een complexiteitswinst met (ongeveer) factor γ in de filteroperaties. Daarenboven kan de N-punts FFT in de echotak vervangen worden door een N/γ-punts FFT in een geïnterpoleerde structuur en γ N/γ-punts FFT's in een gedecimeerde structuur. Verder vergelijken we de complexiteit van de filteroperatie van PT-EC met t/f domein echo-onderdrukking en tijdsdomein echo-onderdrukking. We besluiten dat, voor gegeven filterlengtes, t/f domein echo-onderdrukking de laagste complexiteit heeft. De complexiteitswinst van PT-EC ten opzichte van TEC is het gevolg van de selectie van de gebruikte tonen. Anderzijds, maakt PT-EC gecombineerd met PT-EQ, het mogelijk de bitsnelheid te optimaliseren voor gegeven filterlengtes. Omdat de PT-EQ bovendien vóór de PT-EC komt, is optimale gezamelijke verkorting per toon vervat in de kostfunctie en kunnen bij de PT-EC kortere filterlengtes aangewend worden voor een gelijkaardige performantie.

Hoofdstuk 8. Besluiten en verder onderzoek

Besluiten

In **deel I** van dit proefschrift hebben we egalisatie in DMT-gebaseerde DSL-modems behandeld. We hebben eerst de bestaande structuur met TEQ en het gekende kanaalverkortingsalgoritme besproken. Dit algoritme komt neer op de minimalisatie van een kwadratische kostfunctie met een beperking, echter zonder rechtstreeks verband met de bitsnelheid. De beperking is een eenheidsnorm, eenheidscoëfficiënt of eenheidsenergie en wordt opgelegd om de nuloplossing te vermijden. We hebben aangetoond dat een eenheidsenergiebeperking op de doelimpulsresponsie en/of op de TEQ tot dezelfde oplossing leiden voor de doelimpulsresponsie en de TEQ op een schaalfactor na en dus resulteren in dezelfde bitsnelheid.

Omdat het kanaalverkortingsalgoritme een aantal duidelijke nadelen vertoont, hebben we een alternatief TEQ-initialisatie-algoritme ontwikkeld. Door het invoegen van gewichtsmatrices in de kostfunctie en in de beperking, kunnen we de ongebruikte tonen expliciet negeren. Dit resulteert in een gevoelige performantieverbetering in upstream. We merken echter op dat het voorgestelde algoritme nog steeds niet overeenkomt met bitsnelheidsoptimalisatie.

Vervolgens hebben we de ontvangerstructuur zelf gewijzigd. Deze nieuwe structuur bevat geen klassieke TEQ meer (*i.e.* een reëel filter in het tijdsdomein). Maar elke gebruikte toon heeft zijn eigen (complex) filter na demodulatie (egalisatie per toon). Door het minimaliseren van een kwadratische kostfunctie per toon (MMSE), zijn we in staat om de bitsnelheid per toon te optimaliseren. Zowel in up- als downstream bekomen we een verbeterde performantie. We hebben aangetoond dat de complexiteit tijdens datatransmissie (voor gegeven filterlengte) vergelijkbaar is voor PT-EQ en TEQ wanneer alle tonen gebruikt worden. Bovendien laat PT-EQ toe om de filterlengte per toon te optimaliseren. Het nadeel van PT-EQ ten opzichte van TEQ is het grotere geheugen, nodig om alle filtercoëfficiënten te bewaren.

We hebben de combinatie van PT-EQ en een vensterfunctie (in het tijdsdomein) bestudeerd. De efficiënte implementatie van PT-EQ kan niet gecombineerd worden met een vensterfunctie. Een vensterfunctie is echter wel equivalent met een bepaalde set van PT-EQ's. Hieruit volgt dat een vensterfunctie kan geïmplementeerd worden na demodulatie als een deel van de globale PT-EQ's en dus ook kan geoptimaliseerd worden per toon.

Als bovengrens voor de PT-EQ hebben we SIMO-egalisatie gesimuleerd. We hebben aangetoond dat SIMO-egalisatie slechts aanleiding geeft tot een kleine performantieverbetering voor een grote complexiteitsstijging.

Directe initialisatie, door middel van het minimaliseren van de MMSE per toon, heeft een hoge complexiteit. We hebben daarom recursieve initialisatie gebaseerd op trainingssymbolen bestudeerd. Omdat de autocorrelatiematrix van de filteringang een zeer grote eigenwaardenspreiding heeft, is LMS-gebaseerde initialisatie zeer traag. RLS-gebaseerde initialisatie bereikt wel een goede performantie met een aanvaardbaar aantal trainingsymbolen. We hebben, meer bepaald, het RLS-algoritme met inverse updating toegepast op de PT-EQ's. Door de gemeenschappelijke ingangen van de PT-EQ's, *i.e.* de reële verschiltermen, eerst te verwerken, kan een behoorlijke complexiteitswinst bekomen worden.

Om de complexiteit tijdens initialisatie verder te verlagen, hebben we toongroepering voorgesteld. De optimale PT-EQ worden alleen berekend voor de middelste tonen van elke groep met directe of recursieve initialisatie. Deze egalisatoren worden vervolgens hergebruikt voor de andere tonen in dezelfde groep. Met een goed gekozen groepgrootte daalt de bitsnelheid slechts weinig terwijl de initialisatiecomplexiteit die afhankelijk is van het aantal gebruikte tonen, wordt gedeeld door de groepgrootte.

In **deel II** hebben we echo-onderdrukking voor DMT-gebaseerde DSL-modems bestudeerd. Na een bespreking van de in de literatuur voorgestelde t/f domein echo-onderdrukking, hebben we de combinatie met egalisatie bestudeerd. Meestal wordt de TEQ vóór de echo-onderdrukking toegepast om gezamelijke kanaalverkorting mogelijk te maken, wat kortere echofilters mogelijk maakt. Gezamelijke kanaalverkorting vertoont echter dezelfde nadelen als kanaalverkorting op zich: er is geen rechtstreeks verband met de bitsnelheid.

Wanneer de TEQ wordt ontworpen om alleen het *far end* kanaal te verkorten, wordt de echo-impulsresponsie in het algemeen verlengd. Om de verlenging te voorkomen, hebben we aangetoond dat de TEQ en echo-onderdrukking mogen omgewisseld worden. Deze structuur wordt eerder als een overgangsschema beschouwd om uiteindelijk eerst t/f domein echo-onderdrukking en dan PT-EQ toe te passen. Met de laatst genoemde structuur zijn we in staat om de bitsnelheid te optimaliseren voor een gegeven echofilter. We hebben aangetoond dat de complexiteit van 'eerst-TEQ-daarna-echo' vergelijkbaar is met 'eerst-echo-daarna-PT-EQ'.

Vervolgens hebben we echo-onderdrukking per toon voorgesteld als een alternatief voor echo-onderdrukking in DMT-gebaseerde systemen. Zoals we de TEQ na de FFT geplaatst hebben, hebben we ook de tijdsdomein echo-onderdrukker na de FFT geplaatst. Het voordeel van deze structuur is dat de SNR per toon kan geoptimaliseerd worden door een (uitgebreide) kostfunctie per toon. Aangepaste en efficiëntere schema's voor asymmetrische modems werden afgeleid. We hebben de complexiteit van de filteroperatie van PT-EC vergeleken met t/f domein echo-onderdrukking. Voor gegeven filterlengte, heeft t/f domein echo-onderdrukking de laagste complexiteit. Maar omdat PT-EC de bitsnelheid optimaliseert, kunnen kortere filterlengtes gebruikt worden voor vergelijkbare performantie.

Verder onderzoek

Directe gezamelijke initialisatie van de PT-EC en PT-EQ is eerder complex omdat een uitgebreid MMSE-probleem per toon opgelost moet worden. Het zou dan ook nuttig zijn om recursieve initialisatie te bestuderen voor PT-EC gecombineerd met PT-EQ. In eerste instantie, zou men het RLS schema met inverse updating kunnen uitbreiden. In vergelijking met t/f domein echo-onderdrukking, dat slechts een 1-taps LMS algoritme per toon nodig heeft, is er voor PT-EC nood aan een eenvoudiger initialisatie-algoritme.

Met efficiënte echo-onderdrukkingsalgoritmen wordt het mogelijk de modemstructuur te herorganiseren om hogere bitsnelheden mogelijk te maken. Men kan de tonen opnieuw toewijzen aan up- en downstream, zodat beide banden (gedeeltelijk) overlappen of aan elkaar grenzen. Het is ook noodzakelijk de analoge en digitale zend- en ontvangstfilters te herontwerpen. Bovendien zal het echosignaal het dynamisch bereik van het ontvangen signaal vergroten wat invloed heeft op het aantal bits in de A/D converter van de ontvanger.

Interfererende up- en downstream signalen veroorzaken niet alleen een echoprobleem maar ook een NEXT-probleem. NEXT-onderdrukking kan vereenvoudigd worden indien de ontvanger beschikt over referentiesignalen. In dat geval is NEXT-onderdrukking gelijkaardig aan echo-onderdrukking. In de CO kunnen dergelijke signalen aanwezig zijn en gebruikt worden in bijvoorbeeld het ontwerp van een NEXT-onderdrukker per toon. Wanneer geen referentiesignalen beschikbaar zijn, zoals in RT, wordt het NEXT-probleem moeilijker. Het ontwerp van NEXT-onderdrukkingsalgoritmen is een interessant onderwerp voor verder onderzoek.

Een tweede overspraakprobleem is FEXT. FEXT bestaat altijd tussen diensten van hetzelfde type in dezelfde kabelbundel. In het huidige VDSL-ontwerp wordt NEXT vermeden door FDD, pulsvorming en synchronisatie. FEXT blijkt echter een belangrijke stoorbron te zijn. Efficiënte FEXT-onderdrukkingsalgoritmen vormen een nuttig onderwerp voor verder onderzoek.

Naast overspraak afkomstig van gelijkaardige diensten, bestaat er ook overspraak van andere diensten. Voor VDSL blijken lokale netwerken gebaseerd op *Home Phoneline Networking Alliance* (HPNA) een belangrijke overspraakbron te zijn [40]. HPNA gebruikt de bestaande telefoondraden bij de abonnee om een lokaal netwerk te voorzien. De aangewende frequentieband ligt in het VDSL-spectrum. Bij HPNA-installatie wordt er geen isolatie voorzien tussen de telefoonbedrading in het huis van de abonnee en het toegangsnetwerk naar de abonnee. Bijgevolg kunnen de HPNA-signalen in het toegangsnetwerk terechtkomen waar ze in een bundel van telefoondraden overspraak veroorzaken in de VDSL-signalen van naburige abonnees. Huidige HPNA-onderdrukkingsalgoritmen zijn eerder complex. Er is dan ook nood aan efficiëntere algoritmen.

Een ander interessant onderwerp is de toepassing en vergelijking van TEQ en PT-EQ in andere domeinen zoals *HIgh PErformance Radio Local Area Network type 2* (HIPERLAN/2) [43]. HIPERLAN/2 gebruikt OFDM als modulatietechniek. Wanneer de impulsresponsie van het kanaal langer is dan de cyclische prefix, ontstaan interferenties tussen de verschillende dragers en kan egalisatie een hogere bitsnelheid mogelijk maken.

Chapter 1

Introduction

Since the invention of the telephone, a worldwide telephone network has been developed. Although originally designed for ordinary telephone services (Plain Old Telephone Service or POTS), the existing telephone network is nowadays increasingly used for broadband communications. This evolution is motivated by the search for economical solutions to provide broadband applications, such as teleconferencing and fast internet access, over existing media.

During the last decades, a number of new digital techniques for high-speed data transmission over the telephone loop, have been designed or are still being designed. These solutions are generically referred to as *Digital Subscriber Lines* (xDSL). Two of these, more specifically *Asymmetric Digital Subscriber Line* (ADSL) and *Very high bit rate Digital Subscriber Line* (VDSL), are of particular interest in this thesis. The standard modulation scheme for ADSL is the so-called *Discrete Multitone* (DMT) technique, which is a multicarrier technique similar to Orthogonal Frequency Division Multiplexing (OFDM). For VDSL, DMT is one of the two modulation candidates in standardization.

This thesis deals with the design of equalization and echo cancellation structures for DMT-based receivers. Our main motivation is the application to DMT-based digital subscriber lines.

1.1 Media for broadband communication

Three important media for wired broadband communication to and from the customer premises are: the subscriber telephone loop (made from twisted pair copper wires), the coaxial cable and the optical fiber. Besides wireless communication is a fourth option for high-speed communication.

Optical fiber allows the highest bit rates. However, nowadays it is economically infeasible to bring the fiber to the home of every customer. Therefore fiber is usually adopted in hybrid configurations where it is brought into the neighborhood of the customers. To allow a fast and economic installation of broadband connections, one re-uses existing networks to bridge the last leg. This can be the telephone or the cable network. Both networks have an inherently different structure.

The telephone loops are installed for bidirectional communication originally intended for POTS. Each customer has his own telephone line to the central office. Coaxial cable, on the other hand, is originally installed for unidirectional transmission of television signals (broadcasting), but is increasingly being adapted for bidirectional communication. This medium is shared by several customers in the same region and as a result, the available bandwidth of the coaxial cable is shared among these customers.

In this thesis, we consider broadband communication over the subscriber telephone loop. ADSL makes a broadband connection over the subscriber telephone loop from the customer premises to the central office. VDSL, on the other hand, allows even higher bit rates than ADSL but over a shorter distance. Therefore VDSL makes a broadband connection over the subscriber telephone loop from the customer premises to an optical network unit located in a street cabinet. The cabinet is connected to the central office by optical fiber.

An overview of xDSL techniques and a comparison with the traditional voice band modem are given in section 1.4.

1.2 Multicarrier modulation

Multicarrier modulation [15, 16] is a general name for modulation schemes that partition the available bandwidth into parallel, independent and orthogonal subchannels. By exploiting orthogonality between the subchannels, data can be sent in parallel without intersymbol interference by modulating a subcarrier in each band. Multicarrier modulation has applications in wired as well as wireless communication systems.

The first multicarrier systems arose from Frequency Division Multiplexing (FDM): the subbands are completely separated in frequency. However, in the late 60's, it was proven that the subbands can have spectral overlap with neighboring bands without resulting intercarrier and intersymbol interferences after reception [19, 51, 95].

The early multicarrier systems needed filters and oscillators to QAM modulate a carrier in each band. In 1971, the use of a Discrete Fourier Transform (DFT) to digitally implement the modulation and demodulation was proposed, by Weinstein [137, 52, 53]. Its main advantage is a cost-effective implementation

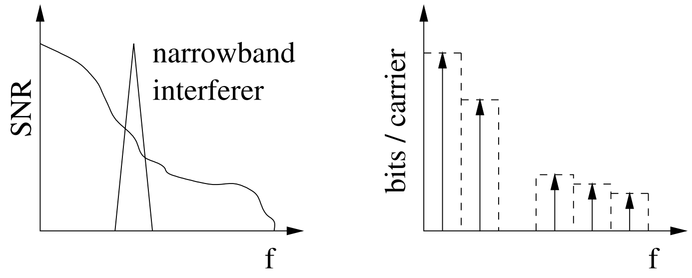

Figure 1.1: Each subchannel carries a number of bits according to its SNR when adaptive bit loading can be applied.

by means of a Fast Fourier transform (FFT). A DFT divides the frequency band into *overlapping*, but mathematically orthogonal, subchannels with sinc-shaped spectra.

A popular DFT-based multicarrier technique is *Orthogonal Frequency Division Multiplexing* (OFDM) [1, 16, 41] which has many wireless applications. OFDM is standardized in Europe for digital audio and video broadcasting. More recently, OFDM is adopted in drafted standards for Wireless Local Area Networks (WLAN) [43, 126, 127]. The outdoor and the indoor channel are characterized by multi path propagation and so have a large delay spread (similar to a long impulse response). When the symbol period is small with respect to the delay spread, intersymbol interference arises. This is seen in the frequency domain as frequency-selectivity. OFDM enables to divide the bandwidth in multiple frequency-flat subchannels without intersymbol interference. In chapter 2 we will explain how this is actually done.

To improve the capacity of a multicarrier system, one may apply so-called *adaptive bit loading* [16, 29, 32, 68, 77, 78]. Each subchannel is allocated an amount of energy and a number of bits according to its Signal-to-Noise Ratio (SNR), as shown in **Fig. 1.1**. However, adaptive bit loading is only feasible when there is a feedback channel from the receiving end of the communication link to the transmitting end. In broadcasting, there is no such feedback channel and a fixed number of bits is assigned to the carriers. For WLAN, adaptive bit loading is proposed as a means to improve capacity [124]. When applied in the latest DSL systems, OFDM combined with adaptive bit loading is known as *Discrete Multitone* (DMT). The term 'subcarrier' is equivalent to 'tone'. DMT-based ADSL requires equalization to keep the tones orthogonal because the channel impulse response is rather 'long', see [16, 28, 30, 32, 93] and chapters 2 and 3.

Other multicarrier modulation techniques have been presented, *e.g.* based on wavelets (Discrete Wavelet Multitone, DWMT) [2, 97], and based on filter-banks (Filtered Multitone, FMT) [24, 25]. Wavelets and filter-banks have a much better spectral containment and thus less spectral overlap than sinc functions, associated with a DFT-based modulation. When the orthogonality between subcarriers can not be maintained because of severe channel distortion and insufficient equalization, sinc functions result in more intersymbol and intercarrier interference (ISI and ICI) than the presented alternatives. Because of the sinc sidelobes, DMT is also less robust to narrowband interference (see section 1.5).

1.3 Duplexing

In a DSL system, two directions of communication are possible: communication from the Central Office (CO) to the Remote terminal (RT), located in the customer premises, is called *downstream* communication, while communication from RT to CO is called *upstream* communication. If transmission in both directions takes place over the same loop, the transmitter and receiver at one end are coupled to the loop by a *hybrid* [21, 74]. A perfectly balanced hybrid prevents leakage of transmitted signals into the receiver. However, due to large variations in the subscriber loops, a fixed hybrid can not be exactly balanced for all loops and hence leakage occurs.

A duplexing technique [74] is adopted to separate up- and downstream signals. In a *Time Division Duplexing* (TDD) system, both directions of communication are separated in time. In a *Frequency Division Duplexing* (FDD) system, they are separated in frequency. Another option is to use the same frequency band simultaneously in both directions. The transmitted signal will then cause echo in the received signal and an echo canceller [83] is needed to reduce the echo that leaks through the hybrid. *Echo cancellation* (EC) techniques for single carrier modulation have been developed in [31, 56, 58, 132]. More recently, a number of echo cancellation techniques suited for multicarrier modulation have been presented in literature [3, 17, 18, 33, 34, 54, 55, 67, 139, 141].

These duplexing techniques are represented in a time-frequency plane in **Fig. 1.2**.

The term 'full-duplex' is often used to refer to a simultaneous communication in both directions. If a full-duplex system operates on a single medium, FDD or echo cancellation is required.

1.4 Digital subscriber lines

A traditional *voice band modem* [74, 89] transmits data over the subscriber telephone loop in the frequency band 300-3400Hz (POTS band). The reason for this small bandwidth is that this type of modem makes an end to end connection across the public switched telephone network which is designed for speech signals with 4kHz bandwidth.

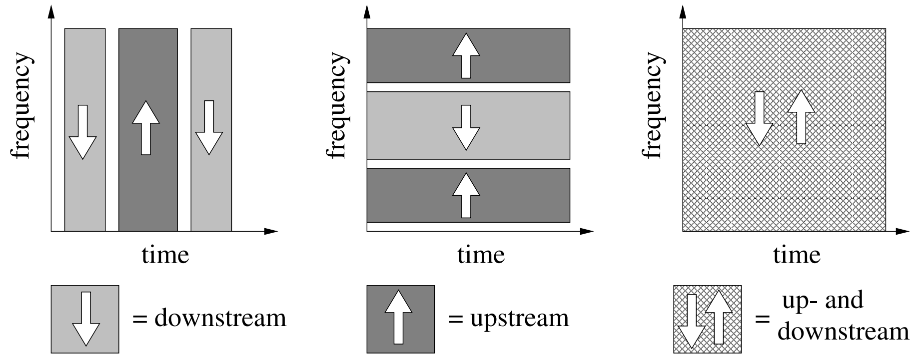

Figure 1.2: Duplexing techniques: time division duplexing, frequency division duplexing and echo cancellation

However, the subscriber telephone loop itself (*i.e.* the local loop between RT and CO only) consists of twisted pair copper wire which has a much larger bandwidth. A digital subscriber line makes use of this bandwidth by means of specially designed modems at both ends of the loop. For instance, ADSL uses a frequency band up to 1.104MHz and can offer downstream bit rates around 6Mbits/s depending on the loop length. In the following, we give a brief overview of xDSL techniques [16, 20, 21, 91]. Their evolution is towards wider bandwidth in order to achieve increasing bit rates.

The first DSL system is basic rate *Integrated Services Digital Network* (ISDN). It provides a symmetric bit rate (*i.e.* the same bit rate in both directions) of 160kbits/s in a bandwidth of 40kHz. ISDN, as standardized in North America, is a full-duplex system applying echo cancellation. A different ISDN system, using TDD, also exists in Japan [85].

The next generation DSL is *High bit rate Digital Subscriber Line* (HDSL) [23, 28, 73] which provides a symmetric rate of 1.536Mbits/s over two wire pairs in 200kHz bandwidth (USA) or 2.048Mbits/s over two or three pairs (Europe). The wire pairs operate in full-duplex mode with echo cancellation. HDSL can provide symmetric high-speed data links and is also used for multiplexing multiple voice band channels in one twisted pair.

Asymmetric Digital Subscriber Line (ADSL) [10, 22, 66, 72, 75, 79] provides a large downstream and a smaller upstream bit rate. The asymmetry of ADSL is specially suited for applications such as internet access and video-on-demand. ADSL is approximately 150 times faster than the fastest voice band modem. The actual supported rate depends, among other things, on the loop length. Target bit rates are 6Mbit/s and 640kbits/s in down- and upstream respectively within a range of 4km from the Central Office (CO). The bandwidth of 1.104MHz is divided by the (discrete) modulation scheme into multiple carriers

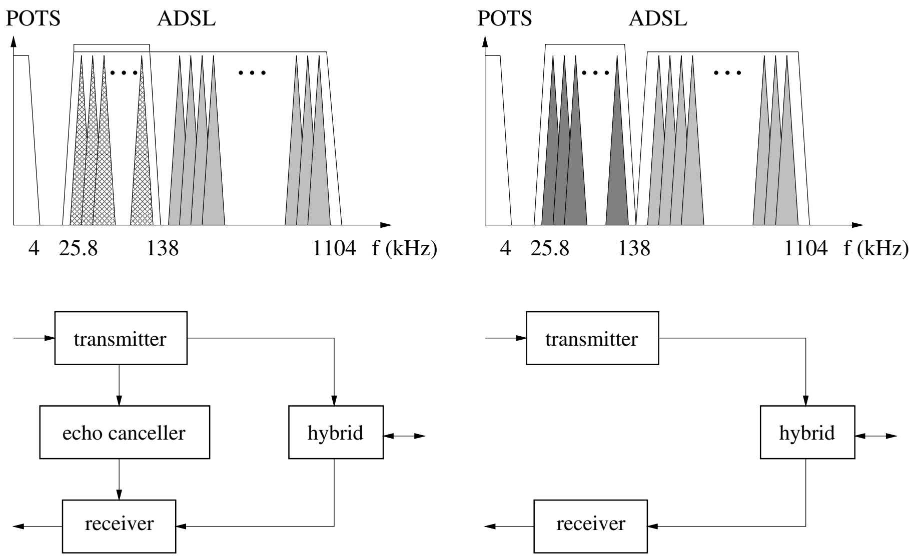

Figure 1.3: In the left set-up the lowest tones are used in upstream as well as in downstream and echo cancellation is required. In the right set-up different tones are assigned to up- and downstream, both frequency bands are separated by filters (FDD). The lowest tones are only used in upstream.

or tones, hence the name Discrete Multitone (DMT). A subset of tones may be used in both directions of communication, which however necessitates echo cancellation, or one may apply FDD and assign a different subset of tones to both directions, as shown in **Fig. 1.3**.

ADSL has to coexist with services like POTS or ISDN on the same twisted pair. The spectral compatibility is achieved by not assigning any bits to the lowest tones (frequency division multiplexing) and by the insertion of a POTS (or ISDN) splitter at both ends of the subscriber line. The POTS (or ISDN) splitter combines and separates the ADSL signal and the POTS (or ISDN) signal for joint transmission over the twisted pair. Hence, POTS (or ISDN) and ADSL services can be used simultaneously. The ADSL modems and POTS splitters at both ends of the loop are schematicly represented in **Fig. 1.4**. A fast deployment of ADSL is expected to be obstructed by the amount of time needed to install a splitter in all customer houses. This has motivated the design of splitterless ADSL, also known as the G.Lite specification [71]. Although POTS and splitterless ADSL are separated in frequency, there can be interference between both services due to nonlinearities in the POTS devices and the DSL modem. To avoid interference from splitterless ADSL into POTS, the splitterless ADSL modem detects changing states of POTS devices. As soon as a POTS device goes off-hook, the splitterless ADSL is interrupted and a fast-

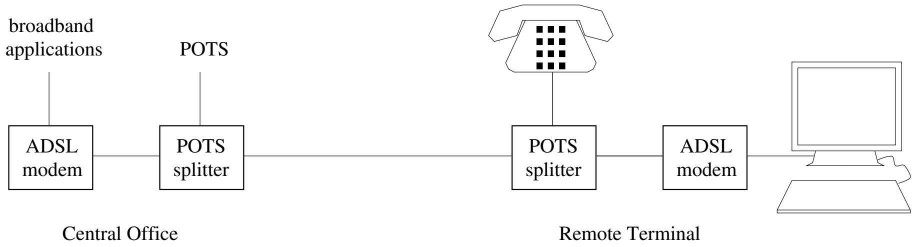

Figure 1.4: A POTS splitter is inserted between the ADSL modem and the subscriber loop to provide coexistence of ADSL with POTS.

retrain algorithm computes a lower bit rate with lower power consumption. During POTS occurrence, splitterless ADSL operates at this lower bit rate. When the POTS device goes on-hook, splitterless ADSL continuous operating at its initial bit rate.

The successor of ADSL is *Very high bit rate Digital Subscriber Line* (VDSL) [11, 35, 36, 42, 98, 103]. Coexistence with POTS or ISDN on the same line is also required. To provide even larger bit rates, its bandwidth is 10 times higher than for ADSL. It can provide symmetric as well as asymmetric (with down/up =8/1) bit rates and is intended to work over short loops. VDSL achieves 52Mbits/s downstream combined with 6.4Mbits/s upstream or a symmetric rate of 26Mbits/s over 300m. The largest target range is 1.5km for which an asymmetric rate of 13Mbits/s combined with 1.6Mbits/s is supported. Because of these short ranges, VDSL will often be used in hybrid fiber/copper configurations where it will bridge the last copper drop [133]. The digital subscriber loop then connects the subscriber to an optical network unit, located in a street cabinet, which is in its turn connected by fiber to the CO. This configuration is known as fiber-to-the-cabinet. Today, there is not yet a standardized modulation scheme for VDSL. The two candidates are on the one hand single carrier modulation including Quadrature Amplitude Modulation (QAM) [38] and Carrierless Amplitude/Phase modulation (CAP) [59, 87, 100] (related to QAM) and on the other hand DMT. A comparison between single carrier and multicarrier modulation is given in [96]. A recently proposed duplexing technique for DMT-based VDSL is the so-called Zipper [14, 60, 61, 62, 63, 64, 65, 81, 88, 104, 107]. Zipper can be thought of as an FDD system, where each frequency band is just one tone, see **Fig. 1.5**. However, in classical FDD, frequency bands are completely separated in frequency, whereas the tones in a DMT-based system are not. But because the tones are kept mathematically orthogonal, they can be used as a means of 'orthogonal duplexing'. The tones can be partitioned between up- and downstream in a huge number of ways, even at run-time. Therefore Zipper results in a very flexible system.

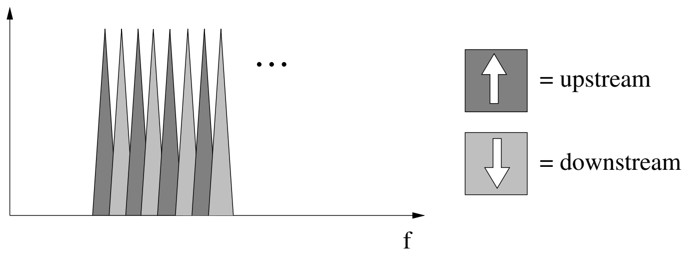

Figure 1.5: In a Zipper system each tone can be used in a different direction of communication.

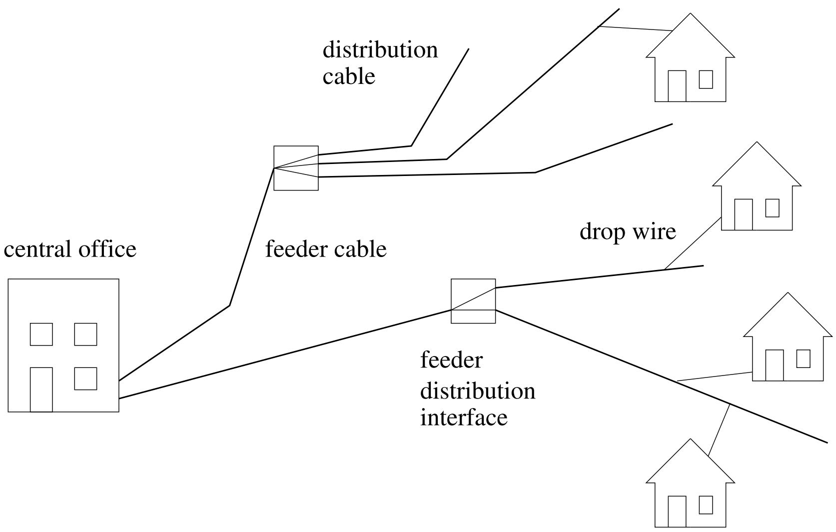

Figure 1.6: Telephone access network of twisted pairs.

1.5 Twisted pair network impairments

In this section, we give a brief overview of the topology of the telephone network in order to understand its major impairments [35, 37, 49, 85, 99, 138], influencing the performance of xDSL systems [13, 30, 69, 70, 101].

A twisted pair contains two insulated copper wires twisted around each other. The pairs are grouped into cables and the number of pairs in a cable decreases from the CO to RT. An overview of the telephone access network is given in **Fig. 1.6**. Starting from CO, the twisted pairs are first collected into binder groups containing tens of pairs. Up to 50 binder groups are collected themselves into large feeder cables. The feeder cable links the CO to a feeder distribution

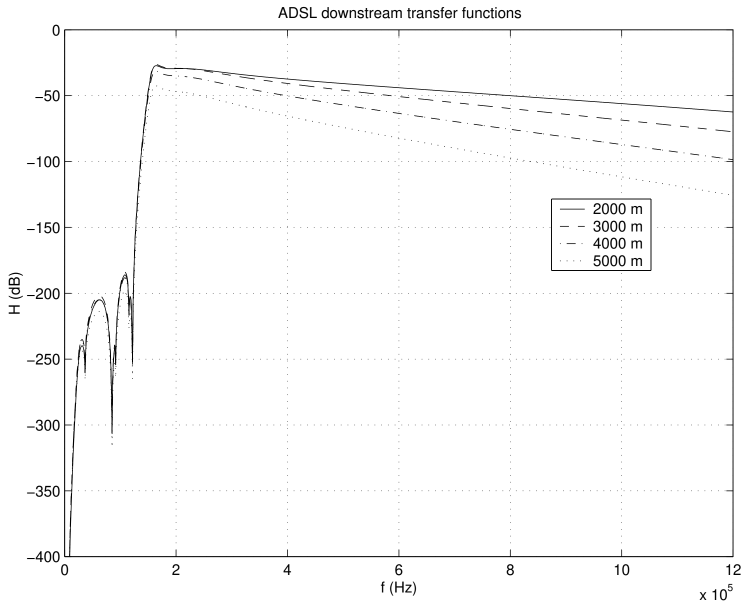

Figure 1.7: ADSL downstream transfer functions for different loop lengths (including transmit and receive filters, 26 AWG).

interface (FDI) where the pairs are cross-connected to pairs in distribution cables (containing tens of pairs). Finally a drop wire connects the twisted pair in a distribution cable to a customers house.

The total loop length, gauge and type of twisting are all important properties. A longer loop results in a larger *attenuation*, see **Fig. 1.7**. The gauge of a wire, often expressed in American Wire Gauge (AWG), may change in an FDI. Typical values are 26 to 19 AWG, corresponding to 0.4 to 0.91mm. Finer gauges are generally found in the large feeder cables whereas further along the loop, coarser gauges are used. The twist length or pitch is varied between neighboring pairs in a cable to limit electromagnetic interference (crosstalk), see below.

A *bridged tap* [134] is an unused, unterminated twisted pair section connected in parallel to a subscriber telephone loop. They may result from multiple connections from one pair in a feeder cable to several pairs in distribution cables for easy deleting and adding new customers. Alternatively, a bridged tap may result from the repair of broken links where an extra twisted pair is connected over the fracture and the broken sections are left in the telephone network. An in-house network of twisted pair copper wire also acts as a bridged tap. At a bridged tap, the signal is split into two parts. One part is reflected at the

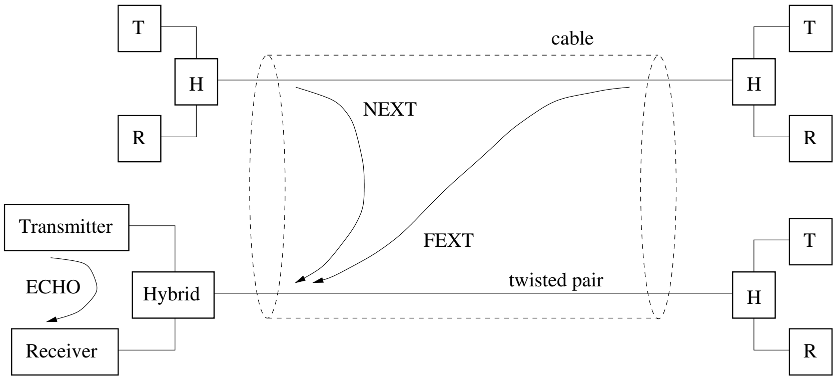

Figure 1.8: Two types of crosstalk may occur: near end crosstalk (NEXT) and far end crosstalk (FEXT). Echo originates from a modem's own transmitter.

open-circuited end of the bridged tap and adds again to the other part. If twice the length of the bridged tap equals half the wavelength of the signal (or an odd multiple of half the wavelength), then both components interfere destructively. This is seen in the attenuation characteristic of the loop as notches.

Standardization bodies like ANSI (American National Standards Institue) and ETSI (European Telecommunications Standards Institute) have defined test loops which consist of sections of different lengths and gauges with or without bridged taps to evaluate the ADSL/VDSL performance. We will use some of these in simulations.

Because twisted pairs are grouped in binders, unwanted electromagnetic coupling between different pairs occurs, known as *crosstalk*. A distinction is made between *Near End Crosstalk* (NEXT) and *Far End Crosstalk* (FEXT). In **Fig. 1.8**, it is seen that NEXT originates from an adjacent transmitter on a different pair. Echo can be considered as a special kind of NEXT, as echo is caused by a modems own transmitter. FEXT originates from a remote transmitter on a different pair. Both NEXT and FEXT increase with frequency (NEXT $\sim f^{3/2}$ and FEXT $\sim f^2$). When transmitters and receivers at both ends of the binder are co-located, NEXT is much more severe than FEXT, because FEXT is attenuated by the loop transfer function. However, FEXT can be a severe impairment too. A typical situation is shown in **Fig. 1.9**, where RT's are located at different distances from the CO (and their twisted pairs are grouped in the same binder). The FEXT from a near RT into the upstream signal from a far RT is destructive for the latter upstream signal. Power back-off is a method to reduce this FEXT by lowering the transmit power of the near RT with respect to the far RT. A power back-off scheme is presented in [108].

In general, crosstalk can arise from the same type of xDSL service on a dif-

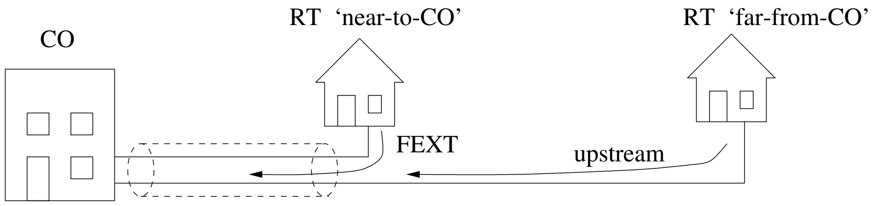

Figure 1.9: Severe FEXT from a near RT into the upstream signal from a far RT.

ferent pair in a binder, *i.e.* self-crosstalk, or from another type, *i.e.* alien crosstalk. NEXT and echo occur only if up- and downstream signals are simultaneously transmitted in the same bandwidth. FEXT exists always between xDSL services of the same type in a binder.

Radio Frequency Interference (RFI) results from Amplitude Modulation (AM) radio and amateur radio operating in the same frequency range as xDSL. This impairment is especially important for VDSL. All specified amateur radio bands are above 1.8MHz which coincide only with the VDSL bandwidth. The AM bands however partially overlap with the ADSL band too. There are two types of interference to be concerned with. *Ingress* is interference from a radio transmitter into xDSL and *egress* is the radiation caused by xDSL into a radio receiver. Drop wires and aerial wires are most vulnerable for RFI. Techniques to suppress RFI ingress and egress are presented in [105, 106, 109] and [12] respectively.

Finally, there is also background noise from *thermal noise* and *impulse noise* [86].

1.6 Problem statement

DMT divides the available bandwidth into parallel tones. The incoming serial bitstream is divided into parallel streams, which are used to QAM-modulate the different tones by means of an inverse fast Fourier operation. After modulation, a cyclic prefix is appended to each symbol. If the prefix is longer than the channel impulse response, demodulation can be implemented by means of a fast Fourier transform, followed by a (complex) 1-taps frequency domain equalizer (FEQ) per tone to compensate for the channel amplitude and phase effects, as will be explained in chapter 2. A long prefix however results in a large overhead with respect to the bit rate. On the other hand, if the prefix is shorter than the channel impulse response, interferences between different symbols and carriers arise.

As an example, in ADSL the channel impulse response is significantly longer than the prefix length. An existing solution for this problem is to insert a (real) T-taps time domain equalizer (TEQ) *before demodulation*, to shorten the channel impulse response. Many TEQ initialization algorithms have been developed in literature. The major part of these compute a TEQ such that the cascade of the channel impulse response and the TEQ forms a FIR channel with length shorter than the cyclic prefix. This criterion leads to a minimum mean square error (MMSE) problem without direct relation to the resulting bit rate, which is a major disadvantage. Moreover, the bit rate is a non-smooth function of the decision delay, see chapter 2, which hampers optimal alignment of the receiver. **Equalization** in DMT-based systems is studied in part I. We consider the TEQ-based receiver as well as a new receiver structure.

Further, we look at **echo cancellation** structures in part II. Echo cancellers are important in two set-ups. With (partly) overlapping up- and downstream bands, as shown in figure 1.3, echo cancellation may allow to achieve higher overall bit rate. Second, echo cancellation may be employed in an FDD set-up as an alternative to the high orders of highly selective transmit and receive filters. Although in the latter set-up separated tones are used in up- and downstream, echo may occur. In general, a certain transmitted tone will not only cause echo in the corresponding received tone, but will cause echo in all received tones, due to interferences in the echo signal, similar to the interferences in the far end signal.

Remark that interfering up- and downstream tones not only cause an echo problem, but also a NEXT problem, as shown in figure 1.8. Furthermore, the dynamic range of the received signal will be increased by the echo signal, which in turns influences the number of necessitated bits in the receiver's A/D converter. In this thesis, we do not aim at optimizing the complete modem architecture when echo cancellation is employed. Instead, we compare echo cancellation structures for given channel impulse responses and noise environments.

1.7 Thesis survey and contributions

In this section, a general overview of the thesis is given.

In *chapter 2*, we give an introduction to some basic concepts, such as DMT modulation, decision delay, time and frequency domain equalization. Further, we derive the data models for different DMT-based system set-ups. These data models are used in the following chapters.

In **part I**, we study **equalization** for DMT-based systems in detail. We review some TEQ design procedures, presented in literature, and aim at improving upon the TEQ performance based on the well-known MMSE channel shortening. *In a first attempt, we maintain the receiver structure*, *i.e.* the TEQ remains in the system and we only change the TEQ initialization algorithm.

In a second attempt, we change the receiver structure. In fact, each tone then has its own optimal (complex) TEQ, but now implemented *after demodulation*. We show that the latter structure clearly outperforms MMSE channel shortening.

In *chapter 3*, we review TEQ design based on MMSE channel shortening and introduce a new TEQ initialization algorithm. A significant bit rate increase is obtained in upstream. The cost functions of these algorithms are quadratic and have a unique global minimum. As a result, the optimization itself is rather simple. However, the drawback of these algorithms is that the cost function does not correspond to bit rate optimization. Finally, we review the optimal TEQ design algorithm, called geometric SNR, which comes down to a nonlinear optimization problem.

Then we develop per tone equalization in *chapter 4*. The new receiver structure has no TEQ anymore before demodulation, but each tone now has its own equalizer, after demodulation, which optimizes the SNR per tone. Increased bit rate is obtained in upstream as well as in downstream. Furthermore, the bit rate is a smooth function of the decision delay in contrast to the TEQ bit rate. The complexity during data transmission for TEQ and per tone equalization are shown to be similar. Moreover, the number of taps can be optimized per tone, and as a result, a complexity reduction may be obtained. Further, we study the combination of per tone equalization and windowing, which is a technique to suppress RFI.

Computation of the optimal per tone equalizers, as in chapter 4, results in a high computational cost. Therefore there is need of computational more efficient initialization. In *chapter 5*, we develop an initialization scheme based on recursive least squares with inverse updating. To reduce initialization complexity even further, tone grouping is proposed.

The publications related to part I are

- K. Van Acker, G. Leus, M. Moonen, S. Claes and O. van de Wiel. An Improved Optimization Algorithm for Time Domain Equalizer Design in ADSL Modems. In *Proc. International Workshop on Copper Wire Access Systems*, pages 117-123, Budapest, Hungary, October 1997.

- K. Van Acker, G. Leus, M. Moonen, S. Claes and O. van de Wiel. Improved Time Domain Equalization for ADSL. In *Proc. ProRISC Workshop on Circuits, Systems and Signal Processing*, pages 615-620, Mierlo, The Netherlands, November 1997.

- K. Van Acker, G. Leus, M. Moonen, O. van de Wiel and T. Pollet. Per Tone Equalization for DMT Receivers. In *Proc. IEEE Global Telecommunications Conference (GLOBECOM)*, pages 2311-2315, Rio de Janeiro, Brazil, December 1999.

- K. Van Acker, G. Leus, M. Moonen, O. van de Wiel and T. Pollet. Per Tone Equalization for DMT-based Systems. In *IEEE Transactions on Communications*, accepted for publication.

- K. Van Acker, T. Pollet, G. Leus, and M. Moonen. Combination of Per Tone Equalization and Windowing in DMT-Receivers. In *Proc. Fifth Bayona Workshop on Emerging Technologies in Telecommunications*, pages 49-53, Bayona, Spain, September 1999.

- K. Van Acker, T. Pollet, G. Leus and M. Moonen. Combination of Per Tone Equalization and Windowing in DMT-Receivers. Internal Report 99-46b, ESAT-SISTA, K.U.Leuven (Leuven, Belgium), submitted to *Signal Processing*, 1999.

- K. Van Acker, G. Leus, M. Moonen and T. Pollet. Frequency Domain Equalization with Tone Grouping in DMT/ADSL Receivers. In *Proc. Asilomar Conference on Signals, Systems and Computers*, pages 1067-1070, Pacific Grove, California, October 1999.

- K. Van Acker, G. Leus, M. Moonen and T. Pollet. RLS-based Initialization for Per Tone Equalizers in DMT-Receivers. In *Proc. European Signal Processing Conference (Eusipco)*, Tampere, Finland, September 2000.

- K. Van Acker, G. Leus, M. Moonen and T. Pollet. RLS-based Initialization for Per Tone Equalizers in DMT-Receivers. Internal Report 00-12b, ESAT-SISTA, K.U.Leuven (Leuven, Belgium), submitted to *IEEE Transactions on Communications*, 2000.

- K. Van Acker, G. Leus, M. Moonen and O. van de Wiel. Multicarrier receiver. European patent application (EP 0 969 637).

- K. Van Acker, G. Leus, M. Moonen, T. Pollet and O. van de Wiel. Multicarrier receiver with per-carrier RLS frequency domain equalization. European patent application (EP 0 967 763).

In **part II**, we study **echo cancellation** for DMT-based systems. We first review an echo canceller presented in literature and then develop a new echo canceller based on the 'per tone' principle that we also have adopted in part I.

In *chapter 6*, we review time/frequency domain echo cancellation [54, 55]. Mostly the TEQ is applied before the echo cancellation. We show that the order of equalization and echo cancellation can be reversed. Our aim is to apply finally first time/frequency domain echo cancellation and then per tone equalization. The advantage of the latter structure is the ability to optimize the SNR per tone given a certain echo canceller in time/frequency domain implementation.

We introduce per tone echo cancellation in *chapter 7*. We start with a simplified scheme containing a multitaps per tone equalizer and a 1-taps per tone echo canceller per tone which is sufficient in the specific case of aligned transmit and receive symbols and, of an echo impulse response which is shorter than the cyclic prefix. To approach the general echo cancellation problem, we propose a multitaps per tone echo canceller combined with a multitaps per tone equalizer. This structure enables to optimize the SNR per tone for given echo cancellation and equalization filter lengths.

The publications related to part II are

- K. Van Acker, G. Leus, M. Moonen and T. Pollet. Combination of Echo Cancellation and Equalization in DMT-based ADSL modems. Internal Report 00-32, ESAT-SISTA, K.U.Leuven (Leuven, Belgium), submitted to *IEEE Transactions on Communications*, 2000.
- K. Van Acker, M. Moonen and T. Pollet. Per Tone Echo Cancellation for DMT-based Systems. Internal Report 00-101 , ESAT-SISTA, K.U.Leuven (Leuven, Belgium), submitted to the *International Conference on Acoustics, Speech and Signal Processing (ICASSP 2001)*, 2000.
- K. Van Acker, M. Moonen and T. Pollet. Per Tone Echo Cancellation for DMT-based Systems. Internal Report 00-119 , ESAT-SISTA, K.U.Leuven (Leuven, Belgium), submitted to *IEEE Transactions on Communications*, 2000.

Finally, in *chapter 8*, we summarize the conclusions and give suggestions for further research.

Chapter 2

Concepts

In this chapter we first explain the DMT modulation technique and the mathematics behind it. In section 2.1, important concepts such as cyclic prefix, time domain equalization, frequency domain equalization, intersymbol and intercarrier interference are reviewed because they turn out to be important in this thesis.

Afterwards, the well-known TEQ design procedure based on minimum mean square error (MMSE) channel shortening and its relation with the decision delay is explained. We state the important disadvantages of MMSE channel shortening which have led us to the design of improved equalization structures.

Then, the channel capacity derived by Shannon, the SNR gap and the formula to compute the bit rate are reviewed. A brief overview of adaptive bit loading algorithms is given.

Data models for the received DMT far end signal and echo signal are described in section 2.2. We start with a basic DMT data model of the received signal, suitable for ADSL signals. We further extend the basic model to include the echo signal, oversampling, decimation and interpolation. The VDSL data model is slightly different from the ADSL data model in that a cyclic suffix, pulse shaping and windowing are adopted.

Finally, conclusions are drawn in section 2.3.

2.1 Discrete multitone

The DMT transmitter and receiver are presented in **Fig. 2.1** and **Fig. 2.2** respectively [15, 28]. The appropriate sampling frequencies are noted in dashed frames. In the transmitter, the following operations are performed.

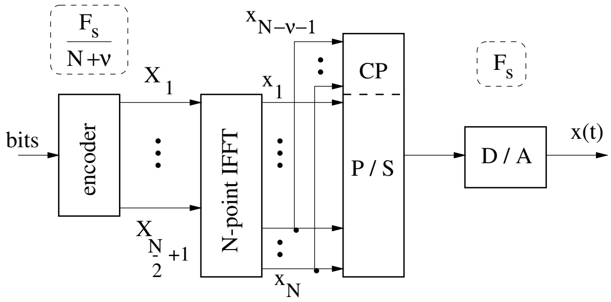

Figure 2.1: DMT Transmitter

- A serial bit stream is divided into $\frac{N}{2}+1$ parallel bit streams. The number of bits b_i assigned to a parallel bit stream depends on the SNR of the corresponding tone $i = 1 \dots \frac{N}{2}+1$. The b_i bits are further mapped onto a complex[1] subsymbol X_i. 2^{b_i} possible complex values form the constellation for tone i.
- An N-point IFFT is performed on the Hermitian-symmetric vector

$$\begin{bmatrix} X_1 & \dots & X_N \end{bmatrix}^{\mathrm{T}} = \begin{bmatrix} X_1 & \dots & X_{N/2+1} & X^*_{N/2} & \dots & X^*_2 \end{bmatrix}^{\mathrm{T}} \quad (2.1)$$

  to result in a real vector of N samples $[x_1 \dots x_N]^{\mathrm{T}}$. The N sized vectors are the DMT symbols in frequency and time domain respectively. We will use the following notation to describe this modulation step

$$\begin{bmatrix} x_1 \\ \vdots \\ x_N \end{bmatrix} = \mathcal{I}_N \cdot \begin{bmatrix} X_1 \\ \vdots \\ X_N \end{bmatrix} \quad (2.2)$$

  with $\mathcal{I}_N$ the $N \times N$ IDFT-matrix.
- The last ν samples of a time domain symbol are repeated as a so-called *Cyclic Prefix* (CP) [92] in front of the symbol.
- Finally, the prefixed time domain symbol is converted from parallel to serial and from digital to analog. The continuous time signal $x(t)$ is sent through the channel. In this model, the 'channel' represents the combination of transmit filters, physical channel as well as receive filters.

The sample rate is denoted as F_s and so the symbol rate is $\frac{F_s}{N+\nu}$.

[1]except for the tone 1 and $\frac{N}{2}+1$ which have to be real

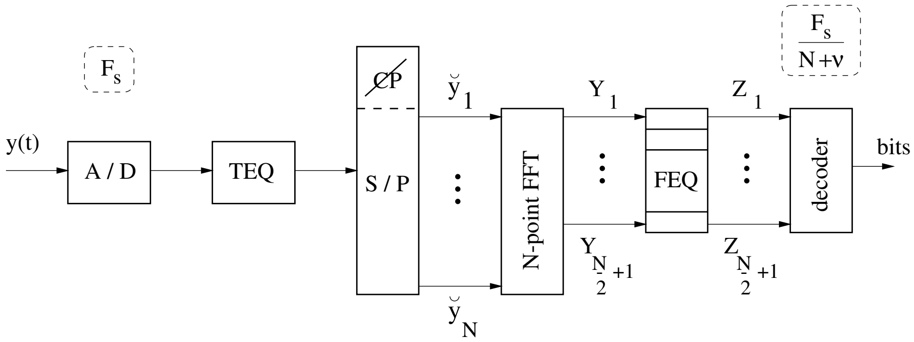

Figure 2.2: DMT Receiver

In the receiver, basically (ignoring the equalization) the reverse operations occur.

- The received continuous time signal $y(t)$ is first analog to digital converted.
- The received discrete signal y_l is filtered with a Finite Impulse Response (FIR) filter, called *Time domain EQualizer* (TEQ) [28].
- The filtered sequence $\breve{y}_l$ is converted from serial to parallel.
- The ν samples corresponding to the cyclic prefix are discarded.
- An FFT operation demodulates the filtered received symbol

$$\begin{bmatrix} Y_1 \\ \vdots \\ Y_N \end{bmatrix} = \mathcal{F}_N \cdot \begin{bmatrix} \breve{y}_1 \\ \vdots \\ \breve{y}_N \end{bmatrix} \tag{2.3}$$

  where $\mathcal{F}_N$ is the $N \times N$ DFT matrix and where the output is Hermitian-symmetric.
- A 1-taps *Frequency domain EQualizer* (FEQ) D_i equalizes each tone separately.
- The equalized FFT output Z_i is decoded to reproduce the transmitted bits.

We will now explain in more detail the function of the cyclic prefix and the equalizers [93]. For this purpose, we adopt a discrete-time model of the channel impulse response $\mathbf{h}$.

A crucial aspect is that the channel impulse response length can be smaller or larger than the prefix length. In the first case, only frequency domain equalization is required, while in the second case both frequency and time domain equalization are required, as will be explained.

2.1.1 Case 1: Order of h is smaller than or equal to ν

Assume that $\mathbf{h} = [h_0 \dots h_\nu]$ (the following derivation holds for shorter channels too). A received symbol can be written as the convolution of a transmitted symbol and the channel impulse response plus noise

$$\begin{bmatrix} y_1 \\ \vdots \\ y_N \end{bmatrix} = \begin{bmatrix} h_\nu & \dots & h_0 & 0 & \dots & 0 \\ 0 & h_\nu & \dots & h_0 & 0 & \\ & \ddots & \ddots & & \ddots & \ddots \\ 0 & \dots & 0 & h_\nu & \dots & h_0 \end{bmatrix} \cdot \left[\frac{\mathbf{O} \mid \mathbf{I}_\nu}{\mathbf{I}_N} \right] \cdot \begin{bmatrix} x_1 \\ \vdots \\ x_N \end{bmatrix} + \begin{bmatrix} n_1 \\ \vdots \\ n_N \end{bmatrix} \tag{2.4}$$

with n_l the channel noise. The first matrix in the right hand side is a Toeplitz matrix of the channel coefficients. The second matrix extends the transmitted symbol with the cyclic prefix. The product of these two matrices produces a circulant matrix. Hence, equation (2.4) can be written as

$$\begin{bmatrix} y_1 \\ \vdots \\ y_N \end{bmatrix} = \overbrace{\begin{bmatrix} h_0 & 0 & \dots & 0 & h_\nu & \dots & h_1 \\ h_1 & h_0 & 0 & \dots & 0 & h_\nu & \dots \\ \dots & h_1 & h_0 & 0 & \dots & 0 & h_\nu \\ h_\nu & \dots & h_1 & h_0 & 0 & \dots & 0 \\ 0 & h_\nu & \dots & h_1 & h_0 & 0 & \dots \\ & & \ddots & & \ddots & \ddots & \\ 0 & \dots & 0 & h_\nu & \dots & h_1 & h_0 \end{bmatrix}}^{\mathbf{C}} \cdot \begin{bmatrix} x_1 \\ \vdots \\ x_N \end{bmatrix} + \begin{bmatrix} n_1 \\ \vdots \\ n_N \end{bmatrix} \tag{2.5}$$

Hence, the linear convolution with the channel impulse response is equivalent to a circular convolution because of the cyclic prefix insertion. By multiplying both sides with $\mathcal{F}_N$ and applying equation (2.2), one obtains

$$\mathcal{F}_N \cdot \begin{bmatrix} y_1 \\ \vdots \\ y_N \end{bmatrix} = \mathcal{F}_N \cdot \mathbf{C} \cdot \mathcal{I}_N \cdot \begin{bmatrix} X_1 \\ \vdots \\ X_N \end{bmatrix} + \mathcal{F}_N \cdot \begin{bmatrix} n_1 \\ \vdots \\ n_N \end{bmatrix} \tag{2.6}$$

The left hand side represents the FFT output in the receiver, ignoring the TEQ. In the right hand side, one can apply the eigenvalue decomposition of a

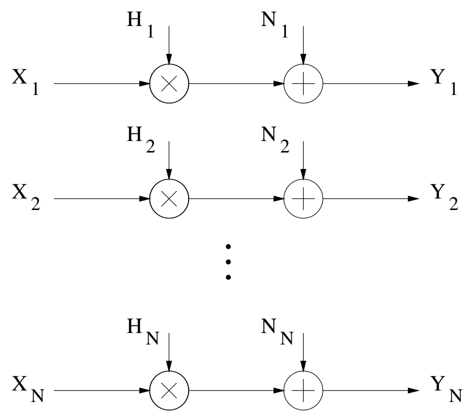

Figure 2.3: Frequency domain interpretation of DMT modulation

circulant matrix. The eigenvectors of a circulant matrix form a DFT matrix and its eigenvalues are equal to the FFT of the first column of $\mathbf{C}$. Hence

$$\begin{bmatrix} Y_1 \\ \vdots \\ Y_N \end{bmatrix} = \begin{bmatrix} H_1 & 0 & \dots \\ 0 & \ddots & 0 \\ \dots & 0 & H_N \end{bmatrix} \cdot \begin{bmatrix} X_1 \\ \vdots \\ X_N \end{bmatrix} + \begin{bmatrix} N_1 \\ \vdots \\ N_N \end{bmatrix}$$

$$\text{with} \quad \begin{bmatrix} H_1 \\ \vdots \\ H_N \end{bmatrix} = \mathcal{F}_N \cdot \begin{bmatrix} h_0 \\ \vdots \\ h_\nu \\ \mathbf{0} \end{bmatrix} \tag{2.7}$$

In conclusion, the DMT technique indeed divides the channel $\mathbf{h}$ in N parallel (independent), flat subchannels each having a channel gain H_i and additive noise N_i. This frequency domain interpretation is shown in **Fig. 2.3**. A 1-taps filter D_i per tone (FEQ) is sufficient to compensate for the channel's amplitude and phase effects.

2.1.2 Case 2: Order of h is larger than ν

When the channel impulse response is longer than the cyclic prefix, *i.e.* $\mathbf{h} = [h_0 \dots h_L]$ with $L > \nu$, interferences arise [94, 102]. To describe the types of interference, we consider a received symbol at time index k. Because $L > \nu$, the transmitted symbol at time $k-1$ will contribute to the received symbol at time k

$$\begin{bmatrix} y_1^{(k)} \\ \vdots \\ y_N^{(k)} \end{bmatrix} = \left[\begin{array}{c|cccccc} \mathbf{O} & h_L & \dots & h_0 & 0 & \dots & 0 \\ & 0 & h_L & \dots & h_0 & 0 & \\ & & \ddots & \ddots & & \ddots & \ddots \\ & 0 & \dots & 0 & h_L & \dots & h_0 \end{array} \right] \cdot \begin{bmatrix} \mathbf{P} & \mathbf{O} \\ \mathbf{O} & \mathbf{P} \end{bmatrix} \cdot \begin{bmatrix} x_1^{(k-1)} \\ \vdots \\ x_N^{(k-1)} \\ x_1^{(k)} \\ \vdots \\ x_N^{(k)} \end{bmatrix} \tag{2.8}$$

with $\mathbf{P} = \left[\begin{array}{c|c} \mathbf{O} & \mathbf{I}_\nu \\ \hline \multicolumn{2}{c}{\mathbf{I}_N} \end{array} \right]$. The Toeplitz matrix of the channel impulse response is zero padded to have $2(N+\nu)$ columns. For a compact notation, the noise is left out for the time being. If this time domain symbol would be fed directly to the demodulating FFT, one has

$$\begin{aligned} \begin{bmatrix} Y_1^{(k)} \\ \vdots \\ Y_N^{(k)} \end{bmatrix} = {} & \mathcal{F}_N \overbrace{\left[\begin{array}{c|ccc} \mathbf{O} & h_L & \dots & h_{\nu+1} \\ & 0 & \ddots & \vdots \\ & \ddots & 0 & h_L \\ & & \ddots & 0 \end{array} \right]}^{\mathbf{T}^{(k-1)}} \mathbf{P} \begin{bmatrix} x_1^{(k-1)} \\ \vdots \\ x_N^{(k-1)} \end{bmatrix} \\ & + \mathcal{F}_N \overbrace{\begin{bmatrix} h_\nu & \dots & h_0 & 0 & \dots & & \dots & 0 \\ h_{\nu+1} & h_\nu & \dots & h_0 & 0 & & & \vdots \\ \vdots & \ddots & \ddots & & \ddots & \ddots & & \\ h_L & \dots & & & \dots & h_0 & 0 & \\ 0 & h_L & \dots & & & \dots & h_0 & 0 \\ 0 & 0 & h_L & \dots & & & \dots & h_0 \end{bmatrix}}^{\mathbf{T}^{(k)}} \mathbf{P} \begin{bmatrix} x_1^{(k)} \\ \vdots \\ x_N^{(k)} \end{bmatrix} \end{aligned} \tag{2.9}$$

$\mathbf{T}^{(k-1)}$ and $\mathbf{T}^{(k)}$ are both Toeplitz matrices. Substituting formula (2.2), the demodulated received symbol becomes

$$\begin{bmatrix} Y_1^{(k)} \\ \vdots \\ Y_N^{(k)} \end{bmatrix} = \mathcal{F}_N \mathbf{T}^{(k-1)} \mathbf{P} \mathcal{I}_N \begin{bmatrix} X_1^{(k-1)} \\ \vdots \\ X_N^{(k-1)} \end{bmatrix} + \mathcal{F}_N \mathbf{T}^{(k)} \mathbf{P} \mathcal{I}_N \begin{bmatrix} X_1^{(k)} \\ \vdots \\ X_N^{(k)} \end{bmatrix} \tag{2.10}$$

The products $\mathbf{T}^{(k-1)}\mathbf{P}$ and $\mathbf{T}^{(k)}\mathbf{P}$ are not circulant. Therefore pre- and post-multiplying with $\mathcal{F}_N$ and $\mathcal{I}_N$ respectively does not produce diagonal matrices.

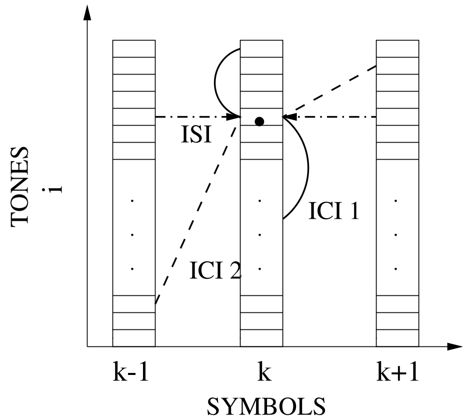

Figure 2.4: Intercarrier and intersymbol interference

The unwanted contributions in $Y_i^{(k)}$ from subsymbols different from $X_i^{(k)}$ are interferences. In **Fig. 2.4** it is shown that the interference can be split in 3 types [94].

1. *Intercarrier Interference of type 1* (ICI1): All elements $a_{i_1 i_2}$ $(i_1 \neq i_2)$ in matrix $\mathbf{A}^{(k)} = \mathcal{F}_N \mathbf{T}^{(k)} \mathbf{P} \mathcal{I}_N$ result in interference from one subsymbol in another subsymbol transmitted on a different tone during the same symbol period. In other words, $X_{i_2}^{(k)}$ causes ICI1 in $X_{i_1}^{(k)}$ with $i_2 \neq i_1$.

2. *Intersymbol Interference* (ISI): All diagonal elements $a_{i_1 i_1}$ in matrix $\mathbf{A}^{(k-1)} = \mathcal{F}_N \mathbf{T}^{(k-1)} \mathbf{P} \mathcal{I}_N$ result in interference from one subsymbol in another subsymbol transmitted on the same tone during a different symbol period. In other words, $X_{i_1}^{(k-1)}$ causes ISI in $X_{i_1}^{(k)}$.

3. *Intercarrier Interference of type 2* (ICI2): All elements $a_{i_1 i_2}$ $(i_1 \neq i_2)$ in matrix $\mathbf{A}^{(k-1)} = \mathcal{F}_N \mathbf{T}^{(k-1)} \mathbf{P} \mathcal{I}_N$ result in interference from one subsymbol in another subsymbol transmitted on a different tone during a different symbol period. In other words, $X_{i_2}^{(k-1)}$ causes ICI2 in $X_{i_1}^{(k)}$ with $i_2 \neq i_1$.

Depending on the length of the channel impulse response, there may be ISI and ICI2 from more than 1 symbol.

Downstream ADSL uses a symbol and a prefix of length $N = 512$ and $\nu = 32$ respectively. The tone spacing is F_{tsp}=4312.5Hz. Thus, the sample frequency is $F_s = N * F_{tsp} = 2.208$MHz. The length of the channel impulse response is a few hundred taps at $F_s = 2.208$MHz, hence significantly longer than the prefix length. In upstream, one can use a symbol and a prefix size of length

$N = 128$ and $\nu = 8$ with the same tone spacing (the upstream symbol size may be smaller because there are less used tones, as can be seen in figure 1.3). It turns out that also for upstream communication, the impulse response is significantly longer than the prefix.

To cope with interferences, one could lengthen the prefix. However, a longer prefix represents a larger efficiency loss ($\frac{\nu}{N+\nu}$). To make the efficiency loss smaller, one could make the symbol size N larger. But then a larger symbol size increases the latency.

Another solution is to reduce the effective channel length by means of a FIR filter before demodulation. This is the function of the TEQ [28]. If a TEQ can be found that effectively reduces the channel length to the length of the prefix, the analysis of case 1 basically applies with the shortened channel substituted for the original channel. In practice, it turns out that designing an appropriate TEQ is a difficult task.

2.1.3 TEQ design

The T-taps TEQ is mostly designed based on a Minimum Mean Square Error (MMSE) criterion to shorten the channel impulse response (CIR) to a $(\nu + 1)$-taps target impulse response (TIR). An exhaustive number of TEQ designs are presented in literature [4, 5, 6, 7, 26, 27, 28, 75, 80, 84, 122, 123, 125, 135, 136]. An important parameter in TEQ design is the so-called *decision delay*. Assume a given impulse response $\mathbf{h} = [h_0 \dots h_L]$. Then, briefly, one may shorten $\mathbf{h}$ to $[h_0 \dots h_\nu 0 \dots 0]$, where the decision delay is then zero, or one may shorten $\mathbf{h}$ to $[0 \dots 0 h_\delta \dots h_{\delta+\nu} 0 \dots 0]$, with decision delay δ. Which delay is chosen depends on the MMSE. According to **Fig. 2.5**, one searches for a TEQ $\mathbf{w}$, a TIR $\mathbf{b}$ and a decision delay δ such that J is minimized

$$\min_{\mathbf{w},\mathbf{b},\delta} J$$

$$\text{with} \quad J = \mathcal{E}\left\{e_l^2\right\} = \mathcal{E}\left\{\left(\left[x_{l-\delta} \dots x_{l-\nu-\delta} | y_l \dots y_{l-T+1}\right] \cdot \begin{bmatrix} -\mathbf{b} \\ \mathbf{w} \end{bmatrix}\right)^2\right\} \qquad (2.11)$$

subject to a certain constraint to avoid the zero solution, see chapter 3, with $\mathbf{b} = [b_0 \dots b_\nu]^{\mathrm{T}}$, $\mathbf{w} = [w_0 \dots w_{T-1}]^{\mathrm{T}}$, x_l and y_l transmitted and received signal samples respectively with l the sample index.

TEQ procedures based on MMSE channel shortening (such as those used in current ADSL modems) have considerable disadvantages.

1. The MMSE is not related to the maximal achievable bit rate by the DMT system.
2. The obtained bit rate is a non-smooth function of the delay which hampers choosing the decision delay.

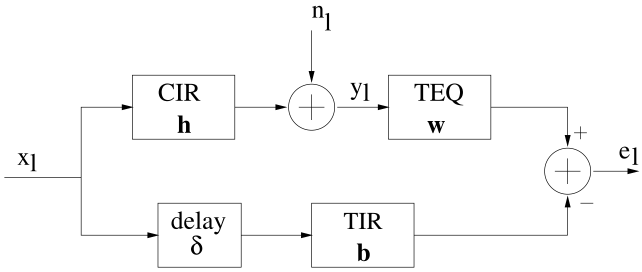

Figure 2.5: TEQ design by MMSE channel shortening

An additional disadvantage of the TEQ is that all tones are equalized with one filter, which as such limits the performance of the DMT-system. In [8, 9], it is shown that the optimal, in the sense of maximal bit rate, TEQ coefficients are the solution of a highly nonlinear cost function, which appears to be difficult to optimize [82].

2.1.4 Alternative equalization structures

Equalization in a DMT-system basically relies on a cyclic prefix insertion and a 1-taps frequency domain equalizer per tone. This prevents interferences (ISI and ICI) provided that the cyclic prefix is long enough. When the order of the channel impulse response is larger than the prefix length, additional equalization techniques are called for. One can apply time domain equalization (TEQ) to shorten the channel impulse response, which is mostly adopted. But, alternatively, one can apply equalization in the frequency domain (without TEQ).

The disadvantages of the TEQ have led us to the design of an alternative receiver structure based on so-called per tone equalization (PT-EQ). PT-EQ is applied after demodulation with the FFT. Each used tone then has its own optimal equalizer while the complexity during data transmission is kept at the same level. We develop PT-EQ in chapter 4.

In literature [93, 128, 129, 130], other forms of equalization have been presented. Multiple-input/multiple-output (MIMO) equalization is also applied after demodulation with the FFT. MIMO can be considered as a more general receiver structure than PT-EQ since it combines multiple FFT outputs for the equalization of tone i, whereas PT-EQ only considers the FFT ouput of tone i as input to the equalizer of tone i. Single-input/single-output (SIMO) equalization is an even more general structure where the cascade of the FFT and the MIMO equalization is replaced by a bank of parallel filters. Hence, SIMO enables even higher bit rates. However, it was noted in literature that the performance comparison was not constrained by complexity issues. Remark

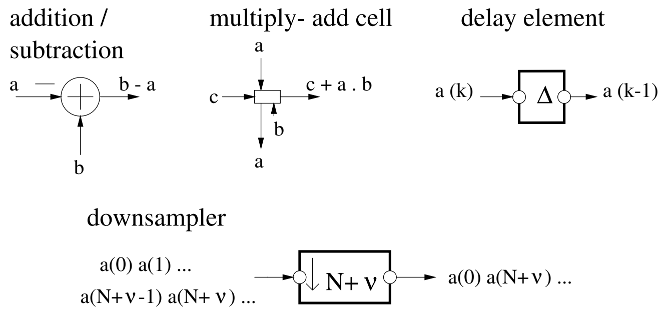

Figure 2.6: Signal flow graph building blocks

that, in contrast with TEQ and PT-EQ, there is no cyclic prefix involved in the MIMO and SIMO equalizers presented in [93, 128, 129, 130].

In chapter 4, we make a comprehensive comparison of PT-EQ with TEQ. Furthermore, we compare PT-EQ and SIMO equalization.

2.1.5 Signal flow graphs

DMT receivers based on a new equalization structure (PT-EQ) will be derived in chapter 4 and represented as signal flow graphs (SFG), building blocks of which are given in **Fig. 2.6**. The addition/subtraction block adds/subtracts the numbers a and b. A multiply-add block multiplies the numbers a and b and adds the product to c. A delay element delays the input signal over one sample period. Finally, a downsampler with factor f only selects one out of f successive input samples.

The (discrete part of the) TEQ-based receiver, as defined in figure 2.2, can also be represented by this type of SFG which is shown in **Fig. 2.7**. The input is the discrete time signal y_l, $\mathbf{w}_{T\times 1} = [w_0\, w_1 \dots w_{T-1}]^{\mathrm{T}}$ is the (real) T-taps TEQ and D_i the (complex) 1-taps FEQ for tone i. The tapped delay line with $(N+\nu)$-downsamplers is equivalent to a serial to parallel conversion and a prefix discard.

2.1.6 Capacity and bit loading

The maximal number of bits (capacity) that can be transmitted over a flat (sub)channel is derived by Shannon and is equal to

$$c_i = \log_2(1 + SNR_i) \quad \text{with} \quad SNR_i = \frac{E_i \cdot |H_i|^2}{\sigma_i^2} \tag{2.12}$$

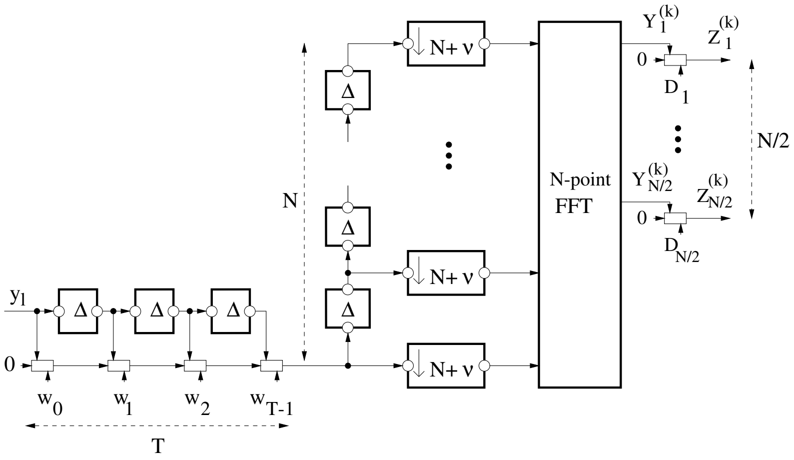

Figure 2.7: T-taps TEQ with 1-taps FEQ per tone

where E_i is the symbol energy and σ_i^2 is the noise variance on tone i. The capacity of the channel is the sum of the capacities of the subchannels, if they are independent. In conclusion, the optimal bit loading algorithm allocates an amount of energy and a number of bits to each tone under a total energy constraint

$$\max \sum_i c_i \quad \text{such that} \quad \sum E_i = E \tag{2.13}$$

This constrained maximization is solved by the water-filling solution: each tone gets an amount of energy E_i such that $E_i + \sigma_i^2/|H|_i^2 = K = \text{cte}$ and $\sum E_i = E$. The solution fills the noise-to-signal curve $\sigma_i^2/|H|_i^2$ with energy (equivalent to water) up to a constant level K. So, the capacity achieving energy distribution depends on the channel SNR $|H|_i^2/\sigma_i^2$.

It is known that infinite complexity is required to achieve the theoretical channel capacity. Hence, a realistic system transmits at a data rate below the theoretical capacity. The gap Γ measures the distance in SNR between theoretical capacity and actual bit rate

$$b_i = \log_2(1 + \frac{SNR_i}{\Gamma}) \quad \text{with} \quad SNR_i = \frac{E_i \cdot |H_i|^2}{\sigma_i^2} \tag{2.14}$$

The gap is a function of the bit error probability P_e aimed at [46]. For instance, with $P_e = 10^{-7}$, the gap is 9.8 dB. On the one hand, by applying coding, the gap can be reduced. On the other hand, a noise margin is required to make the system noise robust, and therefore the gap is again artificially increased. The total gap is then

$$\Gamma = 9.8 - \gamma_c + \gamma_m \tag{2.15}$$

with γ_c the coding gain and γ_m the noise margin. In ADSL the required bit error probability is $P_e = 10^{-7}$ for all used tones and Γ is tone independent. Formulas (2.14) and (2.15) will be adopted in simulations.

Adaptive loading algorithms compute an energy distribution and a bit allocation for a bit rate below capacity. A loading algorithm can maximize the margin at given data rate [29], or can maximize the data rate at given margin [77, 78], under a total energy constraint. The algorithm proposed in [77] is a three-step algorithm. Firstly, one decides which tones are turned on and off based on the water-filling solution. Secondly, the available energy is distributed over the used tones. Two distribution methods are proposed: flat energy and water-filling. The flat energy distribution has slightly worse performance than the water-filling solution (2% loss) but is less complex. Finally, the number of bits is computed with formula (2.14). The numbers of bits have to be rounded to an integer value and then the allocated energies are scaled accordingly. The transmit energy mask then gets a saw-tooth shape.

2.1.7 Pulse shaping and windowing

The duplexing scheme for DMT-based VDSL is the Zipper technique [14, 60, 61, 62, 63, 64, 65, 81, 88, 104, 107]. Orthogonal tones carry signals in up- or downstream direction without applying time domain equalization. The orthogonality is maintained by means of the extended cyclic prefix and an additional cyclic extension at the end of each symbol (*Cyclic Suffix (CS)*). Ideally, the length of this cyclic suffix is equal to the largest channel delay which exists in the considered binder. When synchronization between all transmitters at both ends in one binder, is perfect and the channel impulse response are sufficiently short, there is no echo nor NEXT in the system. Unfortunately, in reality there will be some echo and NEXT due to insufficient lengths of the cyclic extensions and due to insufficient synchronization.

To lower the echo and NEXT, pulse shaping [64] is adopted in the DMT-based VDSL transmitter, shown in **Fig. 2.8**. The number of outputs of each block is indicated below the figure. A symbol of size N first gets a cyclic prefix and suffix of size $\nu+\beta/4$. Then a non-rectangular window (mostly with raised cosine shape) with a roll-off interval of size $\beta/2$ at both sides of the symbol, is applied, see **Fig. 2.9**. Successive symbols overlap in the $\beta/2$-roll-off region. Therefore, the transmitted symbols have finally size $N + 2\nu$. The effect of a raised cosine function with respect to a rectangular function is seen in **Fig. 2.10**. A raised cosine function lowers the sidelobes.

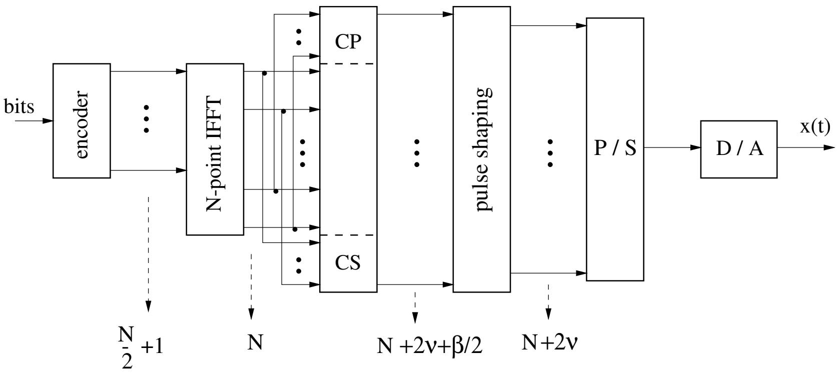

Figure 2.8: DMT-based VDSL Transmitter

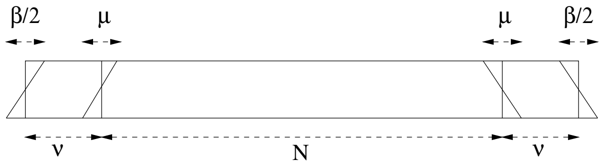

Figure 2.9: A VDSL-symbol of size N having cyclic extensions of size ν. Pulse shaping at the transmitter is determined by β and windowing at the receiver by μ.

The DMT-based VDSL receiver is shown in **Fig. 2.11**. A part of the cyclic prefix and suffix is discarded. The remaining parts are used for windowing. Windowing prevents Radio Frequency Interference (RFI) to leak into too many neighboring tones by lowering the sidelobes at the receiver [109]. A non-rectangular window with a roll-off interval of μ samples at both sides of the symbol, is applied, see also **Fig. 2.9**. Afterwards, the first $\mu/2$ samples (head) are folded on the symbol tail, and the last $\mu/2$ samples (tail) are folded on the symbol head, see **Fig. 2.12**. This operation does not introduce ISI nor ICI because the window has certain symmetry properties. The symmetry requires that when folding the tail on the symbol head and the head on the symbol tail, the resulting function is rectangular.

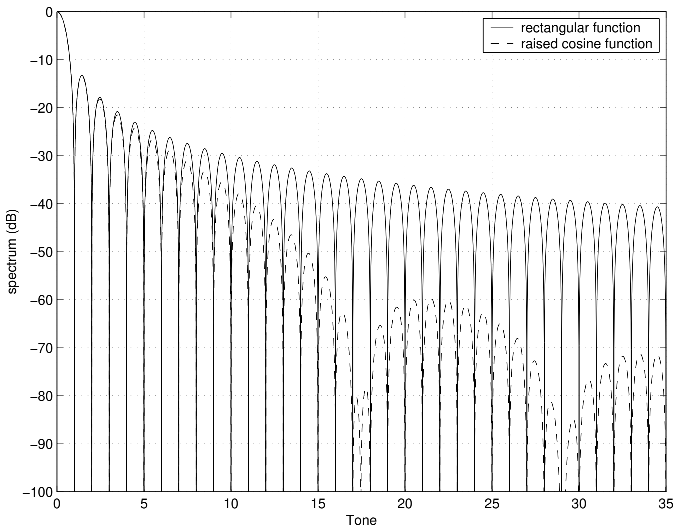

Figure 2.10: Spectrum of a tone when a rectangular or a raised cosine function is applied.

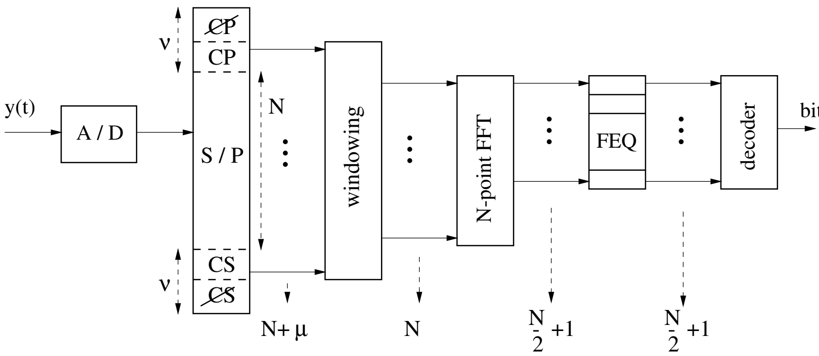

Figure 2.11: DMT-based VDSL Receiver

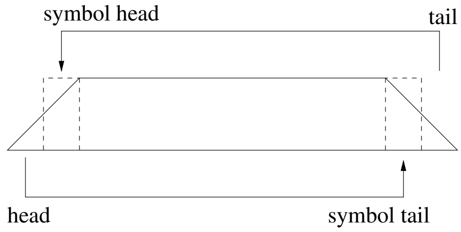

Figure 2.12: Folding operation

2.2 Data models

In this section, we describe a set of data models for the received DMT signal. We start with the basic data model where the transmit IDFT and receive DFT have the same size. This data model is further extended to include the echo signal, oversampling, decimation and interpolation. All these DMT data model are suitable for describing ADSL signals because they incorporate a cyclic prefix, *i.e.* a cyclic extension in front of the symbol.

Finally a data model suitable for VDSL signals is given which includes a cyclic prefix as well as a cyclic suffix, pulse shaping and windowing.

2.2.1 Basic data model

In the basic data model, the IDFT in the transmitter and the DFT in the receiver have the same size N, according to figures 2.1 and 2.2. Hence, transmitted and received symbol size (expressed in samples) is N. At the receiver, the signal is sampled at a sample rate of $N+\nu$ samples per symbol, *i.e.* without oversampling.

The following notation is adopted in the description of the DMT system: k is the time index of a symbol, $X_i^{(k)}$ is a complex subsymbol for tone i ($i = 1 \ldots N$) of the far end signal to be transmitted at symbol period k, $Y_i^{(k)}$ the demodulated output for tone i (after the FFT) and $Z_i^{(k)}$ the final output (after frequency domain equalization). Note that $X_i^{(k)} = X_{N-(i-2)}^{*(k)}$, $i = 2 \ldots \frac{N}{2}$ and that similar equations hold for $Y_i^{(k)}$. Further, ν denotes the length of the cyclic prefix, $s = N+\nu$ the length of a symbol including prefix, $\bar{\mathbf{h}} = [h_L \ldots h_0 \ldots h_{-K}]$ the far end channel impulse response in reverse order[2], n_l additive channel noise and y_l the received signal, with l being the sample index.

[2] $\bar{\mathbf{h}}$ denotes vector $\mathbf{h}$ with its elements in reverse order.

To describe the data model, we consider three successive symbols[3] $X_{1:N}^{(c)}$ to be transmitted at $c = k-1, k, k+1$ respectively. The kth symbol is the symbol of interest, the previous and the next symbol are used to include interferences with neighboring symbols in our model. The received signal may then be specified as follows

$$\begin{aligned}
\overbrace{\begin{bmatrix} y_{k\cdot s+\nu-T+2+\delta} \\ \vdots \\ y_{(k+1)\cdot s+\delta} \end{bmatrix}}^{\mathbf{y}} &= \left[\mathbf{O}_{(1)} \left| \begin{matrix} \boxed{\bar{\mathbf{h}}} & 0 & \cdots \\ & \ddots & \ddots \\ 0 & \cdots & \boxed{\bar{\mathbf{h}}} \end{matrix} \right| \mathbf{O}_{(2)} \right] \cdot \begin{bmatrix} \mathbf{P} & \mathbf{O} & \mathbf{O} \\ \mathbf{O} & \mathbf{P} & \mathbf{O} \\ \mathbf{O} & \mathbf{O} & \mathbf{P} \end{bmatrix} \cdot \\
& \begin{bmatrix} \mathcal{I}_N & \mathbf{O} & \mathbf{O} \\ \mathbf{O} & \mathcal{I}_N & \mathbf{O} \\ \mathbf{O} & \mathbf{O} & \mathcal{I}_N \end{bmatrix} \cdot \overbrace{\begin{bmatrix} X_{1:N}^{(k-1)} \\ X_{1:N}^{(k)} \\ X_{1:N}^{(k+1)} \end{bmatrix}}^{\hat{\mathbf{x}}} + \overbrace{\begin{bmatrix} n_{k\cdot s+\nu-T+2+\delta} \\ \vdots \\ n_{(k+1)\cdot s+\delta} \end{bmatrix}}^{\mathbf{n}} \\
&= \mathbf{H}\cdot\hat{\mathbf{x}} + \mathbf{n}
\end{aligned} \tag{2.16}$$

Here, T is the equalizer length. $\mathbf{O}_{(1)}$ and $\mathbf{O}_{(2)}$ are zero matrices of size $(N+T-1) \times (N+\nu-T+1-L+\nu+\delta)$ and $(N+T-1) \times (N+\nu-K-\delta)$ respectively. The matrix containing the channel impulse response is Toeplitz. Matrix $\mathbf{P} = \left[\begin{array}{c|c} \mathbf{O} & \mathbf{I}_\nu \\ \hline \multicolumn{2}{c}{\mathbf{I}_N} \end{array}\right]$ adds the cyclic prefix. The $\mathcal{I}_N$ matrices are $N \times N$ IDFT matrices and modulate the input symbols. The zero reference decision delay corresponds to the so-called head $[h_{-K} \dots h_{-1}]$ and the tail $[h_{\nu+1} \dots h_L]$ which maximize the energy in $[h_0 \dots h_\nu]$. The decision delay δ is further considered as the relative delay with respect to this reference delay, and is a design parameter.

2.2.2 Data model with echo

If echo is present, one can model the echo as part of the additive noise n_l or, one can model the echo in a similar way as the far end signal, *i.e.* as a DMT-modulated signal. The latter has an advantage in that in this way phase (and hence delay-) information of the echo-signal is included in the model. This improves the design of echo cancellers, see chapter 7.

In this echo model, the far end and echo signals are assumed to have the same symbol and prefix size, *i.e.* N and ν. Further, $U_i^{(k)}$ is a complex subsymbol for tone i ($i = 1 \dots N$) of the echo signal transmitted at symbol period k. $\bar{\mathbf{h}}_E$ is the echo channel impulse response in reverse order. The received signal then becomes

[3] Vector $X_{1:N}^{(c)}$ denotes vector $[X_1^{(c)} \dots X_N^{(c)}]^{\mathrm{T}}$.

$$
\begin{aligned}
\overbrace{\begin{bmatrix} y_{k\cdot s+\nu-T+2+\delta_1} \\ \vdots \\ y_{(k+1)\cdot s+\delta_1} \end{bmatrix}}^{\mathbf{y}} &= \left[\begin{array}{c|ccc|c} \mathbf{O}_{(1)} & \boxed{\bar{\mathbf{h}}} & 0 & \cdots & \mathbf{O}_{(2)} \\ & & \ddots & \ddots & \\ & 0 & \cdots & \boxed{\bar{\mathbf{h}}} & \end{array}\right] \cdot \hat{\mathbf{P}} \cdot \hat{\mathcal{I}}_N \cdot \overbrace{\begin{bmatrix} X_{1:N}^{(k-1)} \\ X_{1:N}^{(k)} \\ X_{1:N}^{(k+1)} \end{bmatrix}}^{\hat{\mathbf{x}}} + \\
& \left[\begin{array}{c|ccc|c} \mathbf{O}_{(3)} & \boxed{\bar{\mathbf{h}}_E} & 0 & \cdots & \mathbf{O}_{(4)} \\ & & \ddots & \ddots & \\ & 0 & \cdots & \boxed{\bar{\mathbf{h}}_E} & \end{array}\right] \cdot \hat{\mathbf{P}} \cdot \hat{\mathcal{I}}_N \cdot \overbrace{\begin{bmatrix} U_{1:N}^{(k-1)} \\ U_{1:N}^{(k)} \\ U_{1:N}^{(k+1)} \end{bmatrix}}^{\hat{\mathbf{u}}} + \\
& \overbrace{\begin{bmatrix} n_{k\cdot s+\nu-T+2+\delta_1} \\ \vdots \\ n_{(k+1)\cdot s+\delta_1} \end{bmatrix}}^{\mathbf{n}} \\
&= \mathbf{H} \cdot \hat{\mathbf{x}} + \mathbf{H}_E \cdot \hat{\mathbf{u}} + \mathbf{n}
\end{aligned} \tag{2.17}
$$

$\mathbf{O}_{(1)}$ and $\mathbf{O}_{(2)}$ are zero matrices of size $(N+T-1) \times (N+\nu-T+1-L+\nu+\delta_1)$ and $(N+T-1) \times (N+\nu-K-\delta_1)$ respectively. Matrix $\hat{\mathbf{P}} = \mathrm{diag}(\mathbf{P}, \mathbf{P}, \mathbf{P})$ and $\hat{\mathcal{I}}_N = \mathrm{diag}(\mathcal{I}_N, \mathcal{I}_N, \mathcal{I}_N)$ are block diagonal matrices. The zero reference decision delay of the far end signal corresponds to the head $[h_{-K} \ldots h_{-1}]$ and the tail $[h_{\nu+1} \ldots h_L]$ that maximize the energy in $[h_0 \ldots h_\nu]$. Finally, δ_1 is the relative decision delay of the far end signal. Analogous definitions hold for the corresponding echo parameters $\mathbf{O}_{(3)}$, $\mathbf{O}_{(4)}$, $\bar{\mathbf{h}}_E$, L_E, K_E and δ_2.

The input to the echo canceller (echo reference signal) is modeled by

$$
\begin{aligned}
\overbrace{\begin{bmatrix} u_{k\cdot s+\nu-T_E+2+\delta_3} \\ \vdots \\ u_{(k+1)\cdot s+\delta_3} \end{bmatrix}}^{\mathbf{u}} &= \left[\begin{array}{c|c|c} \mathbf{O}_{(5)} & \mathbf{I} & \mathbf{O}_{(6)} \end{array}\right] \cdot \hat{\mathbf{P}} \cdot \hat{\mathcal{I}}_N \cdot \hat{\mathbf{u}} \\
&= \mathbf{H}_r \cdot \hat{\mathbf{u}}
\end{aligned} \tag{2.18}
$$

with T_E the length of the echo cancellation filter, $\mathbf{O}_{(5)}$ and $\mathbf{O}_{(6)}$ zero matrices of size $(N+T_E-1) \times (N+\nu-T_E+1+\nu+\delta_3)$ and $(N+T_E-1) \times (N+\nu-\delta_3)$ respectively. There are three delays in the data model: δ_1 for the far end signal, δ_2 for the echo signal and δ_3 for the echo reference signal. δ_2 and δ_3 are related to each other.

2.2.3 Two-fold oversampled receiver

In the case of a two-fold oversampled receiver (receiver sampling rate $2F_s$), one has a vector $\mathbf{y}$ consisting of so-called even (e) and odd (o) samples, *i.e.* there are now $2N$ samples per symbol.

$$
\begin{aligned}
\overbrace{\begin{bmatrix} y_{k\cdot s+\nu-T+2+\delta_1,e} \\ y_{k\cdot s+\nu-T+2+\delta_1,o} \\ \vdots \\ y_{(k+1)\cdot s+\delta_1,e} \\ y_{(k+1)\cdot s+\delta_1,o} \end{bmatrix}}^{\mathbf{y}} = & \left[\begin{array}{c|ccc|c} & \boxed{\begin{matrix}\bar{\mathbf{h}}_e \\ \bar{\mathbf{h}}_o\end{matrix}} & \begin{matrix}0\\0\end{matrix} & \cdots & \\ \mathbf{O}_{(1)} & \ddots & \ddots & & \mathbf{O}_{(2)} \\ & \begin{matrix}0\\0\end{matrix} & \cdots & \boxed{\begin{matrix}\bar{\mathbf{h}}_e \\ \bar{\mathbf{h}}_o\end{matrix}} & \end{array}\right] \cdot \hat{\mathbf{P}} \cdot \hat{\mathcal{I}}_N \cdot \overbrace{\begin{bmatrix} X_{1:N}^{(k-1)} \\ X_{1:N}^{(k)} \\ X_{1:N}^{(k+1)} \end{bmatrix}}^{\hat{\mathbf{x}}} + \\
& \left[\begin{array}{c|ccc|c} & \boxed{\begin{matrix}\bar{\mathbf{h}}_{E,e} \\ \bar{\mathbf{h}}_{E,o}\end{matrix}} & \begin{matrix}0\\0\end{matrix} & \cdots & \\ \mathbf{O}_{(3)} & \ddots & \ddots & & \mathbf{O}_{(4)} \\ & \begin{matrix}0\\0\end{matrix} & \cdots & \boxed{\begin{matrix}\bar{\mathbf{h}}_{E,e} \\ \bar{\mathbf{h}}_{E,o}\end{matrix}} & \end{array}\right] \cdot \hat{\mathbf{P}} \cdot \hat{\mathcal{I}}_N \cdot \overbrace{\begin{bmatrix} U_{1:N}^{(k-1)} \\ U_{1:N}^{(k)} \\ U_{1:N}^{(k+1)} \end{bmatrix}}^{\hat{\mathbf{u}}} + \\
& \overbrace{\begin{bmatrix} n_{k\cdot s+\nu-T+2+\delta_1,e} \\ n_{k\cdot s+\nu-T+2+\delta_1,o} \\ \vdots \\ n_{(k+1)\cdot s+\delta_1,e} \\ n_{(k+1)\cdot s+\delta_1,o} \end{bmatrix}}^{\mathbf{n}}
\end{aligned} \tag{2.19}
$$

The matrices $\mathbf{O}_{(.)}$ now have twice as many rows as compared to equation (2.17). The vector $\mathbf{y}$ can be split into a vector of even samples $\mathbf{y}_e$ and a vector of odd samples $\mathbf{y}_o$, both of which may be specified by means of a formula of the form (2.17). The corresponding impulse responses are $\bar{\mathbf{h}}_e$, $\bar{\mathbf{h}}_{E,e}$ and $\bar{\mathbf{h}}_o$, $\bar{\mathbf{h}}_{E,o}$ and the noise vectors are $\mathbf{n}_e$ and $\mathbf{n}_o$.

It is clear that the models of section 2.2.1 and 2.2.2 are special cases of this model.

2.2.4 Decimated DMT signal

In case of a decimated signal the size of the receiver DFT is κ times smaller than the transmit IDFT.

In downstream, there are around 220 used tones. Adding its hermitian symmetric part, leads to an IDFT with at least size 512, *i.e.* the smallest power of 2 larger than two times 220. With a tone spacing of 4312.5Hz, one frequency domain period of the discrete signal occupies a bandwidth of 2.208MHz. There is only as small frequency gap between the used tones and their complex conjugate tones for the roll-off of low-pass filters. If the frequency gap would be larger, filter orders could be reduced. By increasing the IDFT size to 1024, one basically adds 512 extra zeros between the 220 used tones and their complex conjugate tones, resulting in a larger frequency gap. Adding zeros in frequency domain corresponds to an implicit interpolation per symbol. Similarly, in upstream, there are around 25 tones (with the same tone spacing). Therefore, strictly spoken, an IDFT-DFT pair of size 64 would be sufficient. However, one uses an 128-point FFT. In conclusion, the increase in IDFT-DFT size, and so complexity, is due to facilitate filter design.

The decimated data model then becomes

$$\begin{aligned}\overbrace{\begin{bmatrix} y_{k\cdot\frac{s}{\kappa}+\frac{\nu}{\kappa}-T+2+\delta} \\ \vdots \\ y_{(k+1)\cdot\frac{s}{\kappa}+\delta} \end{bmatrix}}^{\mathbf{y}} &= \left[\begin{array}{c|cccc|c} & \boxed{\bar{\mathbf{h}}} & 0 & \cdots & & \\ & \mathbf{o}_{\kappa\times 1} & \boxed{\bar{\mathbf{h}}} & & & \\ \mathbf{O}_{(1)} & & & \ddots & & \mathbf{O}_{(2)} \\ & 0 & \cdots & & \boxed{\bar{\mathbf{h}}} & \end{array}\right] \cdot \\ & \hat{\mathbf{P}} \cdot \hat{\mathcal{I}}_N \cdot \overbrace{\begin{bmatrix} X_{1:N}^{(k-1)} \\ X_{1:N}^{(k)} \\ X_{1:N}^{(k+1)} \end{bmatrix}}^{\hat{\mathbf{x}}} + \overbrace{\begin{bmatrix} n_{k\cdot\frac{s}{\kappa}+\frac{\nu}{\kappa}-T+2+\delta} \\ \vdots \\ n_{(k+1)\cdot\frac{s}{\kappa}+\delta} \end{bmatrix}}^{\mathbf{n}} \\ &= \mathbf{H}_{\frac{1}{\kappa}} \cdot \hat{\mathbf{x}} + \mathbf{n}\end{aligned} \tag{2.20}$$

The symbol and prefix size (expressed in samples) at the transmitter are respectively N and ν. At the receiver, they are κ times smaller: $\frac{N}{\kappa}$ and $\frac{\nu}{\kappa}$. The channel impulse response is sampled at the highest rate (corresponding to the transmitter) and has length $K+L+1$. The matrix containing the channel impulse response is not Toeplitz anymore because in each row vector $\bar{\mathbf{h}}$ is shifted over κ elements with respect to the previous row. The zero matrices $\mathbf{O}_{(1)}$ and $\mathbf{O}_{(2)}$ have respectively size $(\frac{N}{\kappa}+T-1) \times (N+\nu-(T-1)\kappa-L+\nu+(\kappa-1)+\delta\kappa)$ and $(\frac{N}{\kappa}+T-1) \times (N+\nu-K-\delta\kappa)$. The relative decision delay δ is determined at the receiver, hence at low rate.

2.2.5 Interpolated DMT signal

In case of an interpolated DMT signal the receiver DFT is κ times larger than the transmitter IDFT.

Let us assume a DMT set-up with a downstream IDFT-DFT pair of size 512 and an upstream IDFT-DFT pair of size 128. When describing the echo seen at RT, one has a a transmit 128-point IDFT and a receive 512-point DFT. In this case, an interpolated DMT signal model for echo applies. At CO, one has a decimated DMT signal model for the echo.

The interpolated data model is

$$\begin{aligned}\overbrace{\begin{bmatrix} y_{k\cdot s\cdot\kappa+\nu\cdot\kappa-T+2+\delta} \\ \vdots \\ y_{(k+1)\cdot s\cdot\kappa+\delta}\end{bmatrix}}^{\mathbf{y}} &= \left[\begin{array}{c|ccc|c} \mathbf{O}_{(1)} & \boxed{\bar{\mathbf{h}}} & 0 & \cdots & \mathbf{O}_{(2)} \\ & & \ddots & \ddots & \\ & 0 & \cdots & \boxed{\bar{\mathbf{h}}} & \end{array}\right] \cdot \\ & \hat{\mathbf{P}}^{\text{in}} \cdot \hat{\mathcal{I}}_N \cdot \overbrace{\begin{bmatrix} X_{1:N}^{(k-1)} \\ X_{1:N}^{(k)} \\ X_{1:N}^{(k+1)} \end{bmatrix}}^{\hat{\mathbf{x}}} + \overbrace{\begin{bmatrix} n_{k\cdot s\cdot\kappa+\nu\cdot\kappa-T+2+\delta} \\ \vdots \\ n_{(k+1)\cdot s\cdot\kappa+\delta}\end{bmatrix}}^{\mathbf{n}} \\ &= \mathbf{H}_\kappa \cdot \hat{\mathbf{x}} + \mathbf{n}\end{aligned} \tag{2.21}$$

The symbol and prefix size (expressed in samples) at the transmitter are respectively N and ν. At the receiver, they are κ times larger: κN and $\kappa\nu$. The channel impulse response is sampled at the high rate (corresponding to the receiver) and has length $K+L+1$. Matrix $\hat{\mathbf{P}}^{\text{in}} = \text{diag}(\mathbf{P}^{\text{in}}, \mathbf{P}^{\text{in}}, \mathbf{P}^{\text{in}})$ is a block diagonal matrix that adds the prefices to the symbols and interpolates the data with factor κ, hence $\mathbf{P}^{\text{in}} = \begin{bmatrix}\mathbf{e}_1 & \mathbf{e}_{\kappa+1} & \ldots & \mathbf{e}_{\kappa\cdot s-\kappa+1}\end{bmatrix} \cdot \mathbf{P}$, with $\mathbf{e}_i$ is the ith basis vector of size $\kappa s \times 1$. The zero matrices $\mathbf{O}_{(1)}$ and $\mathbf{O}_{(2)}$ have respectively size $(\kappa N+T-1) \times (\kappa(N+\nu)-T+1-L+\kappa\nu+\delta)$ and $(\kappa N+T-1) \times (\kappa(N+\nu)-K-\delta)$. The relative decision delay δ is determined at the receiver, hence at high rate.

2.2.6 Data model with pulse shaping and windowing

The VDSL data model of the received signal differs from the ADSL model in that an additional cyclic suffix is used and that pulse shaping at the transmitter and windowing at the receiver is applied. The following notation is adopted (see figure 2.9). The symbol size at transmit and receive side are both equal to N. The final cyclic extensions (prefix as well as suffix) have size ν and pulse shaping is determined by β. The total symbol size is $N + 2\nu + \frac{\beta}{2}$. Successive symbols are overlapped in the roll-off interval. Hence, after overlapping, each symbol has $\acute{s} = N + 2\nu$ samples. Windowing at the receiver is determined by μ. The received signal (before windowing) can then be described as follows

$$
\overbrace{\begin{bmatrix} y_{k\cdot\acute{s}+\nu-\frac{\mu}{2}-T+2+\delta_1} \\ \vdots \\ y_{k\cdot\acute{s}+\nu+N+\frac{\mu}{2}+\delta_1} \end{bmatrix}}^{\mathbf{y}} = \left[\begin{array}{c|ccc|c} \mathbf{O}_{(1)} & \boxed{\bar{\mathbf{h}}} & 0 & \cdots & \mathbf{O}_{(2)} \\ & & \ddots & \ddots & \\ & 0 & \cdots & \boxed{\bar{\mathbf{h}}} & \end{array}\right] \cdot \begin{bmatrix} \boxed{\mathbf{I}} & \mathbf{O} & \mathbf{O} \\ \mathbf{O} & \boxed{\mathbf{I}} & \mathbf{O} \\ \mathbf{O} & \mathbf{O} & \boxed{\mathbf{I}} \end{bmatrix} \cdot
$$

$$
\hat{\mathbf{C}} \cdot \hat{\mathcal{I}}_N \cdot \overbrace{\begin{bmatrix} X_{1:N}^{(k-1)} \\ X_{1:N}^{(k)} \\ X_{1:N}^{(k+1)} \end{bmatrix}}^{\hat{\mathbf{x}}} + \overbrace{\begin{bmatrix} n_{k\cdot\acute{s}+\nu-\frac{\mu}{2}-T+2+\delta_1} \\ \vdots \\ n_{k\cdot\acute{s}+\nu+N+\frac{\mu}{2}+\delta_1} \end{bmatrix}}^{\mathbf{n}}
$$

$$
= \mathbf{H} \cdot \hat{\mathbf{x}} + \mathbf{n} \tag{2.22}
$$

with $\hat{\mathbf{C}} = \text{diag}(\mathbf{C}, \mathbf{C}, \mathbf{C})$ where $\mathbf{C} = \left[\begin{array}{cc|c} \mathbf{O} & \mathbf{O} & \mathbf{C}_1 \\ \hline & \mathbf{I}_N & \\ \hline \mathbf{C}_2 & \mathbf{O} & \mathbf{O} \end{array}\right]$ appends the pulse shaped cyclic prefix and suffix. $\mathbf{C}_1$ and $\mathbf{C}_2$ are diagonal matrices of size $\nu + \beta/4$ which contain the pulse shaping coefficients. $\boxed{\mathbf{I}}$ is an identity matrix of size $N + 2\nu + \beta/2$. Corresponding to a $\beta/2$-overlap between successive symbols, there is an overlap of $\beta/2$ rows between successive identity matrices, as indicated in formula (2.22). The zero matrices $\mathbf{O}_{(1)}$ and $\mathbf{O}_{(2)}$ have respectively size $(N+T-1+\mu) \times (N+3\nu-T+1-L+\delta_1-\mu/2+\beta/4)$ and $(N+T-1+\mu) \times (N+3\nu-K-\delta_1-\mu/2+\beta/4)$.

In this data model, one has $N + T - 1 + \mu$ samples per received symbol. The parameter T enables to study the effect of T-taps equalization. The μ extra samples are required for the windowing operation to be applied at the receiver.

An analogous model can be built for the echo signal, and, if an oversampled receiver is applied, for even and odd far end signal and echo signal. The total received signal is then

$$
\overbrace{\begin{bmatrix} y_{k\cdot\acute{s}+\nu-\mu/2-T+2+\delta_1} \\ \vdots \\ y_{k\cdot\acute{s}+\nu+N+\mu/2+\delta_1} \end{bmatrix}}^{\mathbf{y}} = \mathbf{H} \cdot \hat{\mathbf{x}} + \mathbf{H}_E \cdot \hat{\mathbf{u}} + \mathbf{n} \tag{2.23}
$$

The transmitted echo signal, *i.e.* the reference echo signal, is modeled by

$$\overbrace{\begin{bmatrix} u_{k\cdot \acute{s}+\nu-T_E+2+\delta_3} \\ \vdots \\ u_{k\cdot \acute{s}+\nu+N+\delta_3} \end{bmatrix}}^{\mathbf{u}} = \left[\ \mathbf{O}_{(5)} \mid \mathbf{I} \mid \mathbf{O}_{(6)}\ \right] \cdot \begin{bmatrix} \boxed{\mathbf{I}} & \mathbf{O} & \mathbf{O} \\ \mathbf{O} & \boxed{\mathbf{I}} & \mathbf{O} \\ \mathbf{O} & \mathbf{O} & \boxed{\mathbf{I}} \end{bmatrix} \cdot \hat{\mathbf{C}} \cdot \hat{\mathcal{I}_N} \cdot \hat{\mathbf{u}} \qquad (2.24)$$

$$= \mathbf{H}_r \cdot \hat{\mathbf{u}}$$

with the zero matrices $\mathbf{O}_{(5)}$ and $\mathbf{O}_{(6)}$ respectively of size $(N+T_E-1) \times (N+3\nu-T_E+1+\delta_3+\mu/2+\beta/4)$ and $(N+T-1) \times (N+3\nu-\delta_3-\mu/2+\beta/4)$.

2.3 Conclusions

In this chapter, we have reviewed DMT modulation. We have explained concepts such as cyclic prefix, TEQ, FEQ, intersymbol and intercarrier interference.

TEQ design based on MMSE channel shortening is shortly reviewed. This design procedure is generally applied in ADSL but has some important disadvantages. The cost function does not correspond to bit rate optimization and the resulting bit rate is a non-smooth function of the decision delay. The disadvantages of the TEQ are the motivation for the search for new equalization structures, profoundly studied in part I of the thesis.

Bit rate formulas have been given and are further adopted in simulations.

Finally, we have presented data models which will be used throughout this thesis. The first data models are based on a cyclic prefix and are suitable for ADSL. Data models for far end signal with external noise, echo, oversampling, decimation and interpolation are given. Then a VDSL data model with cyclic prefix as well as a cyclic suffix, pulse shaping and windowing is presented.

Part I

Equalization

Chapter 3

Time domain equalization

Equalization is required in a DMT-system to combat intercarrier and intersymbol interference. Basically, the equalization relies on the insertion of a cyclic prefix and a 1-taps frequency domain equalizer per tone. However, when the order of the channel impulse response is larger than the prefix length, interferences arise, as explained in chapter 2. Hence, additional equalization techniques are called for. In this chapter, we discuss time domain equalization to shorten the channel impulse response. This technique is mostly adopted. However, remark that one can also apply equalization in the frequency domain, *e.g.* per tone equalization (see chapter 4), multiple-input/multiple-output and single-input/multiple-output equalization [93].

MMSE channel shortening is a well-known time domain equalizer design approach for DMT. The cost function is quadratic and has a unique global minimum which leads to low-complexity algorithms. To avoid the trivial zero solution, the minimization is subject to a certain constraint. Although this design procedure is very popular, it has some important disadvantages resulting from the fact that MMSE channel shortening is not equivalent with bit rate optimization.

In section 3.1, we give a comprehensive review of MMSE channel shortening subject to a unit norm, a unit tap or a unit energy constraint on the equalizer taps itself or on the so-called target impulse response. We show that there is a connection between the solutions for a unit energy constraint on the received signal of interest, on the total received signal and on both signals simultaneously.

To improve the performance of the MMSE channel shortening, we propose a new algorithm called 'Weighted MMSE', in section 3.2. It differs from previously presented algorithms in that the unused tones are explicitly disregarded in the cost function as well as in the constraint, by introducing weight matrices.

Simulations show that weighted MMSE significantly improves performance in the upstream direction.

The disadvantages of MMSE channel shortening and in a smaller amount of weighted MMSE are formulated in section 3.3. In section 3.4, we review TEQ design based on other cost functions (geometric SNR and shortening SNR). Simulation results are given in section 3.5. Performance of MMSE channel shortening with different constraints and weighted MMSE is shown. Finally, conclusions are drawn in section 3.6.

3.1 MMSE Channel shortening

A DMT system avoids intersymbol and intercarrier interference if a cyclic prefix with sufficient length is added to each transmitted symbol. The prefix length has to be equal to (or longer than) the order of the channel impulse response (CIR) $\mathbf{h}$ and results in an efficiency loss $\mathcal{O}(\mathbf{h})/(N+\mathcal{O}(\mathbf{h}))$ with N the symbol size and $\mathcal{O}(\mathbf{h})$ the order of $\mathbf{h}$. For ADSL, this efficiency loss is unacceptably high.

Therefore, typically a T-taps time domain equalizer (TEQ) $\mathbf{w}$ is introduced before demodulation (*e.g.* in ADSL with $T=32$ in downstream and $T=64$ in upstream) to equalize the CIR to a shorter target impulse response (TIR) such that it 'fits' into a given cyclic prefix length ν. The efficiency loss then decreases to $\nu/(N+\nu)$.

Several algorithms are proposed in literature [4, 5, 6, 7, 26, 27, 28, 75, 80, 84, 122, 123, 125, 135, 136] that search for a TIR with length $\nu+1$ that is closest to the convolution of CIR and TEQ. This basic approach is shown in **Fig. 3.1**. One searches for a TEQ $\mathbf{w}$, a TIR $\mathbf{b}$ and a decision delay δ_{tot} such that the following cost function is minimized

$$J=\mathcal{E}\left\{e_l^2\right\}=\mathcal{E}\left\{\left(\left[x_{l-\delta_{\text{tot}}}\dots x_{l-\nu-\delta_{\text{tot}}}|y_l\dots y_{l-T+1}\right]\cdot\begin{bmatrix}-\mathbf{b}\\ \mathbf{w}\end{bmatrix}\right)^2\right\} \tag{3.1}$$

with $\mathbf{b}=[b_0\dots b_\nu]^{\mathrm{T}}$, $\mathbf{w}=[w_0\dots w_{T-1}]^{\mathrm{T}}$, x_l and y_l transmitted and received signal samples respectively with l the sample index. Remark that δ_{tot} is the 'total' decision delay introduced by the channel and is written as the sum $\delta+\delta_0-1$. The reference delay δ_0 indicates the first sample of the maximal energy interval of length $\nu+1$ in $\mathbf{h}$ and δ denotes here the 'relative' decision delay, see also section 2.2.1. To avoid trivial solutions (*i.e.* zero vectors $\mathbf{w}$ and $\mathbf{b}$), a non-triviality constraint is applied which is a unit norm, unit tap or unit energy constraint on either $\mathbf{w}$ or $\mathbf{b}$.

Cost function (3.1) can be written in several ways. One can consider a "data driven"approach, where one uses knowledge of the data samples x_l and y_l, or

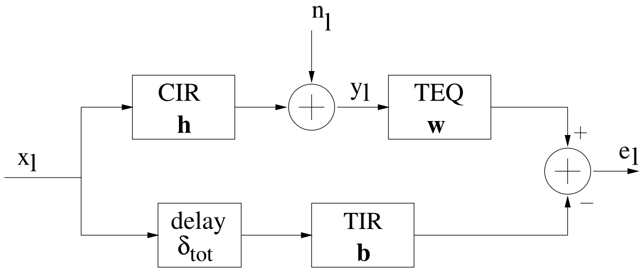

Figure 3.1: TEQ design by MMSE channel shortening

an “impulse response identification based”approach, where one incorporates explicitly the channel $\mathbf{h}$ in the cost function. (When the autocorrelation of y is computed using the identified channel impulse response, both approaches give exactly the same solution.)

In the following sections, MMSE, TEQ and TIR solutions are given for a certain delay δ_{tot}. To find the minimum value for J, the MMSE has to be computed for several delays and the minimum has to be selected.

3.1.1 Data driven computation

By writing the square in equation (3.1) explicitly and taking the expected value of the data, cost function J can be written by means of autocorrelation and crosscorrelation matrices of signals x and y

$$\begin{aligned} J &= \begin{bmatrix} -\mathbf{b}^{\mathrm{T}} & \mathbf{w}^{\mathrm{T}} \end{bmatrix} \cdot \begin{bmatrix} \mathbf{R}_{xx} & \mathbf{R}_{xy} \\ \mathbf{R}_{yx} & \mathbf{R}_{yy} \end{bmatrix} \cdot \begin{bmatrix} -\mathbf{b} \\ \mathbf{w} \end{bmatrix} \\ &= \mathbf{b}^{\mathrm{T}} \cdot \mathbf{R}_{xx} \cdot \mathbf{b} - 2 \cdot \mathbf{w}^{\mathrm{T}} \cdot \mathbf{R}_{yx} \mathbf{b} + \mathbf{w}^{\mathrm{T}} \cdot \mathbf{R}_{yy} \cdot \mathbf{w} \end{aligned} \tag{3.2}$$

subject to a certain non-triviality constraint. We explore unit norm, unit tap and unit energy constraints for the MMSE channel shortening approach. For each constraint, the solution of the minimization problem is given in terms of the correlation matrices.

Remark that, for each constraint, an interpretation of the solution can also be given in terms of the original data matrices of the transmitted signal x_l and the received signal y_l, *i.e.* matrices $\mathbf{X}$ and $\mathbf{Y}$. These data matrices are a $p \times (\nu+1)$ and a $p \times T$ Toeplitz matrix respectively with $p \geq \nu + 1$ and $p \geq T$. The cost function is then rewritten as $J = \|\mathbf{Y}\mathbf{w} - \mathbf{X}\mathbf{b}\|_2^2$. The Least Squares (LS) and the Total Least Squares (TLS) [48] interpretation of a unit tap and a unit norm constraint respectively are given in [39]. Unit energy constraints are related to principal angles between subspaces [48], see below.

Correlation matrices

In our TEQ design simulations, we neglect the prefix structure and assume that all tones are used. Therefore, the transmitted signal x is assumed to be white and $\mathbf{R}_{xx}$ is a diagonal matrix (with on the diagonal psd_x).

These assumptions also imply that $\mathbf{R}_{xx}$, $\mathbf{R}_{yy}$ and $\mathbf{R}_{xy}$ are time invariant.

Remark that matrix $\mathbf{R}_{xy}$ (and $\mathbf{R}_{yx}$) depends on the delay δ_{tot}. This can be seen by writing signal y as the convolution of signal x with the channel impulse response $\mathbf{h}$ plus noise n as in the impulse identification based computation of section 3.1.2. The crosscorrelation matrix $\mathbf{R}_{xy}$ becomes

$$\begin{aligned}
\mathbf{R}_{xy} &= \mathcal{E}\left\{\begin{bmatrix} x_{l-\delta_{\text{tot}}} \\ \vdots \\ x_{l-\nu-\delta_{\text{tot}}} \end{bmatrix} \cdot \begin{bmatrix} y_l \ldots y_{l-T+1} \end{bmatrix}\right\} \\
&= \mathcal{E}\left\{\begin{bmatrix} x_{l-\delta_{\text{tot}}} \\ \vdots \\ x_{l-\nu-\delta_{\text{tot}}} \end{bmatrix} \cdot \begin{bmatrix} x_l \ldots x_{l-\theta-T+2} | n_l \ldots n_{l-T+1} \end{bmatrix} \cdot \begin{bmatrix} \mathbf{H} \\ \hline \mathbf{I}_T \end{bmatrix}\right\}
\end{aligned} \tag{3.3}$$

with $\theta = \text{length}(\mathbf{h})$ and $\mathbf{H}$ an $(\theta + T - 1) \times T$ Toeplitz matrix formed with the impulse response $\mathbf{h}$

$$\mathbf{H} = \begin{bmatrix} \boxed{\quad\mathbf{h}\quad} & 0 & \cdots & 0 \\ 0 & \boxed{\quad\mathbf{h}\quad} & 0 & \cdots \\ \vdots & \ddots & \ddots & \ddots & \vdots \\ 0 & \cdots & 0 & \boxed{\quad\mathbf{h}\quad} \end{bmatrix}^{\mathrm{T}} \tag{3.4}$$

From the second line of formula (3.3) it is clear that the expected value of the multiplication of the first vector with the second vector, results in a delay dependent matrix. Furthermore, assuming that the transmitted signal x is independent of the noise n, one can write

$$\mathbf{R}_{xy} = \begin{bmatrix} \mathbf{O}_{(\nu+1)\times\delta_{\text{tot}}} \ \mathbf{R}_{xx} \ \mathbf{O} \mid \mathbf{O} \end{bmatrix} \cdot \begin{bmatrix} \mathbf{H} \\ \hline \mathbf{I}_T \end{bmatrix} \tag{3.5}$$

Unit norm constraint

When subjected to a unit norm constraint, the minimization comes down to an eigenvalue problem, as described in [4, 7, 44, 122, 123].

For the norm on $\mathbf{b}$, one has

$$\boxed{\min_{\mathbf{w},\mathbf{b}} J \ \text{ such that } \ \|\mathbf{b}\|_2^2 = 1} \tag{3.6}$$

For a given delay δ_{tot}, the optimal $\mathbf{w}$, for a given $\mathbf{b}$, can be found by $\partial J/\partial \mathbf{w} = 0$

$$\mathbf{w} = \mathbf{R}_{yy}^{-1} \cdot \mathbf{R}_{yx} \cdot \mathbf{b} \tag{3.7}$$

$\mathbf{w}$ can now be eliminated in equation (3.2), which leads to

$$\min_{\mathbf{b}} J = \min_{\mathbf{b}} \mathbf{b}^{\mathrm{T}} \cdot \mathbf{R}_{x|y} \cdot \mathbf{b} \quad \text{with} \quad \mathbf{R}_{x|y} = \mathbf{R}_{xx} - \mathbf{R}_{xy} \cdot \mathbf{R}_{yy}^{-1} \cdot \mathbf{R}_{yx} \tag{3.8}$$

The minimum[1] is given by the unit norm eigenvector $\mathbf{b}$ corresponding to the smallest eigenvalue of matrix $\mathbf{R}_{x|y}$ and so $\min_{\mathbf{b}} J = \lambda_{\min}$.

Similarly, a unit norm constraint on $\mathbf{w}$ leads to

$$\boxed{\min_{\mathbf{w},\mathbf{b}} J \quad \text{such that} \quad \|\mathbf{w}\|_2^2 = 1} \tag{3.9}$$

The gradient $\partial J/\partial \mathbf{b} = 0$ gives

$$\mathbf{b} = \mathbf{R}_{xx}^{-1} \cdot \mathbf{R}_{xy} \cdot \mathbf{w} \tag{3.10}$$

and substituting this in the cost function J results in

$$\min_{\mathbf{w}} J = \min_{\mathbf{w}} \mathbf{w}^{\mathrm{T}} \cdot \mathbf{R}_{y|x} \cdot \mathbf{w} \quad \text{with} \quad \mathbf{R}_{y|x} = \mathbf{R}_{yy} - \mathbf{R}_{yx} \cdot \mathbf{R}_{xx}^{-1} \cdot \mathbf{R}_{xy} \tag{3.11}$$

The optimal $\mathbf{w}$ is then the eigenvector corresponding to the minimum eigenvalue of matrix $\mathbf{R}_{y|x}$.

As in [135], one can also apply a unit norm constraint on the vector containing TIR and TEQ, $[-\mathbf{b}^{\mathrm{T}}\mathbf{w}^{\mathrm{T}}]^{\mathrm{T}}$, resulting in

$$\boxed{\min_{\mathbf{w},\mathbf{b}} J \quad \text{such that} \quad \|\mathbf{b}\|_2^2 + \|\mathbf{w}\|_2^2 = 1} \tag{3.12}$$

From the corresponding Lagrangean, it is seen that the minimum is given by the unit norm eigenvector corresponding to the smallest eigenvalue of the following eigenvalue problem

$$\begin{bmatrix} \mathbf{R}_{xx} & \mathbf{R}_{xy} \\ \mathbf{R}_{yx} & \mathbf{R}_{yy} \end{bmatrix} \cdot \begin{bmatrix} -\mathbf{b} \\ \mathbf{w} \end{bmatrix} = \begin{bmatrix} -\mathbf{b} \\ \mathbf{w} \end{bmatrix} \cdot \lambda \tag{3.13}$$

[1] The solution is equal to the minimum of the corresponding Lagrangean $\mathcal{L} = J + \lambda(1 - \mathbf{b}^{\mathrm{T}}\mathbf{b})$ with λ a Lagrange multiplier. The minimum is given by putting the gradients $\partial\mathcal{L}/\partial\mathbf{w}$, $\partial\mathcal{L}/\partial\mathbf{b}$ and $\partial\mathcal{L}/\partial\lambda$ to zero.

Unit tap constraint

Alternatively, a unit tap constraint may be imposed on the TEQ or the TIR, see [4, 7, 26, 75, 76, 80, 136], which results in a least squares problem. When the kth tap of the TIR is constrained to 1, the optimization problem becomes

$$\boxed{\min_{\mathbf{w},\mathbf{b}} J \quad \text{such that} \quad \mathbf{e}_k^{\mathrm{T}}\mathbf{b} = 1} \tag{3.14}$$

with $\mathbf{e}_k$ the kth basis vector of size $\nu + 1$. The solution is given by[2]

$$\mathbf{w} = \mathbf{R}_{yy}^{-1} \cdot \mathbf{R}_{yx} \cdot \mathbf{b} \tag{3.15}$$

$$\mathbf{b} = \frac{\mathbf{R}_{x|y}^{-1} \cdot \mathbf{e}_k}{\mathbf{e}_k^{\mathrm{T}} \cdot \mathbf{R}_{x|y}^{-1} \cdot \mathbf{e}_k} \tag{3.16}$$

The optimal $\mathbf{b}$ and $\mathbf{w}$ are found by minimizing the cost function for all possible k $(1 \leq k \leq \nu + 1)$.

Similarly, an unit tap constraint on the TEQ leads to

$$\boxed{\min_{\mathbf{w},\mathbf{b}} J \quad \text{such that} \quad \mathbf{e}_k^{\mathrm{T}}\mathbf{w} = 1} \tag{3.17}$$

with $\mathbf{e}_k$ the kth basisvector of size T. The solution is given by

$$\mathbf{b} = \mathbf{R}_{xx}^{-1} \cdot \mathbf{R}_{xy} \cdot \mathbf{w} \tag{3.18}$$

$$\mathbf{w} = \frac{\mathbf{R}_{y|x}^{-1} \cdot \mathbf{e}_k}{\mathbf{e}_k^{\mathrm{T}} \cdot \mathbf{R}_{y|x}^{-1} \cdot \mathbf{e}_k} \tag{3.19}$$

for every k $(1 \leq k \leq T)$.

In [75], it is stated that this method involves intensive computation and that, if LMS is applied as in [27], a significant number of iterations is required. Therefore, a fast algorithm (with monic constraint on $\mathbf{b}$) is developed in [75, 76]. It is based on the approximation of a Toeplitz correlation matrix by a circulant matrix and has near-optimal performance. Also in [80], a cost-effective algorithm for channel shortening with monic constraint on $\mathbf{b}$ is developed, called two-channel autoregressive modeling.

Al-Dhahir *et al* [4, 7] have shown that a unit norm constraint results in a lower MMSE than a unit tap constraint. It is also noted that the index k of the unit tap has no crucial influence on the MMSE, but that the effect of the delay parameter is significant.

[2]This can again be found by putting the three gradients of the Lagrangean $\mathcal{L} = J + \lambda(1 - \mathbf{e}_k^{\mathrm{T}}\mathbf{b})$ to zero.

Unit energy constraint

The unit norm constraint may be modified by applying weighting to result in a constraint of the type $\mathbf{b}^{\mathrm{T}}\mathbf{W}\mathbf{b} = 1$ [4, 7]. Minimization of the quadratic cost function J in formula (3.2) combined with this unit energy constraint comes down to a generalized eigenvalue problem.

Two unit energy constraints are of particular interest: a unit energy constraint on the received signal of interest, $\mathbf{b}^{\mathrm{T}}\mathbf{R}_{xx}\mathbf{b} = 1$, and a unit energy constraint on the total received signal, $\mathbf{w}^{\mathrm{T}}\mathbf{R}_{yy}\mathbf{w} = 1$.

Let us first apply both unit energy constraints simultaneously. The minimization problem then becomes

$$\boxed{\min_{\mathbf{w},\mathbf{b}} J \quad \text{such that} \quad \mathbf{b}^{\mathrm{T}}\mathbf{R}_{xx}\mathbf{b} = 1 \quad \text{and} \quad \mathbf{w}^{\mathrm{T}}\mathbf{R}_{yy}\mathbf{w} = 1} \tag{3.20}$$

Hence, the Lagrangean is

$$\mathcal{L}(\mathbf{w}, \mathbf{b}, \lambda', \lambda'') = J + \lambda'(1 - \mathbf{b}^{\mathrm{T}}\mathbf{R}_{xx}\mathbf{b}) + \lambda''(1 - \mathbf{w}^{\mathrm{T}}\mathbf{R}_{yy}\mathbf{w}) \tag{3.21}$$

and the minimum corresponds to its four gradients equal to zero. This leads to

$$\mathbf{w}^{\mathrm{T}}\mathbf{R}_{yx}\mathbf{b} = 1 - \lambda' = 1 - \lambda'' = 1 - \lambda \tag{3.22}$$

$$\begin{bmatrix} \mathbf{O} & \mathbf{R}_{yx} \\ \mathbf{R}_{xy} & \mathbf{O} \end{bmatrix} \cdot \begin{bmatrix} \mathbf{w} \\ \mathbf{b} \end{bmatrix} = \begin{bmatrix} \mathbf{R}_{yy} & \mathbf{O} \\ \mathbf{O} & \mathbf{R}_{xx} \end{bmatrix} \cdot \begin{bmatrix} \mathbf{w} \\ \mathbf{b} \end{bmatrix} \cdot (1 - \lambda) \tag{3.23}$$

and the minimum of the cost function becomes

$$\min_{\mathbf{w},\mathbf{b}} J = 2 - 2(1 - \lambda) \tag{3.24}$$

Hence, the TEQ $\mathbf{w}$ and the TIR $\mathbf{b}$ are the solution of the generalized eigenvalue problem (3.23), corresponding to the maximal eigenvalue $(1-\lambda)_{max}$. Moreover, the eigenvalues of this problem, $(1 - \lambda)$, are the cosines of the principal angles between the spaces[3] spanned by the received signal y and the transmitted signal x.

In appendix 3.A, it is shown that the largest eigenvalue of the generalized eigenvalue problem (3.23) is equal to the largest singular value of matrix $\mathbf{A} = (\mathbf{R}_{yy}^{-1/2})^T \cdot \mathbf{R}_{yx} \cdot \mathbf{R}_{xx}^{-1/2}$, *hence* $(1 - \lambda)_{max} = \cos\theta_1 = \sigma_1$, *with matrix* $\mathbf{R}^{1/2}$ *the Cholesky factor [48] of matrix* $\mathbf{R}$ *and with* θ_1 *the smallest principal angle.*

[3] More specifically, formulating the cost function and the constraints by means of the data matrices $\mathbf{Y}$ and $\mathbf{X}$ themselves, *i.e.* $J = \|\mathbf{Y}\mathbf{w} - \mathbf{X}\mathbf{b}\|_2^2$ such that $\mathbf{b}^{\mathrm{T}}\mathbf{X}^{\mathrm{T}}\mathbf{X}\mathbf{b} = 1$ and $\mathbf{w}^{\mathrm{T}}\mathbf{Y}^{\mathrm{T}}\mathbf{Y}\mathbf{w} = 1$, the eigenvalues are the cosines of the principal angles between the column spaces of the data matrices $\mathbf{Y}$ and $\mathbf{X}$, *i.e.* $\mathbf{w}^{\mathrm{T}}\mathbf{Y}^{\mathrm{T}}\mathbf{X}\mathbf{b} = 1 - \lambda = \cos\theta$, which is similar to formula (3.22).

Let us now consider the first constraint only. The minimization problem becomes[4]

$$\boxed{\min_{\mathbf{w},\mathbf{b}} J \quad \text{such that} \quad \mathbf{b}^{\mathrm{T}}\mathbf{R}_{xx}\mathbf{b} = 1} \tag{3.25}$$

Putting the gradient $\partial J/\partial \mathbf{w}$ to zero leads to formula (3.7) and substituting this in cost function J leads to formula (3.8) but now constrained to $\mathbf{b}^{\mathrm{T}}\mathbf{R}_{xx}\mathbf{b} = 1$. With $\mathbf{R}_{xx}^{1/2}$ the Cholesky factor of $\mathbf{R}_{xx}$, we define $\mathbf{c} = \mathbf{R}_{xx}^{1/2}\mathbf{b}$. The minimum is then given by

$$\mathbf{w} = \mathbf{R}_{yy}^{-1} \cdot \mathbf{R}_{yx} \cdot \mathbf{b} \tag{3.26}$$

$$\mathbf{b} = \mathbf{R}_{xx}^{-1/2} \cdot \mathbf{c} \tag{3.27}$$

$$\min_{\mathbf{c}} J = \min_{\mathbf{c}} \mathbf{c}^{\mathrm{T}} \cdot (\mathbf{R}_{xx}^{-1/2})^{\mathrm{T}} \cdot \mathbf{R}_{x|y} \cdot \mathbf{R}_{xx}^{-1/2} \cdot \mathbf{c} \quad \text{such that} \quad \|\mathbf{c}\|_2^2 = 1 \tag{3.28}$$

Hence, the minimum is given by the unit norm eigenvector $\mathbf{c}$ corresponding to the smallest eigenvalue of $(\mathbf{R}_{xx}^{-1/2})^{\mathrm{T}} \cdot \mathbf{R}_{x|y} \cdot \mathbf{R}_{xx}^{-1/2}$. Remark that if the transmitted signal x is assumed to be white, this solution is the same as for the unit norm constraint on $\mathbf{b}$ (note however, that in an FDD set-up, the transmitted signal is certainly non-white.)

Similarly, one can apply $\mathbf{w}^{\mathrm{T}}\mathbf{R}_{yy}\mathbf{w} = 1$ and define $\mathbf{R}_{yy}^{1/2}$ as the Cholesky factor of $\mathbf{R}_{yy}$.

$$\boxed{\min_{\mathbf{w},\mathbf{b}} J \quad \text{such that} \quad \mathbf{w}^{\mathrm{T}}\mathbf{R}_{yy}\mathbf{w} = 1} \tag{3.29}$$

The gradient $\partial J/\partial \mathbf{b} = 0$ and the resulting cost function are given by formulas (3.10) and (3.11). With $\mathbf{d} = \mathbf{R}_{yy}^{1/2}\mathbf{w}$, the minimum is given by

$$\mathbf{b} = \mathbf{R}_{xx}^{-1} \cdot \mathbf{R}_{xy} \cdot \mathbf{w} \tag{3.30}$$

$$\mathbf{w} = \mathbf{R}_{yy}^{-1/2} \cdot \mathbf{d} \tag{3.31}$$

$$\min_{\mathbf{d}} J = \min_{\mathbf{d}} \mathbf{d}^{\mathrm{T}} \cdot (\mathbf{R}_{yy}^{-1/2})^{\mathrm{T}} \cdot \mathbf{R}_{y|x} \cdot \mathbf{R}_{yy}^{-1/2} \cdot \mathbf{d} \quad \text{such that} \quad \|\mathbf{d}\|_2^2 = 1 \tag{3.32}$$

with $\mathbf{d}$ the unit norm eigenvector corresponding to the smallest eigenvalue of $(\mathbf{R}_{yy}^{-1/2})^{\mathrm{T}} \cdot \mathbf{R}_{y|x} \cdot \mathbf{R}_{yy}^{-1/2}$.

In appendix 3.A, it is proven that the solutions for both unit energy constraints simultaneously, the first constraint only and the second constraint only are related. The respective TEQs $\mathbf{w}_0$, $\mathbf{w}_1$ and $\mathbf{w}_2$ are dominant eigenvectors of matrix $\mathbf{B} = \mathbf{R}_{yy}^{-1}\mathbf{R}_{yx}\mathbf{R}_{xx}^{-1}\mathbf{R}_{xy}$. Simulations have shown that the largest eigenvalue appears only once as eigenvalue of $\mathbf{B}$ (algebraic multiplicity is 1, although the

[4]Hence, the Lagrangean is $\mathcal{L} = J + \lambda(1 - \mathbf{b}^{\mathrm{T}}\mathbf{R}_{xx}\mathbf{b})$ and its minimum corresponds to the three gradients equal to zero.

	both constraints	$\mathbf{b}^{\mathrm{T}}\mathbf{R}_{xx}\mathbf{b} = 1$	$\mathbf{w}^{\mathrm{T}}\mathbf{R}_{yy}\mathbf{w} = 1$
TEQ	$\mathbf{w}_0 = \mathbf{R}_{yy}^{-1/2} \cdot \mathbf{U}(:,1)$	$\mathbf{w}_1 = \sigma_1 \cdot \mathbf{w}_0$	$\mathbf{w}_2 = \mathbf{w}_0$
TIR	$\mathbf{b}_0 = \mathbf{R}_{xx}^{-1/2} \cdot \mathbf{V}(:,1)$	$\mathbf{b}_1 = \mathbf{b}_0$	$\mathbf{b}_2 = \sigma_1 \cdot \mathbf{b}_0$
cost function	$J = 2(1 - \sigma_1)$	$J = 1 - \sigma_1^2$	$J = 1 - \sigma_1^2$

Table 3.1: Solutions for TEQ, TIR and cost function when both unit energy constraints are applied simultaneously and when only one unit energy constraint is applied. The symbols σ_1, $\mathbf{U}(:,1)$ and $\mathbf{V}(:,1)$ are the largest singular value and the first left and right singular vector respectively of matrix $\mathbf{A} = (\mathbf{R}_{yy}^{-1/2})^{\mathrm{T}} \cdot \mathbf{R}_{yx} \cdot \mathbf{R}_{xx}^{-1/2}$.

next eigenvalue is close to the largest). Therefore, *the TEQs* $\mathbf{w}_0$*,* $\mathbf{w}_1$ *and* $\mathbf{w}_2$ *are parallel* and hence, result in the same bit rate. A similar conclusion holds for the TIRs. An overview of the solutions for TEQ, TIR and cost function is given in **Table 3.1**.

These results can geometrically be interpreted by means of the data matrices $\mathbf{Y}$ and $\mathbf{X}$ as follows. The three optimization problems find a TEQ and a TIR corresponding to the smallest principal angle between the column spaces of $\mathbf{Y}$ and $\mathbf{X}$, *i.e.* the maximal cosine of the principal angles, $\cos\theta_1 = \sigma_1$. When both unit energy constraints are applied simultaneously, the vectors $\mathbf{Yw}$ and $\mathbf{Xb}$ have both unit norm and the squared distance between these vectors is given by $J = 2(1 - \cos\theta_1)$. When only one constraint is applied, *e.g.* $\|\mathbf{Xb}\|_2^2 = 1$, vector $\mathbf{Xb}$ has unit norm. It can be shown that vector $\mathbf{Yw}$ is then the orthogonal projection of vector $\mathbf{Xb}$ in the column space of $\mathbf{Y}$. Hence, the norm of vector $\mathbf{Yw}$ is $\|\mathbf{Yw}\|_2^2 = \cos^2\theta_1$ and the squared distance is given by $J = 1 - \cos^2\theta_1 = \sin^2\theta_1$. A similar conclusion holds for the constraint $\|\mathbf{Yw}\|_2^2 = 1$.

3.1.2 Impulse response identification based computation

TEQ design algorithms based on impulse response identification are given for unit norm, unit tap and unit energy constraints. These algorithms are used for TEQ simulations in section 3.5.

Unit norm constraint

One can write the received samples y_l in equation (3.1) as the convolution of the transmitted samples x_l with $\mathbf{h}$ plus additive channel noise n_l. The cost function J, subject to a unit norm constraint on the TIR $\mathbf{b}$, then becomes

$$
\begin{aligned}
J &= \mathcal{E}\left\{ \left(\left[y_{l:-1:l-T+1} | x_{l-\delta_{\text{tot}}:-1:l-\nu-\delta_{\text{tot}}} \right] \cdot \begin{bmatrix} \mathbf{w} \\ -\mathbf{b} \end{bmatrix} \right)^2 \right\} \\
&= \mathcal{E}\left\{ \left(\left[x_{l:-1:l-\theta-T+2} | n_{l:-1:l-T+1} \right] \cdot \left[\begin{array}{c|c} \mathbf{H} & \begin{array}{c} \mathbf{O}_{\delta_{\text{tot}}\times(\nu+1)} \\ \hline \mathbf{I}_{\nu+1} \\ \hline \mathbf{O} \end{array} \\ \hline \mathbf{I}_T & \mathbf{O} \end{array} \right] \cdot \begin{bmatrix} \mathbf{w} \\ -\mathbf{b} \end{bmatrix} \right)^2 \right\}
\end{aligned} \tag{3.33}
$$

where the subscript of y, and similarly the subscripts of x and n, are Matlab notation and defined as in $[y_{l:-1:l-T+1}] = [y_l\, y_{l-1} \ldots y_{l-T+1}]$. $\mathbf{H}$ is a Toeplitz matrix with the impulse response $\mathbf{h}$, given in formula (3.4). Writing the square of the error explicitly and taking the expected value of the data matrices, J can finally be written as

$$
J = \left\| \underbrace{\begin{bmatrix} \underline{\mathbf{R}}_{xx}^{1/2} & \mathbf{O} \\ \mathbf{O} & \mathbf{R}_{nn}^{1/2} \end{bmatrix} \cdot \left[\begin{array}{c|c} \mathbf{H} & \begin{array}{c} \mathbf{O}_{\delta_{\text{tot}}\times(\nu+1)} \\ \hline \mathbf{I}_{\nu+1} \\ \hline \mathbf{O} \end{array} \\ \hline \mathbf{I}_T & \mathbf{O} \end{array} \right]}_{\mathbf{A}} \cdot \begin{bmatrix} \mathbf{w} \\ -\mathbf{b} \end{bmatrix} \right\|_2^2 \quad \text{such that} \quad \|\mathbf{b}\|_2^2 = 1 \tag{3.34}
$$

where $\mathbf{R}^{1/2}$ means the Cholesky factor of $\mathbf{R}$, and $\underline{\mathbf{R}}_{xx}$ is a $(\theta+T-1)\times(\theta+T-1)$ correlation matrix of the transmitted signal x.

With the unit norm constraint on $\mathbf{b}$, the minimum of J is given by

$$
\begin{aligned}
[\mathbf{Q}, \mathbf{R}] &= \text{qr}(\mathbf{A}) \\
[\mathbf{U}, \mathbf{S}, \mathbf{V}] &= \text{svd}(\mathbf{R}(T+1:T+\nu+1, T+1:T+\nu+1)) \\
\mathbf{b}_{opt} &= \mathbf{V}(:, \nu+1) \\
\mathbf{w}_{opt} &= \mathbf{R}(1:T, 1:T)^{-1} \cdot \mathbf{R}(1:T, T+1:T+\nu+1) \cdot \mathbf{b}_{opt}
\end{aligned} \tag{3.35}
$$

where we adopted a Matlab notation: function 'qr' computes the QR decomposition [48], function 'svd' computes the singular value decomposition [48], $\mathbf{R}(a:b, c:d)$ equals the submatrix of $\mathbf{R}$ containing rows a up to b and columns c up to d and $\mathbf{R}(:, c:d)$ equals the submatrix of $\mathbf{R}$ containing all rows of $\mathbf{R}$ and columns c up to d.

Similarly, when constraining the norm on $\mathbf{w}$ to one, the cost function J becomes

$$
J = \left\| \begin{bmatrix} \underline{\mathbf{R}}_{xx}^{1/2} & \mathbf{O} \\ \mathbf{O} & \mathbf{R}_{nn}^{1/2} \end{bmatrix} \cdot \left[\begin{array}{c|c} \begin{array}{c} \mathbf{O}_{\delta_{tot}\times(\nu+1)} \\ \hline \mathbf{I}_{\nu+1} \\ \hline \mathbf{O} \end{array} & \mathbf{H} \\ \hline \mathbf{O} & \mathbf{I}_T \end{array} \right] \cdot \begin{bmatrix} -\mathbf{b} \\ \mathbf{w} \end{bmatrix} \right\|_2^2 \quad \text{such that} \quad \|\mathbf{w}\|_2^2 = 1 \tag{3.36}
$$

and the optimal $\mathbf{w}$ and $\mathbf{b}$ are given by

$$\begin{aligned}
[\mathbf{U},\mathbf{S},\mathbf{V}] &= \mathrm{svd}\left(\begin{bmatrix}\mathbf{H}(1:\delta_{\mathrm{tot}},:)\\ \mathbf{H}(\delta_{\mathrm{tot}}+\nu+2:\theta+T-1,:)\\ \mathbf{R}_{nn}^{1/2}/\mathrm{psd}_x^{1/2}\end{bmatrix}\right)\\
\mathbf{w}_{opt} &= \mathbf{V}(:,T)\\
\mathbf{b}_{opt} &= \mathbf{H}(\delta_{\mathrm{tot}}+1:\delta_{\mathrm{tot}}+\nu+1,:)\cdot\mathbf{w}_{opt}
\end{aligned}\tag{3.37}$$

When constraining the sum of the norm on $\mathbf{b}$ and the norm on $\mathbf{w}$ to one, one minimizes

$$J = \left\| \underbrace{\begin{bmatrix}\underline{\mathbf{R}}_{xx}^{1/2} & \mathbf{O}\\ \mathbf{O} & \mathbf{R}_{nn}^{1/2}\end{bmatrix}\cdot\left[\begin{array}{c|c}\mathbf{O}_{\delta_{tot}\times(\nu+1)} & \\ \hline \mathbf{I}_{\nu+1} & \mathbf{H}\\ \hline \mathbf{O} & \\ \hline \mathbf{O} & \mathbf{I}_T\end{array}\right]}_{\mathbf{A}}\cdot\begin{bmatrix}-\mathbf{b}\\ \mathbf{w}\end{bmatrix}\right\|_2^2$$

$$\text{such that}\quad \|\mathbf{b}\|_2^2+\|\mathbf{w}\|_2^2=1 \tag{3.38}$$

and the minimum is given by

$$\begin{aligned}
[\mathbf{Q},\mathbf{R}] &= \mathrm{qr}(\mathbf{A})\\
[\mathbf{U},\mathbf{S},\mathbf{V}] &= \mathrm{svd}(\mathbf{R})\\
\mathbf{b}_{opt} &= -\mathbf{V}(1:\nu+1,\nu+T+1)\\
\mathbf{w}_{opt} &= \mathbf{V}(\nu+2:\nu+T+1,\nu+T+1)
\end{aligned}\tag{3.39}$$

Unit tap constraint

Applying a unit tap constraint leads to the following least squares problem

$$J = \left\| \begin{bmatrix}\underline{\mathbf{R}}_{xx}^{1/2} & \mathbf{O}\\ \mathbf{O} & \mathbf{R}_{nn}^{1/2}\end{bmatrix}\cdot\left[\begin{array}{c|c} & \mathbf{O}_{\delta_{\mathrm{tot}}\times(\nu+1)}\\ \hline \mathbf{H} & \mathbf{I}_{\nu+1}\\ \hline & \mathbf{O}\\ \hline \mathbf{I}_T & \mathbf{O}\end{array}\right]\cdot\begin{bmatrix}\mathbf{w}\\ -\mathbf{b}\end{bmatrix}\right\|_2^2$$

$$\text{such that}\quad \begin{cases} b_k = 1 \quad (1\le k\le \nu+1)\\ \text{or}\\ w_k=1 \quad (1\le k\le T)\end{cases} \tag{3.40}$$

Unit energy constraint

Optimizing J subject to a unit energy constraint on the received signal of interest, $\mathbf{b}^{\mathrm{T}}\mathbf{R}_{xx}\mathbf{b} = 1$, leads to the minimization of J with

$$J = \left\| \begin{bmatrix} \underline{\mathbf{R}}_{xx}^{1/2} & \mathbf{O} \\ \mathbf{O} & \mathbf{R}_{nn}^{1/2} \end{bmatrix} \cdot \left[\begin{array}{c|c} & \mathbf{O}_{\delta_{\mathrm{tot}}\times(\nu+1)} \\ \cline{2-2} \mathbf{H} & \mathbf{I}_{\nu+1} \\ \cline{2-2} & \mathbf{O} \\ \hline \mathbf{I}_T & \mathbf{O} \end{array}\right] \cdot \begin{bmatrix} \mathbf{w} \\ -\mathbf{b} \end{bmatrix} \right\|_2^2 \quad \text{such that} \quad \mathbf{b}^{\mathrm{T}}\mathbf{R}_{xx}\mathbf{b} = 1 \tag{3.41}$$

By applying Cholesky factorization, we define $\mathbf{c} = \mathbf{R}_{xx}^{1/2}\mathbf{b}$ and the cost function becomes

$$J = \left\| \begin{bmatrix} \underline{\mathbf{R}}_{xx}^{1/2} & \mathbf{O} \\ \mathbf{O} & \mathbf{R}_{nn}^{1/2} \end{bmatrix} \cdot \left[\begin{array}{c|c} & \mathbf{O}_{\delta_{\mathrm{tot}}\times(\nu+1)} \\ \cline{2-2} \mathbf{H} & \mathbf{I}_{\nu+1} \\ \cline{2-2} & \mathbf{O} \\ \hline \mathbf{I}_T & \mathbf{O} \end{array}\right] \cdot \begin{bmatrix} \mathbf{I}_T & \mathbf{O} \\ \mathbf{O} & \mathbf{R}_{xx}^{-1/2} \end{bmatrix} \cdot \begin{bmatrix} \mathbf{w} \\ -\mathbf{c} \end{bmatrix} \right\|_2^2$$

$$\text{such that} \quad ||\mathbf{c}||_2^2 = 1 \tag{3.42}$$

which may be solved analogously to formula (3.35).

The optimization subject to a unit energy constraint on the total received signal, $\mathbf{w}^{\mathrm{T}}\mathbf{R}_{yy}\mathbf{w} = 1$, may be solved in a similar way. However, we know that the resulting TEQ is equal up to a scaling factor and so that equal capacity is achieved when one unit energy constraint is applied or when both unit energy constraints are applied simultaneously.

3.1.3 Frequency domain approach of MMSE cost function

The cost function (3.1) can be written by means of circular convolution if the training sequence x is periodic and if the channel noise in y is averaged out or neglected such that the received signal y is also periodic. After Fourier transforming the error, one obtains for tone i

$$E_i = -B_i \cdot X_i + W_i \cdot Y_i \quad \text{with} \quad i = 1 : \frac{N}{2} + 1 \tag{3.43}$$

The training algorithms for the TEQ, by Chow *et al* [27], minimize the mean square of this frequency domain error for all tones. Adaptation of the TEQ and TIR is done in the frequency domain. After each adaptation step, a windowing is performed in the time domain. Windowing means here searching for T or $\nu+1$ consecutive taps with highest energy in the (IDFT of the frequency domain)

TEQ and TIR respectively. To avoid the trivial solution, the energy in the TIR is constrained.

Wang *et al* [135] consider a cost function which is a weighted sum of the frequency domain error for all tones. The weights are introduced to control the TEQ spectral response. A unit norm on the total parameter vector (containing TEQ and TIR) again results in an eigenvalue problem. It is shown that TEQ solutions corresponding to several smallest eigenvalues can also shorten the CIR. In [136], the authors optimize the same cost function with a unit tap constraint.

3.1.4 Channel shortening with virtual noise

The odd behavior of the channel shortening algorithm applied in an FDM set-up, is described by Van Kerckhove *et al* in [125]. When the TEQ $\mathbf{w}$ is normed to unity, the solution of the algorithm is a TEQ with its energy mainly concentrated in the stop band. In a DMT receiver, the TEQ is followed by an FFT which acts like a filter bank of sinc filters and these have considerable sidelobes. The sidelobes pick up noise in a wide frequency band and adds this noise to the narrow band signal of interest. Hence, stop band noise, enhanced by the TEQ, will leak into the pass band and cause the SNR of the used tones to drop. Therefore it is important to control the TEQ's spectral response.

The concentration of the TEQ energy in the stop band is seen as follows. Let H_i be the channel transfer function on tone i. The transfer function is split in a stop and a pass band section as follows

$$H_{1:\frac{N}{2}+1} = \begin{bmatrix} H^{stop} \\ H^{pass} \end{bmatrix} \approx \begin{bmatrix} \mathbf{0} \\ H^{pass} \end{bmatrix} \tag{3.44}$$

where a high pass downstream channel is assumed. Zero error in equation (3.43) is obtained for

$$B_i \approx W_i \cdot H_i \tag{3.45}$$

Splitting this equation in stop and pass band, one has

$$\begin{bmatrix} B^{stop} \\ B^{pass} \end{bmatrix} \approx \begin{bmatrix} W^{stop} \\ W^{pass} \end{bmatrix} \odot \begin{bmatrix} \mathbf{0} \\ H^{pass} \end{bmatrix} \tag{3.46}$$

with $\odot$ representing a componentwise multiplication. From the first block row of formula (3.46), it follows that $B^{stop} \approx \mathbf{0}$. It is seen that the unit norm constraint on $\mathbf{w}$ or equivalently on $W_{1:N}$, can not avoid a TEQ solution with its main energy concentrated in the stop band and a minor energy in the pass band, so $W^{stop} \neq \mathbf{0}$ and $W^{pass} \approx \mathbf{0}$ and as a result $B \approx \mathbf{0}$ for all tones. This leads to the undesirable behavior where the signal of interest is blocked and the stop band noise is amplified by the TEQ.

Note that for a unit normed B, the TIR B can not be zero for all tones. From the first block row of formula (3.46), it follows that $B^{stop} \approx \mathbf{0}$ and as such $B^{pass} \neq \mathbf{0}$. But from the first block row it also follows that W^{stop} remains unconstrained.

To solve this problem, a modified optimization criterion is proposed in [125], to concentrate the TEQ energy in the pass band. The MSE of equation (3.1) is modified by adding an additional term which enables to shape the TEQ spectral response. The constrained MSE (in the time domain) is

$$J_{constr} = J + \psi \cdot E_{sr} \tag{3.47}$$

with ψ the suppression factor and E_{sr} the energy of the TEQ W over the tones in the suppression region (the tones where one wants to suppress the energy of the TEQ). It is demonstrated in [125] that the extra term is equivalent to the insertion of a virtual (*i.e.* a mathematically injected) noise in the suppression region. The PSD of the virtual noise equals ψ in this region and is zero elsewhere.

3.2 Weighted MMSE

In an attempt to improve the performance of the shortening algorithm, we modify the cost function as well as the constraint. Unlike [125], our algorithm explicitly disregards the unused tones. The non-triviality constraint is imposed only on the used tones such that trivial solutions in the pass band are avoided. This is achieved by introducing weight matrices. The cost function still is quadratic and has a unique global minimum.

Remark that this approach is not equivalent to bit rate optimization as is performed by the geometric TEQ [8] which leads to a nonlinear optimization hence in general without a unique minimum.

3.2.1 Cost function

Our aim is to take into account the DMT nature of the input and output samples in the cost function. However, remark that, for mathematical tractability of the correlation matrices, we will make some assumptions in section 3.2.2, *i.e.* we neglect the prefix structure and assume that all tones are used. In section 3.2.5, we will show how the presented cost function can be modified such that the prefix and used tones are taken into account.

The starting formula contains a set of exactly N equations with N being the symbol size. The shortening error is minimized over the complete symbol length, so the cost function becomes

$$J = \mathcal{E}\left\{\left\| \underbrace{\begin{bmatrix} y_l & y_{l-1} & \cdots & y_{l-T+1} \\ y_{l+1} & y_l & & \vdots \\ \vdots & \ddots & & \\ y_{l+N-1} & \cdots & & y_{l+N-T} \end{bmatrix}}_{\mathbf{Y}} \cdot \mathbf{w} - \right.\right.$$

$$\left.\left. \underbrace{\begin{bmatrix} x_{l-\delta_{\text{tot}}} & x_{l-\delta_{\text{tot}}-1} & \cdots & x_{l-\delta_{\text{tot}}-\nu} \\ x_{l-\delta_{\text{tot}}+1} & x_{l-\delta_{\text{tot}}} & & \vdots \\ \vdots & \ddots & & \\ x_{l-\delta_{\text{tot}}+N-1} & \cdots & & x_{l-\delta_{\text{tot}}+N-1-\nu} \end{bmatrix}}_{\mathbf{X}} \cdot \mathbf{b} \right\|_2^2 \right\} \tag{3.48}$$

It is noted that the data matrices have a Toeplitz structure. This cost function is then modified by minimizing only over the used tones. Therefore the set of equations is transformed to the frequency domain, leading to

$$J = \mathcal{E}\left\{\|\mathbf{S} \cdot \mathcal{F}_N \cdot (\mathbf{Y} \cdot \mathbf{w} - \mathbf{X} \cdot \mathbf{b})\|_2^2\right\} \tag{3.49}$$

$\mathcal{F}_N$ is the N-point DFT-matrix, $\mathbf{S}$ is an $N \times N$ selector matrix, *i.e.* a diagonal matrix with ones on the positions corresponding to the used tones and its complex conjugates, and zeros elsewhere, *i.e.* $\mathbf{S}(i,i) = \mathbf{S}(N-i+2, N-i+2)$, $i = 2 \ldots \frac{N}{2}$. By writing the output samples y_l as a function of x_l and the additive channel noise n_l, as in equation (3.33), one obtains

$$J = \mathcal{E}\left\{\left\| \mathbf{S} \cdot \mathcal{F}_N \cdot \left[\begin{array}{c|c} \mathbf{X}^{ext} & \mathbf{N} \end{array}\right] \cdot \left[\begin{array}{c|c} \mathbf{H} & \begin{array}{c} \mathbf{O}_{\delta_{\text{tot}} \times (\nu+1)} \\ \hline \mathbf{I}_{\nu+1} \\ \hline \mathbf{O} \end{array} \\ \hline \mathbf{I}_T & \mathbf{O} \end{array}\right] \cdot \begin{bmatrix} \mathbf{w} \\ -\mathbf{b} \end{bmatrix} \right\|_2^2 \right\} \tag{3.50}$$

with

$$\mathbf{X}^{ext} = \left[\begin{array}{ccc|c|cc} x_l & \cdots & x_{l-\delta_{\text{tot}}+1} & & \cdots & x_{l-\theta-T+2} \\ \vdots & \ddots & \ddots & \mathbf{X} & \ddots & \\ x_{l+N-1} & \cdots & & & \cdots & \end{array}\right] \tag{3.51}$$

and

$$\mathbf{N} = \begin{bmatrix} n_l & n_{l-1} & \cdots & n_{l-T+1} \\ n_{l+1} & n_l & & \vdots \\ \vdots & \ddots & & \\ n_{l+N-1} & \cdots & & n_{l+N-T} \end{bmatrix} \tag{3.52}$$

$\mathbf{X}^{ext}$ is an $N \times (\theta - 1 + T)$ Toeplitz matrix, and an 'extension' of $\mathbf{X}$. $\mathbf{N}$ is a Toeplitz matrix of noise samples. Modified data matrices with tilde are defined as

$$\begin{aligned}\widetilde{\mathbf{X}} &= \mathbf{S} \cdot \mathcal{F}_N \cdot \mathbf{X} \\ \widetilde{\mathbf{X}}^{ext} &= \mathbf{S} \cdot \mathcal{F}_N \cdot \mathbf{X}^{ext} \\ \widetilde{\mathbf{N}} &= \mathbf{S} \cdot \mathcal{F}_N \cdot \mathbf{N}\end{aligned} \tag{3.53}$$

3.2.2 Correlation matrices

To solve this least squares problem by QR decomposition, the (Cholesky factors of the) correlation matrices of noise and transmitted signal samples are needed. The noise correlation matrix becomes

$$\begin{aligned}\widetilde{\mathbf{R}}_{nn} &= \mathcal{E}\left\{\widetilde{\mathbf{N}}^{\mathrm{H}} \cdot \widetilde{\mathbf{N}}\right\} \\ &= \mathcal{E}\left\{\left(\mathbf{N}^{\mathrm{H}} \cdot \mathcal{F}_N^{\mathrm{H}} \cdot \mathbf{S}^{\mathrm{H}}\right) \cdot \left(\mathbf{S} \cdot \mathcal{F}_N \cdot \mathbf{N}\right)\right\} \\ &= \mathcal{E}\left\{\mathbf{N}^{\mathrm{H}} \cdot \mathcal{F}_N^{\mathrm{H}} \cdot \mathbf{S} \cdot \mathcal{F}_N \cdot \mathbf{N}\right\}\end{aligned} \tag{3.54}$$

The $\mathbf{S}$ matrix selects the appropriate rows and columns in $\mathcal{F}_N$ and $\mathcal{F}_N^{\mathrm{H}}$ respectively. The product $\mathcal{F}_N^{\mathrm{H}} \cdot \mathbf{S} \cdot \mathcal{F}_N$ forms an $N \times N$ real, symmetric circulant weight matrix, see appendix 3.B for a proof. This leads to

$$\widetilde{\mathbf{R}}_{nn} = \mathcal{E}\left\{\mathbf{N}^{\mathrm{H}} \cdot \begin{bmatrix} a & b & c & \dots & c & b \\ b & a & b & \ddots & & \vdots \\ c & b & \ddots & & & \\ \vdots & \ddots & & & & \\ b & c & \dots & & & a \end{bmatrix} \cdot \mathbf{N}\right\} \tag{3.55}$$

with $a, b, c... \in \mathbb{R}$ (an expression for these elements is derived in appendix 3.B). For white additive channel noise, $\widetilde{\mathbf{R}}_{nn}$ reduces to a simple expression, namely

$$\widetilde{\mathbf{R}}_{nn} = \begin{bmatrix} N \cdot a & (N-1) \cdot b & \dots & (N-T+1) \cdot f \\ (N-1) \cdot b & N \cdot a & \ddots & \vdots \\ \vdots & \ddots & & \\ (N-T+1) \cdot f & \dots & & N \cdot a \end{bmatrix} \cdot \mathcal{E}\left\{n_l^2\right\} \tag{3.56}$$

where the elements of the real, symmetric Toeplitz matrix are computed by making the sum of the diagonals of the weight matrix of equation (3.55), see also appendix 3.B.

For mathematical tractability, in calculating $\widetilde{\mathbf{R}}_{xx}^{ext}$, some assumptions are made such that it is formed similar to $\widetilde{\mathbf{R}}_{nn}$. The prefix structure is neglected in $\mathbf{X}^{ext}$ and it is assumed that all tones are used, therefore the input samples x_l can assumed to be white. As already mentioned, the optimization itself is made over the tones that are effectively used. This leads to

$$\begin{aligned}\widetilde{\mathbf{R}}_{xx}^{ext} &\approx \mathcal{E}\left\{\widetilde{\mathbf{X}}^{ext,\mathrm{H}} \cdot \widetilde{\mathbf{X}}^{ext}\right\} \\ &\approx \mathcal{E}\left\{\left(\mathbf{X}^{ext,\mathrm{H}} \cdot \mathcal{F}_N^{\mathrm{H}} \cdot \mathbf{S}^{\mathrm{H}}\right) \cdot \left(\mathbf{S} \cdot \mathcal{F}_N \cdot \mathbf{X}^{ext}\right)\right\} \\ &\approx \mathbf{T} \cdot \mathcal{E}\left\{x_l^2\right\}\end{aligned} \tag{3.57}$$

$\mathbf{T}$ is a real symmetric Toeplitz matrix. It is formed similar to equation (3.56). However its dimension is larger, namely $(\theta - 1 + T) \times (\theta - 1 + T)$, and the $\theta - 1 + T - N$ outer off-diagonals consist of zeros

$$\mathbf{T} = \begin{bmatrix} N \cdot a & (N-1)\cdot b & \dots & b & 0 & \dots & 0 \\ (N-1)\cdot b & \ddots & \ddots & & b & 0 & \vdots \\ \vdots & \ddots & & & & \ddots & \ddots \\ b & & & & & & \\ 0 & b & & & & & \\ \vdots & 0 & \ddots & & \ddots & & \\ 0 & \dots & \ddots & & & & N \cdot a \end{bmatrix} \tag{3.58}$$

3.2.3 Constraint

The non-triviality constraint

$$\mathcal{E}\left\{\left\|\widetilde{\mathbf{X}} \cdot \mathbf{b}\right\|_2^2\right\} = 1 \tag{3.59}$$

is considered. It can be written as

$$\mathcal{E}\left\{\left(\mathbf{b}^{\mathrm{H}} \cdot \mathbf{X}^{\mathrm{H}} \cdot \mathcal{F}_N^{\mathrm{H}} \cdot \mathbf{S}^{\mathrm{H}}\right) \cdot \left(\mathbf{S} \cdot \mathcal{F}_N \cdot \mathbf{X} \cdot \mathbf{b}\right)\right\} = 1 \tag{3.60}$$

In matrix $\mathbf{X}$, we now explicitly take the cyclic prefix into account, because this leads to a simple expression for the constraint. Matrix $\mathbf{X}$ can be circularly extended to an $N \times N$ circulant matrix $\mathbf{X}^{circ}$. Accordingly, vector $\mathbf{b}$ is zero padded. Hence, the constraint becomes

$$\mathcal{E}\left\{\begin{bmatrix}\mathbf{b}^{\mathrm{H}} & \mathbf{0}_{1\times(N-\nu-1)}\end{bmatrix} \cdot \mathbf{X}^{circ,\mathrm{H}} \cdot \mathcal{F}_N^{\mathrm{H}} \cdot \mathbf{S} \cdot \mathcal{F}_N \cdot \mathbf{X}^{circ} \cdot \begin{bmatrix}\mathbf{b} \\ \mathbf{0}_{(N-\nu-1)\times 1}\end{bmatrix}\right\} = 1 \tag{3.61}$$

After insertion of an $\mathcal{I}_N \cdot \mathcal{F}_N$ pair between the circulant matrix and the TIR and applying the eigenvalue decomposition of $\mathbf{X}^{circ}$, one obtains

$$\mathcal{E}\left\{B^{\mathrm{H}} \cdot \mathrm{diag}(X^{\mathrm{H}}) \cdot \mathbf{S} \cdot \mathrm{diag}(X) \cdot B\right\} = 1 \tag{3.62}$$

with $B = \mathcal{F}_N \cdot \begin{bmatrix} \mathbf{b} \\ \mathbf{0} \end{bmatrix}$ and $X = \mathcal{F}_N \cdot \mathbf{X}^{circ}(:,1)$. This means

$$\boxed{\sum\nolimits_{i=used\ tone} |B_i|^2 \cdot \mathcal{E}\left\{|X_i|^2\right\} = 1} \tag{3.63}$$

So, as far as the constraint is concerned, the prefix and the used tones are taken into account. It is further assumed that $\mathcal{E}\left\{|X_i|^2\right\}$ is constant for the used tones. Practically, the constraint is then computed as follows

$$\begin{aligned} B^{\mathrm{H}} \cdot \mathbf{S} \cdot B &= 1/\mathcal{E}\left\{|X_i|^2\right\} \\ \begin{bmatrix} \mathbf{b}^{\mathrm{H}} & \mathbf{0} \end{bmatrix} \cdot \mathcal{F}_N^{\mathrm{H}} \cdot \mathbf{S} \cdot \mathcal{F}_N \cdot \begin{bmatrix} \mathbf{b} \\ \mathbf{0} \end{bmatrix} &= \\ \mathbf{b}^{\mathrm{H}} \cdot \mathbf{R}^{\mathrm{H}} \cdot \mathbf{Q}^{\mathrm{H}} \cdot \mathbf{Q} \cdot \mathbf{R} \cdot \mathbf{b} &= \end{aligned} \tag{3.64}$$

where $\mathbf{Q} \cdot \mathbf{R}$ is the QR factorization of $\mathbf{S} \cdot \mathcal{F}_N(:, 1:\nu+1)$. With $\mathbf{c} = \mathbf{R} \cdot \mathbf{b}$, the cost function to be minimized then becomes

$$J = \left\| \begin{bmatrix} (\widetilde{\mathbf{R}}_{xx}^{ext})^{1/2} & \mathbf{O} \\ \mathbf{O} & (\widetilde{\mathbf{R}}_{nn})^{1/2} \end{bmatrix} \cdot \left[\begin{array}{c|c} & \mathbf{O}_{(\delta_{\mathrm{tot}}-1)\times(\nu+1)} \\ \cline{2-2} \mathbf{H} & \mathbf{I}_{\nu+1} \\ \cline{2-2} & \mathbf{O} \\ \hline \mathbf{I}_T & \mathbf{O} \end{array} \right] \cdot \begin{bmatrix} \mathbf{I}_T & \mathbf{O} \\ \mathbf{O} & \mathbf{R}^{-1} \end{bmatrix} \cdot \begin{bmatrix} \mathbf{w} \\ -\mathbf{c} \end{bmatrix} \right\|_2^2 \tag{3.65}$$

subject to $\mathbf{c}^{\mathrm{H}} \cdot \mathbf{c} = 1/\mathcal{E}\left\{|X_i|^2\right\}$ which is a given constant, say c. This cost function may be solved similar to equation (3.35). The effect of constant c is only a scaling of the unit norm solution for $\mathbf{c}$ by $\sqrt{c}$ and so $\mathbf{b}$ and $\mathbf{w}$ are scaled by the same value. As a scaling of the TEQ $\mathbf{w}$ does not alter the SNR of the tones, and hence the bit rate of the DMT system, the constraint $\mathbf{c}^{\mathrm{H}} \cdot \mathbf{c}$ can arbitrary be set to 1.

3.2.4 Interpretation

This constraint is meaningful because of the following reason. The solution of the constrained MMSE problem is equal to the solution of the unconstrained

MMSE problem

$$\min_{\mathbf{w},\mathbf{b}} \frac{\begin{bmatrix}\mathbf{w}^{\mathrm{H}} & -\mathbf{b}^{\mathrm{H}}\end{bmatrix} \cdot \begin{bmatrix}\widetilde{\mathbf{R}}_{yy} & \widetilde{\mathbf{R}}_{yx} \\ \widetilde{\mathbf{R}}_{xy} & \widetilde{\mathbf{R}}_{xx}\end{bmatrix} \cdot \begin{bmatrix}\mathbf{w} \\ -\mathbf{b}\end{bmatrix}}{\mathbf{b}^{\mathrm{H}} \cdot \widetilde{\mathbf{R}}_{xx} \cdot \mathbf{b}} \tag{3.66}$$

where the matrices $\widetilde{\mathbf{R}}$ are correlations of $\widetilde{\mathbf{Y}} = \mathbf{S} \cdot \mathcal{F}_N \cdot \mathbf{Y}$ and $\widetilde{\mathbf{X}} = \mathbf{S} \cdot \mathcal{F}_N \cdot \mathbf{X}$.

This formula can be seen as a sort of 1/SNR in the subband of the used tones. For every value of subband signal energy in the denominator, the subband MMSE in the numerator is minimized as shown in equation (3.65), with the subband energy taken as the sum of the energies of the used tones. Remark that this optimization criterion does not yet correspond to the ultimate goal, namely SNR optimization for each tone separately (see chapter 4).

Let us now consider the cost function (3.49) for one particular tone i

$$\begin{aligned} J_i &= \mathcal{E}\left\{\left|\mathcal{F}_N(i,:) \cdot (\mathbf{Y} \cdot \mathbf{w} - \mathbf{X} \cdot \mathbf{b})\right|^2\right\} \\ &= \mathcal{E}\left\{\left|\mathcal{F}_N(i,:) \cdot \mathbf{Y} \cdot \mathbf{w} - \mathcal{F}_N(i,:) \cdot \mathbf{X}^{circ} \cdot \mathcal{I}_N \cdot \mathcal{F}_N \cdot \begin{bmatrix}\mathbf{b} \\ \mathbf{0}\end{bmatrix}\right|^2\right\} \\ &= \mathcal{E}\left\{\left|\mathcal{F}_N(i,:) \cdot \mathbf{Y} \cdot \mathbf{w} - X_i \cdot B_i\right|^2\right\} \end{aligned} \tag{3.67}$$

If, in the first row of the preceding formula, the prefix is taken into account in matrix $\mathbf{X}$, this matrix can again be circularly extended to matrix $\mathbf{X}^{circ}$, as seen in the second row. The TIR is zero padded to length N. After insertion of an IDFT-DFT pair between the circulant matrix and the TIR and applying the eigenvalue decomposition of a circulant matrix, one obtains the third row.

We will see in chapter 4 that minimization of the latter formula results in the optimal equalizer for tone i, if B_i is set to 1, if the DMT signal structure is included in matrix $\mathbf{Y}$ and if equalizer $\mathbf{w}$ may be complex and different for every tone. One may compare the latter formula with formula (4.7) in chapter 4. Also note that the minimum of J_i (MMSE) does not exactly correspond to the residual ISI-ICI and external noise for tone i after equalization. This would only be the case if the transfer function from tone i at receiver side to tone i at transmitter side equals exactly B_i.

3.2.5 Inclusion of real DMT signal and noise

The presented algorithm may be modified to include the DMT signal structure and the real noise in matrix $\mathbf{Y}$ as follows. For one tone i, the cost function (3.50) is

$$J_i = \mathcal{E}\left\{\left|\mathcal{F}_N(i,:)\cdot\left[\ \mathbf{X}^{ext}\ \middle|\ \mathbf{N}\ \right]\cdot\underbrace{\left[\begin{array}{c|c} \mathbf{H} & \begin{array}{c}\mathbf{O}_{\delta_{\text{tot}}\times(\nu+1)}\\ \hline \mathbf{I}_{\nu+1}\\ \hline \mathbf{O}\end{array}\\ \hline \mathbf{I}_T & \mathbf{O}\end{array}\right]}_{\mathcal{H}}\cdot\begin{bmatrix}\mathbf{w}\\-\mathbf{b}\end{bmatrix}\right|_2^2\right\} \tag{3.68}$$

The order of the DFT matrix $\mathcal{F}_N(i,:)$ and the data matrices $\mathbf{X}^{ext}$ and $\mathbf{N}$ may be changed as follows

$$J_i = \mathcal{E}\left\{\left|\left[x_{l-\theta-T+2:l+N-1}\cdot\mathbf{D}_{(\theta+T-1),i}\middle|n_{l-T+1:l+N-1}\cdot\mathbf{D}_{(T),i}\right]\cdot\mathcal{H}\cdot\begin{bmatrix}\mathbf{w}\\-\mathbf{b}\end{bmatrix}\right|_2^2\right\} \tag{3.69}$$

with $\mathbf{D}_{(T),i} = \begin{bmatrix} 0 & \cdots & \boxed{\mathcal{F}_N(i,:)} \\ & \vdots & \vdots \\ \boxed{\mathcal{F}_N(i,:)} & 0 & \cdots \end{bmatrix}^{\mathrm{T}}$ containing T DFT's for tone i. Analogous to the basic data model of equation (2.16), one can then write the transmitted signal x as a function of the frequency domain symbols

$$\begin{bmatrix} x_{l-\theta-T+2} \\ \vdots \\ x_{l+N-1}\end{bmatrix} = \begin{bmatrix}\mathbf{O} & \mathbf{I} & \mathbf{O}\end{bmatrix}\cdot\hat{\mathbf{P}}\cdot\hat{\mathcal{I}}_N\cdot\hat{\mathbf{x}} \tag{3.70}$$

$\hat{\mathbf{x}}$ is defined in equation (2.16) and contains 3 successive DMT symbols, $\hat{\mathbf{P}} = \text{diag}(\mathbf{P},\mathbf{P},\mathbf{P})$ and $\hat{\mathcal{I}}_N = \text{diag}(\mathcal{I}_N,\mathcal{I}_N,\mathcal{I}_N)$. The identity matrix is padded with zero columns, the number of which depends on the delay δ_{tot}. The cost function for tone i can then be written as follows

$$\begin{aligned} J_i &= \mathcal{E}\left\{\left|\left[\hat{\mathbf{x}}^{\mathrm{T}}|\mathbf{n}\right]\cdot\begin{bmatrix}\hat{\mathcal{I}}_N^{\mathrm{T}}\hat{\mathbf{P}}^{\mathrm{T}}\begin{bmatrix}\mathbf{O}\\ \mathbf{D}_{(\theta+T-1),i}\\ \mathbf{O}\end{bmatrix} & \mathbf{O}\\ \mathbf{O} & \mathbf{D}_{(T),i}\end{bmatrix}\cdot\mathcal{H}\cdot\begin{bmatrix}\mathbf{w}\\-\mathbf{b}\end{bmatrix}\right|_2^2\right\} \\ &= \left\|\underbrace{\begin{bmatrix}\mathbf{R}_{\hat{\mathbf{x}}}^{1/2}\hat{\mathcal{I}}_N^{\mathrm{T}}\hat{\mathbf{P}}^{\mathrm{T}}\begin{bmatrix}\mathbf{O}\\ \mathbf{D}_{(\theta+T-1),i}\\ \mathbf{O}\end{bmatrix} & \mathbf{O}\\ \mathbf{O} & \mathbf{R}_{\mathbf{n}}^{1/2}\mathbf{D}_{(T),i}\end{bmatrix}}_{\mathbf{W}_i}\cdot\mathcal{H}\cdot\begin{bmatrix}\mathbf{w}\\-\mathbf{b}\end{bmatrix}\right\|_2^2 \end{aligned} \tag{3.71}$$

where $\mathbf{D}_{(\theta+T-1),i}$ is padded with zero rows, the number of which depends of the delay δ_{tot}. Finally, $\mathbf{W}_i$ is the weight matrix for tone i. The cost function for all used tones then becomes

$$J = \left\| \begin{bmatrix} \mathbf{W}_{i_a} \\ \vdots \\ \mathbf{W}_{i_b} \end{bmatrix} \cdot \left[\begin{array}{c|c} & \mathbf{O}_{\delta_{\text{tot}} \times (\nu+1)} \\ \cline{2-2} \mathbf{H} & \mathbf{I}_{\nu+1} \\ \cline{2-2} & \mathbf{O} \\ \hline \mathbf{I}_T & \mathbf{O} \end{array} \right] \cdot \begin{bmatrix} \mathbf{w} \\ -\mathbf{b} \end{bmatrix} \right\|_2^2 \tag{3.72}$$

where $i_a \ldots i_b$ are the used tones. The disadvantage of this method is the large number of weight matrices to be computed for a cost function that still does not correspond to optimal SNR per tone.

3.3 Main disadvantages of MMSE channel shortening

Shortening the channel impulse response by means of an MMSE criterion (in the time or in the frequency domain), has no direct relation to the optimal bit rate, which results in unsatisfactory performance.

A constraint is necessary to prevent the trivial solution but this has no relation to the bit rate, and hence it may be difficult to select the appropriate constraint.

Besides the non-optimal capacity, another aspect of the unsatisfactory behavior of the MMSE shortening algorithm is the non-smooth behavior of resulting bit rate as a function of the decision delay. Hence an optimal delay is not easily selected beforehand and an exhaustive search over a large range of delays is needed during modem initialization.

3.4 TEQ algorithms based on other cost functions

3.4.1 Geometric signal-to-noise ratio

In [8], Al-Dhahir *et al* derive the optimal criterion to design the TEQ in a DMT receiver. The total number of bits transmitted per DMT symbol is maximized and is given by

$$\begin{aligned} b &= \sum_{i=used \quad tone} b_i \\ &= \sum_{i=used \quad tone} \log_2\left(1+\frac{SNR_i}{\Gamma_i}\right) \\ &= \log_2\left(\prod_{i=used \quad tone}\left(1+\frac{SNR_i}{\Gamma_i}\right)\right) \end{aligned} \tag{3.73}$$

with SNR_i the signal-to-noise ratio on tone i and Γ_i the SNR gap of tone i. The SNR gap reduces the SNR with respect to the theoretical (Shannon) capacity by Γ_i. The SNR gap is a function of the probability of error [46, 8]. It is further assumed that all the used tones have the same probability of error and so $\Gamma_i = \Gamma$.

The geometric SNR is defined as

$$1+\frac{SNR_{geom}}{\Gamma} = \left(\prod_{i=used \quad tone}\left(1+\frac{SNR_i}{\Gamma}\right)\right)^{1/N_u} \tag{3.74}$$

with N_u the number of used tones. So, the number of bits per DMT symbol may be written as

$$b = N_u \cdot \log_2\left(1+\frac{SNR_{geom}}{\Gamma}\right) \tag{3.75}$$

Hence, maximizing the bit rate of the DMT system is equivalent to maximizing the SNR_{geom}, assuming the transmission bandwidth is fixed. In [8] it is assumed that the SNR is high enough so that that the '+1' can be ignored in formula (3.74), and hence the dependence on Γ, which results in

$$SNR_{geom} \approx \left(\prod_{i=used \quad tone}(SNR_i)\right)^{1/N_u} \tag{3.76}$$

which is indeed the geometric mean of the SNRs of the used tones. In [8], the TEQ $\mathbf{w}$ and TIR $\mathbf{b}$ are searched for such that the geometric SNR of equation (3.76) is maximized. Under certain assumptions, a cost function in $\mathbf{b}$ is derived with 2 constraints. The result is a nonlinear constrained optimization problem in general without a unique optimum. Simulation results present improved performance with respect to MMSE channel shortening with unit norm constraint on $\mathbf{b}$.

3.4.2 Shortening signal-to-noise ratio

Perfectly shortening of a CIR $\mathbf{h}$ by a TEQ $\mathbf{w}$ is generally not possible. Melsa *et al* [80] propose a measure for the amount of energy outside the interval of $\nu+1$ elements of $\mathbf{h}*\mathbf{w}$. The Shortening Signal-to-Noise Ratio (SSNR) is defined as the ratio of the largest energy in $\nu+1$ consecutive samples to the energy in the remaining samples. It is noted that the largest energy will not necessarily start on the first sample of $\mathbf{h}*\mathbf{w}$ and so that delay optimization is needed. With $\mathbf{h}_{win}$ representing a window of $\nu+1$ consecutive samples of $\mathbf{h}*\mathbf{w}$ and $\mathbf{h}_{wall}$ the remaining samples, the following optimization problem is solved

$$\min_{\mathbf{w}} \mathbf{h}_{wall}^T \mathbf{h}_{wall} \quad \text{such that} \quad \mathbf{h}_{win}^T \mathbf{h}_{win} = 1 \tag{3.77}$$

The optimal TEQ settings are given by an eigenvalue problem.

The approach is based on shortening such that ISI is minimized. This cost function does not take into account the channel noise. It is noted that the SSNR, like (weighted) MMSE, is possibly not the best measure for TEQ design, because the ultimate goal is maximizing the SNR per tone of the DMT system.

3.5 Simulation results

To compare the performance of different equalizers, simulation results are presented for a set of ADSL channels. We consider 26 AWG 'inline' channels with lengths (0 : 500 : 6000) m and a set of standard channels [10]: T1.601-#7, T1.601-#9, T1.601-#13, CSA-#4, CSA-#6, CSA-#7, CSA-#8, mid-CSA. The standard channels are defined by standardization bodies and are given in [10]. The external noise consists of -140dBm/Hz additive white Gaussian noise (colored by the receiver front-end). An FDM set-up is adopted and the residual echo is taken into account. The transfer functions for the different channels and the noise PSDs are obtained from a simulation model from Alcatel. The channel transfer functions include the model of the copper wire itself as well as the digital and analog transmit and receive filters.

To compute the bit rate, we compute the SNR for each used tone i and take the SNR gap $\Gamma = 9.8$ dB, noise margin $\gamma_m = 6$ dB, coding gain $\gamma_c = 3$ dB. The number of bits b assigned to tone i is

$$b_i = \lfloor \log_2 \left(1 + 10^{\frac{SNR_i - \Gamma - \gamma_m + \gamma_c}{10}}\right) \rfloor \tag{3.78}$$

The bit rate is computed with the formula

$$rate = \left(\sum_{i=used\ tone} b_i\right) \cdot \frac{F_s}{N+\nu} \tag{3.79}$$

with F_s the sample frequency.

Simulation parameters are given in **Table 3.2**. A symmetric rate set-up, as given by the basic data model of section 2.2.1, is assumed.

	down	up
N	512	128
ν	32	8
used tones	39-256	8-30
F_s	2.208 MHz	552 kHz
psd$_x$	-40 dBm/Hz	-38 dBm/Hz

Table 3.2: Simulation parameters

3.5.1 MMSE channel shortening with different constraints

In the following simulations, the TEQs are trained for a white input signal x and colored noise n. In the bit rate computations, the used tones and the prefix structure are taken into account as well as colored noise.

Downstream

Fig. 3.2 shows a comparison of several constraints for a downstream 4km 26 AWG loop with 32-taps TEQ ($T = 32$). In the top figure, the bit rate is plotted for unit tap and unit norm constraints in this order: $w_0{=}1, \ldots, w_{T-1}{=}1, b_0{=}$ $1, \ldots, b_\nu{=}1, ||\mathbf{w}||_2^2{=}1, ||\mathbf{b}||_2^2{=}1$, for a fixed delay $\delta = -8$. The channel shortening cost function (3.1) combined with one of these constraints has no direct relation to the capacity of the system. Hence, it is difficult to predict which constraint will be the best for a certain channel and delay. It is seen in the top figure that the bit rate varies with the constraint and that unit tap constraint on $\mathbf{b}$ results in the largest bit rate for this delay. For a white input signal x, the unit norm constraint on $\mathbf{b}$ corresponds to constant energy of the received signal of interest, *i.e.* $\mathbf{b}^T\mathbf{R}_{xx}\mathbf{b} = 1$, and so this constraint has a physical meaning. Although the channel shortening cost function constrained to $||\mathbf{b}||_2^2 = 1$ does not optimize capacity, it still results in an acceptably large bit rate.

In the bottom figure, the bit rate is plotted as a function of the delay for 4 constraints. The bit rate of the unit tap and unit norm constraint on $\mathbf{b}$ are comparable whereas the unit norm constraint on $\mathbf{w}$ is worse. The unit tap constraint on $\mathbf{w}$ has a smaller delay range in which maximal bit rate is achieved. Remark the non-smooth behavior of the capacity as a function of the delay.

A similar simulation is made with an 8-taps TEQ for the same downstream channel in **Fig. 3.3**. Again, the unit tap and unit norm constraint on $\mathbf{b}$ are comparable whereas the unit norm constraint on $\mathbf{w}$ is worse. The unit tap constraint on $\mathbf{w}$ results in a slightly smaller optimal delay range.

Upstream

Fig. 3.4 shows the bit rate for an upstream 4km 26 AWG loop with 64-taps TEQ ($T = 64$). In the top figure different constraints are compared for a fixed delay $\delta = 30$. The unit tap and unit norm constraint on $\mathbf{w}$ are clearly worse than unit tap and unit norm constraint on $\mathbf{b}$. The bottom figure shows the bit rate as a function of the delay for 4 constraints. The performance of the unit tap and unit norm constraint on $\mathbf{b}$ is comparable. The bit rate is a very non-smooth function of the delay, which is a main disadvantage of the TEQ procedure. To explain the different behavior of the constraints, the transfer functions of the TEQs, *i.e.* $\mathcal{F}_N \cdot [\mathbf{w}^T \mathbf{0}^T]^T$, are plotted for delay 30 in **Fig. 3.5**. A constraint on $\mathbf{b}$ results in a higher gain on the used tones (8-30) than a constraint on $\mathbf{w}$. The latter constraint suffers from noise leakage (see also section 3.1.4).

Fig. 3.6 shows a similar simulation with a 16-taps TEQ ($T = 16$) for the same channel. In the top figure, the delay is fixed at $\delta = 6$. In the bottom figure, the bit rate variation with the delay is plotted for 4 constraints.

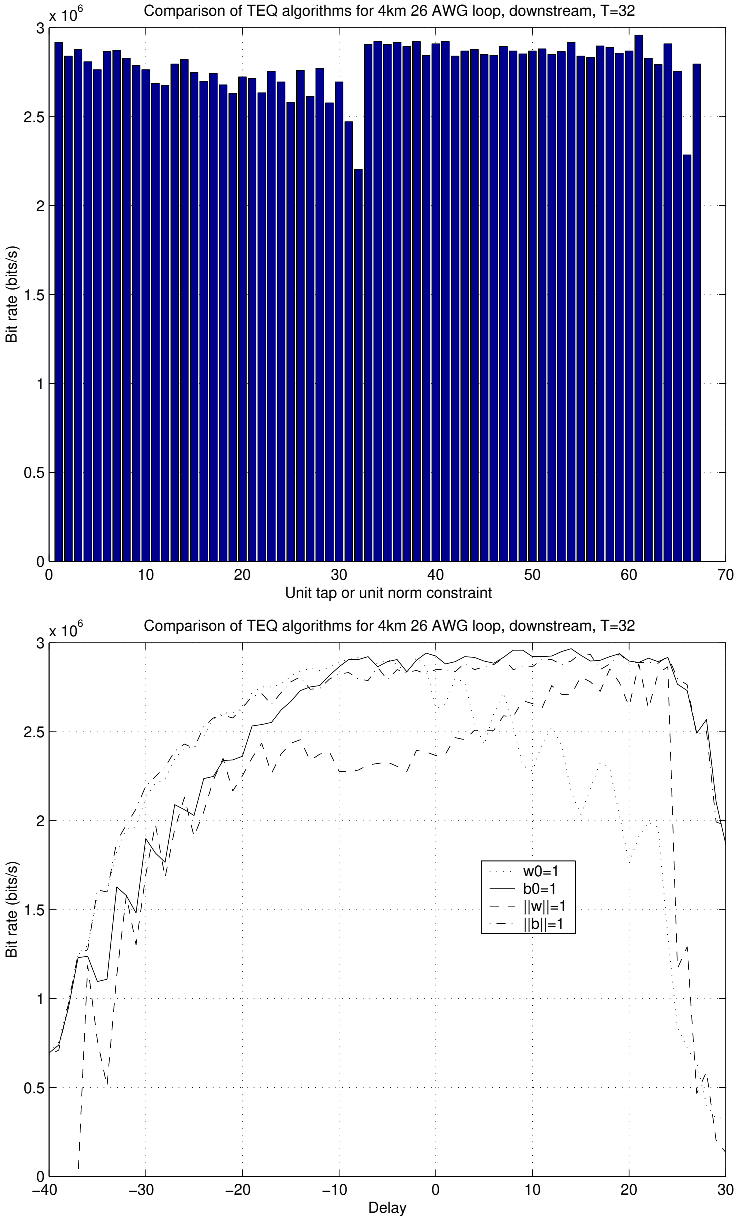

Figure 3.2: Simulations for a downstream 4km 26 AWG loop with 32-taps TEQ. Top: Bit rate as a function of the constraint (w_0=1, …, w_{T-1}=1, b_0=1, …, b_ν= 1, $||\mathbf{w}||_2^2$=1, $||\mathbf{b}||_2^2$=1) for fixed delay -8. Bottom: Bit rate as a function of the delay for 4 constraints.

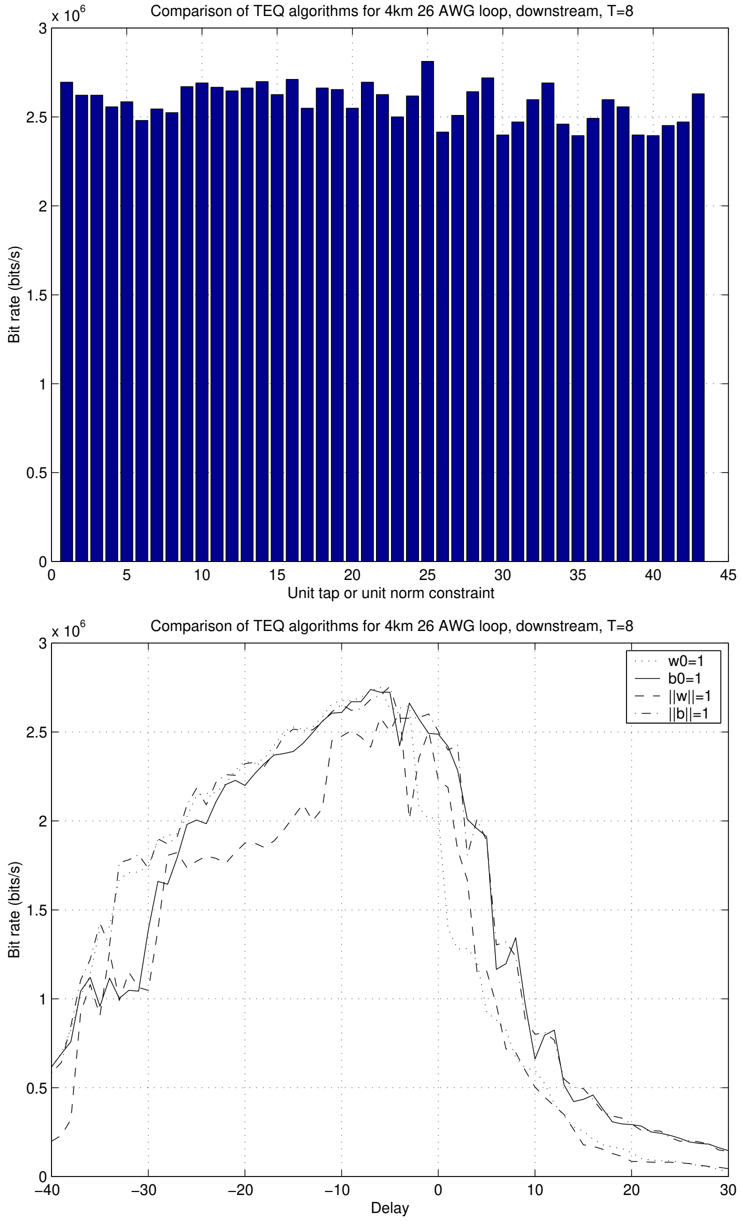

Figure 3.3: Simulations for a downstream 4km 26 AWG loop with 8-taps TEQ. Top: bit rate as a function of the constraint (w_0=1, ..., w_{T-1}=1, b_0=1, ..., b_ν= 1, $||\mathbf{w}||_2^2$=1, $||\mathbf{b}||_2^2$=1) for fixed delay -8. Bottom: bit rate as a function of the delay for 4 constraints.

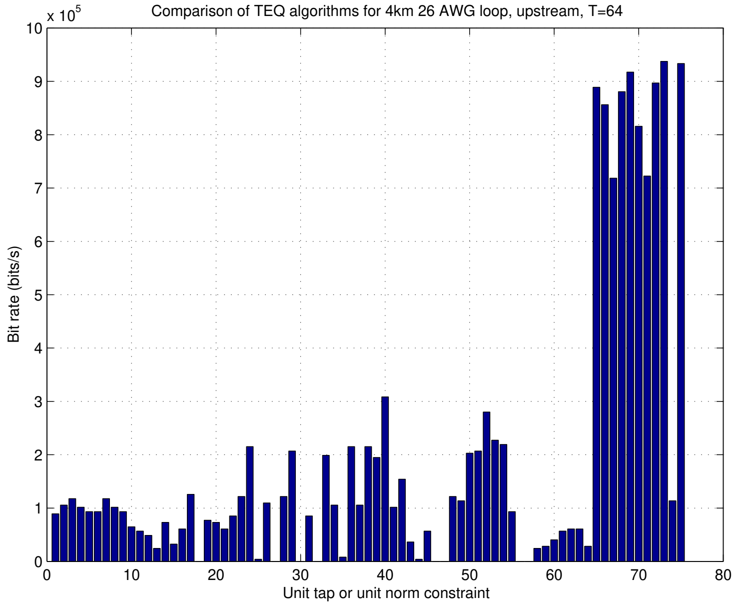

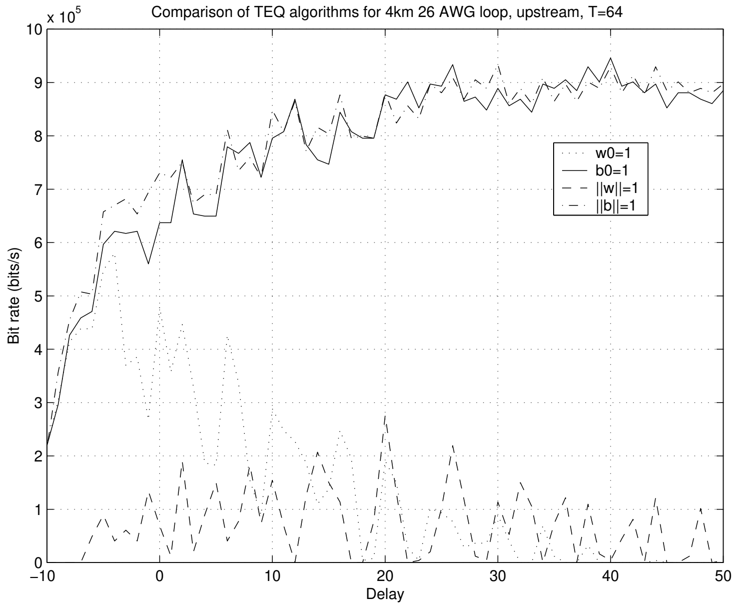

Figure 3.4: Simulations for an upstream 4km 26 AWG loop with 64-taps TEQ. Top: Bit rate as a function of the constraint (w_0=1, ..., w_{T-1}=1, b_0=1, ..., b_ν= 1, $||\mathbf{w}||_2^2$=1, $||\mathbf{b}||_2^2$=1) for fixed delay 30. Bottom: Bit rate as a function of the delay for 4 constraints.

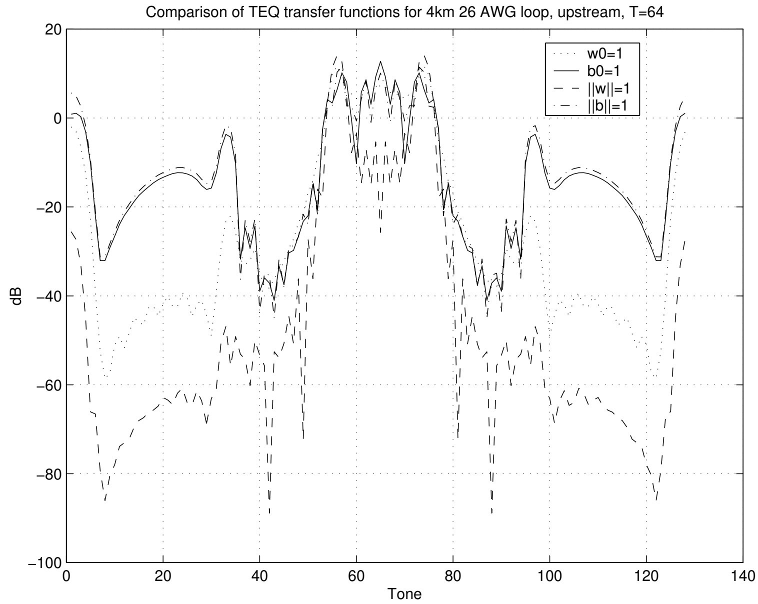

Figure 3.5: Transfer functions of the 64-taps TEQ, *i.e.* $\mathcal{F}_N \cdot [\mathbf{w}^{\mathrm{T}} \mathbf{0}^{\mathrm{T}}]^{\mathrm{T}}$, at delay 30 for 4 constraints. A constraint on $\mathbf{b}$ results in a higher gain on the tones of interest (8-30) than a constraint on $\mathbf{w}$. The latter suffers from noise leakage.

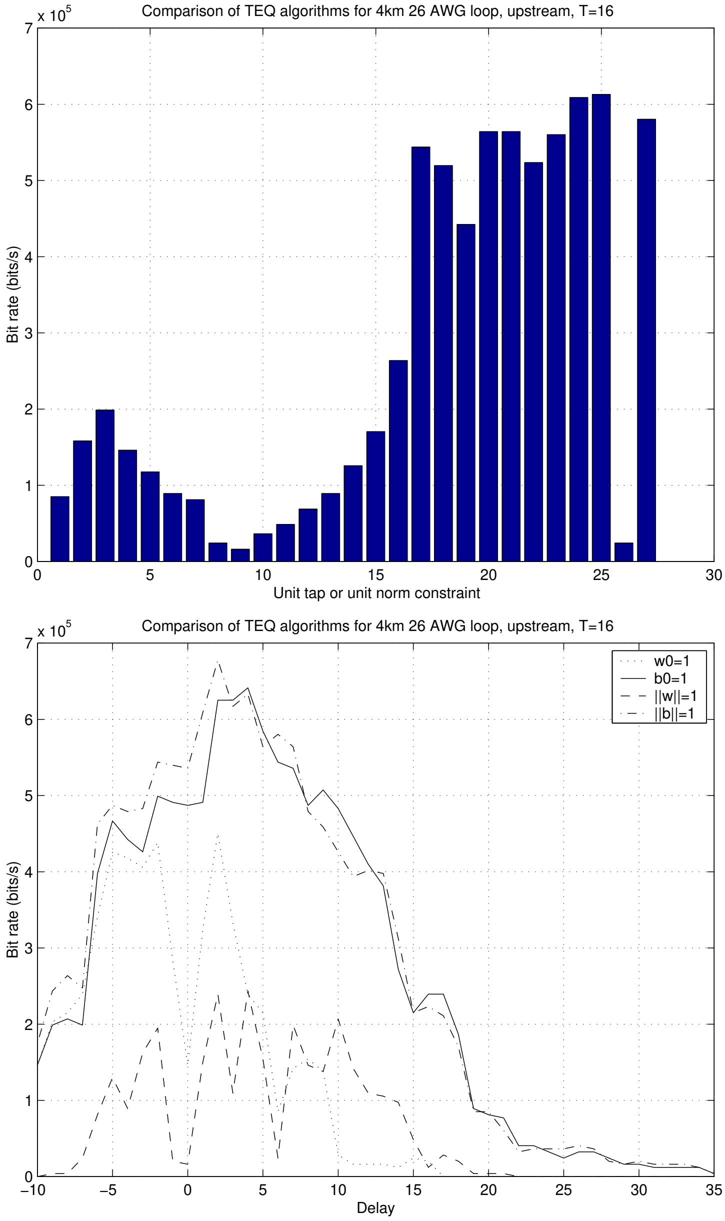

Figure 3.6: Simulations for an upstream 4km 26 AWG loop with 16-taps TEQ. Top: Bit rate as a function of the constraint ($w_0{=}1, \ldots, w_{T-1}{=}1, b_0{=}1, \ldots, b_\nu{=}1, ||\mathbf{w}||_2^2{=}1, ||\mathbf{b}||_2^2{=}1$) for fixed delay 6. Bottom: Bit rate as a function of the delay for 4 constraints.

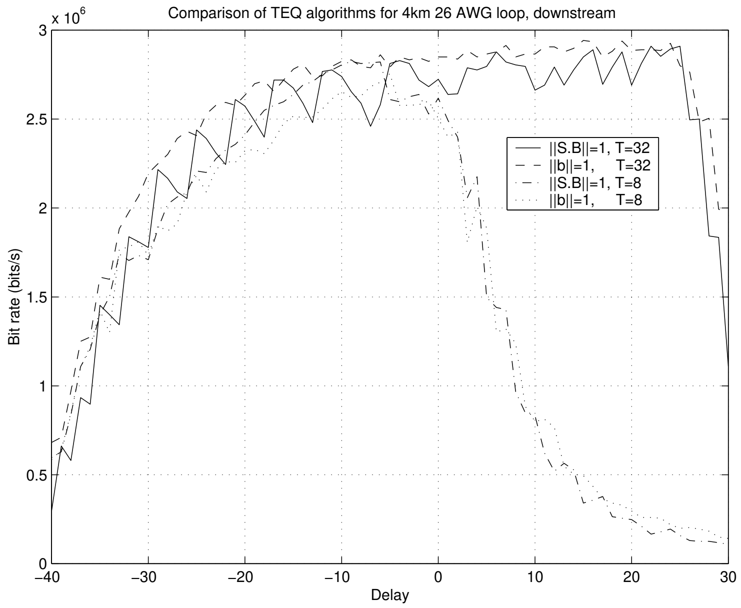

Figure 3.7: Comparison of weighted MMSE with classic channel shortening for a 4km 26 AWG downstream loop.

3.5.2 Weighted MMSE

Downstream

In **Fig. 3.7**, 2 TEQ algorithms are compared for 2 TEQ lengths for a downstream 4km 26 AWG loop. The first algorithm, denoted by $||\mathbf{S} \cdot B||_2^2 = 1$, minimizes cost function (3.65) and takes into account the used tones in the constraint as well as in the cost function (by weighting with $\mathbf{S}$). The second algorithm minimizes the classic channel shortening cost function constrained by $||\mathbf{b}||_2^2 = 1$. The considered TEQ lengths are 8 and 32. For $T = 32$, the weighted algorithm is worse than the classic channel shortening and very delay dependent. For $T = 8$, the weighted algorithm performs better than classic channel shortening.

Upstream

An upstream simulation for a 4km 26 AWG upstream loop is shown in **Fig. 3.8**. The weighted MMSE algorithm is clearly better than the classical channel shortening for $T = 64$ and for $T = 16$. Moreover for a large equalizer length, the delay dependency decreases significantly. In upstream, a relatively small

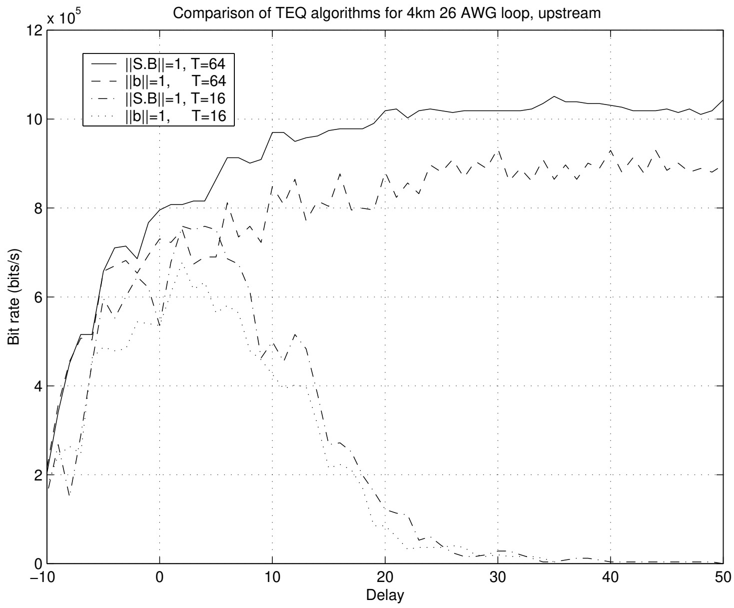

Figure 3.8: Comparison of weighted MMSE with classic channel shortening for a 4km 26 AWG upstream loop.

number of tones is used (only 8 up to 30 of the 65 tones). Probably for this reason, *the performance increase with the weighted criterion is more apparent in upstream than in downstream.*

3.5.3 Overview of TEQ algorithms

Downstream

An overview of the performance of 5 TEQ algorithms is shown in **Fig. 3.9** for downstream with $T = 32$ and fixed delay -8. In the top figure, bit rates are plotted as a function of the loop length for 26 AWG channels. For short loops, the unit tap constraints achieve highest bit rate. For longer loops, the difference between the algorithms is small. However, the unit norm constraint on $\mathbf{w}$ behaves clearly worst. There is no improvement achieved with the weighted MMSE algorithm.

The bottom figure shows bit rates for the reference loops. The unit tap constraint achieves highest bit rate, followed by the unit norm constraint on $\mathbf{b}$. No significant improvement is achieved by the weighted MMSE algorithm.

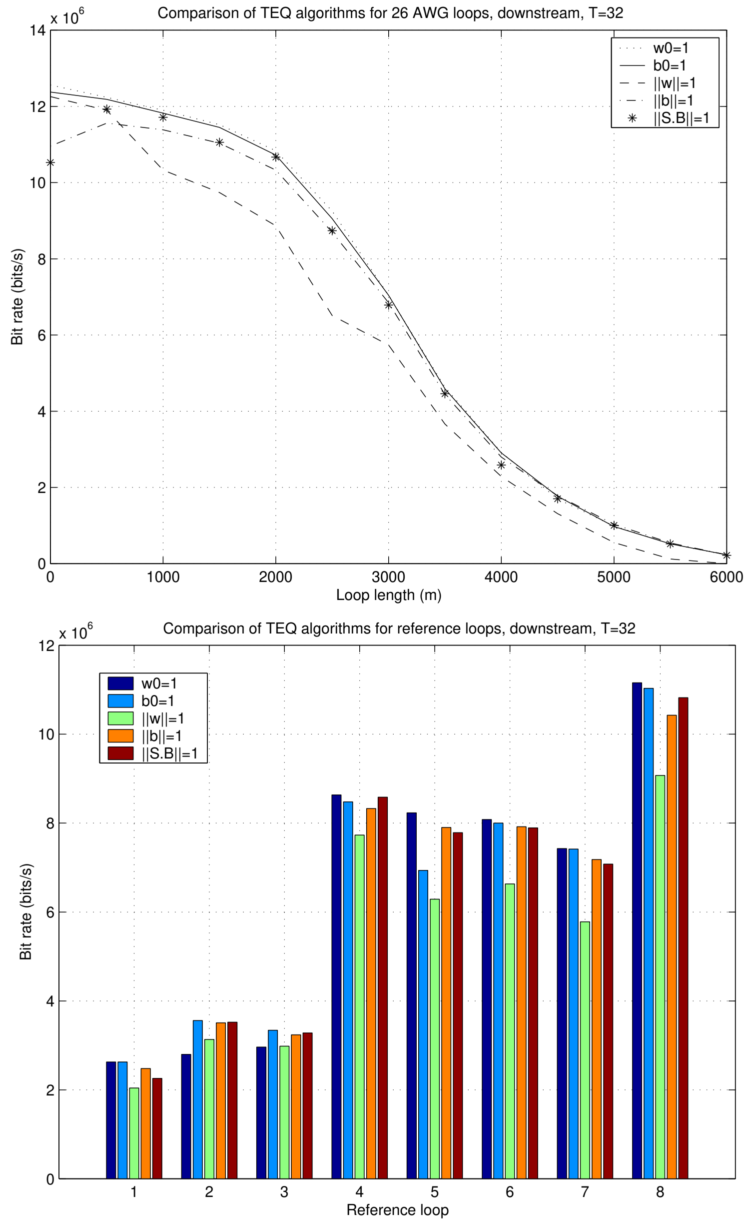

Figure 3.9: Downstream bit rate as a function of the loop length (top) and as a function of the reference loop number (bottom) with a 32-taps TEQ for different TEQ algorithms and fixed delay -8.

Upstream

Similar figures are made for upstream with $T = 64$ and fixed delay 30, the results of which are shown in **Fig. 3.10**. For all simulated loops, the weighted MMSE algorithm achieves a significant improvement with respect to the other algorithms. The unit norm and tap constraint on $\mathbf{b}$ have similar performance. The unit norm and tap constraint on $\mathbf{w}$ both provide low performance.

3.6 Conclusions

In this chapter, we have made an extensive study of TEQ design. First, an overview of existing MMSE channel shortening algorithms subject to different constraints is given. These algorithms do not correspond to bit rate optimization. Hence, it may be difficult to select the appropriate constraint. We have shown that a unit energy constraint on the received signal of interest or on the total received signal or on both signals simultaneously lead to the same solution for the TEQ, up to a scaling factor and, as a result, lead to the same bit rate. Subject to the latter constraints, the channel shortening algorithm can be interpreted as searching for the minimal principal angle between the subspaces defined by the transmitted signal x and the received signal y.

Then, we have modified the classical MMSE algorithm by the introduction of weight matrices in the cost function as well as in the constraint, to explicitly disregard the unused tones. Simplified formulas for the correlation matrices in case of white signal of interest and noise are derived. Optimizing the weighted MMSE can be seen as minimizing a sort of 1/SNR over the subband of used tones.

Further, we have reviewed TEQ design approaches, different from MMSE-based approaches. The geometric SNR optimizes bit rate by means of a nonlinear optimization. Shortening SNR measures the amount of energy outside a prefix-length interval in the shortened channel impulse response and does not correspond to bit rate optimization.

Finally, simulation results are given. The bit rate obtained by MMSE channel shortening varies as a function of the decision delay and the constraint. In downstream, a unit norm constraint on the TEQ behaves worst. In upstream, unit norm and unit tap constraints on the TIR are clearly better than similar constraints on the TEQ. The weighted MMSE shows a significant performance increase in upstream. However, remark that the modified weighted cost function still does not correspond to bit rate optimization.

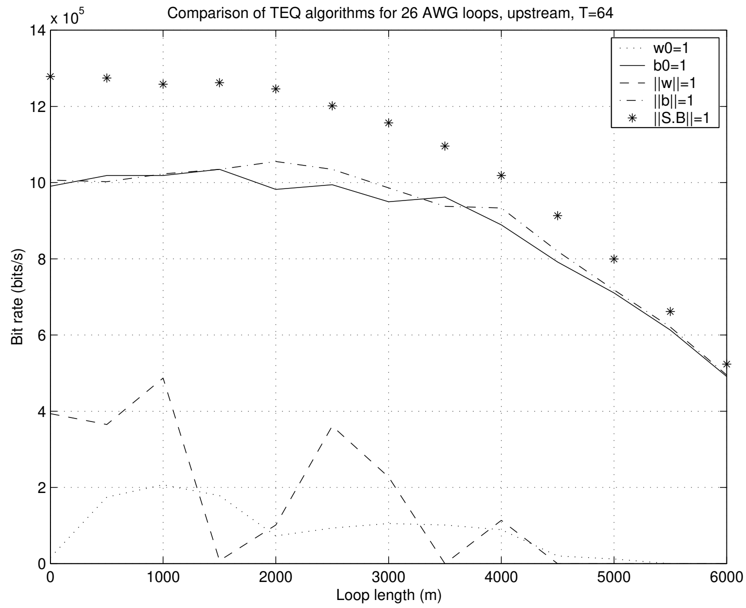

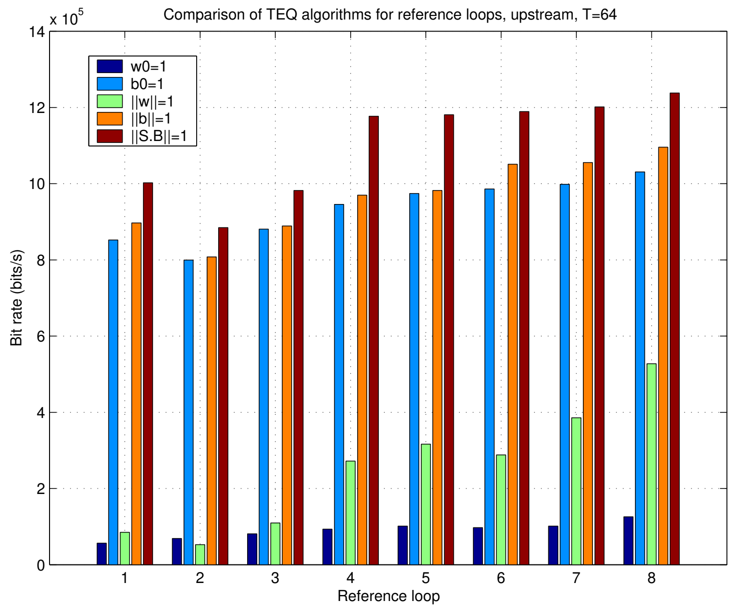

Figure 3.10: Upstream bit rate as a function of the loop length (top) and as a function of the reference loop number (bottom) with a 64-taps TEQ for different TEQ algorithms and fixed delay 30.

3.A Appendix: Unit energy constraints

Property 3.A.1. *The solution of the MMSE channel shortening algorithm subject to both unit energy constraints simultaneously, is given by* $\mathbf{w} = \mathbf{R}_{yy}^{-1/2} \cdot \mathbf{U}(:,1)$, $\mathbf{b} = \mathbf{R}_{xx}^{-1/2} \cdot \mathbf{V}(:,1)$ *and* $J = 2(1-\sigma_1)$ *with* $(\mathbf{U}(:,1), \sigma_1, \mathbf{V}(:,1))$ *the singular triplet of matrix* $\mathbf{A} = (\mathbf{R}_{yy}^{-1/2})^T \cdot \mathbf{R}_{yx} \cdot \mathbf{R}_{xx}^{-1/2}$ *corresponding to the largest singular value.*

Proof:
By applying the Cholesky factorization of matrices $\mathbf{R}_{xx}$ and $\mathbf{R}_{yy}$ in formula (3.23), one can write the generalized eigenvalue problem as

$$\begin{bmatrix} \mathbf{O} & (\mathbf{R}_{yy}^{-1/2})^{\mathrm{T}}\mathbf{R}_{yx}\mathbf{R}_{xx}^{-1/2} \\ (\mathbf{R}_{xx}^{-1/2})^{\mathrm{T}}\mathbf{R}_{xy}\mathbf{R}_{yy}^{-1/2} & \mathbf{O} \end{bmatrix} \cdot \begin{bmatrix} \mathbf{R}_{yy}^{1/2}\mathbf{w} \\ \mathbf{R}_{xx}^{1/2}\mathbf{b} \end{bmatrix} = \begin{bmatrix} \mathbf{R}_{yy}^{1/2}\mathbf{w} \\ \mathbf{R}_{xx}^{1/2}\mathbf{b} \end{bmatrix} \cdot (1-\lambda) \tag{3.80}$$

By substituting

$$\mathbf{A} = (\mathbf{R}_{yy}^{-1/2})^{\mathrm{T}} \cdot \mathbf{R}_{yx} \cdot \mathbf{R}_{xx}^{-1/2} \tag{3.81}$$

$$\mathbf{d} = \mathbf{R}_{yy}^{1/2} \cdot \mathbf{w} \tag{3.82}$$

$$\mathbf{c} = \mathbf{R}_{xx}^{1/2} \cdot \mathbf{b} \tag{3.83}$$

one obtains

$$\begin{bmatrix} \mathbf{O} & \mathbf{A} \\ \mathbf{A}^{\mathrm{T}} & \mathbf{O} \end{bmatrix} \cdot \begin{bmatrix} \mathbf{d} \\ \mathbf{c} \end{bmatrix} = \begin{bmatrix} \mathbf{d} \\ \mathbf{c} \end{bmatrix} \cdot (1-\lambda) \tag{3.84}$$

With $\mathbf{A} = \mathbf{U}\Sigma\mathbf{V}^{\mathrm{T}}$, the singular value decomposition (SVD) of matrix $\mathbf{A}$, the solution is given by the singular triplet of $\mathbf{A}$ corresponding to the largest singular value

$$\mathbf{d} = \mathbf{U}(:,1) \tag{3.85}$$

$$1 - \lambda = \sigma_1 \tag{3.86}$$

$$\mathbf{c} = \mathbf{V}(:,1) \tag{3.87}$$

Hence, the TEQ, TIR and minimum of the cost function are given by

$$\mathbf{w} = \mathbf{R}_{yy}^{-1/2} \cdot \mathbf{U}(:,1) \tag{3.88}$$

$$\mathbf{b} = \mathbf{R}_{xx}^{-1/2} \cdot \mathbf{V}(:,1) \tag{3.89}$$

$$J = 2(1-\sigma_1) \tag{3.90}$$

□

Property 3.A.2. *The solutions of the MMSE channel shortening algorithm subject to both constraints simultaneously or to either to* $\mathbf{b}^T\mathbf{R}_{xx}\mathbf{b} = 1$ *or to* $\mathbf{w}^T\mathbf{R}_{yy}\mathbf{w} = 1$ *are related. The respective TEQ solutions* $\mathbf{w}_0$, $\mathbf{w}_1$ *and* $\mathbf{w}_2$ *are a dominant eigenvector of matrix* $\mathbf{R}_{yy}^{-1} \cdot \mathbf{R}_{yx} \cdot \mathbf{R}_{xx}^{-1} \cdot \mathbf{R}_{xy}$. *Simulations have shown that the largest eigenvalue has algebraic multiplicity one (although the next eigenvalue is close to the largest). Therefore the solutions are equal up to a scaling factor. It is shown that the norms of the solutions are related by* $\|\mathbf{w}_1\|_2^2 = \sigma_1^2 \cdot \|\mathbf{w}_2\|_2^2 = \sigma_1^2 \cdot \|\mathbf{w}_0\|_2^2$. *A similar property holds for the TIR solutions.*

Proof:

The solution with constraint $\mathbf{b}^\mathrm{T}\mathbf{R}_{xx}\mathbf{b} = 1$ only, is determined by formula (3.28) and may be written as

$$\begin{aligned}
\min_{\mathbf{c}} J &= \min_{\mathbf{c}} \mathbf{c}^\mathrm{T} \cdot \left(\mathbf{I} - (\mathbf{R}_{xx}^{-1/2})^\mathrm{T} \cdot \mathbf{R}_{xy} \cdot \mathbf{R}_{yy}^{-1} \cdot \mathbf{R}_{yx} \cdot \mathbf{R}_{xx}^{-1/2}\right) \cdot \mathbf{c} \\
&= 1 - \max_{\mathbf{c}} \mathbf{c}^\mathrm{T} \cdot \left((\mathbf{R}_{xx}^{-1/2})^\mathrm{T} \cdot \mathbf{R}_{xy} \cdot \mathbf{R}_{yy}^{-1} \cdot \mathbf{R}_{yx} \cdot \mathbf{R}_{xx}^{-1/2}\right) \cdot \mathbf{c} \\
&= 1 - \max_{\mathbf{c}} \mathbf{c}^\mathrm{T} \cdot \left(\mathbf{A}^\mathrm{T}\mathbf{A}\right) \cdot \mathbf{c} \quad \text{such that} \quad \|\mathbf{c}\|_2^2 = 1
\end{aligned} \tag{3.91}$$

Hence, the minimum is also given by the eigenvector $\mathbf{c}$ corresponding to the maximal eigenvalue of $\mathbf{A}^\mathrm{T}\mathbf{A}$ with $\mathbf{A}$ given in formula (3.81). Similarly, the solution with constraint $\mathbf{w}^\mathrm{T}\mathbf{R}_{yy}\mathbf{w} = 1$ only, is determined by formula (3.32) and may be written as

$$\begin{aligned}
\min_{\mathbf{d}} J &= \min_{\mathbf{d}} \mathbf{d}^\mathrm{T} \cdot \left(\mathbf{I} - (\mathbf{R}_{yy}^{-1/2})^\mathrm{T} \cdot \mathbf{R}_{yx} \cdot \mathbf{R}_{xx}^{-1} \cdot \mathbf{R}_{xy} \cdot \mathbf{R}_{yy}^{-1/2}\right) \cdot \mathbf{d} \\
&= 1 - \max_{\mathbf{d}} \mathbf{d}^\mathrm{T} \cdot \left((\mathbf{R}_{yy}^{-1/2})^\mathrm{T} \cdot \mathbf{R}_{yx} \cdot \mathbf{R}_{xx}^{-1} \cdot \mathbf{R}_{xy} \cdot \mathbf{R}_{yy}^{-1/2}\right) \cdot \mathbf{d} \\
&= 1 - \max_{\mathbf{d}} \mathbf{d}^\mathrm{T} \cdot \left(\mathbf{A}\mathbf{A}^\mathrm{T}\right) \cdot \mathbf{d} \quad \text{such that} \quad \|\mathbf{d}\|_2^2 = 1
\end{aligned} \tag{3.92}$$

and the minimum is given by the eigenvector $\mathbf{d}$ corresponding to the maximal eigenvalue of $\mathbf{A}\mathbf{A}^\mathrm{T}$. Because the eigenvalues of $\mathbf{A}^\mathrm{T}\mathbf{A}$ and $\mathbf{A}\mathbf{A}^\mathrm{T}$ are equal (they are equal to σ^2, the squared singular values of $\mathbf{A}$), both unit energy constraints result in the same MMSE.

We further call $\mathbf{w}_1$ and $\mathbf{w}_2$ the TEQs corresponding to the first or the second unit energy constraint respectively. Vector $\mathbf{c}$ is such that

$$\mathbf{A}^\mathrm{T}\mathbf{A} \cdot \mathbf{c} = \lambda_{max} \cdot \mathbf{c} \tag{3.93}$$

$$(\mathbf{R}_{xx}^{-1/2})^\mathrm{T} \cdot \mathbf{R}_{xy} \cdot \mathbf{R}_{yy}^{-1} \cdot \mathbf{R}_{yx} \cdot \mathbf{R}_{xx}^{-1/2} \cdot \mathbf{c} = \lambda_{max} \cdot \mathbf{c} \tag{3.94}$$

By multiplying each side with $\mathbf{R}_{yy}^{-1} \cdot \mathbf{R}_{yx} \cdot \mathbf{R}_{xx}^{-1/2}$ and applying forumulas (3.26) and (3.27), one has

$$\mathbf{R}_{yy}^{-1} \cdot \mathbf{R}_{yx} \cdot \mathbf{R}_{xx}^{-1/2} \cdot (\mathbf{R}_{xx}^{-1/2})^{\mathrm{T}} \cdot \mathbf{R}_{xy} \cdot \mathbf{R}_{yy}^{-1} \cdot \mathbf{R}_{yx} \cdot \mathbf{R}_{xx}^{-1/2} \cdot \mathbf{c} = \lambda_{max} \mathbf{R}_{yy}^{-1} \cdot \mathbf{R}_{yx} \cdot \mathbf{R}_{xx}^{-1/2} \cdot \mathbf{c} \quad (3.95)$$

$$\mathbf{R}_{yy}^{-1} \cdot \mathbf{R}_{yx} \cdot \mathbf{R}_{xx}^{-1} \cdot \mathbf{R}_{xy} \mathbf{w}_1 = \lambda_{max} \cdot \mathbf{w}_1 \quad (3.96)$$

Similarly, vector $\mathbf{d}$ is such that

$$\mathbf{A}\mathbf{A}^{\mathrm{T}} \cdot \mathbf{d} = \lambda_{max} \cdot \mathbf{d} \quad (3.97)$$

$$(\mathbf{R}_{yy}^{-1/2})^{\mathrm{T}} \cdot \mathbf{R}_{yx} \cdot \mathbf{R}_{xx}^{-1} \cdot \mathbf{R}_{xy} \cdot \mathbf{R}_{yy}^{-1/2} \cdot \mathbf{d} = \lambda_{max} \cdot \mathbf{d} \quad (3.98)$$

with the same value for λ_{max}. After multiplying each side with $\mathbf{R}_{yy}^{-1/2}$ and applying formula (3.31), one has

$$\mathbf{R}_{yy}^{-1/2} \cdot (\mathbf{R}_{yy}^{-1/2})^{\mathrm{T}} \cdot \mathbf{R}_{yx} \cdot \mathbf{R}_{xx}^{-1} \cdot \mathbf{R}_{xy} \cdot \mathbf{R}_{yy}^{-1/2} \cdot \mathbf{d} = \lambda_{max} \cdot \mathbf{R}_{yy}^{-1/2} \cdot \mathbf{d} \quad (3.99)$$

$$\mathbf{R}_{yy}^{-1} \cdot \mathbf{R}_{yx} \cdot \mathbf{R}_{xx}^{-1} \cdot \mathbf{R}_{xy} \cdot \mathbf{w}_2 = \lambda_{max} \cdot \mathbf{w}_2 \quad (3.100)$$

When both constraints are applied simultaneously, one obtains for the TEQ $\mathbf{w}_0$, from formula (3.23), that

$$\mathbf{R}_{yy}^{-1} \cdot \mathbf{R}_{yx} \cdot \mathbf{R}_{xx}^{-1} \cdot \mathbf{R}_{xy} \cdot \mathbf{w}_0 = \sigma_1^2 \cdot \mathbf{w}_0 \quad (3.101)$$

and from formulas (3.91) and (3.92), it is clear that $\lambda_{max} = \sigma_1^2$. Hence, it is seen that the TEQs $\mathbf{w}_0$, $\mathbf{w}_1$ and $\mathbf{w}_2$ are dominant eigenvectors of the same matrix. Simulations have shown that the algebraic multiplicity of the dominant eigenvalue is one, therefore the three TEQs are parallel.

The scaling factor between the TEQs may be computed as follows. Consider first the SVD of $\mathbf{A} = \mathbf{U}\Sigma\mathbf{V}^{\mathrm{T}}$. Then we know from formulas (3.91) and (3.92) that $\mathbf{c} = \mathbf{V}(:,1)$ and $\mathbf{d} = \mathbf{U}(:,1)$. The norm of $\mathbf{w}_1$ becomes

$$\begin{aligned}
\mathbf{w}_1^{\mathrm{T}}\mathbf{w}_1 &= \mathbf{c}^{\mathrm{T}} \cdot (\mathbf{R}_{xx}^{-1/2})^{\mathrm{T}} \cdot \mathbf{R}_{xy} \cdot (\mathbf{R}_{yy}^{-1})^{\mathrm{T}} \cdot \mathbf{R}_{yy}^{-1} \cdot \mathbf{R}_{yx} \cdot \mathbf{R}_{xx}^{-1/2} \cdot \mathbf{c} \\
&= \mathbf{c}^{\mathrm{T}} \cdot \mathbf{A}^{\mathrm{T}} \cdot (\mathbf{R}_{yy}^{-1/2})^{\mathrm{T}} \cdot \mathbf{R}_{yy}^{-1/2} \cdot \mathbf{A} \cdot \mathbf{c} \\
&= \sigma_1 \cdot \mathbf{U}(:,1)^{\mathrm{T}} \cdot (\mathbf{R}_{yy}^{-1/2})^{\mathrm{T}} \cdot \mathbf{R}_{yy}^{-1/2} \cdot \mathbf{U}(:,1) \cdot \sigma_1 \\
&= \sigma_1^2 \cdot \mathbf{w}_2^{\mathrm{T}}\mathbf{w}_2
\end{aligned} \quad (3.102)$$

So, the scaling factor between the TEQs $\mathbf{w}_1$ and $\mathbf{w}_2$ is the largest singular value of matrix $\mathbf{A}$. From formula (3.31), one obtains $\mathbf{w}_2 = \mathbf{R}_{yy}^{-1/2} \cdot \mathbf{U}(:,1)$. Hence, $\mathbf{w}_2$ is equal to $\mathbf{w}_0$, given in formula (3.88).

A similar derivation can be given for the TIRs. It can be proven that $\mathbf{b}_0$, $\mathbf{b}_1$ and $\mathbf{b}_2$ are dominant eigenvectors of matrix $\mathbf{R}_{xx}^{-1} \cdot \mathbf{R}_{xy} \cdot \mathbf{R}_{yy}^{-1} \cdot \mathbf{R}_{yx}$ and that $||\mathbf{b}_2||_2^2 = \sigma_1^2 \cdot ||\mathbf{b}_1||_2^2 = \sigma_1^2 \cdot ||\mathbf{b}_0||_2^2$. □

Remark that the solutions for $\lambda < \lambda_{max}$ may result in a similar (or even better) bit rate as the solution related to λ_{max}. This is because the cost function does not optimize the bit rate. This is also noted in [135].

3.B Appendix: Correlation matrices for weighted MMSE

Property 3.B.1. *Matrix $\mathcal{F}_N^H \cdot \mathbf{S} \cdot \mathcal{F}_N$ is an $N \times N$ real, symmetric circulant weight matrix, where $\mathcal{F}_N$ is the N-point DFT-matrix and $\mathbf{S}$ is an $N \times N$ selector matrix, i.e. a diagonal matrix with ones on the positions corresponding to the used tones and its complex conjugates, and zeros elsewhere, i.e. $\mathbf{S}(i,i) = \mathbf{S}(N-i+2, N-i+2)$, $i = 2 \ldots \frac{N}{2}$.*

Proof:

- $\mathcal{F}_N^{\mathrm{H}} \cdot \mathbf{S} \cdot \mathcal{F}_N$ is hermitian symmetric.

$$\left(\mathcal{F}_N^{\mathrm{H}} \cdot \mathbf{S} \cdot \mathcal{F}_N\right)^{\mathrm{H}} = \mathcal{F}_N^{\mathrm{H}} \cdot \mathbf{S}^{\mathrm{H}} \cdot \mathcal{F}_N \tag{3.103}$$

- $\mathcal{F}_N^{\mathrm{H}} \cdot \mathbf{S} \cdot \mathcal{F}_N$ is real.
  Consider the element on the mth row and the nth column

$$\begin{aligned}\sum_i e^{j2\pi\frac{m(i-1)}{N}} \cdot e^{-j2\pi\frac{(i-1)n}{N}} &= \sum_i e^{j2\pi\frac{(i-1)p}{N}} \quad \text{with } p = m-n \\ &= \sum_i \cos\left(2\pi\frac{(i-1)p}{N}\right) + j\sin\left(2\pi\frac{(i-1)p}{N}\right)\end{aligned} \tag{3.104}$$

  Because of the structure of matrix $\mathbf{S}$, the complex conjugate tone of every used tone also appears in this sum. Hence, the sum of the second terms is zero and the elements are real.

- $\mathcal{F}_N^{\mathrm{H}} \cdot \mathbf{S} \cdot \mathcal{F}_N$ is circulant.
  The eigenvalue decomposition of this matrix is

$$\mathcal{F}_N \cdot \left(\mathcal{F}_N^{\mathrm{H}} \cdot \mathbf{S} \cdot \mathcal{F}_N\right) \mathcal{I}_N = N \cdot \mathbf{S} \tag{3.105}$$

The eigenvectors are the columns of $\mathcal{I}_N$, the N-point IDFT matrix, and the eigenvalues correspond to the DFT of the first column of $\mathcal{F}_N^{\mathrm{H}} \cdot \mathbf{S} \cdot \mathcal{F}_N$. Hence, it is a circulant matrix. □

Property 3.B.2. *The element of the real symmetric Toeplitz matrix in formula (3.56) are formed by taking the sum of the diagonals of matrix* $\mathcal{F}_N^{H} \cdot \mathbf{S} \cdot \mathcal{F}_N$.

Proof:

Consider the element on the mth row and the nth column of $\widetilde{\mathbf{R}}_{nn}$

$$\widetilde{\mathbf{R}}_{nn}(m,n) = \mathcal{E}\left\{\mathbf{N}(:,m)^{\mathrm{H}} \cdot \mathcal{F}_N^{\mathrm{H}} \cdot \mathbf{S} \cdot \mathcal{F}_N \cdot \mathbf{N}(:,n)\right\} \tag{3.106}$$

Suppose $m < n$ (a similar derivation holds for $m \geq n$). Then the first $N - (n-m)$ elements of the mth column of $\mathbf{N}$ are equal to the last $N - (n-m)$ elements of the nth column because $\mathbf{N}$ is Toeplitz. When developing (3.106), only terms with a product of white noise samples with the same index have to be considered. These are the only terms left after taking the expected value. Now suppose the $n - m + 1$ column of the weight matrix $\mathcal{F}_N^{\mathrm{H}} \cdot \mathbf{S} \cdot \mathcal{F}_N$ starts with the element g then

$$\begin{aligned}\widetilde{\mathbf{R}}_{nn}(m,n) &= \mathcal{E}\left\{\mathbf{N}(:,m)^{\mathrm{H}} \cdot \begin{bmatrix} a & b & \dots & g & \dots & b \\ b & \ddots & \ddots & & g & \vdots \\ \vdots & \ddots & & & & \ddots \\ g & & & & & \\ \vdots & g & & & & \\ b & \dots & \ddots & & & a \end{bmatrix} \cdot \mathbf{N}(:,n)\right\} \\ &= (N - (m-n)) \cdot g \cdot \mathcal{E}\left\{n_l^2\right\}\end{aligned} \tag{3.107}$$

□

Chapter 4

Per tone equalization

In chapter 3, we have seen that the famous MMSE channel shortening algorithm to initialize the TEQ does not result in optimal bit rate and, if one wants to optimize the bit rate for a TEQ-based DMT receiver, a nonlinear cost function has to be minimized. In this chapter, we derive a new equalization structure for DMT-based receivers, called *Per Tone EQualization* (PT-EQ), which allows to optimize the bit rate by means of an MMSE problem for each tone separately. The new DMT receiver has no TEQ anymore, but instead, has a multitaps equalizer for each tone separately. Hence the PT-EQ is performed in the frequency domain, *i.e.* after the FFT. The PT-EQ for a certain tone can be considered as a complex TEQ resulting in the optimal bit rate for that particular tone. As a result, the PT-EQ bit rate forms an upper bound for the TEQ bit rate, assuming the same number of taps.

In section 4.1, the PT-EQ is derived. It is seen that at first sight, the PT-EQ-based receiver needs multiple FFTs per received symbol, which would result in a large complexity increase. However, we show that one FFT per symbol is sufficient and that the other FFTs can be derived by means of so-called difference terms. The FFT output and the difference terms become the inputs of the modified PT-EQs.

The MSE cost function, resulting in optimal SNR for each tone, is derived in section 4.2. Complexity figures (during data transmission) are made for both PT-EQ and TEQ in section 4.3. In section 4.4, we study the combination of PT-EQ and windowing. (Time domain) windowing is developed in literature to decrease the DMT sensitivity for RFI. It turns out that the combination of (time domain) windowing and the efficient version of PT-EQ is not feasible. But, we show that a (time domain) window is equivalent to a certain set of PT-EQs.

Simulation results are given in section 4.5. We compare the performance of

PT-EQ and TEQ and investigate windowing and PT-EQ. SIMO equalization is simulated as an upper bound for PT-EQ. Finally conclusions are drawn in section 4.6.

4.1 Per tone equalization in a DMT modem

Different DMT receivers will be represented as signal flow graphs (SFG). SFG building blocks were shown in figure 2.6. The SFG for the well-known TEQ-based receiver [4, 5, 6, 7, 8, 26, 27, 28, 75, 80, 84, 122, 123, 125, 135, 136] was presented in figure 2.7 and is based on the following operation

$$\begin{bmatrix} Z_1^{(k)} \\ \vdots \\ Z_N^{(k)} \end{bmatrix} = \begin{bmatrix} D_1 & 0 & \cdots \\ 0 & \ddots & 0 \\ \vdots & 0 & D_N \end{bmatrix} \cdot \overbrace{\mathcal{F}_N \cdot (\mathbf{Y} \cdot \mathbf{w})}^{1 \text{ FFT}} \tag{4.1}$$

$$\text{where} \quad \mathbf{Y} = \begin{bmatrix} y_{k\cdot s+\nu+1} & y_{k\cdot s+\nu} & \cdots & y_{k\cdot s+\nu-T+2} \\ y_{k\cdot s+\nu+2} & y_{k\cdot s+\nu+1} & \cdots & y_{k\cdot s+\nu-T+3} \\ & \ddots & \ddots & \\ y_{(k+1)\cdot s} & y_{(k+1)\cdot s-1} & \cdots & y_{(k+1)\cdot s-T+1} \end{bmatrix} \tag{4.2}$$

and $\mathbf{w}_{T\times 1} = [w_0\, w_1 \ldots w_{T-1}]^{\mathrm{T}}$ is the (real) T-taps TEQ, $\mathcal{F}_N$ an $N \times N$ DFT-matrix, D_i the (complex) 1-taps FEQ for tone i, $Z_i^{(k)}$ is the FEQ output for tone i at symbol period k and $\mathbf{Y}$ an $N \times T$ Toeplitz matrix which contains exactly the same received signal samples as vector $\mathbf{y}$ in formula (2.16). For the sake of a compact notation, the decision delay δ is omitted in $\mathbf{Y}$[1].

Our approach is based on transferring the TEQ-operations to the frequency domain (*i.e.* after the FFT-demodulation). For a single tone i, we can rewrite the above operations as follows:

$$\begin{aligned} Z_i^{(k)} &= D_i \cdot \mathrm{row}_i\,(\mathcal{F}_N) \cdot (\mathbf{Y} \cdot \mathbf{w}) \\ &= \mathrm{row}_i\,\underbrace{(\mathcal{F}_N \cdot \mathbf{Y})}_{T \text{ FFTs}} \cdot \underbrace{\mathbf{w} \cdot D_i}_{\mathbf{w}_i} \end{aligned} \tag{4.3}$$

By applying associativity of the matrix product and putting D_i to the right, one has $\mathbf{w} \cdot D_i = (\mathbf{w}_i)_{T\times 1}$ which is a (complex) T-taps FEQ for tone i. The next step then is to allow each tone to have its own optimal TEQ, (be it) implemented as a T-taps FEQ $\mathbf{w}_i$. These T-taps FEQs are further called *Per Tone EQualizers* (PT-EQ). The corresponding receiver structure is shown in **Fig. 4.1**. From formula (4.3), it follows that the latency of the system is the same for the TEQ-approach as for the per tone equalization.

[1]The capital boldface letter $\mathbf{Y}$ is a matrix of received signal samples. The capital letter $Y_i^{(k)}$ (the demodulated output for tone i at symbol period k) is a complex subsymbol.

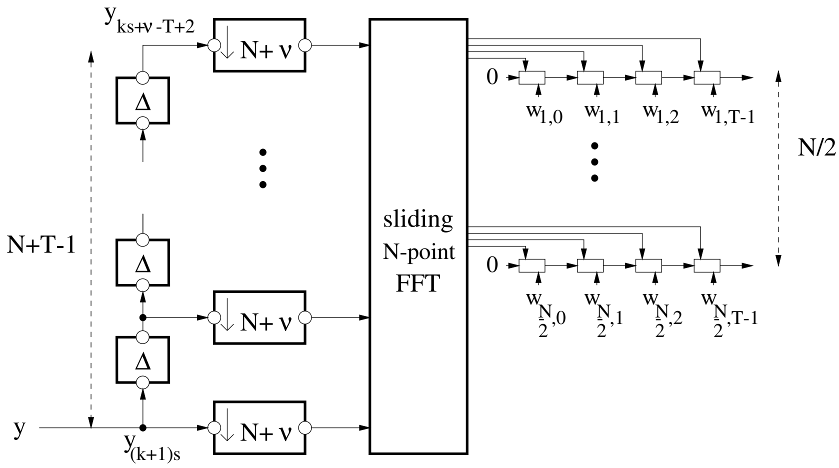

Figure 4.1: T-taps per tone equalizers

Note that, as indicated in the second line of formula (4.3), instead of one FFT-operation per symbol, we now apparently need T FFT-operations (one FFT for each column of $\mathbf{Y}$). Fortunately, because of the Toeplitz structure of $\mathbf{Y}$, these FFTs can be calculated efficiently by means of a sliding FFT [45]. Only one 'full' FFT has to be calculated (for the first column of $\mathbf{Y}$) and the $T-1$ remaining FFTs can be deduced as follows, as is proven in appendix 4.A:

$$\begin{aligned} &(\mathcal{F}_N \cdot \mathbf{Y}(:, m+1)) = (\mathcal{F}_N \cdot \mathbf{Y}(:, m)) \odot \mathbf{p} + \begin{bmatrix} 1 \\ \vdots \\ 1 \end{bmatrix}_{N \times 1} \cdot (y_{k\cdot s+\nu-(m-1)} - y_{k\cdot s+s-(m-1)}) \\ &\mathbf{p}^{\mathrm{T}} = \begin{bmatrix} \alpha^0 & \alpha^1 & \ldots & \alpha^{N-1} \end{bmatrix} \quad \alpha = e^{-j2\pi\frac{1}{N}} \end{aligned} \tag{4.4}$$

where $m = 1 \ldots T-1$. The $\odot$ represents a componentwise multiplication. $\mathbf{Y}(:, m+1)$ is the $(m+1)$st column of $\mathbf{Y}$, and $y_{k\cdot s+\nu-(m-1)}$ is its first element. $\mathbf{Y}(:, m)$ is the mth column of $\mathbf{Y}$, and $y_{k\cdot s+s-(m-1)}$ is its last element. For tone i, all relevant FFT-elements can thus be derived as linear combinations of the ith component of the first FFT (FFT of the first column of $\mathbf{Y}$) and $T-1$ difference terms $y_{k\cdot s+\nu-(m-1)} - y_{k\cdot s+s-(m-1)}$ for $m = 1 \ldots T-1$.

To reduce complexity even further, these linear combinations can then be incorporated in the PT-EQ coefficients such that the global PT-EQ for each tone i has as its inputs the ith output of the FFT and $T-1$ (real) difference terms, see **Fig. 4.2**. The modified per tone equalizers are denoted as $\mathbf{v}_i = [v_{i,0} \ldots v_{i,T-1}]^{\mathrm{T}}$ and can be calculated from the original PT-EQs $\mathbf{w}_i$ as follows

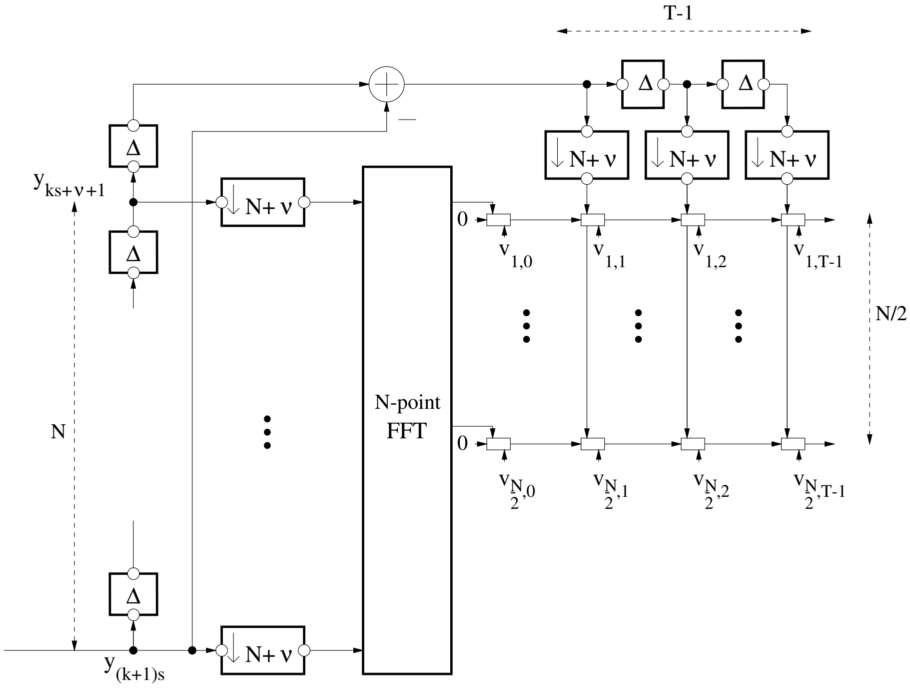

Figure 4.2: Modified T-taps per tone equalizers

$$
\begin{aligned}
\begin{bmatrix} v_{i,0} \\ v_{i,1} \\ \vdots \\ v_{i,T-1} \end{bmatrix} &= \begin{bmatrix} 1 & \alpha^{i-1} & \dots & \alpha^{(i-1)(T-1)} \\ 0 & 1 & \ddots & \ddots \\ \vdots & \ddots & \ddots & \alpha^{(i-1)} \\ 0 & \dots & 0 & 1 \end{bmatrix} \cdot \begin{bmatrix} w_{i,0} \\ w_{i,1} \\ \vdots \\ w_{i,T-1} \end{bmatrix} \\
&= \begin{bmatrix} 1 & -\alpha^{i-1} & 0 & \dots \\ 0 & 1 & \ddots & 0 \\ \vdots & \ddots & \ddots & -\alpha^{(i-1)} \\ 0 & \dots & 0 & 1 \end{bmatrix}^{-1} \cdot \begin{bmatrix} w_{i,0} \\ w_{i,1} \\ \vdots \\ w_{i,T-1} \end{bmatrix}
\end{aligned}
\tag{4.5}
$$

which is proven in appendix 4.B, and leads to the recursion formula

$$v_{i,t+1} \cdot \alpha^{i-1} + w_{i,t} = v_{i,t} \tag{4.6}$$

for tone $i = 1 \dots N$ with $t = 0 \dots T-2$, $v_{i,T-1} = w_{i,T-1}$ and $\alpha = e^{-j2\pi\frac{1}{N}}$ (see also appendix 4.B). SFGs of the recursion are presented in **Fig. 4.3**

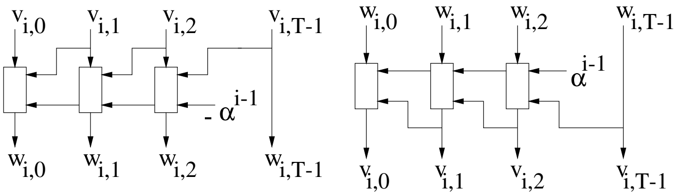

Figure 4.3: Recursions $\mathbf{v}_i$ to $\mathbf{w}_i$ and $\mathbf{w}_i$ to $\mathbf{v}_i$

for transformation from $\mathbf{v}_i$ to $\mathbf{w}_i$ and vice versa. These transformations are important when grouping tones, see section 5.3. The optimal PT-EQ is then only computed for the center tone of a group of tones and afterwards reused by the other tones in the same group. Because the equalizer $\mathbf{v}_i$ has 2 functions, it equalizes the channel for tone i and includes the sliding Fourier transform corresponding to tone i, this equalizer can not be used as such for other tones in the same group. However, the equalizer $\mathbf{w}_i$ can be used as such for other tones of the same group, because this equalizer does not include the sliding Fourier transform for tone i.

As indicated in figure 4.2, the per tone equalization structure works with the $\mathbf{v}_i$'s, while the $\mathbf{w}_i$'s are not computed explicitly (except when tone grouping is used, then the $\mathbf{w}_i$'s are computed for the center tones). The advantages of the per tone approach over the usual TEQ approach will be demonstrated in section 4.5.

4.2 Optimal per tone equalizer taps

For each of the used tones, we find the MMSE-based PT-EQ (for a particular choice of δ) by minimizing the following cost function

$$\begin{aligned}\min_{\mathbf{w}_i} J(\mathbf{w}_i) &= \min_{\mathbf{w}_i} \mathcal{E}\left\{\left|Z_i^{(k)} - X_i^{(k)}\right|^2\right\} \\ &= \min_{\mathbf{w}_i} \mathcal{E}\left\{\left|\bar{\mathbf{w}}_i^{\mathrm{T}} \cdot \begin{bmatrix} \boxed{\mathcal{F}_N(i,:)} & 0 & \cdots \\ & \ddots & \ddots \\ 0 & \cdots & \boxed{\mathcal{F}_N(i,:)} \end{bmatrix} \cdot \mathbf{y} - X_i^{(k)}\right|^2\right\}\end{aligned} \tag{4.7}$$

with $\bar{\mathbf{w}}_i^{\mathrm{T}} = \begin{bmatrix} w_{i,T-1} & \ldots & w_{i,0} \end{bmatrix}$ [2] and $\mathcal{F}_N(i,:)$ the ith row of $\mathcal{F}_N$. The MMSE-based PT-EQ optimizes the SNR for each tone separately, as is proven in property 4.2.1 on page 87.

[2] $\bar{\mathbf{w}}_i$ denotes vector $\mathbf{w}_i$ with its elements in reverse order.

Similarly, the modified PT-EQ $\mathbf{v}_i$ may be computed from

$$\min_{\mathbf{v}_i} J(\mathbf{v}_i) = \min_{\mathbf{v}_i} \mathcal{E}\left\{ \left| \bar{\mathbf{v}}_i^{\mathrm{T}} \cdot \underbrace{\left[\begin{array}{c|c|c} \mathbf{I}_{T-1} & \mathbf{O} & -\mathbf{I}_{T-1} \\ \hline \mathbf{O} & \multicolumn{2}{c}{\mathcal{F}_N(i,:)} \end{array} \right]}_{\mathbf{F}_i} \cdot \mathbf{y} - X_i^{(k)} \right|^2 \right\} \tag{4.8}$$

with $\bar{\mathbf{v}}_i^{\mathrm{T}} = \left[v_{i,T-1} \ldots v_{i,0} \right]$. The first block row in $\mathbf{F}_i$ is seen to extract the difference terms, while the last row corresponds to the single FFT.

Formula (4.8) may be combined with formula (2.16) of the basic data model resulting in an initialization formula which is applicable whenever a channel model is available, as well as signal and noise covariance matrices[3]. The combination with other data models is similar. In the sequel, we use the following notation: $\mathbf{e}_i^{(k)} = \left[0 \ \ldots \ 0 \ 1 \ 0 \ \ldots \ 0 \right]_{1\times 3N}$ with the non-zero entry in the $(N+i)$th column, $\mathbf{H}$ which includes channel convolution, adding of prefix and modulation, see equation (2.16), $\mathbf{R}_{\hat{\mathbf{x}}} = \mathcal{E}\{\hat{\mathbf{x}}\hat{\mathbf{x}}^{\mathrm{H}}\}$ the autocorrelation of vector $\hat{\mathbf{x}}$ and finally $\mathbf{R}_{\mathbf{n}} = \mathcal{E}\{\mathbf{n}\mathbf{n}^{\mathrm{H}}\}$ the autocorrelation of the noise $\mathbf{n}$.

The (zero-mean) transmitted subsymbols $X_i^{(k)}$ are assumed to be circularly symmetric [74], *i.e.* $\mathcal{E}\{(X_i^{(k)})^2\} = 0$. This is true if and only if the real and imaginary part of each subsymbol have the same variance and are independent. Furthermore, it holds that $\mathcal{E}\{X_i^{(k)} \cdot X_i^{(k)*}\} = \mathrm{psd}_x$ and that subsymbols transmitted on different tones or during different symbol periods are independent. These properties make $\mathbf{R}_{\hat{\mathbf{x}}}$ a diagonal matrix with diagonal elements corresponding to the used tones, equal to psd_x and zeros otherwise.

Combining formula (4.8) with (2.16) then results in

$$\begin{aligned} J(\mathbf{v}_i) &= \mathcal{E}\left\{ \left| \bar{\mathbf{v}}_i^{\mathrm{T}} \mathbf{F}_i (\mathbf{H}\hat{\mathbf{x}} + \mathbf{n}) - \mathbf{e}_i^{(k)} \hat{\mathbf{x}} \right|^2 \right\} \\ &= \mathcal{E}\left\{ \left| \begin{bmatrix} \hat{\mathbf{x}}^{\mathrm{H}} & \mathbf{n}^{\mathrm{H}} \end{bmatrix} \cdot \begin{bmatrix} \mathbf{H}^{\mathrm{H}} \mathbf{F}_i^{\mathrm{H}} \bar{\mathbf{v}}_i^* - \mathbf{e}_i^{(k)\mathrm{H}} \\ \mathbf{F}_i^{\mathrm{H}} \bar{\mathbf{v}}_i^* \end{bmatrix} \right|^2 \right\} \\ &= \left\| \begin{bmatrix} \mathbf{R}_{\hat{\mathbf{x}}}^{1/2} & \mathbf{O} \\ \mathbf{O} & \mathbf{R}_{\mathbf{n}}^{1/2} \end{bmatrix} \cdot \begin{bmatrix} \mathbf{H}^{\mathrm{H}} \mathbf{F}_i^{\mathrm{H}} \bar{\mathbf{v}}_i^* - \mathbf{e}_i^{(k)\mathrm{H}} \\ \mathbf{F}_i^{\mathrm{H}} \bar{\mathbf{v}}_i^* \end{bmatrix} \right\|_2^2 \\ &= \left\| \underbrace{\begin{bmatrix} \mathbf{R}_{\hat{\mathbf{x}}}^{1/2} \mathbf{H}^{\mathrm{H}} \mathbf{F}_i^{\mathrm{H}} \\ \mathbf{R}_{\mathbf{n}}^{1/2} \mathbf{F}_i^{\mathrm{H}} \end{bmatrix}}_{\mathbf{U}} \bar{\mathbf{v}}_i^* - \underbrace{\begin{bmatrix} \mathbf{R}_{\hat{\mathbf{x}}}^{1/2} \mathbf{e}_i^{(k)\mathrm{H}} \\ \mathbf{0} \end{bmatrix}}_{\mathbf{d}} \right\|_2^2 \end{aligned} \tag{4.9}$$

[3]Alternatively formula (4.8) may be used for a training sequence based initialization of the per tone equalizers. Efficient implementation schemes for such initialization procedures will be considered in chapter 5.

This least squares problem (for a particular choice of δ) is then solved for each tone i, for instance by a QR decomposition [48] of the compound matrix $\begin{bmatrix}\mathbf{U} & \mathbf{d}\end{bmatrix}$. The resulting signal, ISI-ICI and noise energy for tone i can then be found respectively as

$$S_i = \left|(\mathbf{R}_{\hat{\mathbf{x}}}^{1/2}\mathbf{H}^{\mathrm{H}}\mathbf{F}_i^{\mathrm{H}})_{(N+i,:)}\bar{\mathbf{v}}_i^*\right|^2 \tag{4.10}$$

$$I_i = \left\|\mathbf{R}_{\hat{\mathbf{x}}}^{1/2}\mathbf{H}^{\mathrm{H}}\mathbf{F}_i^{\mathrm{H}}\bar{\mathbf{v}}_i^*\right\|^2 - S_i \tag{4.11}$$

$$N_i = \left\|\mathbf{R}_{\mathbf{n}}^{1/2}\mathbf{F}_i^{\mathrm{H}}\bar{\mathbf{v}}_i^*\right\|^2 \tag{4.12}$$

And the SNR of tone i becomes $SNR_i = \frac{S_i}{I_i+N_i}$.

Property 4.2.1. *The MMSE per tone equalizer, computed by means of the unconstrained least squares set of equations in formula (4.9), optimizes the SNR per tone.*

Proof:
Let us consider first the constrained optimization problem

$$\min_{\mathbf{v}_i}\left\|\begin{bmatrix}\mathbf{u}_i^{\mathrm{H}}\\ \widetilde{\mathbf{U}}\end{bmatrix}\cdot\bar{\mathbf{v}}_i^* - \begin{bmatrix}\mathrm{psd}_x^{1/2}\cdot 1\\ \mathbf{0}\end{bmatrix}\right\|_2^2 \quad \text{subject to} \quad \mathbf{u}_i^{\mathrm{H}}\cdot\bar{\mathbf{v}}_i^* = \mathrm{psd}_x^{1/2} \tag{4.13}$$

where $\mathbf{u}_i^{\mathrm{H}}$ is the $(N+i)$th row of matrix $\mathbf{U}$, *i.e.* the row corresponding to tone i of the symbol of interest, and $\widetilde{\mathbf{U}}$ is a submatrix of $\mathbf{U}$ containing all the other rows. The rows in vector $\mathbf{d}$, defined in formula (4.9), are ordered accordingly resulting in $[\mathrm{psd}_x^{1/2}\ \mathbf{0}]^{\mathrm{T}}$. Formula (4.13) optimizes the SNR for tone i because the constraint corresponds to constant received signal of interest energy while the cost function minimizes the sum of ISI, ICI and noise energy.

Optimization problem (4.13) is equivalent to

$$\min_{\mathbf{v}_i}\left\|\begin{bmatrix}f\cdot\mathbf{u}_i^{\mathrm{H}}\\ \widetilde{\mathbf{U}}\end{bmatrix}\cdot\bar{\mathbf{v}}_i^* - \begin{bmatrix}f\cdot\mathrm{psd}_x^{1/2}\\ \mathbf{0}\end{bmatrix}\right\|_2^2 \quad \text{with} \quad f\to\infty \tag{4.14}$$

By applying the matrix inversion lemma[4], it can be shown that the solution is given by

$$\bar{\mathbf{v}}_i^* = \frac{1}{1+f\mathbf{u}_i^{\mathrm{H}}(\widetilde{\mathbf{U}}^{\mathrm{H}}\widetilde{\mathbf{U}})^{-1}\mathbf{u}_i f}\cdot(\widetilde{\mathbf{U}}^{\mathrm{H}}\widetilde{\mathbf{U}})^{-1}\cdot\mathbf{u}_i\cdot f\cdot\mathrm{psd}_x^{1/2}\cdot f \tag{4.15}$$

[4] $(A+BCD)^{-1} = A^{-1} - A^{-1}B(C^{-1}+DA^{-1}B)^{-1}DA^{-1}$, see [57]

Hence, for every value of f, the solution is parallel to $(\widetilde{\mathbf{U}}^{\mathrm{H}}\widetilde{\mathbf{U}})^{-1} \cdot \mathbf{u}_i$ and as such, results in the same bit rate. The unconstrained optimization problem in formula (4.9) corresponds to the optimization problem in formula (4.14) with $f = 1$. While the solutions for all values of f are parallel, the constrained ($f \to \infty$) and the unconstrained ($f = 1$) optimization problem result in the same bit rate. Hence, the unconstrained optimization problem given in formula (4.9) optimizes the SNR for tone i. □

4.3 Complexity during data transmission

In the following complexity computations, the number of *real multiplications* and *real additions* is considered. A multiplication of a real with a complex number is counted as 2 real multiplications, a multiplication of 2 complex numbers is counted as 4 real multiplications. An addition of 2 complex numbers is counted as 2 real additions.

4.3.1 Constant equalizer length and delay

Because the per tone equalizers work at a downsampled rate with respect to the TEQ, the total complexity of the TEQ-based structure and the modified PT-EQ-based structure is easily shown to be roughly equal for a particular T and N.

Complexity calculations for equalization consisting of TEQ and 1-taps FEQ per tone are presented in **Table 4.1**. F_s is the sample frequency and $\frac{N+\nu}{F_s}$ the symbol duration. N_u denotes the number of used tones. The last row of the table is an approximation where the number of used tones is taken $N_u = \frac{N}{2}$, which is a worst-case scenario, and the symbol duration is $\frac{N}{F_s}$.

The complexity of the PT-EQs $\mathbf{v}_i$ is presented in **Table 4.2**. A cartesian representation of the complex numbers is used. The different terms in the third row (PT-EQ) correspond to the complexities of the following operations: product of complex input with complex tap, $T-1$ products of real input with complex tap, sum of T complex tap outputs and calculation of $T-1$ difference terms. In the last row, similar approximations are used as in table 4.1.

We can conclude that the resulting complexities are comparable and both of order F_sT.

The complexity of the per tone method can be reduced even further by varying the equalizer length per tone and setting the length to zero for non-used tones, see subsection 4.3.2. One the other hand, the influence of a tone dependent decision delay δ_i on the complexity is investigated in subsection 4.3.3.

Example 4.3.1. To give a numerical example of the complexity for a TEQ-based and a PT-EQ-based DMT receiver, we consider an equalizer length T

	# multiplications	# additions
TEQ	F_sT	$F_s(T-1)$
FFT	$\frac{F_s}{N+\nu}\mathcal{O}(N\cdot\log_2(N))$	$\frac{F_s}{N+\nu}\mathcal{O}(N\cdot\log_2(N))$
FEQ Polar representation	$N_u\frac{F_s}{N+\nu}$	$N_u\frac{F_s}{N+\nu}$
TEQ + FEQ	$F_s(T+\frac{N_u}{N+\nu})$	$F_s(T-1+\frac{N_u}{N+\nu})$
approximation	$F_s(T+\frac{1}{2})$	$F_s(T-\frac{1}{2})$

Table 4.1: Complexity of equalization with TEQ and 1-taps FEQ per tone

	# multiplications	# additions
TEQ		
FFT	$\frac{F_s}{N+\nu}\mathcal{O}(N\cdot\log_2(N))$	$\frac{F_s}{N+\nu}\mathcal{O}(N\cdot\log_2(N))$
PT-EQ Cartesian representation	$\frac{F_s}{N+\nu}N_u[4+2(T-1)]$ $=2\frac{F_s}{N+\nu}N_u(T+1)$	$\frac{F_s}{N+\nu}N_u[2+2(T-1)]$ $+\frac{F_s}{N+\nu}(T-1)$ $=\frac{F_s}{N+\nu}(2N_uT+T-1)$
approximation	$F_s(T+1)$	$F_sT+\frac{F_s}{N}(T-1)$

Table 4.2: Complexity of per tone equalizers

equal to 32 in downstream and 64 in upstream. We further consider the parameters given in table 3.2. Hence, we assume there are 218 downstream and 23 upstream used tones (N_u). A numerical complexity comparison is given in **Table 4.3**. Because not all tones are used in downstream and upstream, the complexity of PT-EQ is lower than the complexity of TEQ combined with 1-taps FEQ. $\square$

4.3.2 Tone dependent equalizer length and constant delay

The PT-EQ are schematicly represented in **Fig. 4.4**. T_i is the equalizer length for tone i. i_f and i_l are respectively the first and last used tone, so the number of used tones N_u is now $i_l - i_f + 1$. One FFT is performed per received symbol. Every PT-EQ has one complex input and $T_i - 1$ real inputs which

		# multiplications	# additions
down	TEQ+FEQ	71.5	69.3
down	PT-EQ	58.4	56.8
up	TEQ+FEQ	35.4	34.9
up	PT-EQ	12.1	12.2

Table 4.3: Numerical example of the equalization complexity (in M operations/s) of, on the one hand, T-taps TEQ and 1-taps FEQ and, on the other hand, T-taps PT-EQ. T is 32 and 64 in downstream and upstream respectively. In every case, one FFT per received symbol is performed.

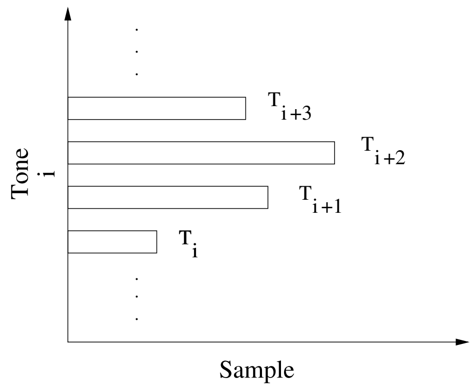

Figure 4.4: Schematic representation of per tone equalizers with tone dependent length T_i

are difference terms of the received samples. A cartesian representation of the complex numbers is again used in the complexity calculations in **Table 4.4**. The different terms in the third row (PT-EQ) correspond to the complexities of the following operations: product of complex input with complex tap, $T_i - 1$ products of real input with complex tap, sum of T_i complex tap outputs and calculation of $T_{i,max} - 1$ difference terms.

Example 4.3.2. To show the complexity reduction by adapting the number of taps per tone, we assume a downstream set-up with 218 used tones. 40 tones have $T = 32$ taps. 178 tones have $T = 8$ taps. Complexity numbers are given in **Table 4.5**. It is seen in section 4.5 that, in downstream, one can lower the number of taps per tone from 32 to 8 in a large range of tones without significant bit rate decrease. Only around the band edges, a high number of

	# multiplications	# additions
TEQ		
FFT	$\frac{F_s}{N+\nu}\mathcal{O}(N \cdot \log_2(N))$	$\frac{F_s}{N+\nu}\mathcal{O}(N \cdot \log_2(N))$
PT-EQ Cartesian representation	$\frac{F_s}{N+\nu}\sum_{i=i_f}^{i_l}[4+2(T_i-1)]$ $= 2\frac{F_s}{N+\nu}(N_u + \sum_{i=i_f}^{i_l} T_i)$	$\frac{F_s}{N+\nu}\sum_{i=i_f}^{i_l}[2+2(T_i-1)]$ $+\frac{F_s}{N+\nu}(T_{\max}-1)$ $=\frac{F_s}{N+\nu}(2\sum_{i=i_f}^{i_l} T_i + T_{\max} - 1)$

Table 4.4: Complexity of per tone equalizers with tone dependent equalizer length and constant delay

		# multiplications	# additions
down	PT-EQ	23.7	22.1

Table 4.5: Numerical example of the equalization complexity (in M operations/s) with variable number of taps per tone: 40 tones have 32 taps and 178 tones have 8 taps. One FFT per received symbol is performed.

taps is needed. In upstream however, a lower number of taps per tone decreases the SNR on all tones. □

4.3.3 Tone dependent equalizer length and delay

A schematic representation of these PT-EQ is shown in **Fig. 4.5**. δ_i is the delay for used tone i and $\Delta_i = \delta_i - \min_i \delta_i$ the delay difference. Still one complete FFT is performed per received symbol which is computed on the time instant corresponding to $\Delta_i = 0$. Because of the tone dependency of δ_i, one needs to compute the FFT for the other used tones by means of sliding FFT. Hence, $\Delta_{\max} = \max_i \Delta_i$ sliding FFTs are computed and so the first $\Delta_{\max}$ difference terms of received signal samples are also computed. For each tone i, an extra number of difference terms equal to $\max(\Delta_i + T_i - 1 - \Delta_{\max}, 0)$ is needed. The total number of necessary difference terms equals $\max_i(\Delta_i + T_i) - 1$. Complexity calculations are presented in **Table 4.6**.

An other possibility could be not to compute the additional sliding FFTs but to increase the equalizer length T_i of every tone i with Δ_i. This comes down to the equalization scheme of the previous subsection. In the complexity calculations one then replaces T_i by $T_i + \Delta_i$ and sets Δ_i equal to zero.

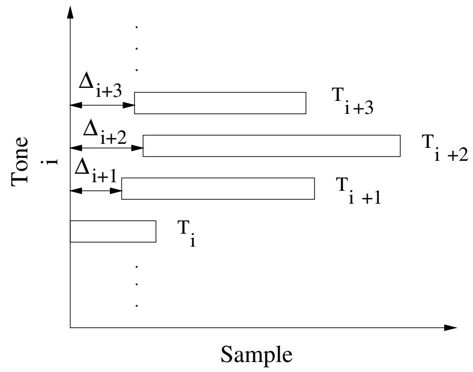

Figure 4.5: Schematic representation of per tone equalizers with different delays Δ_i and lengths T_i

	# multiplications	# additions
TEQ		
FFT	$\frac{F_s}{N+\nu}[\mathcal{O}(N \cdot \log_2(N))$ $+\Delta_{\max}\mathcal{O}(N)]$	$\frac{F_s}{N+\nu}[\mathcal{O}(N \cdot \log_2(N))$ $+\Delta_{\max}\mathcal{O}(N)]$
PT-EQ Cartesian represen- tation	$\frac{F_s}{N+\nu}\sum_{i=i_f}^{i_l}[4+2(T_i-1)]$ $= 2\frac{F_s}{N+\nu}(N_u + \sum_{i=i_f}^{i_l} T_i)$	$\frac{F_s}{N+\nu}\sum_{i=i_f}^{i_l}[2+2(T_i-1)]$ $+\frac{F_s}{N+\nu}(\max_i(\Delta_i+T_i)+\Delta_{\max}-1)$ $= \frac{F_s}{N+\nu}(2\sum_{i=i_f}^{i_l} T_i$ $+\max_i(\Delta_i+T_i)+\Delta_{\max}-1)$

Table 4.6: Complexity of per tone equalizers with tone dependent equalizer length and delay

4.4 Combination of per tone equalization and windowing

DMT is very sensitive to narrow band interference, like RFI, because the FFT filters are sinc shaped and hence, have considerable sidelobes. As a result, a narrow band interferer will hit many tones. To improve robustness to RFI, windowing [109] of the received signal has been used. By applying a time domain window before demodulation, the sidelobes of the sinc filters are significantly lowered, see figure 2.10.

In order to guarantee orthogonality of the tones at the receiver, *i.e.* no in-

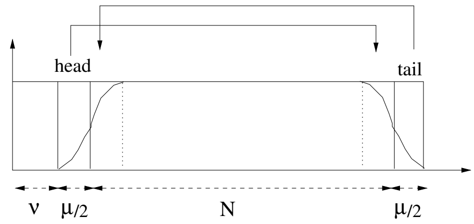

Figure 4.6: A non-rectangular window lowers the DFT sinc filters. The head is folded on the symbol tail end the tail is folded on the symbol head.

troduction of ISI nor ICI by the windowing operation, a part of the cyclic extension is not discarded in the receiver but needed in the windowing operation. In [109], one extends the cyclic prefix with $\frac{\mu}{2}$ samples and add a cyclic suffix of $\frac{\mu}{2}$ samples, see **Fig. 4.6**. At the receiver, the first ν samples are removed and a non-rectangular window (mostly with raised cosine shape) is applied to the remaining $\mu + N$ samples. Afterwards the first and the last $\mu/2$ samples, *i.e.* the head and the tail, are folded such that we end up again with a symbol of length N. The folding operation on the $(N + \mu)$-length symbol ensures that windowing does not introduce ISI nor ICI.

These window and fold operations are equivalent to the multiplication of each time domain symbol of length $\mu + N$ with the following matrix

$$\mathbf{W}_{N\times(\mu+N)} = \begin{bmatrix} 0 & \mathbf{D}_1 & 0 & 0 & \mathbf{D}_3 \\ 0 & 0 & \mathbf{I}_{N-\mu} & 0 & 0 \\ \mathbf{D}_4 & 0 & 0 & \mathbf{D}_2 & 0 \end{bmatrix} \tag{4.16}$$

where the $(\mathbf{D}_i)_{\frac{\mu}{2}\times\frac{\mu}{2}}$ are diagonal matrices with the windowing coefficients.

The modified per tone algorithm is deduced as follows. The output of the frequency domain equalizer becomes

$$\begin{aligned} Z_i^{(k)} &= D_i \cdot \mathrm{row}_i(\mathcal{F}_N) \cdot (\mathbf{W} \cdot \mathbf{Y}_{(\mu+N)\times T} \cdot \mathbf{w}) \\ &= \mathrm{row}_i(\underbrace{\mathcal{F}_N \cdot \mathbf{W}}_{\mathcal{F}_{win}} \cdot \mathbf{Y}) \cdot \mathbf{w}_i \end{aligned} \tag{4.17}$$

The appropriate data model for the received signal y is an extension of the basic data model, given in formula (2.16), in that a prefix as well as a suffix is assumed. This can be achieved by substituting $\mathbf{P} = \left[\begin{array}{c|c} \mathbf{O} & \mathbf{I}_\nu \\ \hline \multicolumn{2}{c}{\mathbf{I}_N} \end{array}\right]$ by

$\left[\begin{array}{cc|c} \mathbf{O} & \mathbf{O} & \mathbf{I}_{\nu+\frac{\mu}{2}} \\ \hline \multicolumn{3}{c}{\mathbf{I}_N} \\ \hline \mathbf{I}_{\frac{\mu}{2}} & \mathbf{O} & \mathbf{O} \end{array}\right]$ and adapting accordingly the number of zero rows in the zero padded Toeplitz matrix with the channel impulse response. Alternatively, one can apply the data model with pulse shaping and windowing, given in formula (2.22), to study VDSL performance. The cost function to be minimized becomes

$$\min_{\mathbf{w}_i} J(\mathbf{w}_i) = \min_{\mathbf{w}_i} \mathcal{E}\left\{ \left| \bar{\mathbf{w}}_i^{\mathrm{T}} \cdot \begin{bmatrix} \boxed{\mathcal{F}_{win}(i,:)} & 0 & \cdots \\ & \ddots & \ddots \\ 0 & \cdots & \boxed{\mathcal{F}_{win}(i,:)} \end{bmatrix} \cdot \mathbf{y} - X_i^{(k)} \right|^2 \right\} \tag{4.18}$$

Remark that matrix $\mathbf{W} \cdot \mathbf{Y}$ is no longer Toeplitz. Therefore applying a sliding FFT on the windowed received samples is not possible. Hence if one wants to combine windowing with per tone equalization, one needs T FFTs as described in equation (4.17), which is expensive. However it will be demonstrated that a (time domain) window is equivalent to a particular set of per tone equalizers. Hence with this frequency domain equivalent representation, we are again able to implement the effect of windowing together with the efficient version of per tone equalization as described by equation (4.8).

Theorem 4.4.1. *A (time domain) window can be represented by a particular set of per tone equalizers.*

Proof:
The taps of the window, *i.e.* the non-zero elements of the matrix $\mathbf{W}$, are denoted as

$$\begin{aligned} &\left[\, d_{-\mu} \ \ \ldots \ \ d_{-1} \,\middle|\, d_0 \ \ \ldots \ \ d_{N-\mu-1} \,\middle|\, d_{N-\mu} \ \ \ldots \ \ d_{N-1} \,\right] \\ &= \\ &\left[\, \mathrm{diag}(\mathbf{D}_4) \ \ \mathrm{diag}(\mathbf{D}_1) \,\middle|\, \mathrm{diag}(\mathbf{I}) \,\middle|\, \mathrm{diag}(\mathbf{D}_2) \ \ \mathrm{diag}(\mathbf{D}_3) \,\right] \end{aligned} \tag{4.19}$$

A crucial assumption is that $d_n + d_{n+N} = 1$, which in general holds true [109]. With $\alpha = e^{-\frac{j2\pi(i-1)}{N}}$, we obtain

$$
\begin{aligned}
\mathcal{F}_{win}(i,:) &= \mathrm{row}_i(\mathcal{F}_N \cdot \mathbf{W}) \\
&= \alpha^{\frac{\mu}{2}} \cdot \left[\, d_{-\mu}\alpha^{N-\mu} \;\; \ldots \;\; d_{-1}\alpha^{N-1} \,\middle|\, d_0\alpha^0 \;\; \ldots \;\; d_{N-1}\alpha^{N-1} \,\right] \\
&= \alpha^{\frac{\mu}{2}} \cdot \left[\, d_{-\mu}\alpha^{N-\mu} \;\; \ldots \;\; d_{-1}\alpha^{N-1} \,\middle|\, 1 \,\right] \cdot \left[\begin{array}{c|c|c} \mathbf{I}_\mu & \mathbf{O} & -\mathbf{I}_\mu \\ \hline \mathbf{O} & \multicolumn{2}{c}{\mathcal{F}_N(i,:)} \end{array}\right] \\
&= \alpha^{\frac{\mu}{2}} \cdot \left[\, d_{-\mu}\alpha^{N-\mu} \;\; \ldots \;\; d_{-1}\alpha^{N-1} \,\middle|\, 1 \,\right] \cdot \begin{bmatrix} 1 & -\alpha & 0 & \\ 0 & 1 & \ddots & 0 \\ & \ddots & \ddots & -\alpha \\ & & 0 & 1 \end{bmatrix} \\
&\qquad \cdot \begin{bmatrix} \boxed{\mathcal{F}_N(i,:)} & 0 & \cdots \\ & \ddots & \ddots \\ 0 & \cdots & \boxed{\mathcal{F}_N(i,:)} \end{bmatrix} \\
&= \bar{\mathbf{g}}_i^{\mathrm{T}} \cdot \begin{bmatrix} \boxed{\mathcal{F}_N(i,:)} & 0 & \cdots \\ & \ddots & \ddots \\ 0 & \cdots & \boxed{\mathcal{F}_N(i,:)} \end{bmatrix}
\end{aligned} \tag{4.20}
$$

In the second line, the ith row of the DFT matrix is multiplied with matrix $\mathbf{W}$. In the third line, we apply that the coefficients $d_0 \ldots d_{N-\mu+1}$ are equal to one, as is clear from formula (4.19) and that $d_n + d_{n+N} = 1$ holds for the other windowing coefficients. Finally, in the fourth line, the matrix which extracts the difference terms and computes one FFT for tone i, is decomposed as a product of two Toeplitz matrices, the last of these containing $\mu + 1$ FFT operations for tone i. It appears that windowing of a symbol with an extra prefix of size μ is equivalent to an $(\mu + 1)$-taps per tone equalizer $\mathbf{g}_i$ for tone i. Remark that this theorem is independent of the data model for the received signal y. $\square$

The overall per tone equalizer then becomes $\mathbf{w}_i \otimes \mathbf{g}_i$. Such equalizer has $T + \mu$ taps, so it needs $T + \mu$ FFTs or, according to formula (4.8) the corresponding modified overall per tone equalizer can be used such that only one FFT and $T + \mu - 1$ difference terms have to be computed.

By optimizing the overall per tone equalizer for each tone, we are now able to implicitly optimize the window in a per tone fashion. Thus by extending the per tone equalizer from T to $T + \mu$ taps, the resulting SNR is always better than for a T-taps equalizer combined with a fixed (time domain) window with an extra cyclic extension of μ samples.

The advantage of a *fixed* window is improved performance (with respect to a receiver without windowing) at low complexity for arbitrary RFI frequencies because the goal of a fixed window is to lower the sidelobes of the FFT filters.

This is in contrast with the per tone equalizers. They may be optimized for certain RFI frequencies and therefore result in optimal performance for these RFI frequencies, but updating is necessary when RFI frequencies are changing. The (μ + 1)-taps per tone equalizers are also more expensive than 1 fixed window.

4.5 Simulation results

4.5.1 Per tone equalization versus TEQ

The performance of PT-EQ is compared with the TEQ, based on $||\mathbf{b}||_2^2 = 1$, for the same set of channels and parameters as in the previous chapter.

The bit rate gain in % for a certain delay is defined as

$$gain = 100 \cdot \frac{rate(T\text{-taps PT-EQ}) - rate(T\text{-taps TEQ})}{rate(T\text{-taps TEQ})} \% \qquad (4.21)$$

Downstream

In **Fig. 4.7** the bit rate as a function of the (relative) delay is given for a downstream 4km 26 AWG loop. The solid line gives the capacity for a 32-taps PT-EQ. This capacity is always higher and significantly smoother than the one given by the dashed-dotted line, for a 32-taps TEQ-based structure computed with the channel shortening procedure with unit norm TIR. Because the capacity of the TEQ for different values of the delay parameter is not a smooth curve, an optimal decision delay is not easily selected beforehand. The PT-EQ however shows a smooth behaviour. Hence, selecting an appropriate decision delay is not so critical.

The dashed line shows the capacity with 8-taps PT-EQs for the used tones for each delay. It is seen that for a comparable performance, one can reduce the equalizer filter length from 32 (for TEQ) down to 8 taps (for PT-EQ). It is worth noting that shorter equalizers have a smaller delay range in which optimum capacity is achieved. Finally the dotted line corresponds to the capacity of an 8-taps TEQ. We have an average[5] bit rate gain of 7,5% for $T = 32$ and 8% for $T = 8$.

Investigation of the SNR distribution over the used tones shows that the traditional approach of computing TEQ taps causes dips in the SNR distribution whereas the PT-EQ has a smooth SNR distribution. This is shown in the bot-

[5]The gain is averaged in the delay range of optimal capacity, *i.e.* (-10:20) for $T = 32$ and (-15:0) for $T = 8$.

tom figure where the SNR is plotted over the used tones for the delay range [-40:10:30], *i.e.* from delay -40 to delay 30 in steps of 10.

Equalization of one tone is now independent of equalization of all the other tones. Hence, the equalization effort may be concentrated on the most affected tones by adjusting T for each tone. Comparing the SNR of 8- and 32-taps PT-EQ, one sees that the main gain of extra taps lies in the lowest tones, *i.e.* near the edges of the used band (or near the cut-off frequency of the transmit/receive filters). Tone dependent equalizer lengths are especially interesting when Radio Frequency Interference (RFI) is present. Longer equalizers in the neighborhood of the interferer improve performance of the system without drastic complexity increase.

Similar conclusions may be drawn from **Fig. 4.8** for the downstream standard loop CSA-#4, which has bridged taps. Remark also the odd behavior of the TEQ in that an 8-taps TEQ may result in a higher capacity than a 32-taps TEQ for a certain delay. This is impossible with PT-EQ for which a higher number of taps always results in higher capacity for a certain delay. The average bit rate gain is 5% for $T = 32$ and 6% for $T = 8$.

Fig. 4.9 shows the bit rate and gain as a function of the loop length for 26 AWG loops for a fixed delay, $\delta = -8$. Hence no delay optimization is done. The average (averaged over the loop length) gain is 8,3% for $T = 32$ and 5,5% for $T = 8$. A similar simulation is done for the reference loops, simulation results of which are given in **Fig. 4.10**. The gain for loops 2 and 3 seems to be very high, however this is due to the fact that delay -8 is not in the optimal delay range for $T = 8$. For reference loop 2, the optimal delay is around -20 and for reference loop 3, the optimal delay is around -17. The average gain is 7.5% for $T = 32$ and 6% for $T = 8$ (loops 2 and 3 not taken into account).

Upstream

Analogous simulations are performed for upstream. **Fig. 4.11** shows the bit rate as a function of the delay and corresponding SNRs as a function of the tones for an upstream 4km 26 AWG loop. With 64-taps PT-EQ, the SNR is increased significantly over the whole tone range with respect to 16-taps PT-EQ. The optimal bit rate for 64-taps TEQ is comparable with the bit rate for 16-taps PT-EQ. The average bit rate gain is 30% for $T = 64$ (in delay range (10:40)) and 45% for $T = 16$ (in delay range (-5:10)). **Fig. 4.12** shows the bit rate and the SNR for upstream standard loop CSA-#4. The bit rate gain is 53% for $T = 64$ and 49% for $T = 16$. The optimal delay for $T = 64$ lies around 30 whereas the optimal delay for $T = 16$ is between 5 and 10.

In **Fig. 4.13**, the bit rate and the gain are plotted as a function of the loop length for 26 AWG loops. No delay optimization is done. The delay for $T = 64$ is fixed at $\delta = 30$ and the delay for $T = 16$ at $\delta = 6$. It is seen that the bit rate for 16-taps PT-EQ is comparable with 64-taps TEQ. The average (averaged over the loop length) gain is 35% for $T = 64$ and 50% for $T = 16$. **Fig. 4.14** shows the bit rate for the reference loops in upstream with fixed delay ($\delta = 30$ and $\delta = 6$). The bit rate for 64-taps PT-EQ is clearly higher than for the other equalizers. 16-taps PT-EQ results in a comparable bit rate as 64-taps TEQ. For loops 2 and 3, it turned out that $\delta = 6$ is not in the optimal delay range for $T = 16$. The optimal delay for loop 2 is situated around $\delta = -5$, and for loop 3 around $\delta = 1$. The average bit rate gain is 33% for $T = 64$ and 46% for $T = 16$ (loops 2 and 3 not taken into account).

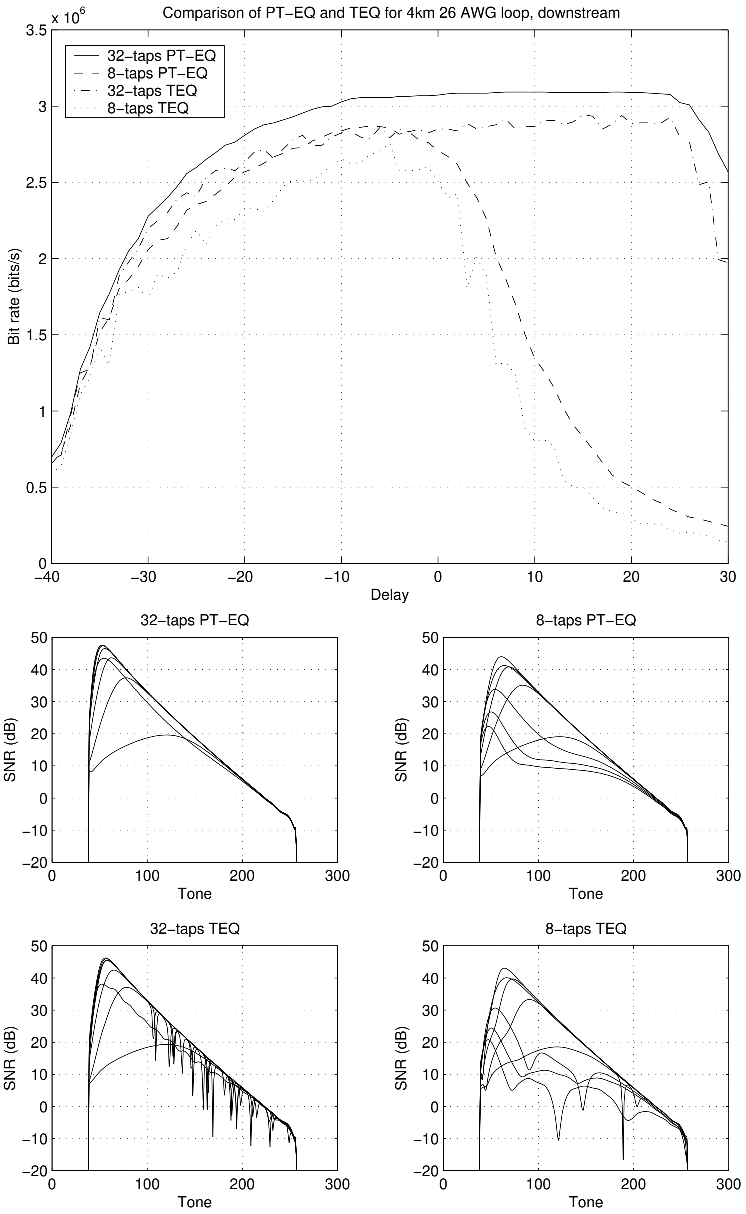

Figure 4.7: Bit rate as a function of the (relative) delay and SNR as a function of the tones (for different delay values) for a downstream 4km 26 AWG loop.

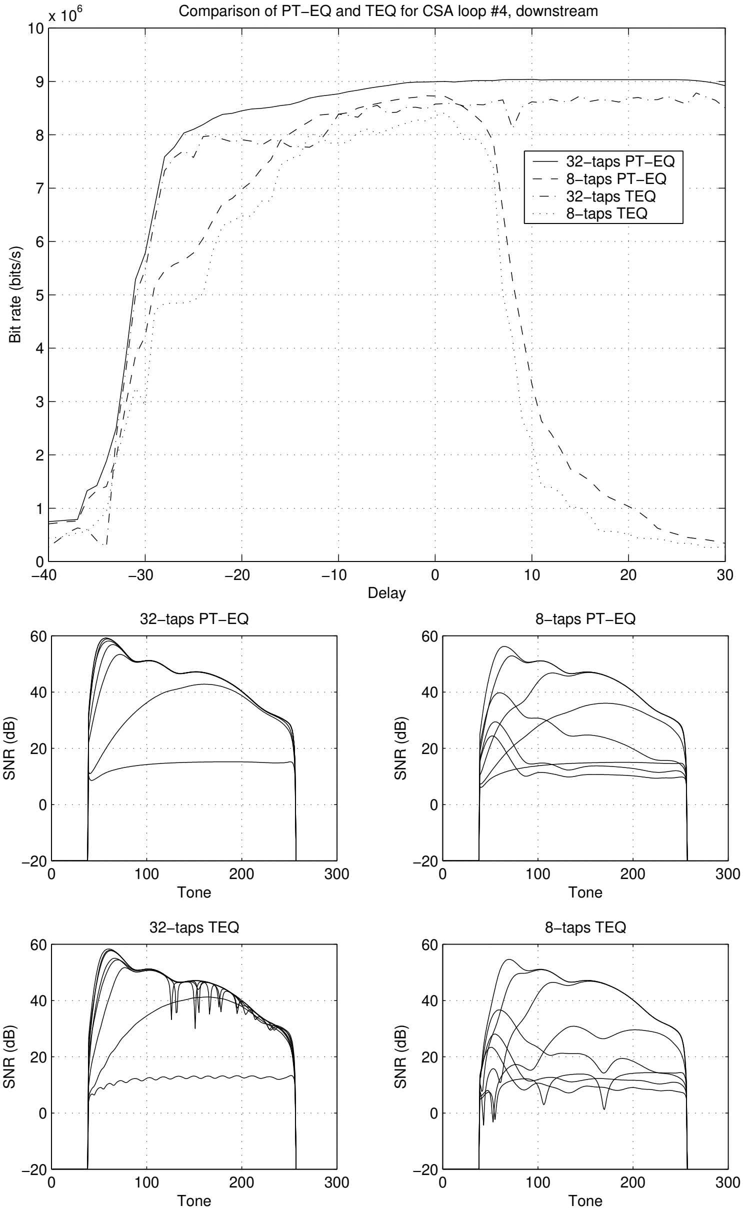

Figure 4.8: Bit rate as a function of the (relative) delay and SNR as a function of the tones for downstream standard loop CSA-#4.

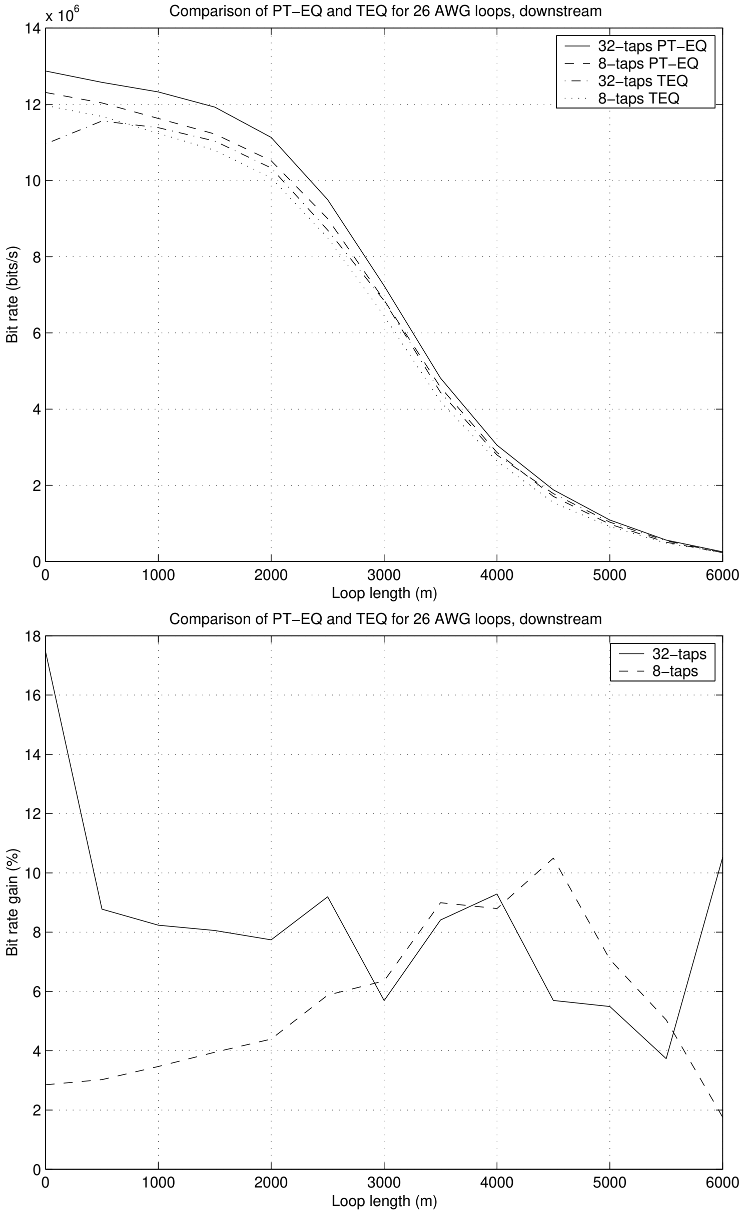

Figure 4.9: Bit rate and gain as a function of loop length for downstream 26 AWG loops with fixed delay -8.

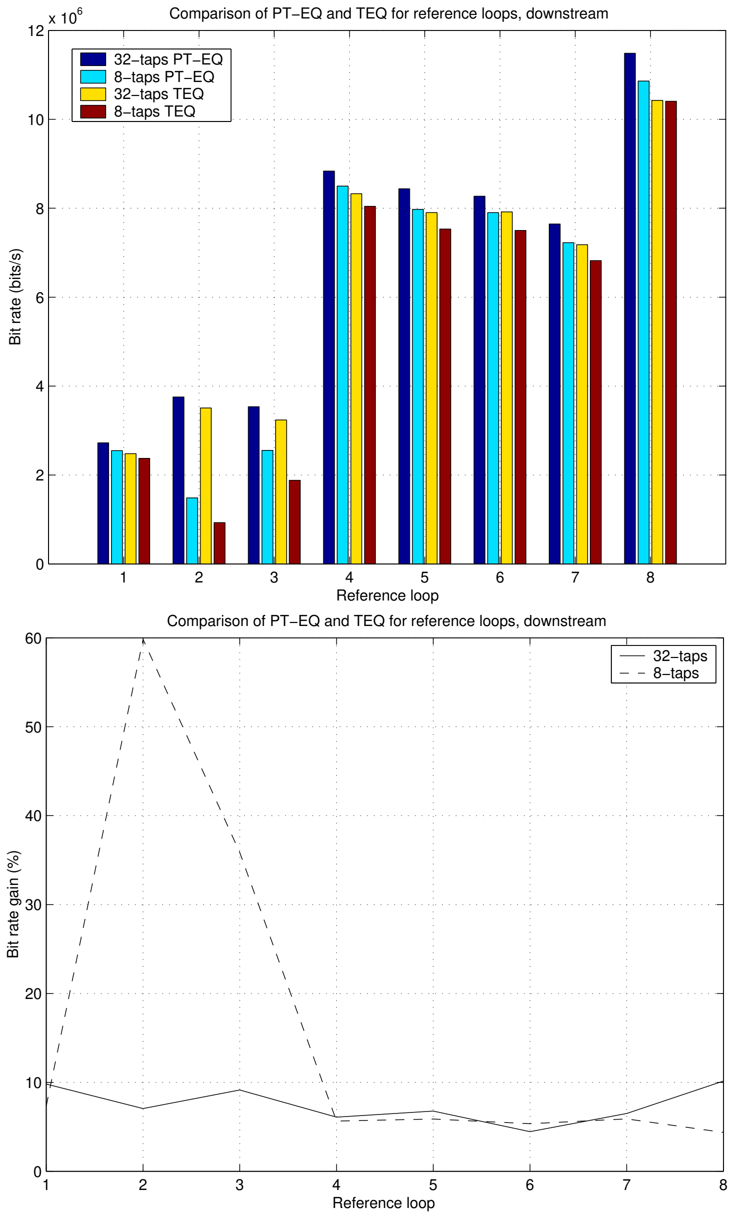

Figure 4.10: Bit rate and gain as a function of loop number for downstream reference loops (T1.601-#7, T1.601-#9, T1.601-#13, CSA-#4, CSA-#6, CSA-#7, CSA-#8, mid-CSA) with fixed delay -8.

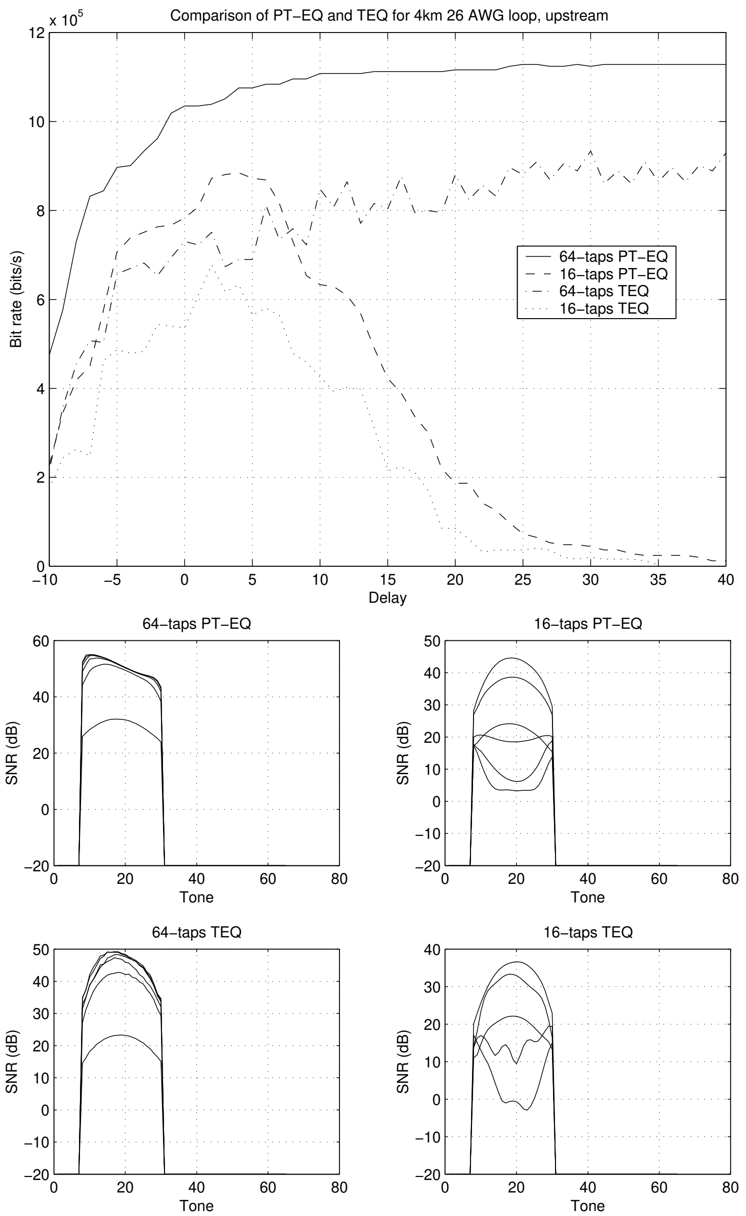

Figure 4.11: Bit rate as a function of the (relative) delay and SNR as a function of the tones for an upstream 4km 26 AWG loop.

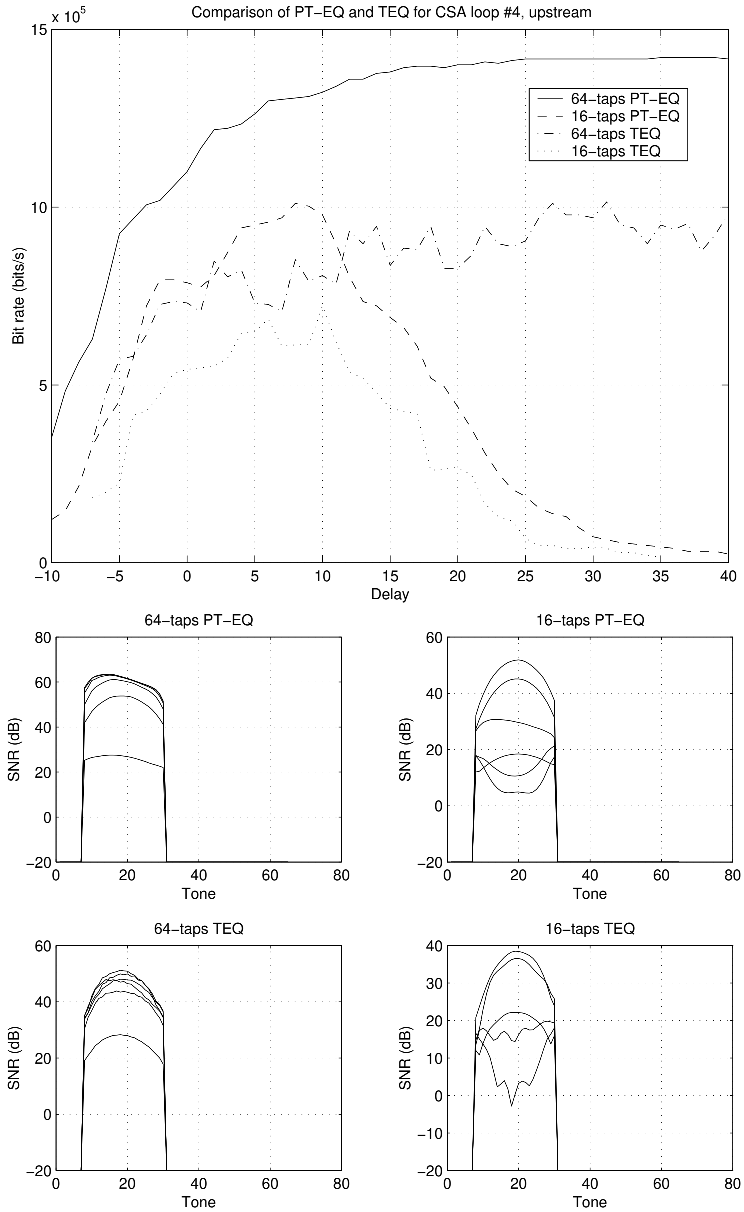

Figure 4.12: Bit rate as a function of the (relative) delay and SNR as a function of the tones for upstream standard loop CSA-#4.

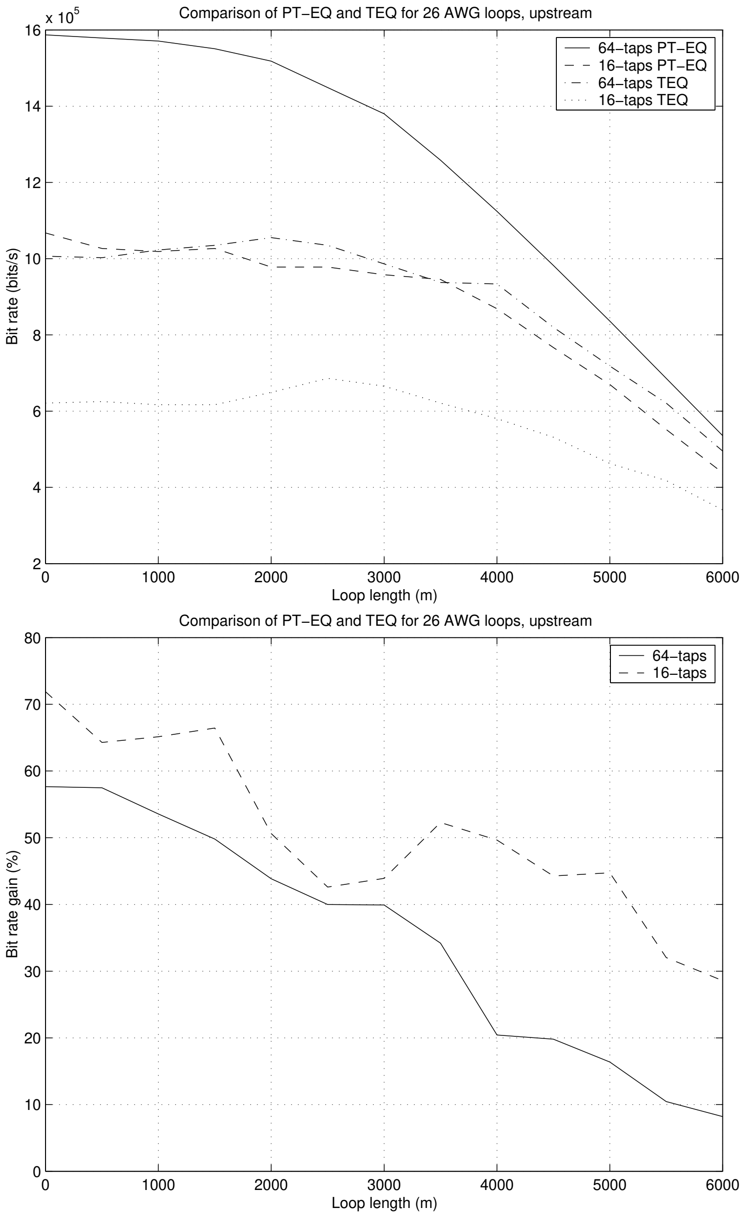

Figure 4.13: Bit rate and gain as a function of loop length for upstream 26 AWG loops with fixed delay 30 (for $T = 64$) and fixed delay 6 (for $T = 16$).

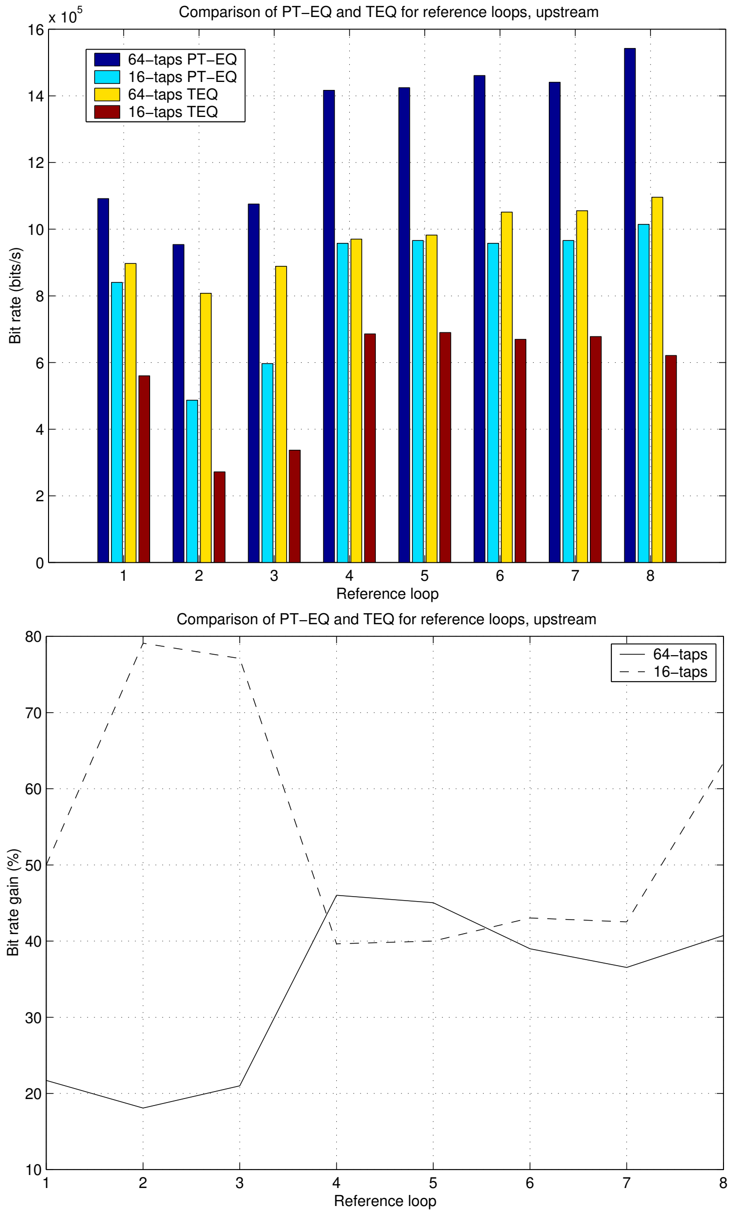

Figure 4.14: Bit rate and gain as a function of loop number for upstream reference loops (T1.601-#7, T1.601-#9, T1.601-#13, CSA-#4, CSA-#6, CSA-#7, CSA-#8, mid-CSA) with fixed delay 30 (for $T = 64$) and fixed delay 6 (for $T = 16$).

4.5.2 Windowing

The robustness of DMT to RFI is investigated. Both windowing and per tone equalization are simulated. The data model of section 2.2.1 is adopted, but to simulate the performance of windowing, we increase the length of the cyclic extension to $\nu + \mu$, with ν the length of the classical prefix and μ the number of extra samples in the cyclic extension for (time domain) windowing. The following scenarios are considered:

- T=16, prefix of length 32, *i.e.* $\nu = 32$ and $\mu = 0$
- T=16, prefix of length 32 combined with a (time domain) window, *i.e.* $\nu = 32$ and $\mu = 44$.
- T=16+22, prefix of length 76, *i.e.* $\nu = 76$ and $\mu = 0$
- T=16+44, prefix of length 76, *i.e.* $\nu = 76$ and $\mu = 0$

The bitrate is given by the following formula:

$$rate = (\sum_{i=used\ tone} b_i) \cdot \frac{F_s}{N + \nu + \mu} \tag{4.22}$$

Higher SNR results in more bits per symbol (first factor). Enlarging the symbol length results in a lower symbol rate (second factor).

A 4km 26 AWG downstream loop is considered. Eight RFI's are added. They are modeled as pure sinusoids with frequencies 150.5, 155.5, 160.5, 163.5, 168.5, 200.5, 203.5, 210.5, each multiplied with the tone spacing (4.3125 kHz). The bitrate as a function of the delay and the SNR corresponding to the highest bitrate are shown. The zero reference delay corresponds to the $\nu + \mu$ samples of the far end channel with highest energy.

For same T, windowing gives rise to a considerable SNR increase and capacity increase, even with the extra cyclic extension overhead (μ samples), as can be seen by comparing dashed-dotted line and dotted line in **Fig. 4.15**.

However, by enlarging the per tone equalizer, one can also achieve high capacity without windowing. This is because the per tone equalizer effectively optimizes the SNR for each tone. Hence, with sufficiently long per tone equalizers, the equalizer is able to model a proper window in its taps. The solid line corresponds to $T = 60$ taps whereas the dashed-dotted line corresponds to $T = 16$ taps with fixed window. Even with $T = 38$, an improved capacity with respect to the fixed window, is obtained.

Note that the ratio between the bit rates of the equalizer/windowing combinations is loop dependent. For instance, for this loop, the equalizer defined by

$T = 16$, $\nu = 32$ and $\mu = 0$ has a significant SNR loss with respect to the other methods on the lowest tones. For this reason, the gap between the bit rates for the first and the second method is so large.

4.5.3 Single-input/multiple-output equalizer

PT-EQ is a special case of the so-called multiple-input/multiple-output (MIMO) equalizer [93, 128]. A MIMO equalizer combines multiple outputs of the demodulating FFT for the equalization of a particular tone. That is, FFT outputs of tones $i' \neq i$ and the FFT output of tone i itself are multiple inputs for the equalizer of tone i, whereas the PT-EQ only considers the FFT output of tone i as input to the equalizer of tone i. In fact, each per tone equalizer forms a single-input/single-output (SISO) equalizer.

Furthermore, a MIMO equalizer could work at symbol rate, *i.e.* the demodulating FFT is applied at symbol rate. Or, one could consider fractionally spaced MIMO equalizers, *i.e.* the FFT is applied at m times the symbol rate. In the special case where $m = N + \nu$, one applies the FFT at sample rate. This is exactly what happens in the PT-EQ-based receiver: a sliding FFT on the received sample sequence provides T successive FFTs as inputs to the PT-EQ.

Finally, an even more general receiver structure is the so-called single-input/multiple-output (SIMO) equalizer where the cascade of the FFT and MIMO equalizer is replaced by a set of parallel filters (one filter for each used tone) [93, 129, 130]. Remark that there was no cyclic prefix involved in the MIMO and SIMO equalizers presented in [93, 128, 129, 130].

In **Fig. 4.16**, we compare PT-EQ and SIMO equalization for a downstream 4km 26 AWG loop. For both methods the symbol size equals $N = 512$ and the cyclic prefix is $\nu = 32$. The PT-EQs have $T = 32$ taps for each used tone. The SIMO equalizers have $N + T - 1 = 543$ taps for each used tone and do not have a demodulating FFT. The stars indicate the SIMO bit rates for the simulated delays. The SIMO bit rate forms indeed an upper bound for the PT-EQ bit rates. But then it is seen that the PT-EQ bit rate is very close to this bound, especially in the optimal delay-range. Moreover, PT-EQ has a much lower complexity than SIMO equalization because part of the receiver is fixed in the demodulating FFT and so less taps have to be initialized.

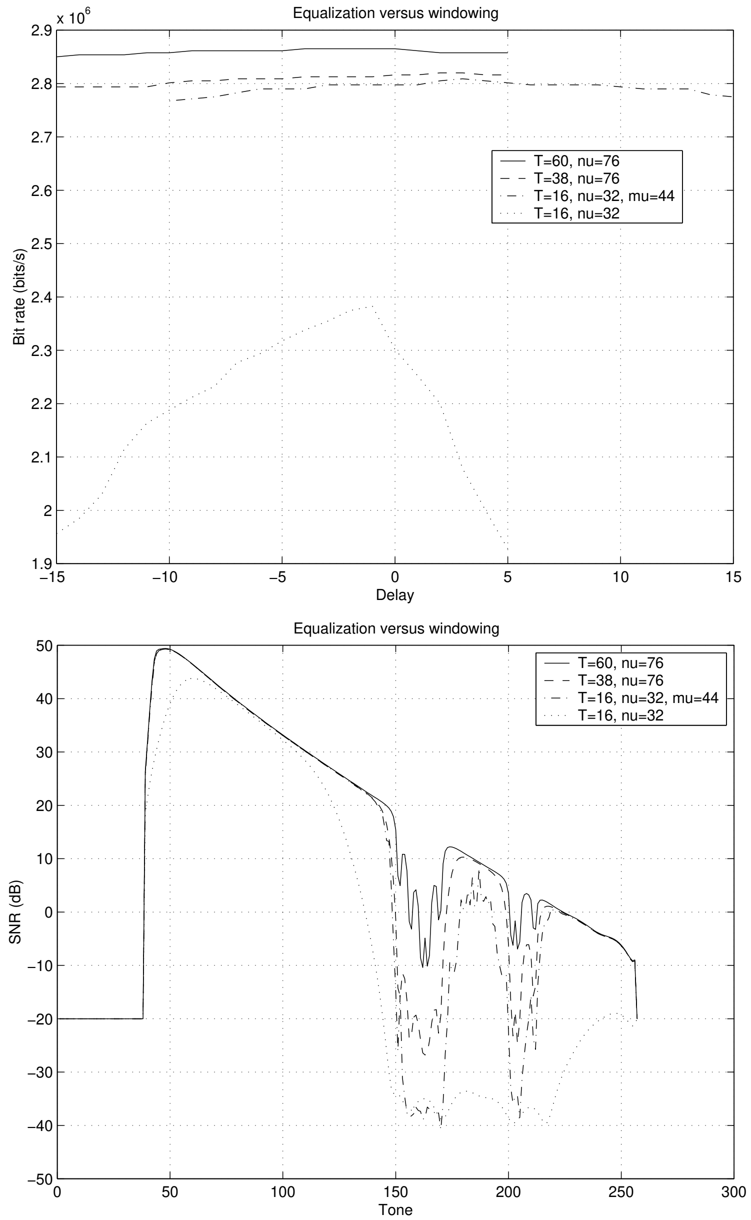

Figure 4.15: Comparison of PT-EQ schemes and windowing for a 4km 26 AWG downstream loop and 8 RFI's.

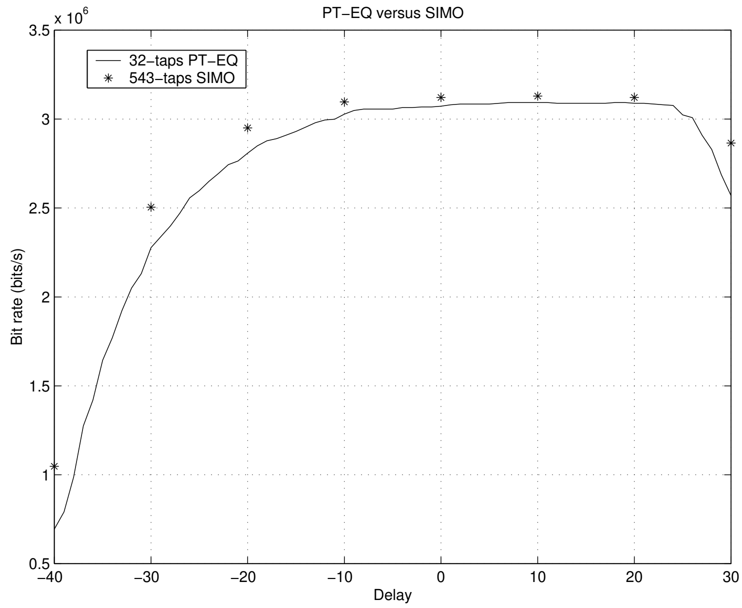

Figure 4.16: Comparison of PT-EQ and SIMO for a 4km 26 AWG downstream loop.

4.6 Conclusions

Per tone equalization has been derived. Each used tone then has its own (complex) TEQ, after demodulation. The large improvement with respect to the TEQ, is that we can optimize the bit rate in a per tone fashion by means of an MMSE problem per tone. The PT-EQ bit rate is an upper bound for the TEQ bit rate and is very smooth as a function of the decision delay, which has been shown in simulations.

The complexity during data transmission has been computed and compared with the complexity of the TEQ. Because T successive FFTs per symbol can be computed efficiently by means of one FFT and $T-1$ difference terms, the complexity of PT-EQ is comparable to the complexity of TEQ, if all tones are used. However, PT-EQ allows optimization of the number of taps per tone and one can set the number of taps to zero for the unused tones, which results in a complexity saving. The drawback of PT-EQ is the increased memory, with respect to a TEQ-based receiver, needed for the storage of the PT-EQ taps.

The combination of PT-EQ and windowing has been studied. Time domain windowing can not be combined with the efficient PT-EQ structure. However, it has been shown that a time domain window is equivalent to a particular set of PT-EQs. Hence, the effect of windowing can be implemented in the frequency domain as a part of the efficient PT-EQs. By optimizing the overall PT-EQ, the window is implicitly optimized in a per tone fashion.

We have compared the performance of PT-EQ and SIMO equalization, where the convolution of the demodulating FFT and the per tone equalizer is considered as one equalizer (for each used tone) that can be optimized per tone. SIMO equalization has been shown to perform only a slight bit rate increase for a large complexity increase with respect to PT-EQ.

4.A Appendix: sliding FFT

Property 4.A.1. *The FFT of successive columns of a Toeplitz matrix can be computed as given by equation (4.4).*

Proof:
Given 2 vectors: $\mathbf{a} = [a_0\, a_1 \ldots a_{N-1}]$ and $\mathbf{b} = [b_0\, b_1 \ldots b_{N-1}] = [c\, a_0\, a_1 \ldots a_{N-2}]$. The FFT of $\mathbf{a}$ is

$$A_{i-1} = \sum_{k=0}^{N-1} a_k e^{-j2\pi \frac{(i-1)k}{N}} \tag{4.23}$$

where $i = 1 \ldots N$ is the tone index. The FFT of $\mathbf{b}$ is

$$\begin{aligned} B_{i-1} &= \sum_{k=0}^{N-1} b_k e^{-j2\pi \frac{(i-1)k}{N}} && (4.24) \\ &= c + \sum_{k=1}^{N-1} a_{k-1} e^{-j2\pi \frac{(i-1)k}{N}} && (4.25) \\ &= c + \left(\sum_{k=0}^{N-2} a_k e^{-j2\pi \frac{(i-1)k}{N}} \right) e^{-j2\pi \frac{(i-1)}{N}} && (4.26) \end{aligned}$$

With phase $\mathbf{p}$ defined as in equation (4.4), one obtains

$$\begin{aligned} \mathbf{p}(i-1) &= e^{-j2\pi \frac{i-1}{N}} && (4.27) \\ A_{i-1} \cdot \mathbf{p}(i-1) &= \left(\sum_{k=0}^{N-2} a_k e^{-j2\pi \frac{(i-1)k}{N}} \right) e^{-j2\pi \frac{i-1}{N}} + a_{N-1} && (4.28) \end{aligned}$$

By comparison of equations (4.26) and (4.28), one obtains

$$B_{i-1} = A_{i-1} \cdot \mathbf{p}(i-1) - a_{N-1} + c \quad \text{for} \quad i = 1 \ldots N \tag{4.29}$$

□

4.B Appendix: per tone equalizers $\mathbf{w}_i$ versus $\mathbf{v}_i$

Property 4.B.1. *The original PT-EQ $\mathbf{w}_i$ and the modified PT-EQ $\mathbf{v}_i$ are related by equation (4.5). An efficient recursion formula is given in equation (4.6).*

Proof:
Without loss of generality, we take $T = 3$ and $N = 4$. Analogous to equation (4.3), we write the demodulated output for the ith tone as:

$$Z_i^{(k)} = \mathcal{F}_4(i,:) \cdot \begin{bmatrix} c & b & a \\ d & c & b \\ e & d & c \\ f & e & d \end{bmatrix} \cdot \mathbf{w}_i \tag{4.30}$$

where the matrix contains received signal samples and $\mathbf{w}_i$ is a 3×1 vector. This expression can be split into a circulant part and a correction on this part, as follows:

$$Z_i^{(k)} = \mathcal{F}_4(i,:) \cdot \left(\begin{bmatrix} c & f & e \\ d & c & f \\ e & d & c \\ f & e & d \end{bmatrix} + \begin{bmatrix} 0 & b-f & a-e \\ 0 & 0 & b-f \\ 0 & 0 & 0 \\ 0 & 0 & 0 \end{bmatrix} \right) \cdot \mathbf{w}_i \tag{4.31}$$

Let A_{i-1} be $\mathcal{F}_4(i,:)$ times the first column of the circulant matrix. The $\mathcal{F}_4(i,:)$ operating on the other columns, which are circular shifts of the first column, gives rise to an additional phase. With $\alpha = e^{-j2\pi\frac{1}{N}}$ (here $N = 4$), the $\mathcal{F}_4(i,:)$ operating on the second matrix is written as a 'normal' FFT-operation[6]:

$$Z_i^{(k)} = A_{i-1} \cdot [\,1 \,|\, \alpha^{i-1} \,|\, \alpha^{(T-1)(i-1)}\,] \cdot \mathbf{w}_i + [\,0 \,|\, (b-f) \,|\, (a-e) + (b-f) \cdot \alpha^{i-1}\,] \cdot \mathbf{w}_i \tag{4.32}$$

One can now write the last expression in an other form by considering A_{i-1} and the differences as inputs of the modified PT-EQ

$$\begin{aligned} Z_i^{(k)} =& A_{i-1} \cdot \underbrace{[1 \,|\, \alpha^{i-1} \,|\, \alpha^{(T-1)(i-1)}] \cdot \mathbf{w}_i}_{v_{i,0}} + (b-f) \cdot \underbrace{[0 \,|\, 1 \,|\, \alpha^{i-1}] \cdot \mathbf{w}_i}_{v_{i,1}} \\ &+ (a-e) \cdot \underbrace{[0 \;\; 0 \;\; 1] \cdot \mathbf{w}_i}_{v_{i,2}} \end{aligned} \tag{4.33}$$

[6] $\mathcal{F}_N(i,:) = [\,1 \,|\, \alpha^{(i-1)\cdot 1} \,|\, \ldots \,|\, \alpha^{(i-1)(N-1)}\,]$

The modified PT-EQ, *i.e.* the PT-EQ with these new inputs, is then found as

$$\begin{bmatrix} v_{i,0} \\ v_{i,1} \\ v_{i,2} \end{bmatrix} = \begin{bmatrix} 1 & \alpha^{i-1} & \alpha^{(T-1)(i-1)} \\ 0 & 1 & \alpha^{i-1} \\ 0 & 0 & 1 \end{bmatrix} \cdot \mathbf{w}_i \tag{4.34}$$

or similarly

$$\begin{bmatrix} v_{i,0} & v_{i,1} & v_{i,2} \end{bmatrix} = \mathcal{F}_4(i,:) \cdot \begin{bmatrix} w_{i,0} & w_{i,1} & w_{i,2} \\ w_{i,1} & w_{i,2} & 0 \\ w_{i,2} & 0 & 0 \\ 0 & 0 & 0 \end{bmatrix} \tag{4.35}$$

From $\begin{bmatrix} 1 & \alpha^{i-1} & \alpha^{(T-1)(i-1)} \\ 0 & 1 & \alpha^{i-1} \\ 0 & 0 & 1 \end{bmatrix}^{-1} = \begin{bmatrix} 1 & -\alpha^{i-1} & 0 \\ 0 & 1 & -\alpha^{i-1} \\ 0 & 0 & 1 \end{bmatrix}$ it follows that a simple recursion formula may be obtained, namely

$$v_{i,t+1} \cdot \alpha^{i-1} + w_{i,t} = v_{i,t} \tag{4.36}$$

for tone $i = 1 \ldots N$ with $t = 0 \ldots T-2$ and $v_{i,T-1} = w_{i,T-1}$. $\square$

SFGs of the recursion are presented in **Fig. 4.3** for transformation from $\mathbf{v}_i$ to $\mathbf{w}_i$ and vice versa.

Chapter 5

Per tone equalizer initialization

The optimal PT-EQs are the solution of an MMSE problem per tone, as explained in the previous chapter. However, this direct PT-EQ computation has a high computational cost. Therefore, in this chapter, we search for a computational efficient scheme and derive a recursive initialization algorithm, *i.e.* based on training symbols.

In section 5.1, we state the cost function to be minimized by the recursive initialization scheme. Due to the large eigenvalue spread of the autocorrelation matrix of the filter input, Least Mean Squares (LMS) based initialization schemes have poor convergence properties, which is clear from the simulation results in section 5.5. For this reason, we develop a recursive initialization scheme based on Recursive Least Squares (RLS).

RLS with inverse updating [90] is explained and adopted to the PT-EQs in section 5.2. The complexity of the RLS scheme is quadratic in the filter length. However, by choosing the order of the inputs such that the real difference terms are applied first and the complex FFT output is applied last to the PT-EQ, the resulting initialization scheme will have a real quadratic part in common for all used tones. An extra complex part is added for each tone separately but this part has a linear complexity.

In section 5.3, we introduce tone grouping as a means to decrease the initialization complexity. The PT-EQ is computed only for the center tone of each group (by direct or recursive initialization). Afterwards this center tone equalizer is recomputed to be applied to the other tones of the same group.

In section 5.4, we compute the complexity of RLS with inverse updating adopted to PT-EQ with and without tone grouping.

Simulation results for tone grouping, LMS and RLS are given in section 5.5. It is seen that RLS achieves good performance with an acceptable number of training symbols. Finally, conclusions are given in section 5.6.

5.1 Recursive initialization

Direct equalizer coefficient computation, based on the knowledge of the channel impulse response as well as the signal and noise characteristics, see section 4.2, has an excessively high computational cost. However, formula (4.8) may also be used for a training sequence based initialization of the per tone equalizers. If a training sequence $X_{1:N}^{(k)}$, $k = 1 \ldots K$, is transmitted, the optimal $\mathbf{v}_i$ for tone i is computed as (compare to formula (4.8))

$$\min_{\mathbf{v}_i} J(\mathbf{v}_i) = \min_{\mathbf{v}_i} \sum_{k=1}^{K} \left| \bar{\mathbf{v}}_i^{\mathrm{T}} \cdot \mathbf{z}_i^{(k)} - X_i^{(k)} \right|^2 \tag{5.1}$$

with $\mathbf{z}_i^{(k)} = \mathbf{F}_i \cdot \mathbf{y}^{(k)}$. This least squares estimation problem may be solved recursively.

LMS-based schemes [50] for the PT-EQs have a low computational complexity ($\mathcal{O}(T)$ per training symbol with T the filter length). Unfortunately, they have poor convergence properties (due to a large eigenvalue spread of the correlation matrix of the filter input) and have indeed been shown to require an excessively large number of training symbols, as can be seen in section 5.5. The slow LMS-based initialization of the equalizer coefficients is inherent to the PT-EQ. The speed of convergence is largely determined by the minimum and maximum of the power spectral density (psd) of the (unequalized) signals at the demodulating FFT outputs. The sliding FFT at the receiver can be seen as a filterbank, each filter implementing a bandpass filter, rejecting signal components far from its central frequency. Because of the spectral containment of the demodulating FFT filter, LMS-based initialization is too slow.

Because of this poor convergence behavior, initialization based on a *Recursive Least Squares (RLS) scheme* [50] for each tone, has been investigated. The results are presented in the following section.

5.2 RLS-based initialization

RLS schemes have a higher computational complexity per training symbol ($\mathcal{O}(T^2)$) than LMS schemes but have optimal convergence properties and hence achieve initialization with an acceptably small number of training symbols. Instead of using the input vector directly in the filter update (as in LMS), the input vector is first transformed by the inverse of the correlation matrix of the input. The resulting so-called kalman vector $\mathbf{k}$ is then used in the filter update. It can be shown that the matrix determining the convergence in the mean of RLS, has T equal eigenvalues. Hence the eigenvalue spread is zero and the convergence is optimal.

More specifically, we use *RLS with so-called inverse updating* [90]. This scheme is based on storing and updating a lower triangular matrix $\mathbf{L}_i^{(k)}$ which is such that $\mathbf{L}_i^{(k)\mathrm{H}} \cdot \mathbf{L}_i^{(k)} = (\mathbf{R}_{\mathbf{z}_i}^{(k)})^{-1}$ for all k, with $\mathbf{R}_{\mathbf{z}_i}^{(k)}$ the correlation matrix of the filter input, $\mathbf{R}_{\mathbf{z}_i}^{(k)} = \sum_{j=1}^{k} \mathbf{z}_i^{(j)*} \cdot \mathbf{z}_i^{(j)\mathrm{T}}$, together with the least squares estimate $\bar{\mathbf{v}}_i^{(k)}$ at iteration k. The following formulas, with the tone index i omitted for compact notation, describe the RLS algorithm:

Algorithm Inverse Updating

For each used tone i

For $k = 1 \ldots K$

Given: $\mathbf{L}^{(k-1)}$, new observation vector $\mathbf{z}^{(k)}$, desired response $X^{(k)}$

Step 1. Form the matrix-vector product

$$\mathbf{a} = -\mathbf{L}^{(k-1)} \cdot \mathbf{z}^{(k)*}$$

Step 2. For $j = 1, \ldots, T$ determine unitary transformations $\mathbf{Q}_j$ so that

$$\left[\begin{array}{c} \mathbf{0} \\ \hline \delta^* \end{array}\right] \Leftarrow \mathbf{Q}_T \mathbf{Q}_{T-1} \ldots \mathbf{Q}_1 \cdot \left[\begin{array}{c} \mathbf{a} \\ \hline 1 \end{array}\right]$$

Step 3. Update $\mathbf{L}^{(k)}$

$$\left[\begin{array}{c} \mathbf{L}^{(k)} \\ \hline -\delta^* \cdot \mathbf{k}^{(k)\mathrm{T}} \end{array}\right] \Leftarrow \mathbf{Q}_T \mathbf{Q}_{T-1} \ldots \mathbf{Q}_1 \cdot \left[\begin{array}{c} \mathbf{L}^{(k-1)} \\ \hline \mathbf{0} \end{array}\right]$$

Step 4. Update $\bar{\mathbf{v}}^{(k)}$

$$\bar{\mathbf{v}}^{(k)} = \bar{\mathbf{v}}^{(k-1)} + \left(-\delta^* \cdot \mathbf{k}^{(k)\mathrm{T}}\right)^{\mathrm{H}} \cdot \left(-\frac{X^{(k)} - \mathbf{z}^{(k)\mathrm{T}} \cdot \bar{\mathbf{v}}^{(k-1)}}{\delta}\right)$$

end

$\bar{\mathbf{v}} = \bar{\mathbf{v}}^{(K)}$

end

In *Step 2*, $\mathbf{Q}_j$ is an elementary unitary transformation[1] acting upon the jth

[1] *i.e.* a transformation matrix that, whenever applied to a vector, modifies (only) two entries of the vector according to

$$\left[\begin{array}{c} a' \\ b' \end{array}\right] = \left[\begin{array}{cc} \cos\theta & e^{j\psi}\sin\theta \\ -e^{-j\psi}\sin\theta & \cos\theta \end{array}\right] \cdot \left[\begin{array}{c} a \\ b \end{array}\right].$$

Such a transformation is represented by a hexagon in the SFGs.

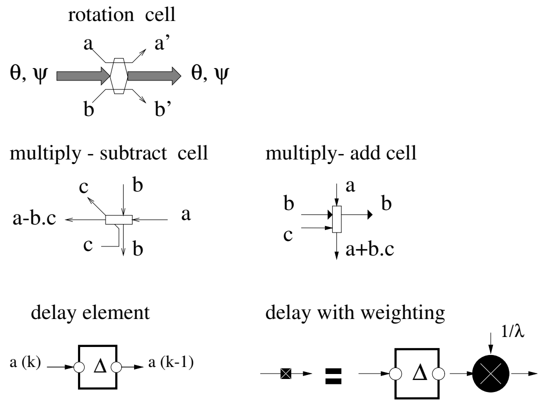

Figure 5.1: SFG building blocks

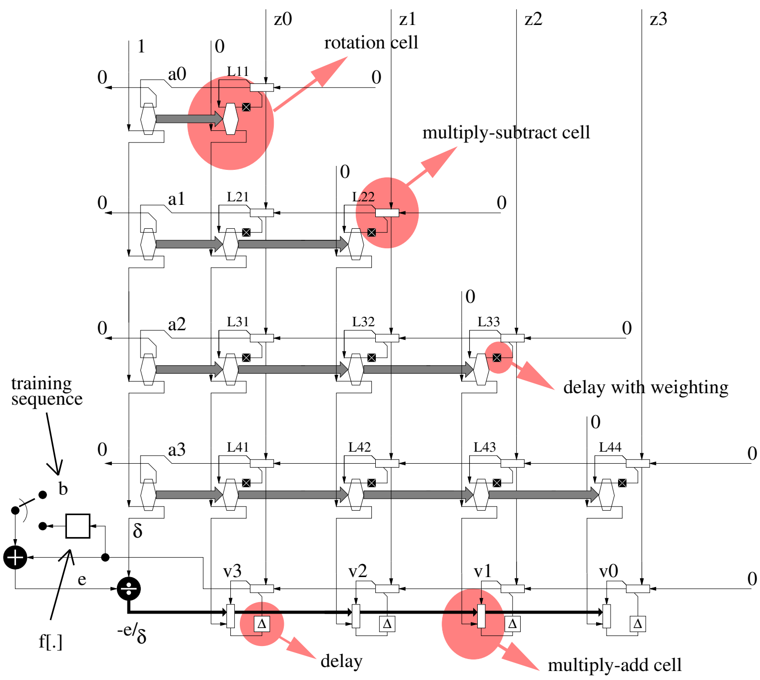

Figure 5.2: SFG for inverse updating RLS-based equalization.

and the last component of $\mathbf{Q}_{j-1}\ldots\mathbf{Q}_1\cdot\left[\mathbf{a}^T|1\right]^T$, such that the jth component is zeroed. For further details, we refer to [90]. To represent this algorithm in a SFG, we define a number of building blocks in **Fig. 5.1**. **Fig. 5.2** then gives

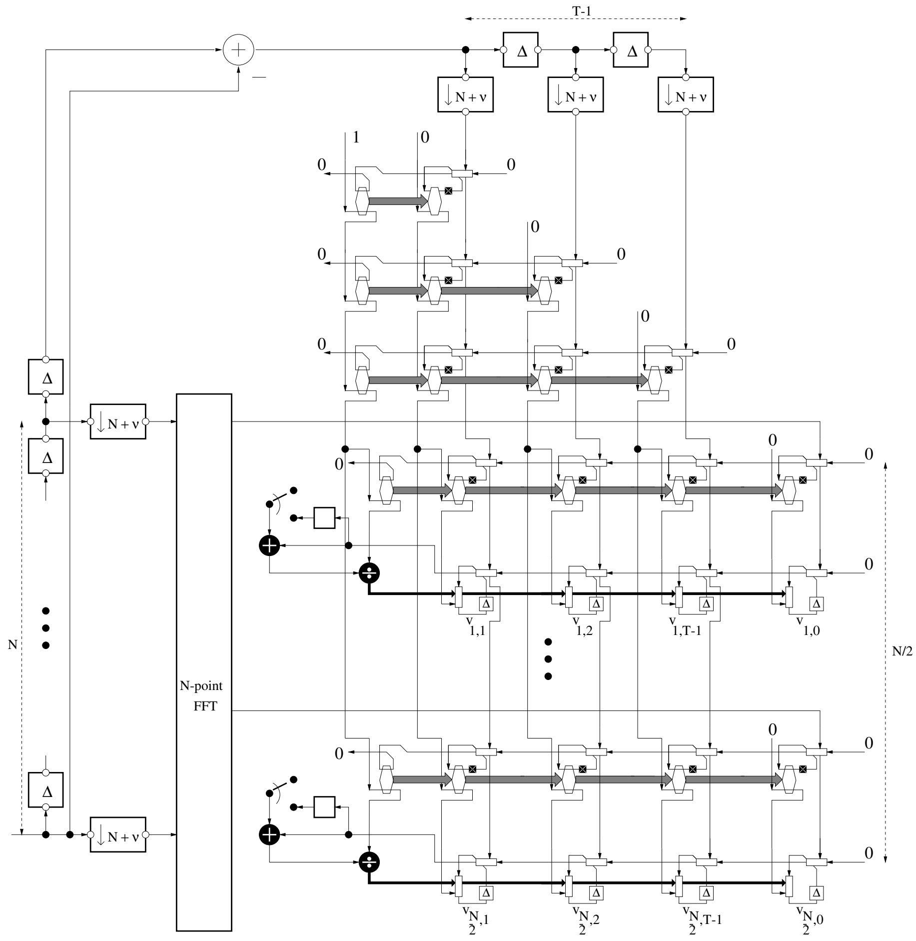

Figure 5.3: SFG for inverse updating RLS-based per tone equalization

the SFG for the RLS algorithm with inverse updating (for $T = 4$). Note that $f[.]$ is a decision device. The output of this device may be used as the so-called desired response input, for further training in 'decision-directed mode', during data transmission.

By applying this algorithm to PT-EQ, one obtains **Fig. 5.3** (for $T = 4$). Per received symbol, one FFT and $T-1$ difference terms are computed. Every used tone has a T-taps PT-EQ with as inputs the FFT output for that tone and $T-1$ difference terms. An important aspect in view of the overall computational complexity, is that the $T-1$ real inputs (the difference terms) give rise to a real triangular part in the SFG which is common to all the used tones, *i.e.*

matrix $\mathbf{L}^{(k)}_{(1:T-1,1:T-1)}$. The complex FFT output is taken as the Tth input to the adaptive filter. This input makes the row $\mathbf{L}^{(k)}_{(T,:)}$ complex, and different for different tones. The update of the filter coefficients is also executed separately for each tone. Remark that the filter coefficients are updated in the following order $[v_{i,1} \ldots v_{i,T-1}\, v_{i,0}]$ where $v_{i,0}$, the tap with complex input signal (FFT output), is the right-most coefficient in the SFG.

5.3 Tone grouping

To achieve optimal capacity, the minimization of equation (4.8) (for direct initialization) or equation (5.1) (for recursive initialization) should be carried out for each tone. However, to reduce initialization complexity, one can group tones and compute an optimal per tone equalizer only for the center tone of each group, *i.e.* one can compute $\{\mathbf{v}_{i_1}\}_{i_1 \in \Omega}$ where Ω is the set of center tones. Then the equalizer $\mathbf{v}_{i_1}$, with $i_1 \in \Omega$, is reused for the tones $i_2 \neq i_1$ belonging to the group with center tone i_1. When grouping tones, one has to take into account the following.

First, the equalizer $\mathbf{v}_{i_1}$, with $i_1 \in \Omega$, does not only equalize the channel, but also includes the sliding Fourier transform corresponding to tone i_1. Therefore $\mathbf{v}_{i_1}$, with $i_1 \in \Omega$, can not be used as such for other tones $i_2 \neq i_1$ belonging to the group with center tone i_1. The equalizer $\mathbf{w}_{i_1}$, with $i_1 \in \Omega$, on the other hand, can be used as such for other tones $i_2 \neq i_1$, belonging to the group with center tone i_1, because this equalizer does not include the sliding Fourier transform corresponding to tone i_1.

Second, the channel impulse response has a tone dependent amplitude and phase. The optimal equalizer $\mathbf{v}_{i_1}$ and hence, $\mathbf{w}_{i_1}$, for tone i_1, contains a scaling and a rotation according to the amplitude and phase of tone i_1. These scaling and rotation may not be optimal for tones $i_2 \neq i_1$ (belonging to the group with center tone i_1). Therefore, an extra 1-taps FEQ D_i is needed for each non-center tone, similar to the 1-taps FEQ in the TEQ-based DMT receiver. Training of the 1-taps FEQs may be done by means of an LMS algorithm

$$D_i^{(k)} = D_i^{(k-1)} + \rho \cdot Z_i^{(k)} \cdot (X_i^{(k)} - Z_i^{(k)} \cdot D_i^{(k-1)}) \tag{5.2}$$

where $D_i^{(k)}$ is the 1-taps FEQ for tone i at training period k, ρ is the step size, $Z_i^{(k)}$ is the output of the PT-EQ and hence, the input of the extra 1-taps FEQ and finally $X_i^{(k)}$ is the desired subsymbol for tone i at period k. Note that a 1-taps FEQ does not alter the SNR of a tone. The SNR is defined by the T-taps equalizer (TEQ or PT-EQ). In conclusion, grouping provides intermediate solutions, encompassing the TEQ approach and the per tone approach as extreme cases.

Per group, with center tone i_1, we therefore execute the following steps:

Step 1. Compute $\mathbf{v}_{i_1}$.

Step 2. Compute $\mathbf{w}_{i_1}$ corresponding to $\mathbf{v}_{i_1}$ with the recursion formula

$$v_{i_1,t+1} \cdot \alpha^{i_1-1} + w_{i_1,t} = v_{i_1,t} \tag{5.3}$$

with $t = 0 \ldots T-2$, $v_{i_1,T-1} = w_{i_1,T-1}$ and $\alpha = e^{-j2\pi\frac{1}{N}}$, see figure 4.3.

Step 3. For $i_2 \neq i_1$, belonging to the group with center tone i_1, take $\mathbf{w}_{i_2} = \mathbf{w}_{i_1}$.

Step 4. Compute $\mathbf{v}_{i_2}$ from $\mathbf{w}_{i_2}$ with the recursion formula

$$v_{i_2,t+1} \cdot \alpha^{i_2-1} + w_{i_2,t} = v_{i_2,t} \tag{5.4}$$

Step 5. Take $\mathbf{v}_{i_2} \leftarrow D_{i_2} \cdot \mathbf{v}_{i_2}$, with D_{i_2} an additional 1-taps FEQ for tone i_2.

5.4 Initialization complexity

In our complexity computations, only the number of *real multiplications* is counted.

5.4.1 RLS with inverse updating per tone

Initialization complexity, per received symbol, of RLS-based PT-EQ without tone grouping, is given in **Table 5.1**. The real part of $\mathbf{L}$ is common for all used tones, while the complex part of $\mathbf{L}$ and the filter update are performed per tone. A real and a complex rotation are counted as 4 and 9 multiplications respectively.

The real part is quadratic in T but shared by all used tones (common), while the complex part is linear in T and executed for each tone separately (per tone). The latter part will mostly dominate the total complexity, *e.g.* for ADSL downstream transmission, where $N_u >> T$, with N_u the total number of used tones. The per tone part of the complexity is 8.5 times higher than the complexity during data transmission, see table 4.2. By assuming $N_u = \frac{N}{2}$ and the symbol duration $\frac{N}{F_s}$, we have a total complexity of
$\frac{F_s}{N}\frac{1}{2}(5T^2+3T-8)+8.5F_s\cdot(T+1)$ real multiplications per second, where mostly the last term constitutes the dominant part.

Example 5.4.1. Let us assume an equalizer length T equal to 32 in downstream and 64 in upstream and the parameters given in table 3.2. Hence, there are 218 downstream and 23 upstream used tones (N_u). The number of multiplications in downstream are 11 and 496 M operations/s for the common and

		# multiplications
common	matrix vector product	$\frac{(T-1)T}{2}$
	real rotations	$[\frac{(T-1)T}{2}+T-1]4$
	total [M operations/s]	$(2.5T^2+1.5T-4)\frac{F_s}{N+\nu}$
per tone	matrix vector product	$(T-1)2+4$
	complex rotations	$(T+1)9$
	filter update	$(T-1)2+4+4+T4$
	total [M operations/s]	$17(T+1)N_u\frac{F_s}{N+\nu}$

Table 5.1: Initialization complexity of RLS with inverse updating for PT-EQ without tone grouping. The number of real multiplications per received symbol is counted. The total complexity is given in M operations/s

the per tone part respectively. In upstream we have 41 and 103 M operations/s. In downstream, the common part has significantly lower complexity than the per tone part: the common part complexity is only 2% of the per tone part complexity. In upstream, the common part complexity is 40% of the per tone complexity. □

5.4.2 RLS with inverse updating and tone grouping

While performance is almost the same for both per tone and per M tones equalization (for sufficiently small values of M, *e.g.* $M = 11$ in downstream), see section 5.5, it can be shown that the overall complexity drops significantly when tones are grouped:

- Training of PT-EQ of center tones
  The per tone complexity reduces to $17(T+1)\frac{N_u}{M}\frac{F_s}{N+\nu}$ when tones are combined into groups of M tones. This may be approximated by $\frac{8.5}{M}F_s(T+1)$ under the same assumptions as in the previous section.

  Example 5.4.2. Let us take $N = 512$ (ADSL downstream) and $M = 11$ (see section 5.5), which leads to a complexity of roughly $0.8F_sT + 0.005F_sT^2$. It is seen that, in this case, initialization complexity is very comparable to complexity during data transmission, namely $F_s \cdot T$, see section 4.3. □

  Example 5.4.3. Assume M equals 11 and 5 in downstream and upstream respectively and further assume the same parameters as in example 5.4.1. The per tone part of the complexities then become 45.1 and 20.6 M operations/s respectively. □

- Transformations after training (performed once)
  1 recursion has $T-1$ complex multiplications[2] per tone, as seen in figure 4.3.
  - For the center tone of each group, we perform a transformation from $\mathbf{v}_{i_1}$ to $\mathbf{w}_{i_1}$. This requires $4(T-1)$ real multiplications.
  - For each non-center tone, we perform a transformation from $\mathbf{w}_{i_2}$ to $\mathbf{v}_{i_2}$. This requires also $4(T-1)$ real multiplications.

  Hence, the total complexity becomes $4N_u(T-1) \approx 2N(T-1)$ real multiplications.

- 1-taps FEQs for the non-center tones
  Training by means of an LMS algorithm requires $10N_u\frac{F_s}{N+\nu} \approx 5F_s$ real multiplications per second.

5.5 Simulation results

The parameters given in section 3.5, are adopted.

5.5.1 Tone grouping

Downstream

The performance of tone grouping is shown for a 4km 26 AWG downstream channel in **Fig. 5.4**. We compare PT-EQ without tone grouping, PT-EQ with groups of 11 tones, PT-EQ with groups of 51 tones and TEQ (with unit norm TIR). The filter length is $T = 32$. The optimal PT-EQ, *i.e.* direct initialization according to formula (4.9), is computed for the center tones. The top figure represents the bit rate as a function of the decision delay. It is seen that tone grouping with group size of 11 tones results in almost the same performance as PT-EQ without tone grouping. Tone grouping with group size equal to 51, behaves worse. Its performance is comparable to the TEQ performance. The bottom figure represents the SNR as a function of the tones for several values of the decision delay, namely $\delta = [-40 : 10 : 30]$. The stars indicate the center tones. The SNR as a function of the tones, remains smooth for tone grouping with group size 11. With group size 51 however, dips arise in tone ranges

[2] Remark that a complex multiplication with the phase α^{i-1} is just 1 real addition in polar coordinates.

between center tones. The SNR corresponding to the TEQ also shows dips. **Fig. 5.5** shows the optimal 1-taps FEQs after tone grouping with group size 11. It is seen that an amplitude and a phase adaptation are needed after tone grouping. Note however that the 1-taps FEQ does not change the SNR.

Upstream

Similar simulations are shown for a 4km 26 AWG upstream loop in **Fig. 5.5**. We compare PT-EQ without tone grouping, PT-EQ with groups of 5 tones, PT-EQ with groups of 7 tones and TEQ (with unit norm TIR). The filter length is $T = 64$. A small bit rate loss is noted for tone grouping with group size 5 and 7. However, the bit rate is still much larger than the TEQ bit rate. The SNR as a function of the tones is shown in the delay range $\delta = [-10 : 10 : 40]$. The optimal 1-taps FEQs after tone grouping with group size 5, are shown in **Fig. 5.7**.

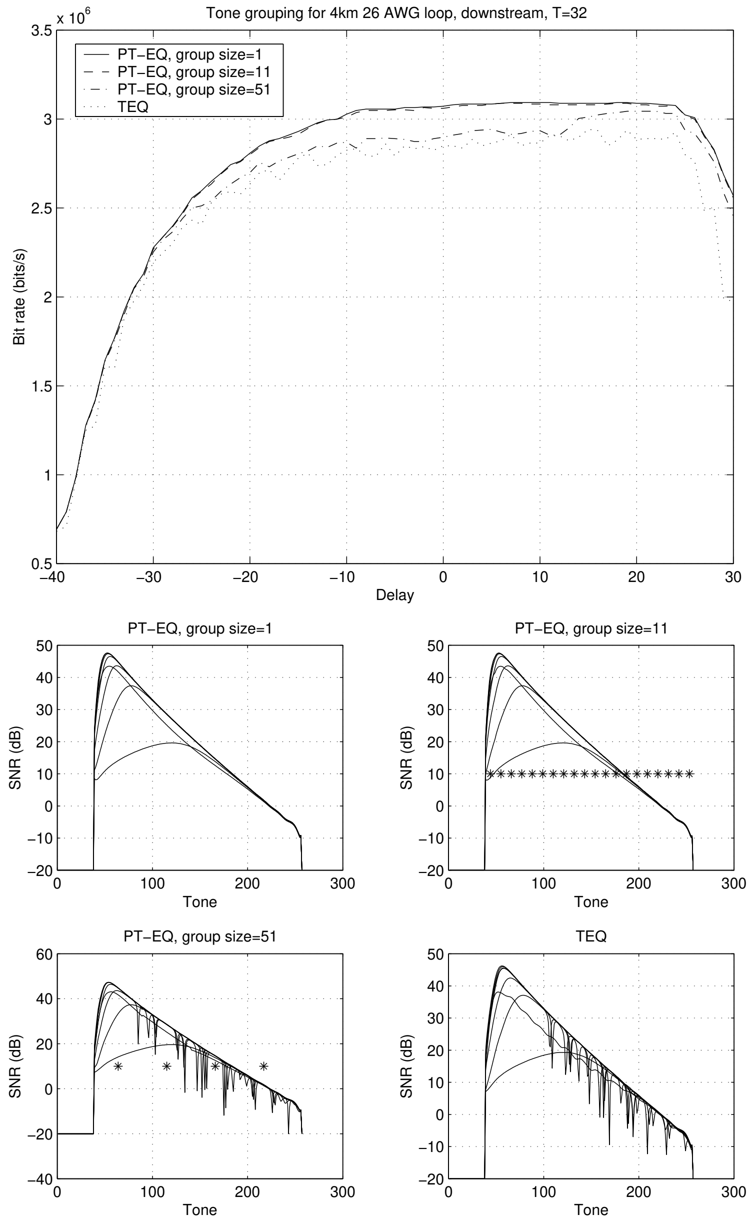

Figure 5.4: Comparison of PT-EQ without tone grouping, with group size 11, with group size 51 and TEQ for a 4km 26 AWG downstream loop. The stars indicate the center tones.

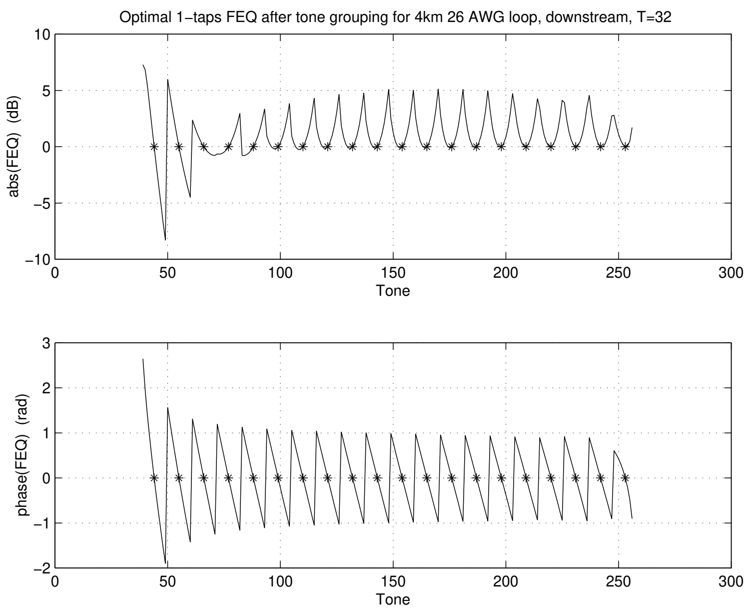

Figure 5.5: Optimal 1-taps FEQs after tone grouping with group size 11 for a 4km 26 AWG downstream loop.

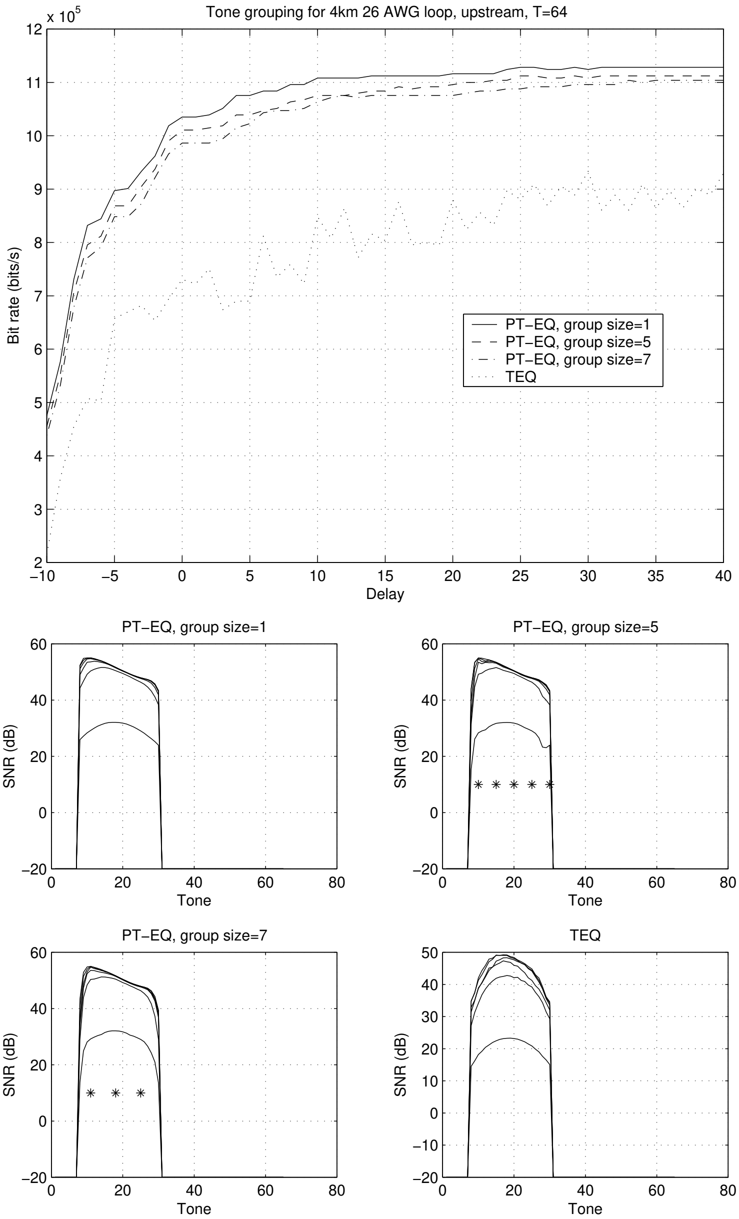

Figure 5.6: Comparison of PT-EQ without tone grouping, with group size 5, with group size 7 and TEQ for a 4km 26 AWG upstream loop.

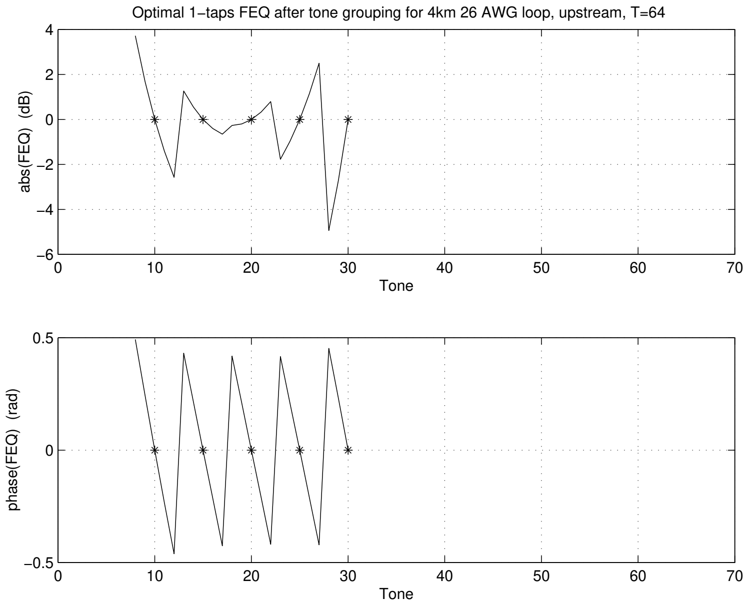

Figure 5.7: Optimal 1-taps FEQs after tone grouping with group size 5 for a 4km 26 AWG upstream loop.

5.5.2 Normalized least mean squares

In this section, the slow convergence of Normalized Least Mean Squares (NLMS) adopted to PT-EQ, is shown. First, the eigenvalues of the autocorrelation matrix of the filter input are computed. This matrix is defined by $\mathbf{R}_{\mathbf{z}_i} = \mathcal{E}\left\{\mathbf{z}_i^{(k)} \cdot \mathbf{z}_i^{(k)\mathrm{H}}\right\}$ with i the tone index and $\mathbf{z}_i^{(k)}$ the PT-EQ input vector for tone i, $\mathbf{z}_i^{(k)} = \mathbf{F}_i \cdot \mathbf{y}^{(k)}$. Refering to equation (4.9), the autocorrelation matrix may be written as

$$\mathbf{R}_{\mathbf{z}_i} = \mathbf{F}_i \cdot \mathbf{H} \cdot \mathbf{R}_{\hat{\mathbf{x}}} \cdot \mathbf{H}^{\mathrm{H}} \cdot \mathbf{F}_i^{\mathrm{H}} + \mathbf{F}_i \cdot \mathbf{R}_{\mathbf{n}} \cdot \mathbf{F}_i^{\mathrm{H}} \tag{5.5}$$

where $\mathbf{F}_i$ incorporates $T-1$ difference terms and 1 FFT operation when applying the modified PT-EQs $\mathbf{v}_i$, or where $\mathbf{F}_i$ alternatively incorporates T FFT operations when studying the basic PT-EQs $\mathbf{w}_i$.

Second, simulation results of the convergence of NLMS is shown. The (complex) updating formula for NLMS is given by

$$\begin{aligned} \bar{\mathbf{v}}_i^{(k)} &= \bar{\mathbf{v}}_i^{(k-1)} + \frac{\rho_i}{\alpha_i^2 + {\mathbf{z}_i^{(k)}}^{\mathrm{H}} \cdot \mathbf{z}_i^{(k)}} \cdot {\mathbf{z}_i^{(k)}}^{*} \cdot e_i^{(k)} \\ e_i^{(k)} &= X_i^{(k)} - {\mathbf{z}_i^{(k)}}^{\mathrm{T}} \cdot \bar{\mathbf{v}}_i^{(k-1)} \end{aligned} \tag{5.6}$$

with ρ_i the step size and α_i a small constant to prevent overflow when ${\mathbf{z}_i^{(k)}}^{\mathrm{H}} \cdot \mathbf{z}_i^{(k)} = 0$. Note that similar formulas apply to the basic PT-EQs $\mathbf{w}_i$. The NLMS algorithm is convergent in the mean and in the mean square if $0 < \mu < 2$. A 10% excess MSE is obtained for $\mu < 0.2$ [50].

Downstream

Simulations are made for a downstream 4km 26 AWG loop. The eigenvalues corresponding to the basic PT-EQs $\mathbf{w}_i$ are shown for each used tone in **Fig. 5.8** for $T = 32$ and $T = 8$ respectively. The delay is fixed at -8. It is seen that the eigenvalue spread is huge, especially on the lowest tones. Hence, the worst convergence is expected on these tones. By decreasing the number of taps from 32 down to 8, the eigenvalue spread does not decrease much. The eigenvalues corresponding to the modified PT-EQs $\mathbf{v}_i$, are different but the spread is of the same order.

The achieved bit rate in function of the number of training symbols (4-QAM) and the optimal bit rate are shown in **Fig. 5.9** for 32-taps PT-EQ (without tone grouping) at delay -8, for the same loop. The SNR for the used tones is also shown after a certain number of training symbols. ρ and α are set to 1 and 0 respectively. The initial values of the PT-EQs are set to $[10\ldots0]^{\mathrm{T}}$. It is clear that convergence is very slow, mainly caused by the lowest tones.

Upstream

For an upstream 4km 26 AWG loop similar simulations are performed. The eigenvalues are shown in **Fig. 5.10** for $T = 64$ at delay 30 and $T = 16$ at delay 6 respectively. The eigenvalue spread is huge on all used tones.

The behavior of NLMS is seen in **Fig. 5.11** for $T = 64$ at delay 30. The bit rate as a function of the number of training symbols, is compared with the optimal rate in the first figure. In the second figure, the evolution of the SNR with the number of training symbols is shown. In upstream, the convergence is slow on all tones.

5.5.3 Recursive least squares

The description of the RLS algorithm with inverse updating is given in section 5.2. The performance of this algorithm is demonstrated for the same loop as used in the previous section.

Downstream

32-taps PT-EQs are simulated at delay -8. The initial values of the PT-EQs are set to $\mathbf{v}_i = [0\ldots010\ldots0]^{\mathrm{T}}$ with '1' in the $(T/2)$th position and the initial triangular matrix is $\mathbf{L}_i = 10^5 \cdot \mathbf{I}_T$. PT-EQ without tone grouping (*i.e.* group size 1) is compared with PT-EQ with tone grouping (group size 11). **Fig. 5.12** shows the bitrate as a function of the number of training symbols for per tone (in solid line) and per 11 tones (in dashed line) equalization. Also the optimal bitrate, computed with direct initialization, is plotted for per tone (in dashed-dotted line) and per 11 tones (in dotted line) equalization. The optimal bit rates are 3.0563 Mbits/s and 3.0482 Mbits/s respectively. The optimal bit rates as well as the bit rates during convergence are almost the same for the grouped and the ungrouped case.

In **Fig. 5.13** the SNR is plotted for per tone equalization (without tone grouping) for different lengths of the training sequence, for the used tones. It is seen that convergence to optimal performance may be achieved with an acceptably short training sequence, typically consisting of 100 symbols.

Upstream

We simulate 64-taps PT-EQ at delay 30 for a 4km 26 AWG upstream loop. The initial values of the PT-EQs are set to $\mathbf{v}_i = [0\ldots010\ldots0]^{\mathrm{T}}$ with '1' in the $(T/2)$th position and and the initial triangular matrix is $\mathbf{L}_i = 10^5 \cdot \sqrt{10^{-4}/10^{-3.8}} \cdot \mathbf{I}_T$. The extra factor in $\mathbf{L}_i$, with respect to downstream, is inserted to take into account the different signal psd adopted in upstream (see also table 3.2).

PT-EQ without tone grouping (*i.e.* group size 1) is compared with PT-EQ with tone grouping (group size 5). **Fig. 5.14** shows the bitrate as a function of the number of training symbols as well as the optimal bit rate. The optimal bit rates are 1.1243 Mbits/s and 1.1081 Mbits/s respectively.

In **Fig. 5.15** the SNR is plotted for per tone equalization (without tone grouping) for different lengths of the training sequence for the used tones. It seen that the PT-EQs in upstream require somewhat more training symbols. However, this is due to the fact that more taps have to be initialized: in our example 64 taps in upstream with respect to 32 taps in downstream.

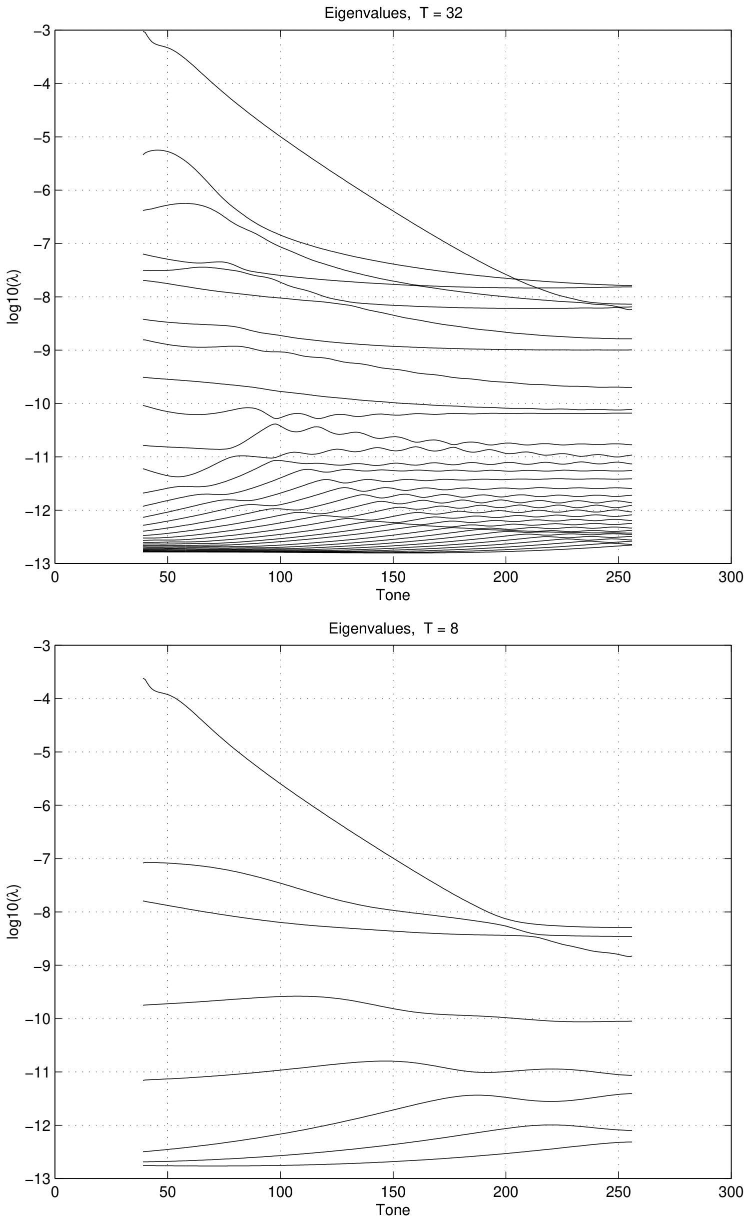

Figure 5.8: T eigenvalues are shown for each used tone. The simulation is made for a 4km 26 AWG downstream loop at delay -8.

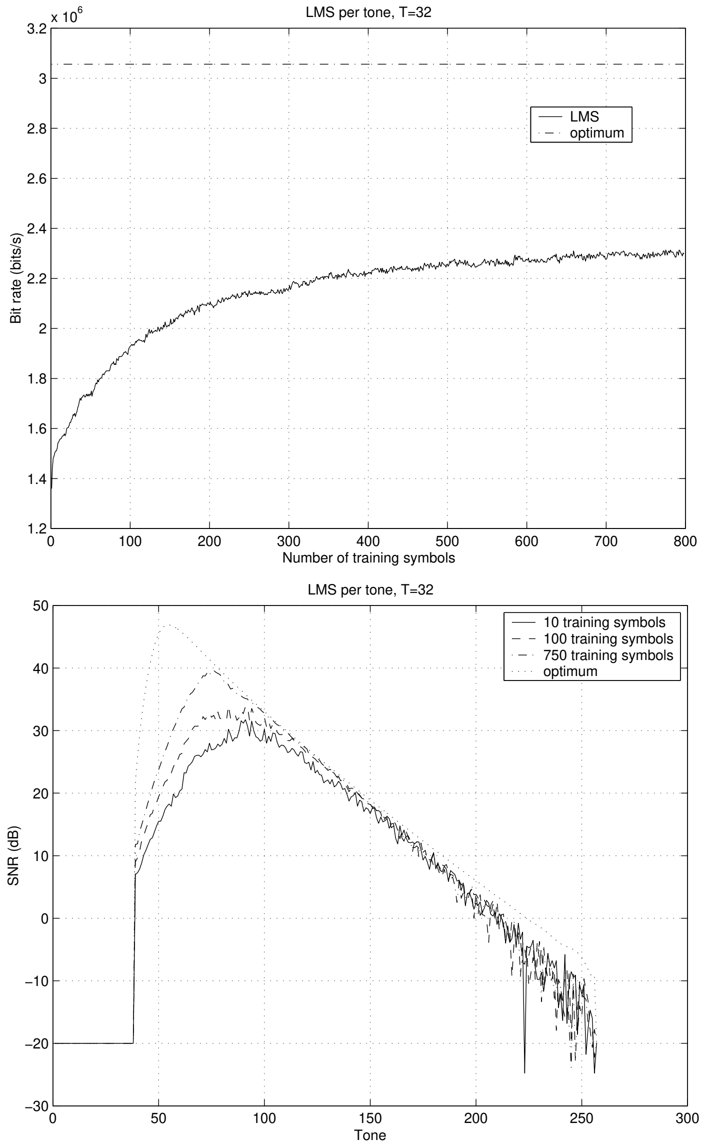

Figure 5.9: Convergence of the NLMS algorithm applied to 32-taps PT-EQ on a 4km 26 AWG downstream loop. The first figure shows the bit rate in function of the number of training symbols as well as the optimal bit rate. In the second figure the evolution of the SNR with the number of training symbols is shown and compared with the optimal SNR for all used tones. The slow convergence is mainly caused by the lowest tones.

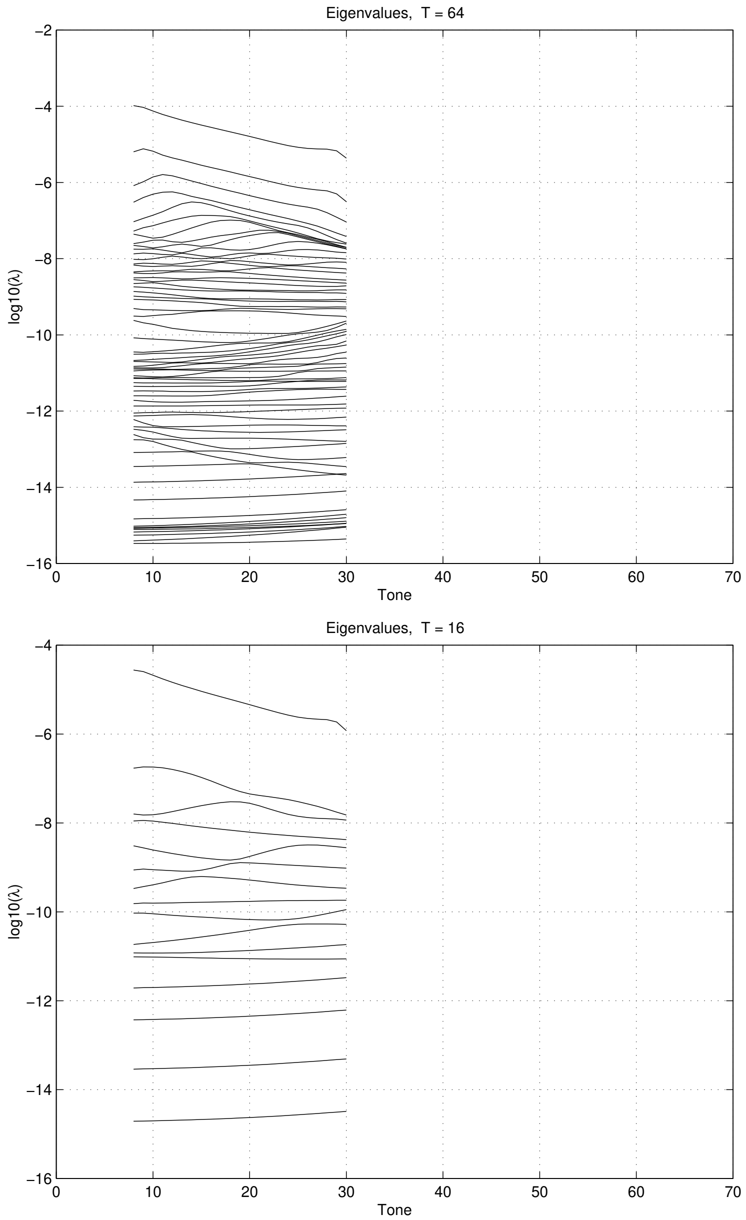

Figure 5.10: T eigenvalues are shown for each used tone. The simulation is made for a 4km 26 AWG upstream loop. The delay is fixed at 30 for $T = 64$ and at 6 for $T = 16$.

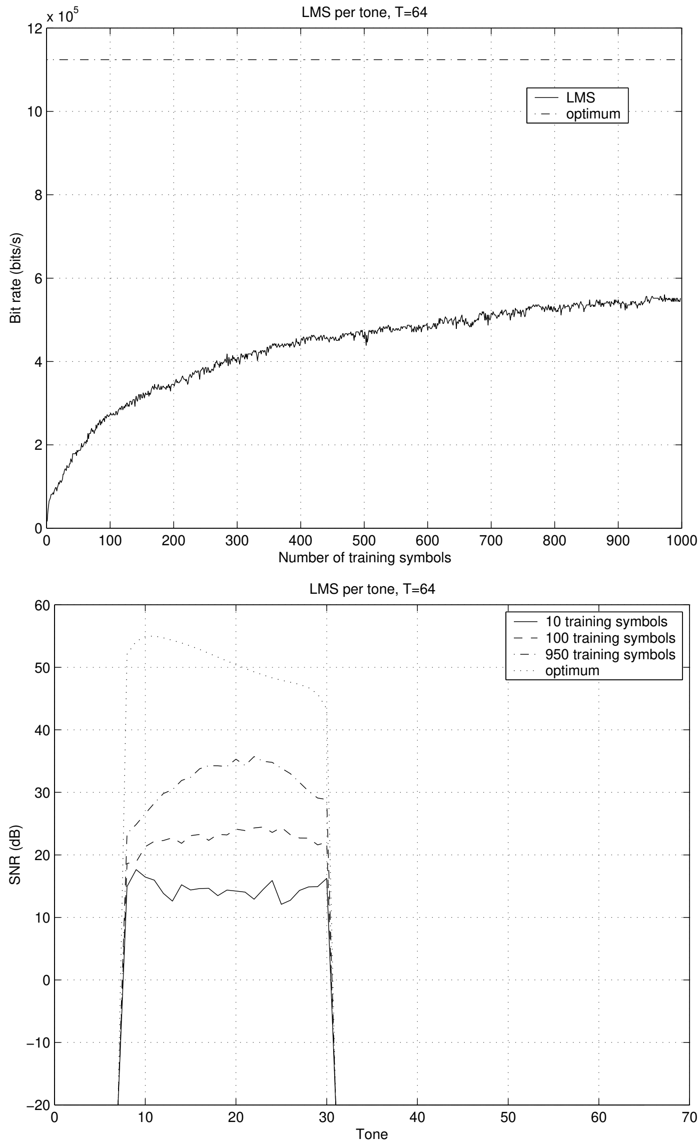

Figure 5.11: Convergence of the NLMS algorithm applied to 64-taps PT-EQ on a 4km 26 AWG upstream loop. The first figure shows the bit rate in function of the number of training symbols as well as the optimal bit rate. In the second figure the evolution of the SNR with the number of training symbols is shown and compared with the optimal SNR for all used tones. The convergence is slow on all used tones.

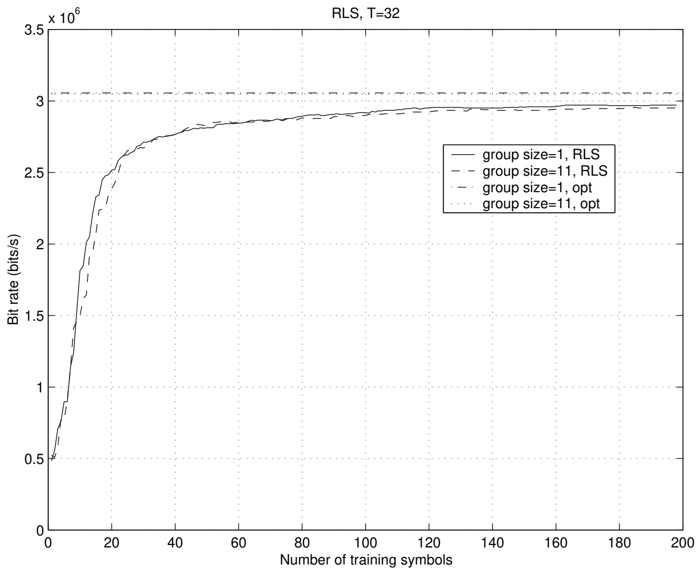

Figure 5.12: Bit rate in function of the number of training symbols and optimal bit rate for 32-tap PT-EQ without and with tone grouping. The simulation is made for a downstream 4km 26 AWG loop

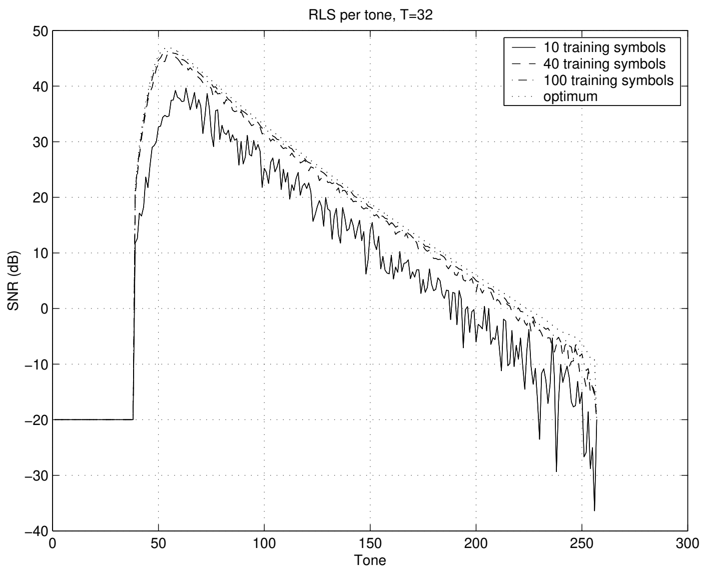

Figure 5.13: Evolution of the SNR for the used tones during training of 32-taps PT-EQ without tone grouping.

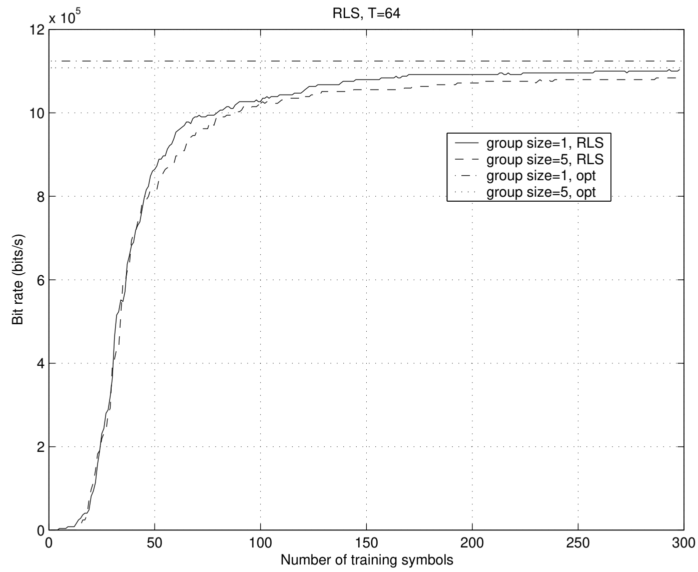

Figure 5.14: Bit rate in function of the number of training symbols and optimal bit rate for 64-tap PT-EQ without and with tone grouping. The simulation is made for an upstream 4km 26 AWG loop

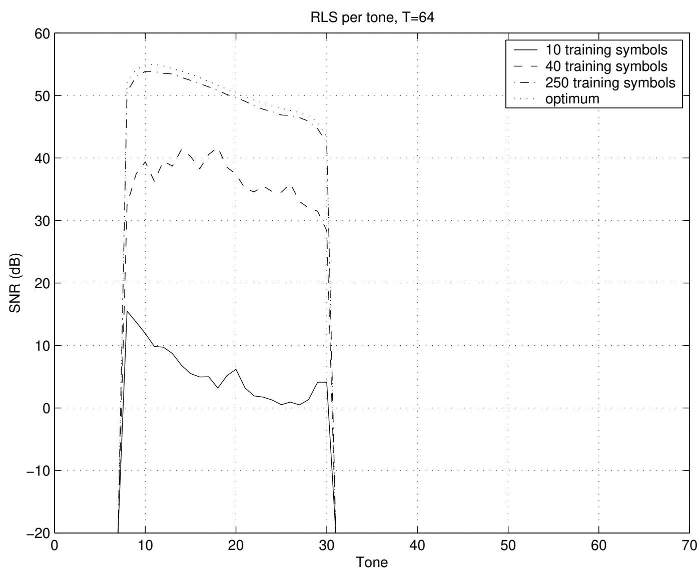

Figure 5.15: Evolution of the SNR for the used tones during training of 64-taps PT-EQ without tone grouping.

5.6 Conclusions

A recursive initialization scheme for the PT-EQs has been proposed. The scheme is based on RLS with inverse updating. Although the RLS complexity is quadratic in the number of filter taps, complexity can be saved considerably. The real difference terms are taken as the first filter inputs which make the quadratic part of the algorithm real and common for all used tones. An additional part of the algorithm is performed for each tone separately. This part is complex but linear in the number of filter taps.

Tone grouping has been proposed to reduce initialization complexity. The optimal PT-EQ is computed only for the center tone and then reused for the other tones in the same group. When the group size is well chosen, performance decreases only slightly with respect to 'full' PT-EQ, while the per tone part initialization complexity is divided by the group size. Tone grouping can be seen as an intermediate solution between TEQ and PT-EQ.

The complexity of RLS with inverse updating adopted to PT-EQ has been computed. It is seen that, when the number of filter taps is smaller than the number of used tones (*e.g.* for ADSL downstream), the quadratic part complexity is only a small fraction of the linear part complexity. Moreover, when tones are grouped, initialization complexity becomes comparable to complexity during data transmission, for ADSL downstream. In ADSL upstream, the quadratic part complexity is more significant due to the larger number of filter taps and the smaller number of used tones.

Finally simulation results have been presented. The autocorrelation matrix of the filter input is seen to have a huge eigenvalue spread. Hence, LMS-based PT-EQ initialization is very slow. RLS, on the other hand, achieves good performance with an acceptable number of training symbols.

Part II

Echo cancellation

Chapter 6

Time/frequency domain echo cancellation and equalization

When up- and downstream signals use the same frequency band simultaneously, the transmitted signal causes echo in the received signal and echo cancellation is needed to reduce the echo that leaks through the hybrid. This concept is shown in chapter 1 (figure 1.3) for a set-up with overlapping up- and downstream tones. However, if one assumes a set-up with separated up- and downstream tones, but with relaxed orders of the filters separating both transmission bands, echo may also occur due to ISI and ICI in the echo signal.

Several echo cancellation structures for DMT transceivers have been developed in literature. The aim of this chapter is to investigate the combination of time/frequency domain echo cancellation [54, 55] and equalization. Therefore, we start in section 6.1 with a review of time/frequency domain echo cancellation, which has been proposed as a cost efficient algorithm to cancel echo in DMT-based systems.

In section 6.2, we study the combination of time/frequency domain echo cancellation and TEQ. Mostly, the TEQ is performed before echo cancellation to enable so-called joint channel shortening of the far end and the echo impulse response allowing a shorter echo cancellation filter. However, MMSE joint channel shortening has no direct relation to the resulting capacity, similarly to far end channel shortening only. On the other hand, if the TEQ is designed to shorten the far end impulse response only, it will in general lengthen the echo path. We show that the order of TEQ and time/frequency domain echo cancellation can be changed, to avoid the possible lengthening.

Applying first time/frequency domain echo cancellation and then TEQ is merely considered as an intermediate scheme to finally apply first time/frequency domain echo cancellation and then per tone equalization. PT-EQ allows to optimize capacity, given a certain echo canceller, in contrast to TEQ. We develop the combination of time/frequency domain echo cancellation and then PT-EQ in section 6.3, which is our main contribution of this chapter.

In section 6.4, we compare the complexity of the combination of time/frequency domain echo cancellation and equalization for several implementations at RT and CO. Simulation results are presented in section 6.5. Finally, conclusions are given in section 6.6.

6.1 T/f domain echo cancellation

Introducing echo cancellation (EC) in an ADSL modem significantly increases the overall complexity of the modem. The echo impulse response can be as long as one DMT symbol, *i.e.* 1/4312.5 Hz = 232 μs or 512 taps at 2.208 MHz. For comparison, the TEQ generally used in RT has only 32 taps working at 2.208 MHz. Hence, the complexity of the EC filter could be as high as 16 times the complexity of the RT-TEQ. Therefore echo cancellation research is mainly aimed at reducing this complexity. Our starting point is the work on EC by Ho and Cioffi [54, 55], where an echo canceller is developed and studied which is implemented partly in the time domain and partly in the frequency domain (t/f domain EC).

An echo canceller performs two tasks: it *emulates the echo* (*i.e.* the filtering operation) and *adapts the filter coefficients*. In the Ho and Cioffi approach

1. the echo emulation is implemented partly in the time domain and partly in the frequency domain. The time domain part dominates the emulation complexity.

2. the adaptation is implemented in the frequency domain and, as a result, has negligible computational complexity.

Briefly, the overall complexity of Ho and Cioffi's scheme is dominated by the time domain part of the echo emulation. With respect to a full time domain echo emulation, a two fold complexity reduction is obtained. Moreover, in a multirate system (*i.e.* transmit IFFT of the echo signal is γ times smaller or larger then the receive FFT) an additional γ fold complexity reduction can be obtained.

By employing a different alignment between transmit and receive symbols an additional two fold complexity reduction can be obtained in the time domain part of the echo emulation [67, 140]. In the following subsections, an overview of this approach will be given and the alternative alignment will be explained.

6.1.1 Echo cancellation by Ho & Cioffi

Echo emulation in a symmetric rate set-up

The received echo signal is equal to the linear convolution of the echo impulse response with the modem's own transmitted DMT signal. This linear convolution can be written as a matrix-vector multiplication of a Toeplitz matrix $\mathbf{U}^{k,k-1}$ consisting of transmitted DMT signal samples with the echo impulse response $\mathbf{h}_E$

$$\mathbf{y}^k = \mathbf{U}^{k,k-1}\mathbf{h}_E + \mathbf{n}^k \tag{6.1}$$

$\mathbf{y}^k = [y_1^k \dots y_N^k]^{\mathrm{T}}$ is a received symbol of size $N \times 1$ at symbol period k prior to EC[1]. $\mathbf{n}^k$ is an $N \times 1$ vector containing the sum of the received far end signal and additive noise at symbol period k. Remark that, as a starting point, we assume a symmetric rate set-up, hence, transmit and receive symbol size (in samples) are both equal to N. $\mathbf{h}_E$ is the M-taps echo impulse response, zero-padded to length N. $\mathbf{U}^{k,k-1}$ is a Toeplitz matrix consisting of transmitted echo samples (*i.e.* echo reference signal samples) at symbol periods k and $k-1$. The actual ordering of the echo samples in this matrix depends on the alignment of the transmitted symbols with respect to the received symbols. For instance, when both symbol streams are aligned, this Toeplitz matrix can be written as

$$\begin{array}{c}
\begin{array}{ccc} \text{symbol } k & \qquad\text{prefix } k & \qquad\qquad\text{symbol } k-1 \end{array} \\
\mathbf{U}^{k,k-1} = \left[\begin{array}{c|ccc|cccc}
u_1^k & u_N^k & \dots & u_{N-\nu+1}^k & u_N^{k-1} & & \dots & u_{\nu+2}^{k-1} \\
u_2^k & u_1^k & \ddots & & \ddots & \ddots & & \vdots \\
\vdots & \ddots & \ddots & & & \ddots & & u_N^{k-1} \\
 & & & & & & & u_{N-\nu+1}^k \\
\vdots & & & & & & & \vdots \\
u_N^k & u_{N-1}^k & \dots & & & \dots & & u_1^k
\end{array}\right]
\end{array} \tag{6.2}$$

with ν the cyclic prefix size.

As a starting point, we assume a complete time domain EC in a symmetric rate set-up. In that case, the echo cancelled received symbol is described by

$$\mathbf{e}^k = \mathbf{y}^k - \mathbf{U}^{k,k-1} \cdot \mathbf{w}_E^k \tag{6.3}$$

where $\mathbf{e}^k = [e_1^k \dots e_N^k]^{\mathrm{T}}$ is an echo cancelled received symbol of size $N \times 1$ at symbol period k, and $\mathbf{w}_E^k$ is the M-taps estimate at symbol period k of the echo impulse response $\mathbf{h}_E$, zero-padded to length N.

[1]Note that, for the sake of a compact notation, the superscript, indicating the symbol period, is denoted as $\mathbf{y}^k$ instead of $\mathbf{y}^{(k)}$.

The t/f domain EC of Ho & Cioffi is based on the fact that any Toeplitz matrix can be written as the sum of a circulant matrix and a correction matrix with only a small number of non-zero elements. Adopting this property to the previously encountered Toeplitz matrix, one can write

$$\mathbf{U}^{k,k-1} = \mathbf{C}^k + \boldsymbol{\chi}^{k,k-1} \tag{6.4}$$

where $\mathbf{C}^k$ is a circulant matrix containing only echo samples at symbol period k, and $\boldsymbol{\chi}^{k,k-1}$ is an upper triangular matrix containing difference terms from echo samples at $k-1$ and k

$$\mathbf{C}^k = \begin{bmatrix} u_1^k & u_N^k & \dots & u_{N-\nu+1}^k & u_{N-\nu}^k & \dots & u_2^k \\ u_2^k & u_1^k & \ddots & \ddots & \ddots & \ddots & \vdots \\ \vdots & \ddots & \ddots & & & \ddots & u_{N-\nu}^k \\ & & & & & & u_{N-\nu+1}^k \\ \vdots & & & & & & \vdots \\ u_N^k & u_{N-1}^k & \dots & & & \dots & u_1^k \end{bmatrix} \tag{6.5}$$

$$\boldsymbol{\chi}^{k,k-1} = \left[\begin{array}{ccccc|cc} 0 & \dots & 0 & \star & \dots & \dots & \star \\ 0 & \ddots & & \ddots & \ddots & \ddots & \vdots \\ \vdots & \ddots & & & 0 & \star & \star \\ & & & & & 0 & \star \\ \vdots & & & & & & \vdots \\ 0 & \dots & & & & \dots & 0 \end{array}\right] \tag{6.6}$$

where $\boldsymbol{\chi}^{k,k-1}$ has an upper triangular part of real numbers, indicated by stars. The number of zeros in the first row is $\nu+1$. The vertical line is drawn after the Mth column, the meaning of which is explained in the next paragraph.

In describing the EC, the following notation is adopted: $\mathcal{F}_N$ is the N-point DFT matrix, $\mathcal{I}_N$ is the N-point IDFT matrix. $U_{1:N}^k = \mathcal{F}_N \cdot [u_1^k \dots u_N^k]^{\mathrm{T}}$ is a frequency domain transmitted (echo) symbol of size $N \times 1$ at symbol period k. $E_{1:N}^k$ is a frequency domain echo cancelled received symbol of size $N \times 1$ at symbol period k. $W_{E,1:N}^k = \mathcal{F}_N \cdot \mathbf{w}_E^k$ is the frequency domain filter of size $N \times 1$ at symbol period k, with $\mathbf{w}_E^k$ the M-taps echo impulse response estimate, zero-padded to length N. Remark that, for the sake of a compact notation, the subscript $1:N$ will be omitted for the vectors of frequency domain values. Let us consider now the echo cancelled received symbol in the frequency domain

$$\begin{aligned} E^k = \mathcal{F}_N \cdot \mathbf{e}^k &= \mathcal{F}_N(\mathbf{y}^k - \mathbf{U}^{k,k-1} \cdot \mathbf{w}_E^k) \\ &= \mathcal{F}_N(\mathbf{y}^k - \boldsymbol{\chi}^{k,k-1} \cdot \mathbf{w}_E^k) - \mathcal{F}_N \cdot \mathbf{C}^k \cdot \mathbf{w}_E^k \end{aligned} \tag{6.7}$$

The simplification of the echo emulation is two-fold. First, by inserting an IDFT-DFT pair between the circulant matrix and the echo filter, one can apply a property of circulant matrices, namely that the eigenvectors of a circulant matrix form an DFT matrix and that its eigenvalues are the Fourier transform of its first column. Hence, the second term in formula (6.7) can be written as

$$\mathcal{F}_N \cdot \mathbf{C}^k \cdot \mathbf{w}_E^k = \underbrace{\mathcal{F}_N \cdot \mathbf{C}^k \cdot \mathcal{I}_N}_{\mathrm{diag}(U^k)} \cdot \underbrace{\mathcal{F}_N \cdot \mathbf{w}_E^k}_{W_E^k} \tag{6.8}$$

which corresponds to only one complex multiplication per tone, namely of the echo subsymbol on that tone with the echo filter on that tone. Second, let us consider the term $\boldsymbol{\chi}^{k,k-1} \cdot \mathbf{w}_E^k$. Because the M-taps echo filter $\mathbf{w}_E^k$ is zero padded to length N, the last $N-M$ columns of matrix $\boldsymbol{\chi}^{k,k-1}$, *i.e.* the columns after the vertical line in formula (6.6), are multiplied with zeros. Therefore, one can substitute the stars in the last $N-M$ columns by zeros without modifying the product $\boldsymbol{\chi}^{k,k-1} \cdot \mathbf{w}_E^k$. To denote this explicitly, we substitute

$$\boldsymbol{\chi}^{k,k-1} \cdot \overbrace{\begin{bmatrix} \mathbf{I}_M & \mathbf{O} \\ \mathbf{O} & \mathbf{O} \end{bmatrix}}^{\mathbf{M}} \cdot \mathbf{w}_E^k \longleftarrow \boldsymbol{\chi}^{k,k-1} \cdot \mathbf{w}_E^k \tag{6.9}$$

in formula (6.7). The two part echo emulation of Ho & Cioffi is then described by

$$\textsf{Echo emulation} \quad E^k = \mathcal{F}_N(\mathbf{y}^k \overbrace{-\boldsymbol{\chi}^{k,k-1}\mathbf{M}\mathbf{w}_E^k}^{\text{time domain EC}}) \overbrace{-\mathrm{diag}(U^k) W_E^k}^{\text{frequency domain EC}} \tag{6.10}$$

The FFT appearing in this equation is the same as the FFT needed for demodulation. The term $\boldsymbol{\chi}^{k,k-1}\mathbf{M}\mathbf{w}_E^k$ represents the convolution of the echo filter with the tail of the previous symbol, *i.e.* symbol $k-1$, (tail echo estimation), minus the convolution of the echo filter with the cyclic extension of the present symbol, *i.e.* k, (cyclic echo elimination). As a result, after the time domain EC, the echo appears to be periodic with period N.

One sees that, if the echo impulse response would be shorter than the cyclic prefix ($M \leq \nu + 1$), the matrix $\boldsymbol{\chi}^{k,k-1}\mathbf{M}$ becomes zero and the linear convolution of the echo impulse response (and also the echo filter) with the transmitted DMT data becomes a circular convolution.

Filter adaptation in symmetric rate set-up

The following *frequency domain filter adaptation* is used

$$\textsf{Filter adaptation} \quad W_E^{k+1} = W_E^k + \rho \ \mathrm{diag}(U^{k^*}) E^k \tag{6.11}$$

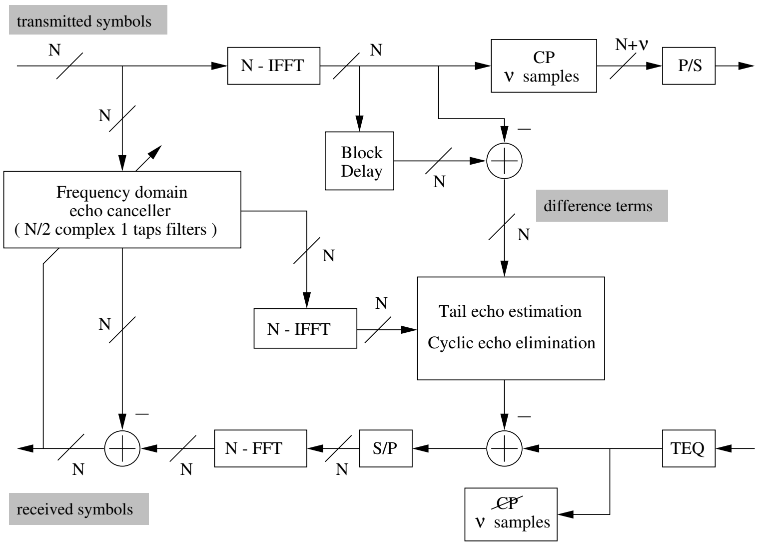

Figure 6.1: T/f domain EC for a symmetric rate transceiver [54, 55].

with ρ the step size. In this update, only the frequency domain part of the filter input is considered. In contrast, the frequency domain blocked version of LMS (FBLMS) has the update

$$W_E^{k+1} = W_E^k + \rho \left(\mathcal{F}_N \boldsymbol{\chi}^{k,k-1} \mathcal{I}_N + \mathrm{diag}(U^k)\right)^{\mathrm{H}} E^k \tag{6.12}$$

where FBLMS forms the filter update with the entire filter input. The method of Ho & Cioffi has a considerably lower complexity per iteration than FBLMS, but then more iterations are needed for convergence because of the simplification in the filter adaptation. Furthermore, simulations have shown that convergence as a function of the total number of operations is faster for formula (6.11).

The *time domain echo filter* $\mathbf{w}_E^k$ is updated by performing an IFFT on W_E^k. To decrease complexity, this IFFT could be performed infrequently (not for every training symbol).

A signal flow graph SFG of this EC is given in **Fig. 6.1**. The $M-\nu-1$ difference terms appearing in $\boldsymbol{\chi}^{k,k-1}\mathbf{M}$, are made in the adder after the block delay, and they are equal to the last $M-\nu-1$ elements of vector $[u_{\nu+2}^{k-1} \dots u_N^{k-1}] - [u_2^k \dots u_{N-\nu}^k]$. Ho & Cioffi proposed adaptations to this t/f domain EC to match in an asymmetric set-up, *i.e.* for an interpolated set-up in RT and a decimated set-up in the CO. Moreover, adaptations for frame-asynchronous operation mode, i.e. without alignment of transmitted and received symbols, are given [54, 55].

Interpolated echo cancellation at RT (frame-synchronous)

At RT the transmit bandwidth is a factor γ smaller than the receive bandwidth[2]. The replications of the smaller bandwidth transmit signal cause echo in the larger receive bandwidth because of non-ideal filter characteristics. Therefore the EC needs to interpolate the transmitted data in frequency and time domain. In frequency domain the interpolation is performed by replicating the data symbol γ times. In time domain $\gamma - 1$ zeros are padded between consecutive time domain samples u. For further details we refer to [54, 55].

A SFG of this algorithm is given in **Fig. 6.2**. The corresponding formulas are

$$\begin{aligned} \text{Echo emulation} \quad & E^k = \mathcal{F}_{\gamma N}(\mathbf{y}^k - \boldsymbol{\chi}^{k,k-1}\mathbf{M}\mathbf{w}_E^k) - \mathrm{diag}(\mathbf{R}\; U^k)W_E^k \\ \text{Filter adaptation} \quad & W_E^{k+1} = W_E^k + \rho\; \mathrm{diag}(\mathbf{R}\; U^{k^*})E^k \end{aligned} \tag{6.13}$$

with $\mathbf{w}_E^k = \mathcal{I}_{\gamma N} W_E^k$ and where $\mathbf{R} = [\mathbf{I}_N; \mathbf{I}_N; \ldots; \mathbf{I}_N]$ contains γ identity matrices of size N, U^k is an echo symbol of size $N \times 1$ (the subscript $1:N$ is omitted) and E^k, $\mathbf{y}^k$, W_E^k are vectors of size $\gamma N \times 1$. This is the efficient implementation of

$$\begin{aligned} \text{Echo emulation} \quad & \mathbf{e}^k = \mathbf{y}^k - \boldsymbol{\chi}^{k,k-1}\mathbf{M}\mathbf{w}_E^k - \mathbf{C}^k\mathbf{w}_E^k \\ \text{Filter adaptation} \quad & \mathbf{w}_E^{k+1} = \mathbf{w}_E^k + \rho\; \mathbf{C}^{k^{\mathrm{H}}}\mathbf{e}^k \end{aligned} \tag{6.14}$$

where $\boldsymbol{\chi}^{k,k-1}$ and the circulant matrix $\mathbf{C}^k$ are interpolated matrices of size $\gamma N \times \gamma N$. Remark that $\mathbf{U}^{k,k-1} = \boldsymbol{\chi}^{k,k-1} + \mathbf{C}^k$ is a $\gamma N \times \gamma N$ Toeplitz matrix.

Decimated echo cancellation at CO (frame-synchronous)

At CO the transmit bandwidth is γ times larger than the receive bandwidth. Due to non-ideal filter characteristics, aliasing occurs and all the symbols of the wide band transmit signal can cause echo in the narrow band receive signal. The EC has to take into account the effects of these aliasing in frequency as well as in time domain. In the frequency domain, this is done by blocking the echo symbol of size γN into γ successive symbols of size N and adding these symbols. The time domain echo signal is decimated by computing only every γth sample. For further details we refer to [54, 55].

The SFG of this algorithm is given in **Fig. 6.3**. The corresponding formulas are

$$\begin{aligned} \text{Echo emulation} \quad & E^k = \mathcal{F}_N(\mathbf{y}^k - \mathbf{D}\boldsymbol{\chi}^{k,k-1}\mathbf{M}\mathbf{w}_E^k) - \frac{1}{\gamma}\mathbf{R}^{\mathrm{T}}\,\mathrm{diag}(U^k)W_E^k \\ \text{Filter adaptation} \quad & W_E^{k+1} = W_E^k + \rho\; \mathrm{diag}(U^{k^*})\mathbf{R}\, E^k \end{aligned} \tag{6.15}$$

[2] At RT, the sample frequency can be a factor γ smaller in the transmitter than in the receiver. It is assumed that the symbol rate in transmitter and receiver are equal. Hence the transmit and receive carrier frequencies are the same.

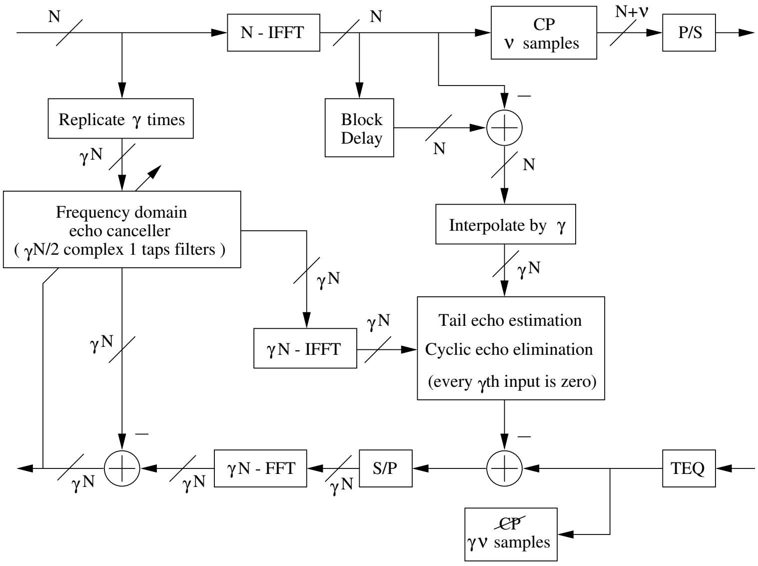

Figure 6.2: Interpolated t/f domain EC at RT [54, 55].

with E^k and $\mathbf{y}^k$ vectors of size $N \times 1$ and W_E^k and U^k vectors of size $\gamma N \times 1$. $\mathbf{D}$ is an $N \times \gamma N$ decimation matrix, $\mathbf{D} = \mathbf{I}_{\gamma N}(1 : \gamma : \gamma N, :)$. Formula (6.15) is the efficient implementation of

$$\begin{aligned} &\textsf{Echo emulation} \quad \mathbf{e}^k = \mathbf{y}^k - \mathbf{D}\boldsymbol{\chi}^{k,k-1}\mathbf{M}\mathbf{w}_E^k - \mathbf{D}\ \mathbf{C}^k\mathbf{w}_E^k \\ &\textsf{Filter adaptation} \quad \mathbf{w}_E^{k+1} = \mathbf{w}_E^k + \rho\ (\mathbf{D}\ \mathbf{C}^k)^{\mathrm{H}}\mathbf{e}^k \end{aligned} \tag{6.16}$$

where $\boldsymbol{\chi}^{k,k-1}$ and $\mathbf{C}^k$ are matrices of size $\gamma N \times \gamma N$ which are decimated by $\mathbf{D}_{N\times\gamma N}$. $\mathbf{U}^{k,k-1} = \boldsymbol{\chi}^{k,k-1} + \mathbf{C}^k$ is a $\gamma N \times \gamma N$ Toeplitz matrix.

Decimated echo cancellation at CO (frame-asynchronous)

In the previous sections, it was assumed that the RT as well as the CO are frame-synchronous, *i.e.* the transmitted and received symbols are aligned in both modems. However, this is in general not possible in reality. Due to the propagation delay of the channel, only one modem can work in a synchronous fashion. Only when twice the propagation delay is an exact multiple of the DMT symbol period, both modems can be frame-synchronous.

In a frame-asynchronous set-up, the cyclic prefix of the transmitted signal can cause echo anywhere in the received symbol, therefore the echo of this cyclic prefix has to be computed. In a frame-synchronous set-up however, the echo caused by the cyclic prefix is added to the cyclic prefix of the received far end

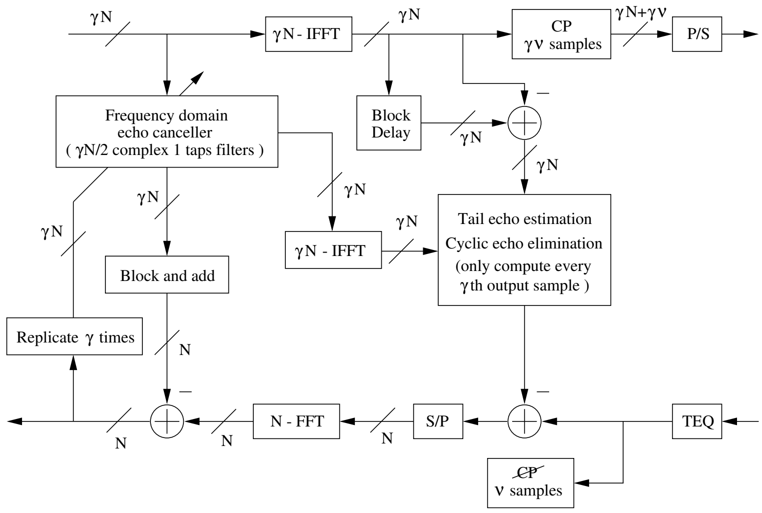

Figure 6.3: Decimated t/f domain EC at CO (frame-synchronous) [54, 55].

signal which is discarded in the receiver.

Ho & Cioffi choose to make the CO frame-asynchronous because this turns out to give the smallest increase in complexity. In their approach, the transmitted signal is decoupled from the received signal by subtracting the echo before demodulating the received symbol. In this way, the EC does not need any knowledge about the misalignment of the transmitted symbols with respect to the received symbols.

The SFG of this algorithm is given in **Fig. 6.4** and is very similar to the SFG for a frame-synchronous EC at CO. The major differences are

- The echo of the transmitted cyclic prefix is computed in the time domain part of the echo emulation by extending the $\mathbf{U}^{k,k-1} = \boldsymbol{\chi}^{k,k-1} + \mathbf{C}^k$ matrix with $\gamma\nu$ rows.

- In the frequency domain part of the echo emulation, the frequency domain echo estimate is modulated (this is an extra IFFT $\mathcal{I}_N$) and a cyclic prefix (CP) is added.

- The prefix of the time domain error symbol is folded and the resulting vector demodulated (extra FFT $\mathcal{F}_N$) to form the frequency domain error vector.

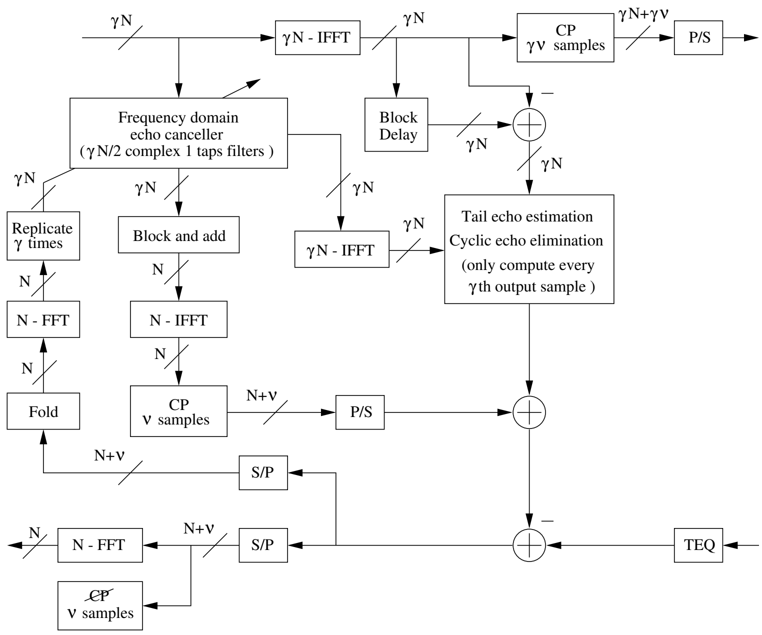

Figure 6.4: Decimated t/f domain EC at CO (frame-asynchronous) [54, 55].

The algorithm is described by the formulas:

$$\begin{aligned} \text{Echo emulation} \quad & \mathbf{e}^k = \mathbf{y}^k - \mathbf{D}\,\boldsymbol{\chi}^{k,k-1}\mathbf{M}\mathbf{w}_E^k - \overbrace{\mathbf{P}\cdot\mathcal{I}_N}^{\mathcal{I}_N \text{ and CP}} \cdot \frac{1}{\gamma}\,\mathbf{R}^{\mathrm{T}}\,\mathrm{diag}(U^k)\,W_E^k \\ \text{Adaptive update} \quad & W_E^{k+1} = W_E^k + \rho\,\mathrm{diag}(U^{k^*})\,\mathbf{R}\cdot \underbrace{\mathcal{F}_N\cdot\mathbf{P}^{\mathrm{T}}}_{\mathcal{F}_N \text{ and CP}} \cdot\mathbf{e}^k \end{aligned} \tag{6.17}$$

with $\mathbf{e}^k$ and $\mathbf{y}^k$ vectors of size $(\nu + N) \times 1$ and W_E^k and U^k vectors of size $\gamma N \times 1$. $\mathbf{P}$ represents the adding of the prefix of size ν to a symbol of size N.

This is the efficient implementation of

$$\begin{aligned} \text{Echo emulation} \quad & \mathbf{e}^k = \mathbf{y}^k - \mathbf{D}\boldsymbol{\chi}^{k,k-1}\mathbf{M}\mathbf{w}_E^k - \mathbf{D}\ \mathbf{C}^k\mathbf{w}_E^k \\ \text{Filter adaptation} \quad & \mathbf{w}_E^{k+1} = \mathbf{w}_E^k + \rho\ (\mathbf{D}\ \mathbf{C}^k)^{\mathrm{H}}\mathbf{e}^k \end{aligned} \tag{6.18}$$

with $\boldsymbol{\chi}^{k,k-1}$ and $\mathbf{C}^k$ matrices of size $\gamma(\nu + N) \times \gamma N$ which are decimated by $\mathbf{D}_{(\nu+N)\times\gamma(\nu+N)}$. $\boldsymbol{\chi}^{k,k-1}$ and $\mathbf{C}^k$ are such that $\mathbf{U}^{k,k-1} = \boldsymbol{\chi}^{k,k-1} + \mathbf{C}^k$ is Toeplitz and consists of the Toeplitz matrix of the frame-synchronous set-up extended with $\gamma\nu$ rows at the beginning corresponding to the cyclic prefix of symbol period k.

	RT	asynchronous CO
size($\boldsymbol{\chi}$)	$\gamma N \times \gamma N$	$\gamma(\nu + N) \times \gamma N$
$\boldsymbol{\chi}$	$\frac{(M-\gamma\nu-1)^2}{2\gamma}$	$\frac{(M-1)^2}{2\gamma}$
asyn.		2 N-point FFTs

Table 6.1: Complexity of t/f domain EC (multiplications/symbol)

Remark that the adder after the block delay has to calculate the last $M-1$ difference terms of the vector $[u_2^{k-1} \dots u_{\gamma N}^{k-1}] - [u_{\gamma N-\gamma\nu+2}^{k} \dots u_{\gamma N}^{k} u_1^k \dots u_{\gamma N-\gamma\nu}^{k}]$.

Complexity

Table 6.1 shows approximate complexities for this approach. Only the complexity of the time domain part of the echo emulation is given (in number of real multiplications per training symbol) because this part dominates complexity and will decrease when applying an alternative alignment. Also the size of the $\boldsymbol{\chi}$ matrix is given and the extra operations for asynchronous mode of operation.

6.1.2 Alternative transmit/receive symbol alignment

Matrix $\boldsymbol{\chi}$ in the previous approach has a non-zero upper triangular part. By applying an alternative symbol alignment, the number of non-zero elements in $\boldsymbol{\chi}$ can be reduced and hence also the corresponding complexity of the time domain part of the echo emulation [140, 67]. In this section we give a matrix interpretation of the algorithm described in [67] and corresponding SFGs which are extensions of the SFGs presented in [54, 55].

Optimal aligned symmetric set-up

The optimal alignment in a symmetric rate set-up is computed as follows. In **Fig. 6.5** an $N \times N$ Toeplitz matrix is drawn with symbol $k-1$ as the symbol of interest. Here n corresponds to the number of different matrix elements from symbol period $k-2$. Hence, $N-\nu-n-1$ corresponds to the number of different matrix elements from symbol period k. The alignment with minimum number of matrix elements from symbol periods other than $k-1$, can then be found by minimizing the cost function

$$\frac{\partial}{\partial n}\left(\frac{n(n+1)}{2} + \frac{(N-\nu-n-1)(N-\nu-n)}{2}\right) = 0 \qquad (6.19)$$

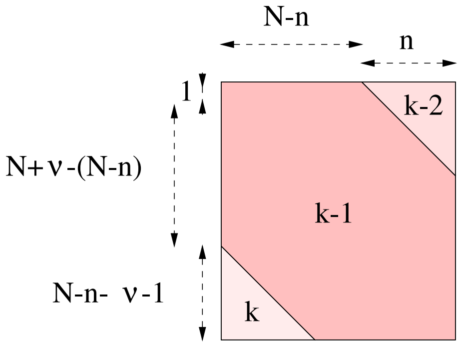

Figure 6.5: Computation of the optimal alignment for an $N \times N$ Toeplitz matrix. $k-1$ is the symbol period of interest. Here n is such that the number of different matrix elements from symbol periods $k-2$ and k is minimal.

The minimum is given by $n = \frac{N-\nu-1}{2}$. However this number is not an integer, therefore we take $n = \frac{N-\nu}{2}$. The Toeplitz matrix $\mathbf{U}^{k,k-1,k-2}$ for the alternative alignment becomes

$$\mathbf{U}^{k,k-1,k-2} = \begin{bmatrix} u^{k-1}_{\frac{N-\nu}{2}} & \cdots & u^{k-1}_1 & u^{k-1}_N & \cdots & u^{k-1}_{N-\nu+1} & u^{k-2}_N & \cdots & u^{k-2}_{\frac{N+\nu}{2}+1} \\ \vdots & \ddots & & & & & & \ddots & \\ u^{k-1}_N & & & & & & & & \ddots \\ u^{k}_{N-\nu+1} & & & & & & & & \\ \vdots & \ddots & & & & & & & \\ u^k_N & & \ddots & & & & & & \\ u^k_1 & & & \ddots & & & & & \\ \vdots & & & & & \ddots & & \ddots & \\ u^k_{\frac{N-3\nu}{2}-1} & & & & & & \ddots & & u^{k-1}_{\frac{N-\nu}{2}} \end{bmatrix} \tag{6.20}$$

which has an upper triangular part containing $\frac{N-\nu}{2}$ samples from symbol period $k-2$ and a lower triangular part containing $\frac{N-\nu-2}{2}$ elements from symbol period k.

The circulant matrix corresponding to this alternative Toeplitz matrix is circularly shifted with respect to the circulant matrix of the Ho & Cioffi approach, see equation (6.5). The element in the first row and the first column is now $u^{k-1}_{\frac{N-\nu}{2}}$ instead of u^k_1

$$\tilde{\mathbf{C}}^{k-1} = \begin{bmatrix} u^{k-1}_{\frac{N-\nu}{2}} & \dots & u^{k-1}_1 & u^{k-1}_N & \dots & u^{k-1}_{N-\nu+1} & u^{k-1}_{N-\nu} & \dots & u^{k-1}_{\frac{N-\nu}{2}+1} \\ \vdots & \ddots & & & & & & \ddots & \\ u^{k-1}_N & & & & & & & & \ddots \\ u^{k-1}_1 & & & & & & & & \\ \vdots & \ddots & & & & & & & \\ u^{k-1}_{\frac{N-\nu}{2}-1} & & \ddots & & & & & & \end{bmatrix} \tag{6.21}$$

$$\boldsymbol{\chi}^{k,k-1,k-2} = \mathbf{U}^{k,k-1,k-2} - \tilde{\mathbf{C}}^{k-1} \tag{6.22}$$

Frame-asynchronous symmetric set-up

In this section, we assume a simplified CO in that is it symmetric but still frame-asynchronous.

For the frame-asynchronous EC at CO, implemented with 2 extra FFTs, a similar optimization can be done. However the needed Toeplitz matrix is rectangular in stead of square and has size $(\nu + N) \times N$. Therefore the optimal alignment will be different. The Toeplitz matrix, leading to minimal complexity, has an upper triangular part containing $n = \frac{N}{2}$ samples from symbol period $k - 2$ and a lower triangular part containing $n = \frac{N-2}{2}$ samples from symbol period k, and thus

$$\mathbf{U}^{k,k-1,k-2} = \begin{bmatrix} u^{k-1}_{\frac{N}{2}-\nu} & \cdots & u^{k-1}_{1} & u^{k-1}_{N} & \cdots & u^{k-1}_{N-\nu+1} & u^{k-2}_{N} & \cdots & u^{k-2}_{\frac{N}{2}+1} \\ \vdots & \ddots & & & & & & \ddots & \\ u^{k-1}_{\frac{N}{2}-1} & & & & & & & & \ddots \\ u^{k-1}_{\frac{N}{2}} & & & & & & & & \\ \vdots & \ddots & & & & & & & \\ u^{k-1}_{N} & & & & & & & & \\ u^{k}_{N-\nu+1} & & & & & & & & \\ \vdots & \ddots & & & & & & & \\ u^{k}_{N} & & \ddots & & & & & & \\ u^{k}_{1} & & & \ddots & & & & & \\ \vdots & & & & \ddots & & & \ddots & \\ u^{k}_{\frac{N}{2}-\nu-1} & & & & & \ddots & & & u^{k-1}_{\frac{N}{2}} \end{bmatrix} \tag{6.23}$$

The corresponding (extended) circulant matrix $\tilde{\mathbf{C}}^{k-1}$ is made by substituting all samples not from symbol period $k-1$ by the circular extension of samples from $k-1$. The (extended) $\boldsymbol{\chi}$ matrix equals $\mathbf{U}^{k,k-1,k-2} - \tilde{\mathbf{C}}^{k-1}$.

An overview of these alignments is given in **Fig. 6.6**. For the alternative alignment, the Toeplitz matrix indicated with ‘AA’ has symbol $k-1$ as symbol of interest. As can be seen, the optimal alignment for RT and CO differ.

When the time domain filter has a length $M < N$, one applies the alignment such that the non-zero portion of the time domain filter multiplies with the center columns of $\mathbf{U}^{k,k-1,k-2}$. This gives rise to the submatrix of $\mathbf{U}^{k,k-1,k-2}$ with minimum number of elements not from symbol period $k-1$. The full matrix $\mathbf{U}^{k,k-1,k-2}$ is independent of the window length, hence the circular shift in $\tilde{\mathbf{C}}^{k-1}$ stays the same. In the subsequent formulas,

$$\mathbf{M} = \begin{bmatrix} \mathbf{O}_{(\gamma N-M)/2} & \mathbf{O} & \mathbf{O} \\ \mathbf{O} & \mathbf{I}_M & \mathbf{O} \\ \mathbf{O} & \mathbf{O} & \mathbf{O}_{(\gamma N-M)/2} \end{bmatrix}.$$

Interpolated echo cancellation at RT (optimal aligned)

At RT, the interpolated EC is based on an $(\gamma N \times \gamma N)$ $\boldsymbol{\chi}$ matrix with an upper triangular part of size $\frac{\gamma N-\gamma\nu}{2}$ and a lower triangular part of size $\frac{\gamma N-\gamma\nu-2}{2}$.

The SFG of the EC at RT with alternative alignment is depicted in **Fig. 6.7**. The main differences with respect to the original alignment are

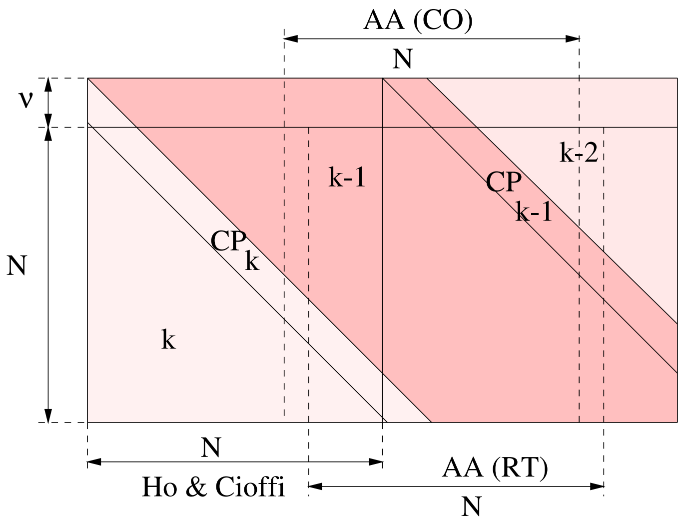

Figure 6.6: Large Toeplitz matrix with 3 symbols to compare the alternative alignment(AA) with the original alignment.

- in the time domain part
  - an extra block delay to account for symbol $u_{1:N}^{k-2}$
  - an extra adder
  - an extra time domain EC to compute the echo caused by the head of the next echo symbol $u_{1:N}^{k}$ and to subtract the echo caused by the cyclic extension of the symbol of interest $u_{1:N}^{k-1}$
- in the frequency domain part
  - an extra block delay because $u_{1:N}^{k-1}$ is the symbol of interest
  - a phase block

Due to the circular shift of the circulant matrix, a phase shift is needed in the EC. The phase shift for tone i equals

$$p_i = e^{-j2\pi \frac{i-1}{\gamma N}(\gamma N - \frac{\gamma N - \gamma\nu}{2}+1)} = e^{-j2\pi \frac{i-1}{\gamma N}\frac{\gamma N+\gamma\nu+2}{2}} \quad \text{for } i = 1 \ldots \gamma N \qquad (6.24)$$

which can be proven by applying equation (4.29). One can implement this phase explicitly in the frequency domain as in **Fig. 6.7**. The formulas describing the EC are

$$\begin{array}{ll} \textsf{Echo emulation} & E^k = \mathcal{F}_{\gamma N}(\mathbf{y}^k - \boldsymbol{\chi}^{k,k-1,k-2}\mathbf{M}\mathbf{w}_E^k) - \mathrm{diag}(\mathbf{p})\mathrm{diag}(\mathbf{R}\ U^{k-1})W_E^k \\ \textsf{Filter adaptation} & W_E^{k+1} = W_E^k + \rho\ \mathrm{diag}(\mathbf{R}\ (U^{k-1})^*)\mathrm{diag}(\mathbf{p}^*)E^k \end{array} \qquad (6.25)$$

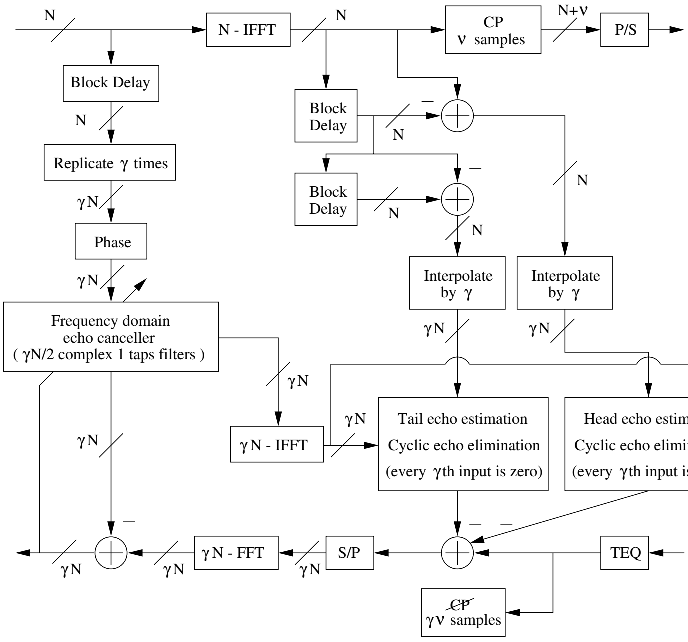

Figure 6.7: Interpolated t/f domain EC at RT with (optimal) alternative alignment. The square matrix $\boldsymbol{\chi}$ has the minimum number of non-zero elements.

with $\boldsymbol{\chi}^{k,k-1,k-2}$ the correction matrix corresponding to the alternative alignment, $\mathbf{p} = [p_1 \dots p_{\gamma N}]$ and $\mathbf{w}_E^k = \mathcal{I}_{\gamma N} W_E^k$.

However, this phase shift can also be included in the frequency domain filter coefficients $\tilde{W}_E^k = \text{diag}(\mathbf{p}) W_E^k$. Because multiplication with a phase shift in the frequency domain is equivalent with a time domain shift, the time domain filter coefficients, $\tilde{\mathbf{w}}_E^k = \mathcal{I}_{\gamma N} \tilde{W}_E^k$, will be shifted over $\frac{\gamma N + \gamma \nu + 2}{2}$ elements. One needs to undo the time domain shift to obtain the right time domain part of the echo estimation by shifting over $-\frac{\gamma N + \gamma \nu + 2}{2}$: $\mathbf{w}_E^k = \text{undo-shift}(\tilde{\mathbf{w}}_E^k)$. The EC is then described by

$$\begin{aligned} \textsf{Echo emulation} \quad & E^k = \mathcal{F}_{\gamma N}(\mathbf{y}^k - \boldsymbol{\chi}^{k,k-1,k-2} \mathbf{M} \mathbf{w}_E^k) - \text{diag}(\mathbf{R}\ U^{k-1}) \tilde{W}_E^k \\ \textsf{Filter adaptation} \quad & \tilde{W}_E^{k+1} = \tilde{W}_E^k + \rho\ \text{diag}(\mathbf{R}\ (U^{k-1})^*) E^k \end{aligned} \tag{6.26}$$

The SFG of this EC is analogous to **Fig. 6.7**. The differences are the removal of the phase shift in the frequency domain and the addition of the 'undo-shift' function after the γN-point IFFT block transforming $\tilde{W}_E^k$.

Remark that the adder before the tail echo estimation in **Fig. 6.7** forms $\frac{N-\nu}{2}$ difference terms, $[u^{k-2}_{\frac{N+\nu+2}{2}} \dots u^{k-2}_N] - [u^{k-1}_{\frac{N-\nu+2}{2}} \dots u^{k-1}_{N-\nu}]$, and the adder before the head echo estimation forms $\frac{N-\nu-2}{2}$ difference terms, $[u^k_{N-\nu+1} \dots u^k_N u^k_1 \dots u^k_{\frac{N-3\nu-2}{2}}] - [u^{k-1}_1 \dots u^{k-1}_{\frac{N-\nu-2}{2}}]$, according to the upper and lower triangle in $\boldsymbol{\chi}$.

Decimated echo cancellation at CO (frame-asynchronous)

For the CO, which works frame-asynchronously, there are two options [140, 67]:

1. One takes the optimal alignment for minimal time domain convolution and adds the 2 extra FFTs for asynchronism as in the original EC for CO [54, 55]. An extended Toeplitz matrix $\mathbf{U}^{k,k-1,k-2}$ of size $\gamma(N+\nu) \times \gamma N$ is needed, similar to formula (6.23) with N and ν substituted by γN and $\gamma\nu$ respectively. Again a fixed phase is added in the frequency domain part of the EC or an 'undo-shift' function in the time domain part. The phase is determined by the $(\gamma\nu+1,1)$-element of the extended Toeplitz matrix, *i.e.* $u^{k-1}_{\frac{\gamma N}{2}}$:

$$p_i = e^{-j2\pi\frac{i-1}{\gamma N}(\gamma N - \frac{\gamma N}{2}+1)} = e^{-j2\pi\frac{i-1}{\gamma N}\frac{\gamma N+2}{2}} \quad \text{for } i = 1 \dots \gamma N \tag{6.27}$$

   The EC is described by

$$\text{Echo emulation} \quad \mathbf{e}^k = \mathbf{y}^k - \mathbf{D}\,\boldsymbol{\chi}^{k,k-1,k-2}\mathbf{M}\mathbf{w}^k_E - \mathbf{P}\,\mathcal{I}_N\,\frac{1}{\gamma}\,\mathbf{R}^{\mathrm{T}}\,\mathrm{diag}(U^{k-1})\,\tilde{W}^k_E$$

$$\text{with} \quad \mathbf{w}^k_E = \text{undo-shift}(\tilde{\mathbf{w}}^k_E) \quad \text{and} \quad \tilde{\mathbf{w}}^k_E = \mathcal{I}_{\gamma N}\tilde{W}^k_E \tag{6.28}$$

$$\text{Filter adaptation} \quad \tilde{W}^{k+1}_E = \tilde{W}^k_E + \rho\ \mathrm{diag}((U^{k-1})^*)\,\mathbf{R}\,\mathcal{F}_N\,\mathbf{P}^{\mathrm{T}}\,\mathbf{e}^k \tag{6.29}$$

   The SFG of the asynchronous EC at CO with extra FFTs is given in **Fig. 6.8**. Remark that the adder before the tail estimation forms $\frac{N}{2}$ difference terms, $[u^{k-2}_{\frac{N+2}{2}} \dots u^{k-2}_N] - [u^{k-1}_{\frac{N-2\nu+2}{2}} \dots u^{k-1}_{N-\nu}]$, and the adder before the head estimation forms $\frac{N-2}{2}$ difference terms, $[u^k_{N-\nu+1} \dots u^k_N u^k_1 \dots u^k_{\frac{N-2\nu-2}{2}}] - [u^{k-1}_1 \dots u^{k-1}_{\frac{N-2}{2}}]$.

2. One discards the ν samples of the received signal first. Hence, the echo on these ν prefix samples does not have to be computed anymore and the 2 extra FFTs can be deleted. But the EC needs the knowledge about the misalignment of the transmitted symbols with respect to the received symbols, which is a function of the propagation delay of the channel δ and thus loop dependent. This is explained in **Fig. 6.9** [3].

[3] It is assumed that the echo filter length M is the same at RT and CO.

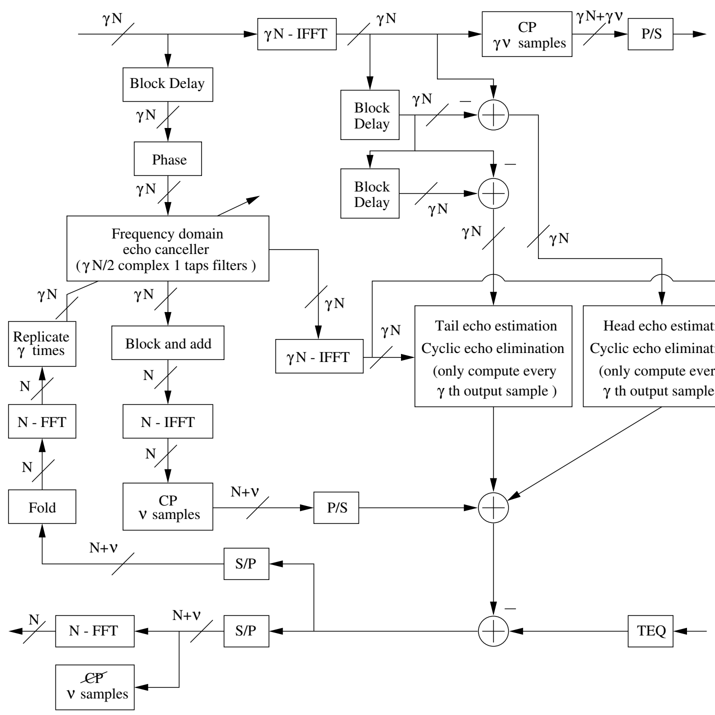

Figure 6.8: Decimated t/f domain EC at CO with (optimal) alternative alignment and 2 extra FFTs for frame-asynchronism. The rectangular matrix $\boldsymbol{\chi}$ has the minimum number of non-zero elements.

The optimal alignment of the echo with respect to the received signal is $-\Delta = \gamma \cdot \nu/2 - M/2$ samples before the symbol. If the optimal alignment is applied at RT, then the deviation of the optimal alignment at CO is $2\delta - 2\Delta$. In this set-up one works again with a Toeplitz matrix $\mathbf{U}^{k,k-1,k-2}$ of size $\gamma N \times \gamma N$ as in the RT case but now $\mathbf{U}^{k,k-1,k-2}$ is not the optimal aligned matrix but delay dependent. Therefore also the phase or the 'undo-shift' operation is delay dependent. This EC for CO is shown in **Fig. 6.10**. Again, the frequency domain phase shift can be substituted by an 'undo-shift' operation in the time domain.

Echo emulation
$$E^k = \mathcal{F}_N(\mathbf{y}^k - \mathbf{D}\boldsymbol{\chi}^{k,k-1,k-2}\mathbf{M}\mathbf{w}_E^k) - \frac{1}{\gamma}\mathbf{R}^{\mathrm{T}}\,\mathrm{diag}(U^{k-1})\tilde{W}_E^k$$
$$\text{with} \quad \mathbf{w}_E^k = \text{undo-shift}(\tilde{\mathbf{w}}_E^k) \quad \text{and} \quad \tilde{\mathbf{w}}_E^k = \mathcal{I}_{\gamma N}\tilde{W}_E^k \quad (6.30)$$

Filter adaptation
$$\tilde{W}_E^{k+1} = \tilde{W}_E^k + \rho\;\mathrm{diag}((U^{k-1})^*)\mathbf{R}\,E^k \quad (6.31)$$

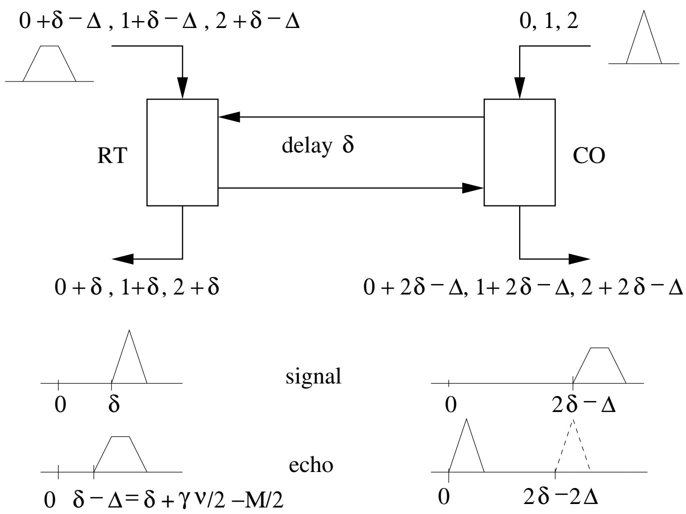

Figure 6.9: The alignment $-\Delta$ of RT is optimal, *i.e.* with minimum number of non zero elements in $\boldsymbol{\chi}$. The deviation of the optimal alignment at CO is $2\delta - 2\Delta$ where δ is the delay of the channel.

Complexity

Complexities are presented in **Table 6.2**. The approximate complexity of the time domain part of the echo emulation is counted in number of real multiplications per symbol. Furthermore the size of matrix $\boldsymbol{\chi}$, the extra operations for asynchronism and the phase shift are given. Depending on the propagation delay of the channel, the first or the second method for the CO is the cheapest one. In section 6.2, this delay dependency of the complexity is illustrated for some values of the propagation delay.

6.2 Order of TEQ and t/f domain echo cancellation

6.2.1 'First-TEQ-then-echo'

In the previous section, it is assumed that a time domain equalizer (TEQ) is applied before the EC, see figures 6.1, 6.2, 6.3, 6.4, 6.7, 6.8, 6.10. Therefore, the TEQ does not explicitly appear in the describing formulas. This approach is further called *'First-TEQ-then-echo'*. The TEQ is part of the echo path and hence the model of this path, $\mathbf{w}_E^k$, will include the TEQ. If the TEQ is designed to shorten the (far end) channel impulse response only, it will in

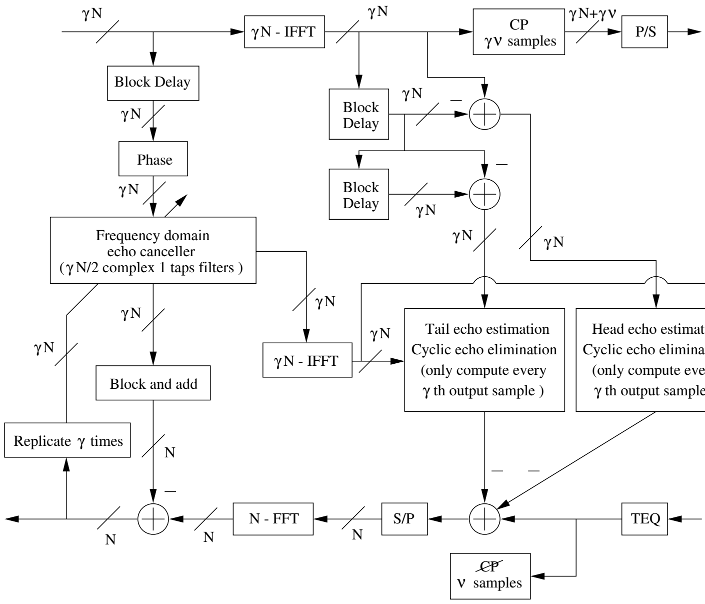

Figure 6.10: Decimated t/f domain EC at CO with alignment dependent of the channel propagation delay. Phase and shape of the time domain correction $\boldsymbol{\chi}$ depend on the misalignment between transmitted and received symbol because the two extra FFTs are removed and the CO works frame-asynchronously.

	RT	CO (opt. align.)	CO
size($\boldsymbol{\chi}$)	$\gamma N \times \gamma N$	$\gamma(\nu + N) \times \gamma N$	$\gamma N \times \gamma N$
$\boldsymbol{\chi}$	$\frac{1}{2\gamma}((\frac{M-\gamma\nu}{2})^2 + (\frac{M-\gamma\nu-2}{2})^2)$	$\frac{1}{2\gamma}((\frac{M}{2})^2 + (\frac{M-2}{2})^2)$	delay dependent
asyn.		2 FFTs	
phase	fixed	fixed	delay dependent

Table 6.2: Complexity of t/f domain EC with alternative alignment (multiplications/symbol).

general lengthen the echo impulse response, thereby necessitating a longer echo filter. If M is the length of the required echo filter without T-taps TEQ in the echo path, the length of the required echo filter in general becomes $M + T - 1$

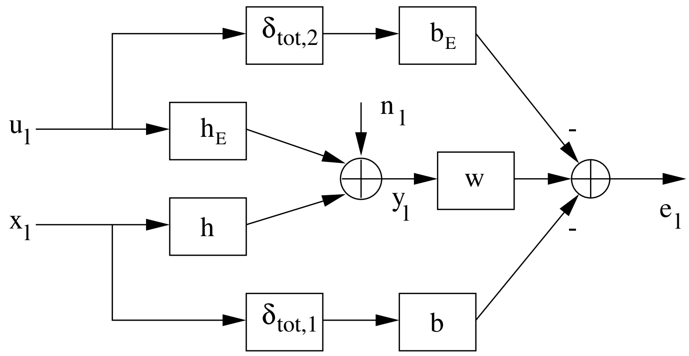

Figure 6.11: Joint channel shortening by an MMSE approach [3].

with the TEQ in the echo path.

A technique called *joint shortening* enables to trade off channel impulse response shortening for echo impulse response shortening [3, 80, 136]. Joint shortening is an extension of the shortening procedure described in chapter 3. **Fig. 6.11** presents the algorithmic approach. Compared to figure 3.1, there is an extra branch for the echo impulse response (EIR) $\mathbf{h}_E$ and for the target echo response $\mathbf{b}_E$. The following MSE criterion is minimized

$$
\begin{aligned}
&\mathcal{E}\{e_l^2\} \\
&= \mathcal{E}\left\{\left(\left[y_{l:-1:l-T+1}|u_{l-\delta_{\text{tot},2}:-1:l-\delta_{\text{tot},2}-\nu_E}|x_{l-\delta_{\text{tot},1}:-1:l-\delta_{\text{tot},1}-\nu}\right]\cdot\begin{bmatrix}\mathbf{w}\\-\mathbf{b}_E\\-\mathbf{b}\end{bmatrix}\right)^2\right\} \\
&= \left\|\begin{bmatrix}\mathbf{R}_{xx}^{1/2} & \mathbf{O} & \mathbf{O}\\ \mathbf{O} & \mathbf{R}_{nn}^{1/2} & \mathbf{O}\\ \mathbf{O} & \mathbf{O} & \mathbf{R}_{uu}^{1/2}\end{bmatrix}\cdot\left[\begin{array}{c|c|c}\mathbf{H} & \mathbf{O} & \begin{array}{c}\mathbf{O}_{\delta_{\text{tot},1}\times(\nu+1)}\\ \mathbf{I}_{\nu+1}\\ \mathbf{O}\end{array}\\ \hline \mathbf{I}_T & \mathbf{O} & \mathbf{O}\\ \hline \mathbf{H}_E & \begin{array}{c}\mathbf{O}_{\delta_{\text{tot},2}\times(\nu_E+1)}\\ \mathbf{I}_{\nu_E+1}\\ \mathbf{O}\end{array} & \mathbf{O}\end{array}\right]\cdot\begin{bmatrix}\mathbf{w}\\-\mathbf{b}_E\\-\mathbf{b}\end{bmatrix}\right\|_2^2
\end{aligned}
\tag{6.32}
$$

In the second line, we adopted an impulse response identification based approach. $\mathbf{H}$ and $\mathbf{H}_E$ are Toeplitz matrices of the CIR $\mathbf{h}$ and EIR $\mathbf{h}_E$ respectively. $\mathbf{R}$ represents the correlation matrix of signal x_l, echo u_l and noise samples n_l respectively. This set of equations is solved under a certain constraint to avoid trivial solutions. This can again be a unit norm, a unit tap or a unit energy constraint, analogous to the channel impulse response shortening in chapter 3.

Because the MMSE criterion and the constraints have no direct relation to optimal bit rate, it may be difficult to select the appropriate constraint.

Knowing that channel impulse response shortening only is already a difficult problem if the criterion is optimal capacity, it is hard to predict whether joint shortening will eventually improve the system performance or not. Two features are important here, namely complexity and capacity. On the one hand, the EC complexity is decreased when the echo path is shortened. But then, on the other hand, joint shortening can lead to a poorer channel response shortening which reduces capacity, unless the TEQ length is increased. This in turn increases the TEQ complexity. The advantage of joint shortening will depend on the effectiveness of the applied algorithm. However, when the applied criterion is optimal shortening of impulse responses in the time domain, it is known that there is no direct correspondence with optimal resulting capacity and hence the obtained capacity will be an unpredictable function of the decision delay, as explained in chapter 3.

6.2.2 'First-echo-then-TEQ'

To avoid the lengthening of the echo path by the TEQ, one can first apply echo cancellation and then equalization. This approach is called *'First-echo-then-TEQ'*.

We derive the formulas describing the 'First-echo-then-TEQ' set-up for the special case of a symmetric-rate modem with alignment of transmit and receive symbols as in formulas (6.10) and (6.11). Extensions to the alternative alignment, asymmetric and asynchronous mode can be made. The t/f domain EC of Ho & Cioffi can be extended to this set-up as follows. The starting formula for 'First-echo-then-TEQ' is

$$E^k = \mathcal{F}_N \cdot \overbrace{\begin{bmatrix} \bar{\mathbf{w}}^{\mathrm{T}} & 0 & \dots \\ 0 & \ddots & \\ \vdots & 0 & \bar{\mathbf{w}}^{\mathrm{T}} \end{bmatrix}}^{\mathcal{T}} \cdot (\mathbf{y}^k_{ext} - \mathbf{U}^{k,k-1}_{ext} \cdot \mathbf{w}^k_E) \tag{6.33}$$

where $\mathbf{w}$ is the T-taps TEQ[4], $\mathcal{T}$ is a Toeplitz matrix with the TEQ coefficients. The number of rows of $\mathbf{y}^k_{ext}$ and $\mathbf{U}^{k,k-1}_{ext}$ is increased with respect to the 'First-TEQ-then-echo' set-up, see formula (6.3), namely to $T-1+N$. The $T-1$ extra rows are added as first rows. Hence, one has $\mathbf{y}^k_{ext} = [y^k_{-T+2} \dots y^k_0 y^k_1 \dots y^k_N]^{\mathrm{T}}$.

[4] $\bar{\mathbf{w}}$ denotes vector $\mathbf{w}$ with its elements in reverse order.

The extended Toeplitz matrix $\mathbf{U}_{ext}^{k,k-1}$ can be written as[5]

$$\mathbf{U}_{ext}^{k,k-1} = \begin{bmatrix} u_{N-T+2}^k & u_{N-T+1}^k & \cdots & & & & \\ \vdots & \ddots & & & & & \\ u_N^k & u_1^k & \ddots & \ddots & & \ddots & \\ u_1^k & u_N^k & \cdots & u_{N-\nu+1}^k & u_N^{k-1} & \cdots & u_{\nu+2}^{k-1} \\ u_2^k & u_1^k & \ddots & & & \ddots & \\ \vdots & \ddots & \ddots & & & & \\ u_N^k & \ddots & & & & & \end{bmatrix} \tag{6.34}$$

This extended Toeplitz matrix is then written as the sum of an extended circulant matrix and an extended correction matrix. The first $T-1$ rows of the extended circulant matrix are equal to the last $T-1$ rows of that matrix. Therefore, one can write analogous to formula (6.4) that

$$\mathbf{U}_{ext}^{k,k-1} = \mathbf{P} \cdot \mathbf{C}^k + \boldsymbol{\chi}_{ext}^{k,k-1} \tag{6.35}$$

where $\mathbf{P} = \left[\begin{array}{c|c} \mathbf{O} & \mathbf{I}_{T-1} \\ \hline \multicolumn{2}{c}{\mathbf{I}_N} \end{array}\right]$ repeats the last $T-1$ rows of $\mathbf{C}^k$ as first rows. The frequency domain echo cancelled received symbol can then be written as

$$\begin{aligned} E^k &= \mathcal{F}_N \cdot \mathcal{T} \cdot \left(\mathbf{y}_{ext}^k - \mathbf{P} \cdot \mathbf{C}^k \cdot \mathbf{w}_E^k - \boldsymbol{\chi}_{ext}^{k,k-1} \cdot \mathbf{w}_E^k\right) \\ &= \mathcal{F}_N \cdot \mathcal{T} \cdot \left(\mathbf{y}_{ext}^k - \boldsymbol{\chi}_{ext}^{k,k-1} \cdot \mathbf{w}_E^k\right) - \mathcal{F}_N \cdot \mathcal{T} \cdot \mathbf{P} \cdot \mathbf{C}^k \cdot \mathbf{w}_E^k \end{aligned} \tag{6.36}$$

The matrix product $\mathcal{T} \cdot \mathbf{P}$ forms a circulant matrix with the zero-padded TEQ coefficients. Therefore, we may now apply twice the property of the eigenvalue decomposition of a circulant matrix in the second term of formula (6.36)

$$\mathcal{F}_N \cdot \mathcal{T} \cdot \mathbf{P} \cdot \mathbf{C}^k \cdot \mathbf{w}_E^k = \underbrace{\mathcal{F}_N \cdot \mathcal{T} \cdot \mathbf{P} \cdot \mathcal{I}_N}_{\mathrm{diag}(\mathcal{F}_N \cdot \begin{bmatrix} \mathbf{w} \\ \mathbf{0} \end{bmatrix})} \cdot \underbrace{\mathcal{F}_N \cdot \mathbf{C}^k \cdot \mathcal{I}_N}_{\mathrm{diag}(U^k)} \cdot \underbrace{\mathcal{F}_N \cdot \mathbf{w}_E^k}_{W_E^k} \tag{6.37}$$

The echo emulation is then described by

$$\textsf{Echo emulation} \quad E_k = \mathcal{F}_N \mathcal{T} \left(\mathbf{y}_{ext}^k - \boldsymbol{\chi}_{ext}^{k,k-1} \mathbf{w}_E^k\right) - \mathrm{diag}(\mathcal{F}_N \begin{bmatrix} \mathbf{w} \\ \mathbf{0} \end{bmatrix}) \mathrm{diag}(U^k) W_E^k \tag{6.38}$$

[5] Note that if $T-1 > \nu$, vector $\mathbf{y}_{ext}^k$ and the first column of $\mathbf{U}_{ext}^{k,k-1}$ will also contain received signal samples at symbol period $k-1$.

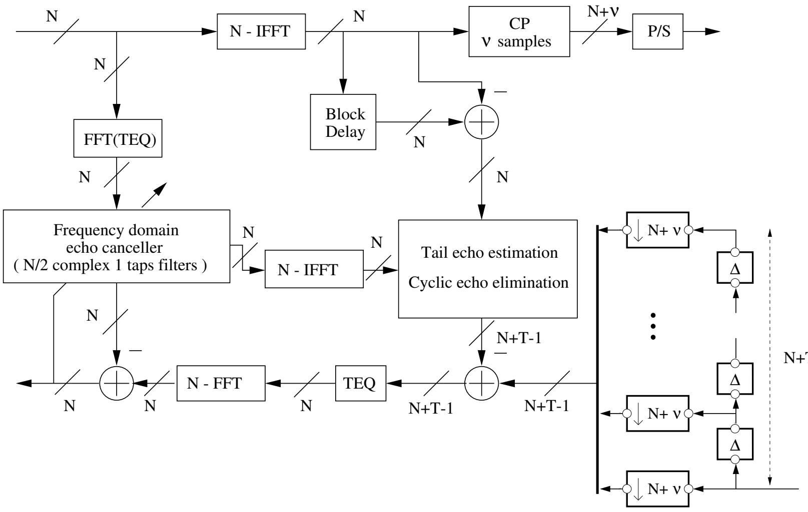

Figure 6.12: EC in a 'First-echo-then-TEQ' symmetric-rate set-up with aligned transmit and receive symbols.

If only the frequency domain part of the filter input is taken into account in the filter adaptation, one has the following updating formula

$$\textsf{Filter adaptation} \quad W_E^{k+1} = W_E^k + \rho\,\mathrm{diag}(U^{k^*}) \cdot \mathrm{diag}(\mathcal{F}_N \begin{bmatrix} \mathbf{w} \\ \mathbf{0} \end{bmatrix})^* \cdot E^k \tag{6.39}$$

The echo filter only models the echo channel, so without TEQ. But the TEQ appears in the error and the filter input and as such influences the adaptation. A SFG for the symmetric rate set-up is given in **Fig. 6.12**. Remark firstly that the removal of the cyclic prefix is incorporated in the tapped delay line (of length $N + T - 1$) with downsamplers (from sample rate to symbol rate). Moreover the tapped delay line allows to model the case where $T - 1 > \nu$. Secondly, the 'TEQ' block has to perform a convolution for N samples per symbol instead of $N + \nu$, because the cyclic prefix is already removed. The SFGs for the alternative alignment, asymmetric rate and asynchronous ECs can be modified to the 'First-echo-then-TEQ' approach in a similar way.

Due to the extra matrix $\mathcal{T}$ in formula (6.38), convergence in the mean is not easily proven for the filter adaptation of the 'First-echo-then-TEQ' scheme. However, our goal is to show how one can change the order of equalization and EC in the DMT transceiver to apply finally per tone equalization instead of TEQ, see section 6.3. Hence, the 'First-echo-then-TEQ' is merely and intermediate scheme. The *'First-echo-then-per tone equalization'* approach allows to optimize capacity, given an EC in the combined t/f domain implementation.

	TEQ	EC (only $\boldsymbol{\chi}$)
First-TEQ-then-EC	$F_s T$	$\frac{F_s}{N+\nu}\frac{(M-\nu-1)^2}{2}$
First-EC-then-TEQ	$\frac{F_s}{N+\nu}(TN+2N)$	$\frac{F_s}{N+\nu}\frac{(M+T-1-\nu-1)^2}{2}$

Table 6.3: Complexity comparison of 'First-TEQ-then-echo' and 'First-echo-then-TEQ' in a symmetric rate set-up with aligned transmit and receive symbols (multiplications/s).

6.2.3 Complexity comparison

We compare the complexity of the 'First-TEQ-then-echo' and 'First-echo-then-TEQ' set-up for a symmetric-rate set-up with aligned transmit and receive symbols.

The number of multiplications is counted for those computations that differ in the two schemes, *i.e.* the TEQ operation in the time domain, the multiplication with the FFT of the TEQ and the size of the time domain echo emulation $\boldsymbol{\chi}$. The multiplication with the FFT of the TEQ is counted as $4N/2$ operations per symbol for Cartesian representation (there are $N/2$ Hermetian symmetric frequency domain taps). A complexity comparison is given in **Table 6.3**[6]. F_s is the sample frequency.

For a given M the 'First-echo-then-TEQ' set-up is more expensive than the 'First-TEQ-then-echo' set-up due to $T-1$ extra rows in the extended $\boldsymbol{\chi}$ matrix and the multiplication with the FFT of the TEQ. However a fair comparison takes into account the possible lengthening of the echo path by the TEQ in the 'First-TEQ-then-echo' set-up. Therefore, one better compares the complexity of 'First-echo-then-TEQ' for a given M with 'First-TEQ-then-echo' for M increased by $T-1$. The corresponding Toeplitz matrix, describing the EC, is shown in **Fig. 6.13** (for $T-1 \leq \nu$). The gray part contains samples from symbol period $k-1$. It is seen that adding $T-1$ extra rows as in the 'First-echo-then-TEQ' approach or adding $T-1$ columns as in the 'First-TEQ-then-echo' approach, for the possible lengthening of the echo path by the TEQ, adds the same number of samples from symbol period $k-1$ to the extended Toeplitz matrix. In conclusion, the same number of non-zero elements is added to the extended $\boldsymbol{\chi}$ matrix and the resulting complexities of the time domain echo emulation are equal.

A similar figure can be made for the alternative alignment with a small upper triangle and a small lower triangle in the Toeplitz matrix, the complexities of

[6] Remark that we assumed an upper triangular matrix $\boldsymbol{\chi}$ in the 'First-echo-then-TEQ' set-up, which is exact for $T-1 \leq \nu$. Slightly adapted formulas apply when $T-1 > \nu$ because then $\boldsymbol{\chi}$ has an upper trapezium part different from zero.

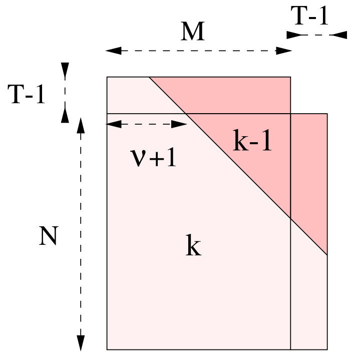

Figure 6.13: A $N \times M$ Toeplitz matrix extended with $T-1$ rows or $T-1$ columns results in the same complexity for the time domain echo emulation. Here the alignment of the Toeplitz matrix is according to [54, 55].

the $\boldsymbol{\chi}$ matrix given in table 6.3 then have an extra factor 1/2.

6.3 T/f domain echo cancellation and per tone equalization

The advantage of applying first EC and then equalization, is that the combined t/f domain EC may subsequently also be combined with per tone equalization (PT-EQ), as an alternative to the usual TEQ scheme. The TEQ initialization problem is a difficult problem, and current procedures are based on an optimization criterion which has no obvious link to the ultimately obtained capacity. This in particular makes a fair comparison between different EC schemes significantly more difficult. The PT-EQs, on the other hand, have an equalizer initialization scheme based on a criterion that has an obvious link to overall capacity, see chapter 4.

Per received symbol, the T-taps PT-EQ for tone i has as its inputs one FFT output for tone i and $T-1$ difference terms

$$Z_i^k = \bar{\mathbf{v}}_i^{\mathrm{T}} \cdot \left[\begin{array}{c|c|c} \mathbf{I}_{T-1} & \mathbf{O} & -\mathbf{I}_{T-1} \\ \hline \mathbf{O} & \multicolumn{2}{c}{\mathcal{F}_N(i,:)} \end{array} \right] \cdot \mathbf{y}_{ext}^k \tag{6.40}$$

where $\mathbf{y}_{ext}^k$ is an $N+T-1$ vector of received samples from symbol period k. The $T-1$ difference terms are independent of the tone index i, so they are common for all PT-EQs. The FFT output is tone dependent. $\bar{\mathbf{v}}_i^{\mathrm{T}} = [v_{i,T-1} \ldots v_{i,0}]$ is the T-taps PT-EQ for tone i. Z_i^k is the equalizer output for tone i at symbol period k. A SFG of PT-EQ is given in figure 4.2.

The t/f domain EC in a symmetric-rate set-up with transmit/receive symbol alignment[7] may be combined with PT-EQ as follows. In a 'First-echo-then-per tone equalization' set-up, the inputs of the PT-EQ should now correspond to received samples after EC. These inputs are given by

$$\begin{bmatrix} \mathbf{e}^k \\ E_i^k \end{bmatrix} = \left[\begin{array}{c|c|c} \mathbf{I}_{T-1} & \mathbf{O} & -\mathbf{I}_{T-1} \\ \hline \mathbf{O} & \multicolumn{2}{c}{\mathcal{F}_N(i,:)} \end{array}\right] \cdot \left(\mathbf{y}_{ext}^k - \mathbf{U}_{ext}^{k,k-1}\ \mathbf{w}_E^k\right) \tag{6.41}$$

Toeplitz matrix $\mathbf{U}_{ext}^{k,k-1}$ is given in formula (6.34), $\mathbf{e}^k$ is a $(T-1)\times 1$ vector of echo cancelled difference terms and E_i^k is the FFT output of echo cancelled received signal samples, for tone i at symbol period k. By applying formula (6.35), one can write the PT-EQ input as

$$\begin{aligned} \begin{bmatrix} \mathbf{e}^k \\ E_i^k \end{bmatrix} &= \left[\begin{array}{c|c|c} \mathbf{I}_{T-1} & \mathbf{O} & -\mathbf{I}_{T-1} \\ \hline \mathbf{O} & \multicolumn{2}{c}{\mathcal{F}_N(i,:)} \end{array}\right] \left(\mathbf{y}_{ext}^k - \boldsymbol{\chi}_{ext}^{k,k-1}\ \mathbf{w}_E^k\right) \\ &\quad - \left[\begin{array}{c|c|c} \mathbf{I}_{T-1} & \mathbf{O} & -\mathbf{I}_{T-1} \\ \hline \mathbf{O} & \multicolumn{2}{c}{\mathcal{F}_N(i,:)} \end{array}\right] \mathbf{P}\mathbf{C}^k\ \mathbf{w}_E^k \end{aligned} \tag{6.42}$$

The second term can be simplified, because

$$\begin{aligned} \left[\begin{array}{c|c|c} \mathbf{I}_{T-1} & \mathbf{O} & -\mathbf{I}_{T-1} \\ \hline \mathbf{O} & \multicolumn{2}{c}{\mathcal{F}_N(i,:)} \end{array}\right] \cdot \mathbf{P} &= \left[\begin{array}{c|c|c} \mathbf{I}_{T-1} & \mathbf{O} & -\mathbf{I}_{T-1} \\ \hline \mathbf{O} & \multicolumn{2}{c}{\mathcal{F}_N(i,:)} \end{array}\right] \cdot \left[\begin{array}{c|c} \mathbf{O} & \mathbf{I}_{T-1} \\ \hline \multicolumn{2}{c}{\mathbf{I}_N} \end{array}\right] \\ &= \begin{bmatrix} \mathbf{O}_{(T-1)\times N} \\ \mathcal{F}_N(i,:) \end{bmatrix} \end{aligned} \tag{6.43}$$

Hence, the second term of formula (6.42) becomes

$$\begin{aligned} \begin{bmatrix} \mathbf{O} \\ \mathcal{F}_N(i,:) \end{bmatrix} \cdot \mathbf{C}^k \cdot \mathbf{w}_E^k &= \begin{bmatrix} \mathbf{O} \\ \mathcal{F}_N(i,:) \end{bmatrix} \cdot \mathbf{C}^k \cdot \mathcal{I}_N \cdot \mathcal{F}_N \cdot \mathbf{w}_E^k \\ &= \begin{bmatrix} \mathbf{O} \\ \mathcal{F}_N(i,:)\mathbf{C}^k\mathcal{I}_N \end{bmatrix} \cdot \mathcal{F}_N \cdot \mathbf{w}_E^k \\ &= \begin{bmatrix} \mathbf{O} \\ \mathrm{row}_i(\mathrm{diag}(U^k)) \end{bmatrix} \cdot W_E^k \\ &= \begin{bmatrix} \mathbf{0}_{(T-1)\times 1} \\ U_i^k \cdot W_{E,i}^k \end{bmatrix} \end{aligned} \tag{6.44}$$

In the first line, we inserted an IDFT-DFT pair, to apply the eigenvalue decomposition property of a circulant matrix in the second line. Finally, we substitute this formula for the second term in formula (6.42) and so, the echo emulation

[7] Similar formulas can be derived for an asymmetric-rate set-up, an asynchronous set-up and alternative alignment.

is described by

Echo emulation

$$\begin{bmatrix} \mathbf{e}^k \\ E_i^k \end{bmatrix} = \left[\begin{array}{c|c|c} \mathbf{I}_{T-1} & \mathbf{O} & -\mathbf{I}_{T-1} \\ \hline \mathbf{O} & \multicolumn{2}{c}{\mathcal{F}_N(i,:)} \end{array}\right] \cdot (\mathbf{y}_{ext}^k \overbrace{-\boldsymbol{\chi}_{ext}^{k,k-1}\ \mathbf{w}_E^k}^{\text{time domain EC}}) \quad \overbrace{- \begin{bmatrix} \mathbf{0} \\ U_i^k\ W_{E,i}^k \end{bmatrix}}^{\text{frequency domain EC}} \tag{6.45}$$

Because of the $(T-1) \times 1$ zero vector in the frequency domain EC part, the *frequency domain echo canceller does not perform any echo cancellation on the difference terms.* This can be understood as follows. Consider again the second term in formula (6.42). Matrix product $\mathbf{PC}^k$ represents the transmitted echo signal samples as if this transmitted echo signal stream were periodic with period N. Hence, by making difference terms of samples that differ exactly N in sample index, these difference terms will be zero. As a result, after the time domain echo canceller, the received samples themselves will still contain residual echo, to be cancelled by the frequency domain echo canceller, but the difference terms do not contain any residual echo anymore.

In the coefficient adaptation, we take only the frequency domain part of the filter input into account, analogous to [54, 55]. The corresponding coefficient adaptation for tone i is then described by

$$\text{Filter adaptation for tone } i \quad \begin{aligned} W_{E,i}^{k+1} &= W_{E,i}^k + \rho \begin{bmatrix} \mathbf{0} \\ U_i^k \end{bmatrix}^{\mathrm{H}} \begin{bmatrix} \mathbf{e}^k \\ E_i^k \end{bmatrix} \\ &= W_{E,i}^k + \rho\ U_i^{k^*}\ E_i^k \end{aligned} \tag{6.46}$$

It is seen that only the last element of the error vector is needed in the coefficient adaptation. This element is the echo cancelled FFT output of tone i. Hence, remarkably enough, the coefficient adaptation reduces to the same coefficient adaptation as in the original EC of Ho & Cioffi. The adaptation for all tones can again be combined into one formula

$$\text{Filter adaptation} \quad W_E^{k+1} = W_E^k + \rho\ \mathrm{diag}(U^{k^*}) E^k \tag{6.47}$$

The convergence-in-the-mean behavior of these filter coefficients is described by a set of eigenvalues given in [54, 55]. A SFG of this algorithm is shown in **Fig. 6.14**. The 'select and extract' block selects N successive samples as input to the FFT block and extracts $T-1$ difference terms according to formula (6.45). The 'PT-EQ' block contains a T-taps per tone equalizer for each used tone.

Compared to 'First-echo-then-TEQ', where the complexity is determined by the size of $\boldsymbol{\chi}$ and the FFT of the TEQ, 'First-echo-then-per tone equalization' has a lower complexity. The size of $\boldsymbol{\chi}$ is the same but the FFT of the TEQ

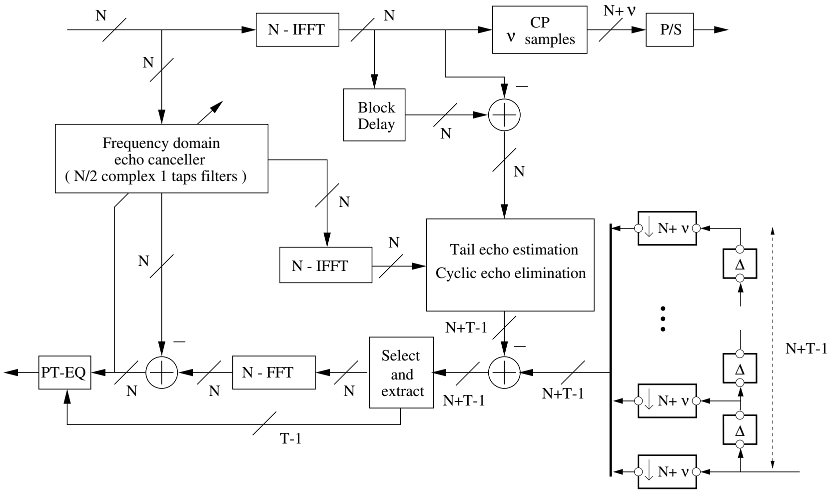

Figure 6.14: Combining t/f domain EC with per tone equalization.

does not appear in the latter SFG. Furthermore, it was shown in chapter 4 that TEQ and PT-EQ have similar complexity during data transmission. Therefore, 'First-echo-then-per tone equalization' and 'First-TEQ-then-echo' have roughly the same complexity, if echo impulse response lengthening by the TEQ is taken into account.

6.4 Complexity comparison

We start with a systematic overview of possible implementations, both at RT and CO for 'First-TEQ-then-echo' and 'First-echo-then-TEQ'. Afterwards, complexities are compared by counting the number of real multiplications per training symbol for those calculations that differ in the different schemes:

- the TEQ operation in time domain
- the multiplication with the FFT of the TEQ
- the size of the time domain echo emulation $\boldsymbol{\chi}$
- 2 extra FFTs for asynchronous operation (counted as $N\log(N)$ or $\gamma N\log(\gamma N)$ per FFT)
- (the phase correction is not counted for)

Complexity computations are made for a downstream IFFT and FFT of size 512 and an upstream IFFT and FFT of size 128. Hence, the interpolation and decimation factor in RT respectively CO are $\gamma = 4$. N equals 128 and ν is 8.

6.4.1 Remote terminal (frame-synchronous or optimal alignment)

At RT, we compare complexity for the following combinations of EC and equalization:

A. 'First-TEQ-then-echo'

1. Original EC of Ho & Cioffi, see **Fig. 6.2**.
   size($\boldsymbol{\chi}$)=$\gamma N \times \gamma N$
2. EC with alternative alignment, see **Fig. 6.7**.
   size($\boldsymbol{\chi}$)=$\gamma N \times \gamma N$

B. 'First-echo-then-TEQ'

1. EC of Ho & Cioffi but with 2 extra FFTs to decouple echo cancellation and TEQ, see **Fig. 6.15**.
   size($\boldsymbol{\chi}$)=$\gamma(\nu + N) \times \gamma N$
2. EC with alternative alignment and 2 extra FFTs.
   size($\boldsymbol{\chi}$)=$\gamma(\nu + N) \times \gamma N$
   The corresponding SFG is similar to **Fig. 6.15** except for the alignment of $\boldsymbol{\chi}$.
3. EC with original alignment without 2 extra FFTs, but with an adjusted size of $\boldsymbol{\chi}$, see **Fig. 6.16**.
   size($\boldsymbol{\chi}$)=$(T - 1 + \gamma N) \times \gamma N$
4. EC with alternative alignment, without 2 extra FFTs, but with an adjusted size of $\boldsymbol{\chi}$
   size($\boldsymbol{\chi}$)=$(T - 1 + \gamma N) \times \gamma N$
   The corresponding SFG is similar to **Fig. 6.16** except for the alignment of $\boldsymbol{\chi}$.

Fig. 6.17 gives a complexity comparison (in multiplications/symbol) for echo cancellation at RT with TEQ size $T = 32$. The complexity is plotted as a function of the length of the echo filter M. It is clear that the alternative alignment gives rise to a large complexity saving for large M. Adding two FFTs at RT to implement the 'First-echo-then-TEQ' approach is disadvantageous because of the large size of the FFTs, namely 512, and $\gamma\nu$ extra rows in the $\boldsymbol{\chi}$ matrix. For a given M the 'First-echo-then-TEQ' set-up without extra FFTs (B.4) is slightly more expensive than the 'First-TEQ-then-echo' set-up due to $T - 1$ extra rows in the $\boldsymbol{\chi}$ matrix. However a fair comparison takes into account the possible lengthening of the echo path by the TEQ, as explained in the previous section.

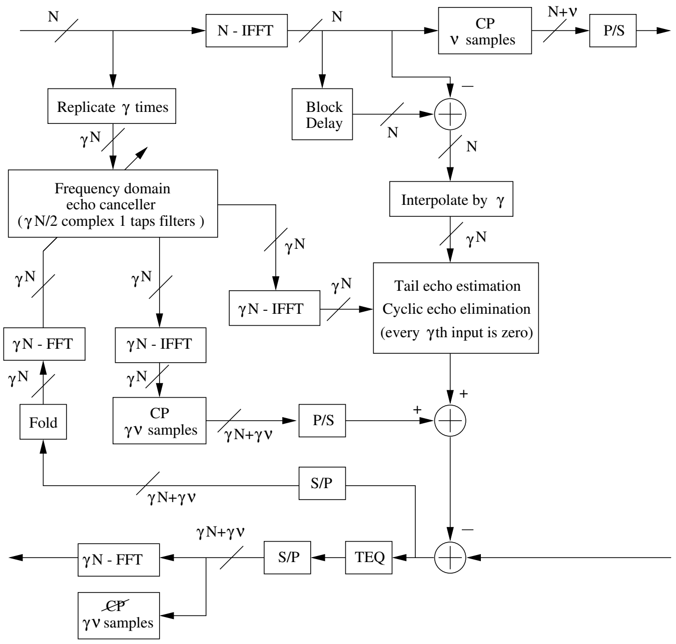

Figure 6.15: Interpolated t/f domain EC at RT (frame-synchronous) in a 'First-echo-then-TEQ' set-up with 2 extra FFTs.

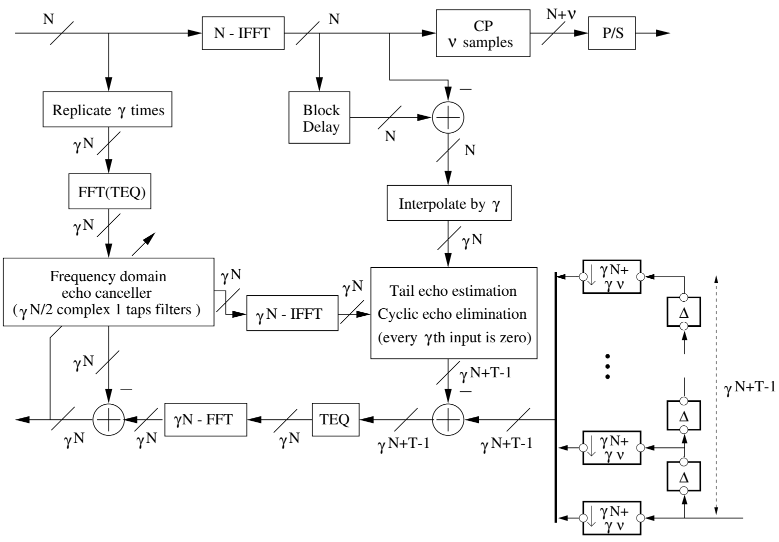

Figure 6.16: Interpolated t/f domain EC at RT (frame-synchronous) in a 'First-echo-then-TEQ' set-up without 2 extra FFTs.

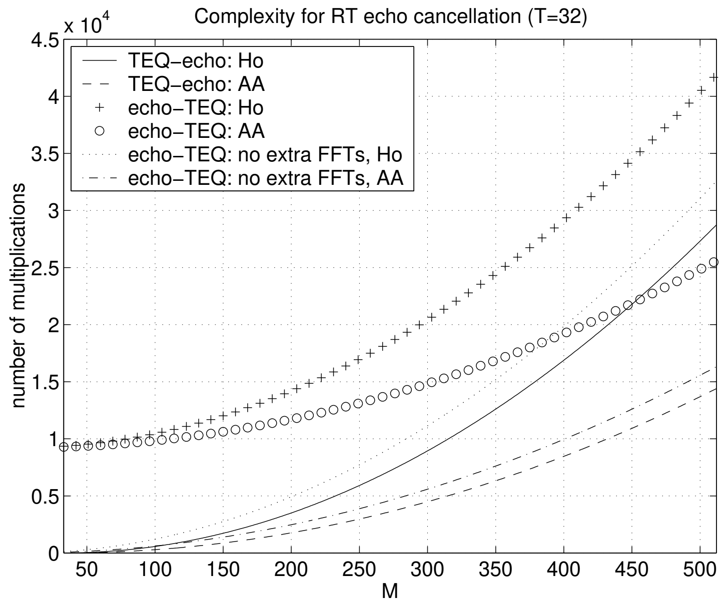

Figure 6.17: Complexity comparison for echo cancellation at RT with TEQ size $T = 32$ (multiplications/symbol).

Note that the complexity of the TEQ is $T\gamma(N+\nu)$ multiplications/symbol for the first 4 schemes and $(T+2)\gamma N$ multiplications/symbol for the last 2 schemes, which is the same for the simulated parameters. Hence the TEQ complexity is not shown in the figure.

6.4.2 Central office (frame-asynchronous)

For the CO the situation is more complicated because the CO works asynchronously. Basically, there are two possibilities. Or 2 extra FFTs are added in the SFG, but then the number of rows in the χ matrix increases with the prefix length. Or matrix $\boldsymbol{\chi}$ remains square, but then the misalignment is dependent of the channel propagation delay.

C. 'First-TEQ-then-echo'

1. Original EC of Ho & Cioffi with 2 FFTs, see **Fig. 6.4**.
   size($\boldsymbol{\chi}$)=$\gamma(\nu+N)\times\gamma N$
2. EC with alternative alignment and 2 FFTs, see **Fig. 6.8**
   size($\boldsymbol{\chi}$)=$\gamma(\nu+N)\times\gamma N$

3. EC without 2 FFTs, *i.e.* alignment dependent of the channel propagation delay, see **Fig. 6.10**.
   size($\boldsymbol{\chi}$)=$\gamma N \times \gamma N$

D. 'First-echo-then-TEQ'

1. EC with original alignment with 2 FFTs.
   size($\boldsymbol{\chi}$)=$\gamma(\nu + N) \times \gamma N$
   The corresponding SFG is similar to **Fig. 6.4** except for the position of the TEQ.
2. EC with alternative alignment with 2 FFTs.
   size($\boldsymbol{\chi}$)=$\gamma(\nu + N) \times \gamma N$
   The corresponding scheme is similar to **Fig. 6.8** except for the position of the TEQ.
3. EC without 2 FFTs, *i.e.* alignment dependent of the channel propagation delay, but with an adjusted size of $\boldsymbol{\chi}$.
   size($\boldsymbol{\chi}$)=$(T - 1 + \gamma N) \times \gamma N$
   The modifications to **Fig. 6.10** to obtain this SFG are analogous to **Fig. 6.16**.

The following schemes are compared: 'First-TEQ-then-echo' with 2 FFTs for the method of Ho & Cioffi and the alternative alignment (schemes C.1 and C.2). Remark that the 'First-echo-then-TEQ' approaches with 2 FFTs (schemes D.1 and D.2) have the same complexity. Finally the 'First-TEQ-then-echo' without FFTs (scheme C.3) is studied. For the latter case the alignment depends on the channel propagation delay δ and the echo filter length M, see figure 6.9. For each M, the following complexities are plotted: the average over all possible alignments, the best and worst alignment and the actual δ. **Fig. 6.18** represents simulations for δ equal to 50 samples.

It is seen that on the average 'First-TEQ-then-echo' with propagation delay dependent alignment is worse than 'First-TEQ-then-echo' with 2 FFTs. Moreover, depending on the propagation delay, the worst complexity arises for another M, which results in a very unpredictable behaviour. So, if $N \log(N)$ is a realistic implementation complexity of an FFT, it is better to choose the set-up with 2 FFTs at CO. Note that the TEQ complexity is not represented in the figure because it is the same for the simulated schemes.

6.5 Simulation results

6.5.1 Alignment in t/f domain echo cancellation

We show the convergence of t/f domain EC for different alignments of transmitted and received signal. The frequency at which the time domain echo

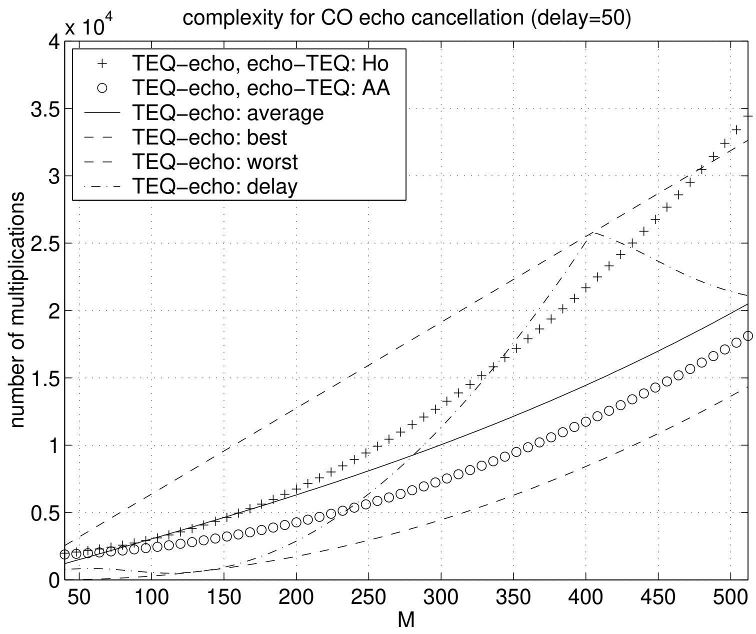

Figure 6.18: Complexity comparison for echo cancellation at CO for channel propagation delay $\delta = 50$ (multiplications/symbol).

filter is updated is varied. This operation is represented in figure 6.1 as the 'IFFT' block between the frequency domain EC and the time domain EC. The updating frequency is given by $\frac{1}{\phi}\frac{F_s}{N+\nu}$.

In these simulations, we assume an echo channel of 300 random taps ($M = 300$) with zero mean and variance $\sigma_h^2 = 10^{-1.5}/300$. Hence, the expected value of the norm$(h)^2$ equals -15dB. The power spectral density of the echo signal (psd$_u$) is -38dBm/Hz at RT which corresponds to the upstream psd, and -40dBm/Hz at CO which is the downstream psd. It is assumed that all tones are used during training. Furthermore, we assume that the background noise is white with psd equal to -140dBm/Hz and that the far end signal is silenced during EC training. We use a 512-point IFFT-FFT pair in downstream and a 128-point IFFT-FFT pair in upstream. Hence, the interpolation and decimation factor in RT and CO respectively are both equal to $\gamma = 4$. The step size is taken as $\rho = \frac{0.2}{psd_u \cdot \lambda_{max}}$. In [54, 55], it is proven that λ_{max} equals 1 at RT and $\frac{N+\nu}{\gamma N}$ at CO. We have plotted the norm of the error and the difference between echo filter and echo channel.

In **Fig. 6.19** and **6.20**, the results are shown for RT. The convergence is plotted for FBLMS, t/f domain EC with original alignment (Fig. 6.2) and alternative

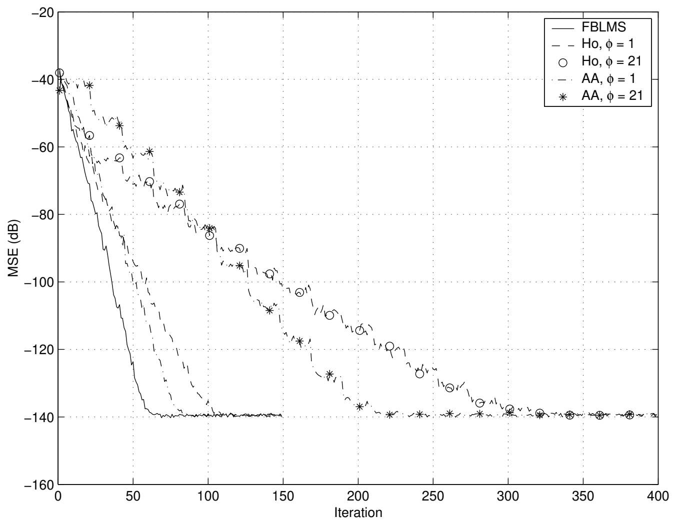

Figure 6.19: Comparison of the MSE for different EC schemes at RT (frequency domain block LMS, t/f domain EC with original alignment and alternative alignment) The updating frequency of the time domain filter is given by ϕ. The echo channel has 300 random taps.

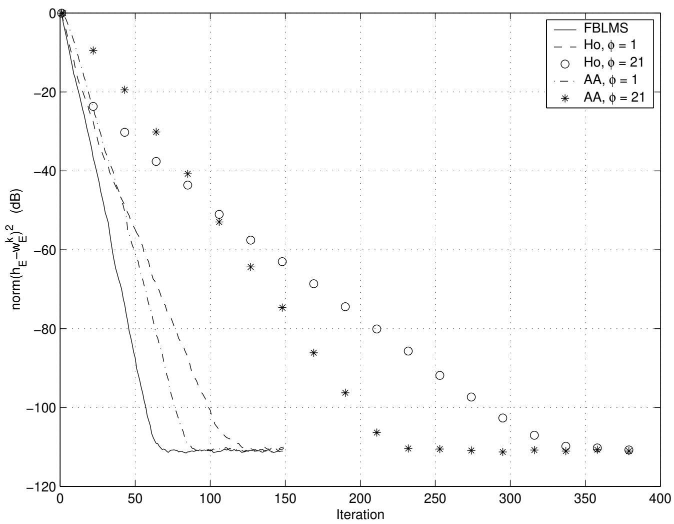

Figure 6.20: Comparison of the residual echo channel for different EC schemes at RT.

alignment (Fig. 6.7). It is seen that frequency domain block LMS converges fastest. This is expected because the complete filter input is used in the filter update. Let us consider now $\phi = 1$. It is seen that the alternative alignment leads to faster convergence than the original alignment [54, 55]. This is because the time domain filter input $\boldsymbol{\chi}$, which is neglected in the filter update, has only half the number of elements with respect to the original alignment and because of our assumption of a random echo channel. The energy in a random echo channel is equally spread over the M taps. The correction term (term with ρ) is equally important for all taps. Hence, in the approximation of the filter input in the updating formula, less approximated samples means a smaller mistake in the correction term and faster convergence.

For a real echo channel, as shown in the next subsection, the speed of convergence is dependent of the distribution of the energy over the taps. In the original alignment, $\boldsymbol{\chi}$ has an upper triangular non-zero part. Hence, the $M-\nu-1$ approximated samples corresponds to the tail of the echo filter. In the alternative alignment, $\boldsymbol{\chi}$ has one upper and one lower smaller triangular part. Thus one has $(M-\nu-1)/2$ samples corresponding to the tail and $(M-\nu-1)/2$ samples corresponding to the head of the echo filter. If for instance, the main energy of the echo impulse response is located in the head, then the original alignment may be faster. Independent of the speed of convergence, it is important to note that the complexity of the alternative alignment is two times lower per iteration step. As such the convergence with the alternative alignment may still be faster as a function of complexity.

Let us now consider $\phi = 21$. Only once per 21 DMT symbols, the time domain echo filter is updated. The influence of the infrequent IFFT is clearly visible. The convergence occurs in steps and is described by the following error[8] (as seen in the time domain)

$$\mathbf{e}^k = \mathbf{y}^k - \left[\begin{array}{c|c} \mathbf{C}^k & \boldsymbol{\chi}^{k,k-1} \cdot \begin{bmatrix} \mathbf{I}_M & \mathbf{O} \\ \mathbf{O} & \mathbf{O} \end{bmatrix} \end{array}\right] \cdot \begin{bmatrix} \mathbf{w}^k_{E,freq} \\ \mathbf{w}^k_{E,time} \end{bmatrix} \tag{6.48}$$

When the infrequent IFFT is computed, $\mathbf{w}^k_{E,time}$ is set equal to $\mathbf{w}^k_{E,freq}$. In the iteration steps in between infrequent IFFTs, $\mathbf{w}^k_{E,time}$ is kept constant and the error can only decrease by iterating on $\mathbf{w}^k_{E,freq}$. The complexity saving in the infrequent IFFT, leads to a poorer convergence performance per iteration step. Hence, there is a trade off between complexity and performance.

Fig. 6.21 and **6.22** show similar simulations for the frame-asynchronous EC at CO with the same echo channel of 300 random taps. The performance of FBLMS, t/f domain EC with original alignment (Fig. 6.4) and alternative alignment (Fig. 6.8) is presented. In the implementation of the asynchronism, the Toeplitz matrix, circulant matrix and χ have $\gamma\nu$ extra rows with respect to

[8] A similar formula holds for the alternative alignment.

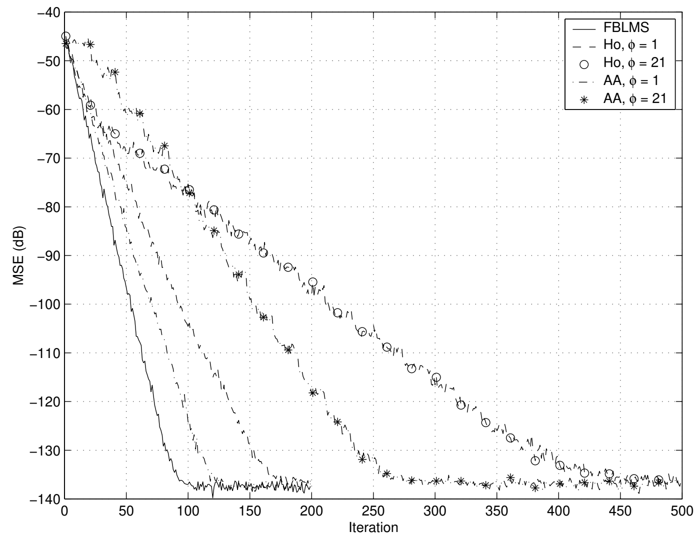

Figure 6.21: Comparison of the MSE for different EC schemes in the asynchronous CO.

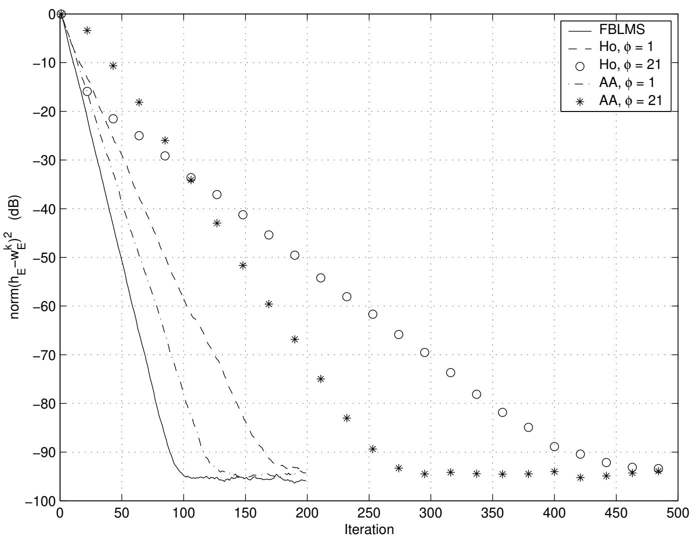

Figure 6.22: Comparison of the residual echo channel for different EC schemes in the asynchronous CO.

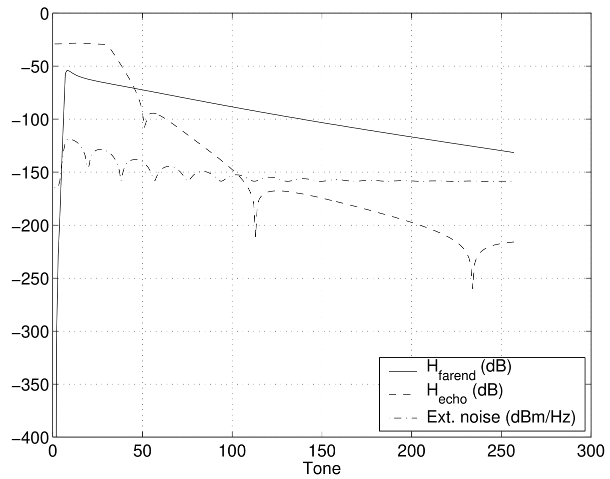

Figure 6.23: Transfer function of farend and echo channel and PSD of the external noise

the EC at RT. Similar conclusions hold for CO. FBLMS has fastest convergence, followed by alternative alignment and then original alignment. When adopting infrequent IFFT, the algorithm is slower.

6.5.2 'First-TEQ-then-echo' versus 'First-echo-then-PT-EQ'

The 'First-TEQ-then-echo' and 'First-echo-then-per tone equalization' approach are demonstrated at RT for channel T1.601-#7 with NEXT from 24 DSL disturbers and -140dBm/Hz background noise, shown in **Fig. 6.23**. A scenario with overlapping up- and downstream tones is considered. The upstream tones are tones 8 up to 30 and the downstream tones are tones 8 up to 256. All IFFT and FFT sizes are $N = 512$ and the cyclic prefix has $\nu = 32$ samples. The psd on the upstream and downstream tones are respectively psd_u=-38dBm/Hz and PSD_x=-40dBm/Hz.

In **Fig. 6.24**, the convergence of 'First-TEQ-then-echo' is shown. A 32-taps TEQ is first computed under the assumption that all echo is cancelled and that only the far end channel has to be shortened. The applied constraint is unit norm TIR. The resulting echo channel is the convolution of echo impulse response and TEQ. The time domain EC is assumed to have $M + T - 1 = 200 + 32 - 1$ non-zero taps. The convergence of the EC is plotted for 2 different schemes: the original alignment and the two fold cheaper alternative alignment. Moreover, the frequency at which the time domain echo filter taps are updated is varied. The step size is $\rho = \frac{0.2}{psd_u \cdot 1}$. During adaptation, the far end signal is set to zero and training symbols are sent on all upstream tones (so, it is assumed that all upstream tones are used during training of the EC). The alternative alignment has slower convergence than the orignal alignment due to the shape of the echo impulse response.

Fig. 6.25 show similar simulations for 'First-echo-then-per tone equalization'. The EC is performed before per tone equalization and as such the equalizers are not involved in the convergence of the EC. The time domain EC is assumed to have $M = 200$ taps.

In both set-ups, the psd of the residual echo is then computed. For a total noise psd containing external noise and residual echo, capacity is computed. The following figures represent signal energy, ISI-ICI, external noise and residual echo. The results of 'First-TEQ-then-echo' are shown in **Fig. 6.26** and **6.27**. In the first scenario, there is no EC. It is clear that the echo is the dominant impairment in the whole frequency range. In the second scenario, the EC of iteration 40 with alternative alignment with $\phi = 1$ (see dashed-dotted line) is applied. The residual echo is still the major impairment on the lowest tones. The respective bit rates are $\boxed{0.507 \text{ Mbits/s}}$ and $\boxed{1.77 \text{ Mbits/s}}$.

The results of 'First-echo-then-per tone equalization' are presented in **Fig. 6.28** and **6.29**. The 32-taps PT-EQ, which optimize the SNR per tone, are computed for a total noise psd containing the external noise and residual echo. The first simulation is made without EC. Only on the lowest tones, the echo is dominant. In the second simulation, the EC of iteration 40 with alternative alignment with $\phi = 1$ (see dashed-dotted line) is applied. The residual echo on the lowest tones is of the same order as the other impairments. The respective bitrates are $\boxed{1.68 \text{ Mbits/s}}$ and $\boxed{2.30 \text{ Mbits/s}}$.

With per tone equalization, one can compute the optimal bit rate given a certain EC. With TEQ, this would not be possible because TEQ initialization by means of channel impulse response shortening has no direct relation with resulting bit rate.

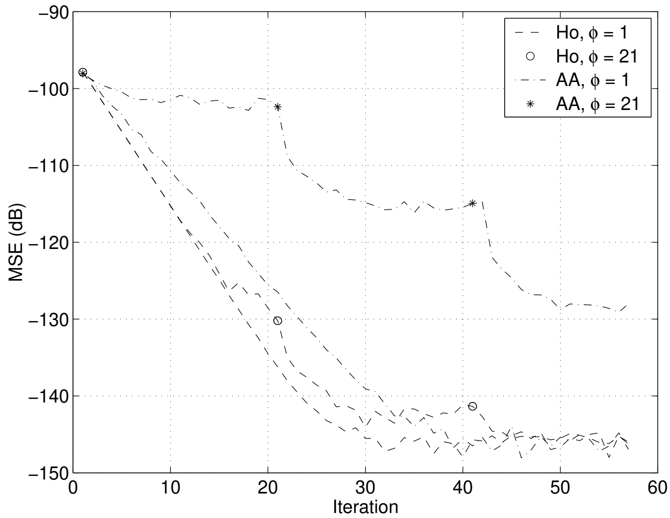

Figure 6.24: Convergence of 'First-TEQ-then-echo' for different ECs. The 32-taps TEQ is part of the total echo path.

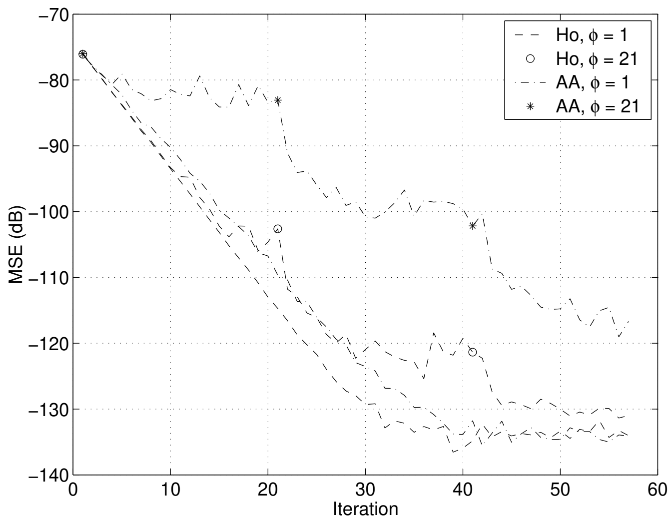

Figure 6.25: Convergence of 'First-echo-then-per tone equalization' for different echo cancellers. The per tone equalizers are not involved in the echo cancellation.

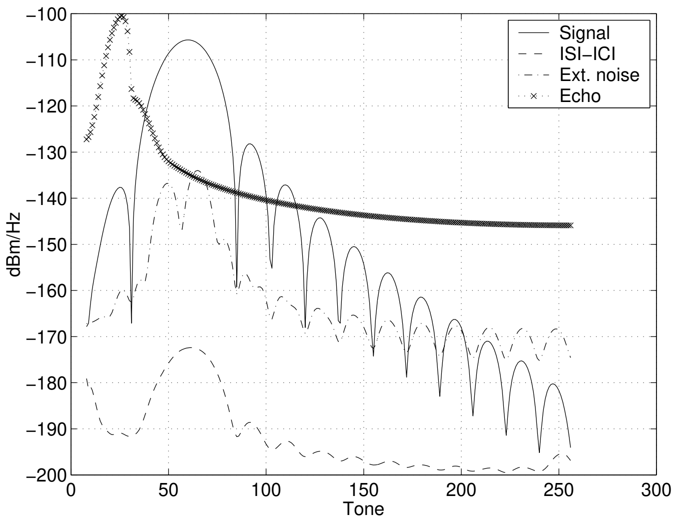

Figure 6.26: Signal and noise levels for 'First-TEQ-then-echo' without EC.

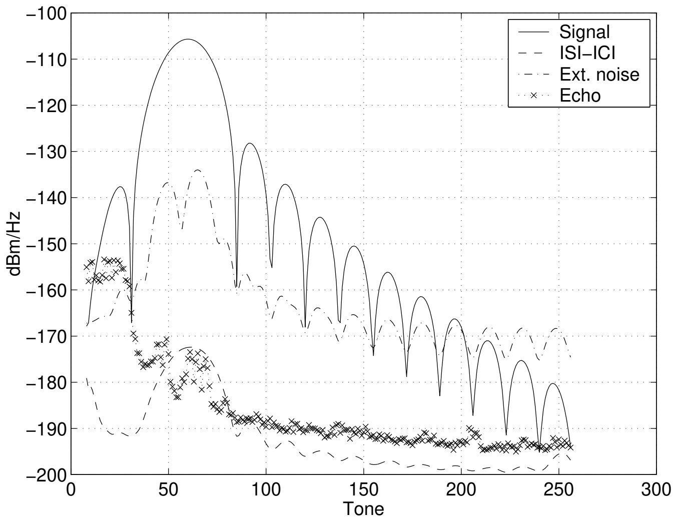

Figure 6.27: Signal and noise levels for 'First-TEQ-then-echo' with EC.

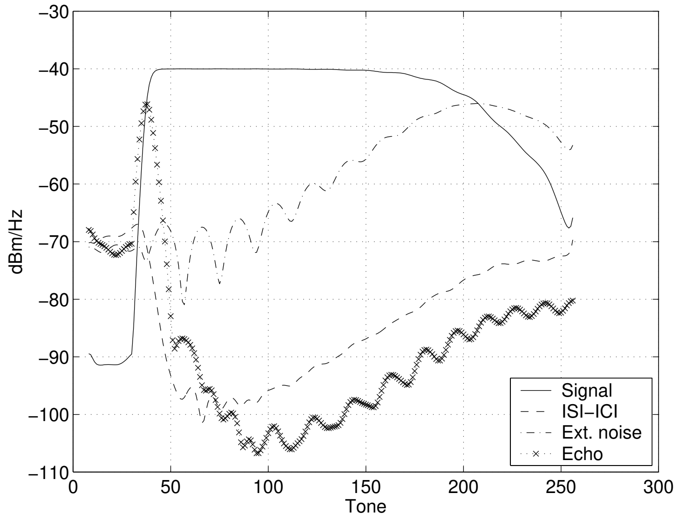

Figure 6.28: Signal and noise levels for 'First-echo-then-per tone equalization' without EC.

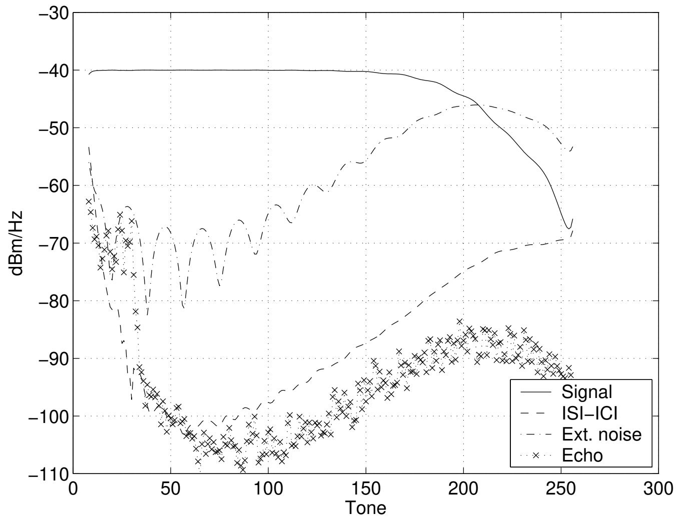

Figure 6.29: Signal and noise levels for 'First-echo-then-per tone equalization' with EC.

6.6 Conclusions

Overlapping up and downstream tones or relaxed filter orders necessitate the use of echo cancellers in DMT transceivers. As a starting point, the t/f domain echo canceller, proposed by Ho & Cioffi has been reviewed. The focus of our study has then been on the combination of this echo canceller and equalization.

First, we have studied the combination of t/f domain echo cancellation and TEQ. Although TEQ is performed mostly before echo cancellation to enable joint channel shortening, and hence, to allow a shorter echo cancellation filter, this approach does not correspond to bit rate optimization. If the TEQ is designed to shorten the far end impulse response only, the TEQ will in general lengthen the echo impulse response. To avoid the possible lengthening of the echo impulse response by the TEQ, we have shown that we can reverse the order of operations and apply first echo cancellation and then equalization.

The main goal of reversing the order is that we can then apply PT-EQ instead of TEQ after t/f domain echo cancellation. And as a result, we can benefit by the property of PT-EQ that it optimizes capacity, given a certain echo canceller. We have shown that, after the time domain part of the echo cancellation, the difference terms (which are inputs to the PT-EQs) do not contain any residual echo anymore. As a result, the frequency domain echo canceller does not perform any echo cancellation on the difference terms, but performs only echo cancellation on the FFT output.

Chapter 7

Per tone echo cancellation

We extend the per tone idea, introduced for equalization in chapter 4, to echo cancellation. The result is a per tone-organized DMT tranceiver with per tone equalization as well as a per tone echo cancellation. In contrast with previously discussed echo cancellation structures, the per tone structure allows to optimize the SNR for each tone separately by means of a quadratic cost function for given filter lengths.

In section 7.1, we start with a simplified echo cancellation scheme in which each used tone has only a 1-taps echo canceller. It is seen that a 1-taps echo canceller is sufficient in the particular case with a 'short' echo impulse response and with aligned transmit and receive symbols.

In general, these conditions do not hold and ISI and ICI arise in the echo signal. Therefore, we introduce a multitaps echo filter per tone in section 7.2. We derive the general structure of per tone equalization combined with per tone echo cancellation and the cost function for joint initialization. The cost function incorporates optimal per tone joint shortening. Further, we derive per tone echo cancellation structures for an interpolated and a decimated set-up and we compute the complexity during data transmission.

In section 7.3, we compare the echo emulation complexity of time/frequency domain echo cancellation and per tone echo cancellation. The combination of per tone echo cancellation with pulse shaping and windowing is explained in section 7.4. Simulations results are given in section 7.5. Finally, conclusions are drawn in section 7.6.

7.1 Per tone equalization and 1-taps per tone echo cancellation

We consider the set-up where we have first a T-taps PT-EQ followed by 1-taps per tone echo cancellers (PT-EC). Compared to t/f domain EC combined with per tone equalization, there is no time domain correction matrix $\boldsymbol{\chi}$ involved in this transceiver. However, the PT-EQ is applied first. This means that the PT-EQ may 'shorten' or equalize the channel impulse response as well as the echo impulse response in a joint fashion. A 1-taps PT-EC is then sufficient to cancel the residual echo on every duplexed[1] tone if the 'shortened' echo impulse response (which is now complex and different for every tone) fits in the cyclic prefix and if the echo signal is frame-synchronous with the received signal, *i.e.* the transmitted echo symbol is aligned with the received symbol. This can be seen as follows. Let us consider the 'shortened' complex echo impulse response $\mathbf{b}_{E_i}$ for tone i

$$\mathbf{b}_{E_i} = \mathbf{h}_E * \mathbf{w}_i \tag{7.1}$$

with $\mathbf{h}_E$ the echo impulse response before equalization or echo cancellation and $\mathbf{w}_i$ the PT-EQ for tone i. Remark that in this interpretation, we implicitly move the PT-EQ before the FFT. This means we change the order of the FFT filter $\mathcal{F}_N(i,:)$ and the PT-EQ $\mathbf{w}_i$ for each tone i. It is clear that this is only done for the interpretation and by no means in the implementation. The received (time domain) echo symbol in frame-synchronous mode can then be written as

$$\overbrace{\begin{bmatrix} u_1^k & u_N^k & \cdots & u_{N-\nu+1}^k & u_N^{k-1} & \cdots & u_{\nu+2}^{k-1} \\ u_2^k & u_1^k & \ddots & & \ddots & \ddots & \vdots \\ \vdots & \ddots & \ddots & & & \ddots & u_N^{k-1} \\ & & & & & & u_{N-\nu+1}^k \\ \vdots & & & & & & \vdots \\ u_N^k & u_{N-1}^k & \cdots & & & \cdots & u_1^k \end{bmatrix}}^{\mathbf{U}^{k,k-1}} \cdot \begin{bmatrix} \mathbf{b}_{E_i} \\ \mathbf{0} \end{bmatrix} \tag{7.2}$$

and the received echo subsymbol in the frequency domain is

$$\mathcal{F}_N(i,:) \cdot \mathbf{U}^{k,k-1} \cdot \begin{bmatrix} \mathbf{b}_{E_i} \\ \mathbf{0} \end{bmatrix} \tag{7.3}$$

The multiplication of the Toeplitz matrix and the zero-padded shortened echo impulse response $\mathbf{b}_{E_i}$ is equivalent to the multiplication of a circulant matrix

[1] A duplexed tone is a tone used in downstream as well as in upstream.

and $\mathbf{b}_{E_i}$ provided that the length of $\mathbf{b}_{E_i}$ is shorter or equal to $\nu + 1$. In fact, we apply formula (6.4)

$$\mathcal{F}_N(i,:) \cdot \mathbf{C}^k \cdot \begin{bmatrix} \mathbf{b}_{E_i} \\ \mathbf{0} \end{bmatrix} + \mathcal{F}_N(i,:) \cdot \overbrace{\boldsymbol{\chi}^{k,k-1} \cdot \begin{bmatrix} \mathbf{b}_{E_i} \\ \mathbf{0} \end{bmatrix}}^{[\mathbf{0}]} \tag{7.4}$$

where the second term vanishes. We insert an IDFT-DFT pair between the circulant matrix and the shortened echo impulse response and apply the eigenvalue decomposition of a circulant matrix

$$\overbrace{\mathcal{F}_N(i,:) \cdot \mathbf{C}^k \cdot \mathcal{I}_N} \cdot \overbrace{\mathcal{F}_N \cdot \begin{bmatrix} \mathbf{b}_{E_i} \\ \mathbf{0} \end{bmatrix}} = \mathrm{row}_i(\mathrm{diag}(U_{1:N}^{(k)})) \cdot B_{E_i} = U_i^{(k)} \cdot B_{E_i,i} \tag{7.5}$$

So, the 'shortened' complex echo path is equivalent to a 1-taps complex echo path per tone $B_{E_i,i}$. This result is similar to a far end impulse response that fits into the cyclic prefix, see section 2.1. In conclusion, a received demodulated and equalized subsymbol $Z_i^{(k)}$ will contain only echo from $U_i^{(k)}$.

A non-duplexed tone i will not experience any echo in frame-synchronous mode if the 'shortened' echo impulse response fits in the prefix, as for a non-duplexed tone $U_i^{(k)} = 0$. **Fig. 7.1** illustrates this receiver structure for $N/2$ used tones, if all tones are duplexed.

The proposed structure is the per tone generalization of the structure consisting of a T-taps TEQ combined with 1-taps PT-EQs for the used tones and 1-taps PT-ECs for the duplexed tones. Finding the optimal TEQ (*i.e.* with maximal capacity) results in a nonlinear optimization problem. Therefore, one usually resorts to an MMSE channel shortening algorithm, see chapter 3. However, by applying PT-EQ instead of TEQ, one has an MMSE problem per tone in the PT-EQ coefficients and the 1-taps PT-EC, which optimizes capacity, and thus leads to the optimal *per tone joint shortening*.

The optimal PT-EQ $\mathbf{v}_i$ and 1-taps PT-EC a_i for a duplexed tone i are the solution of an extended MMSE problem (with respect to formula (4.9)). The data model of formula (2.17) is used, in which the far end and echo signal are explicitly written as a DMT signal, and an extra term to model the echo canceller is added

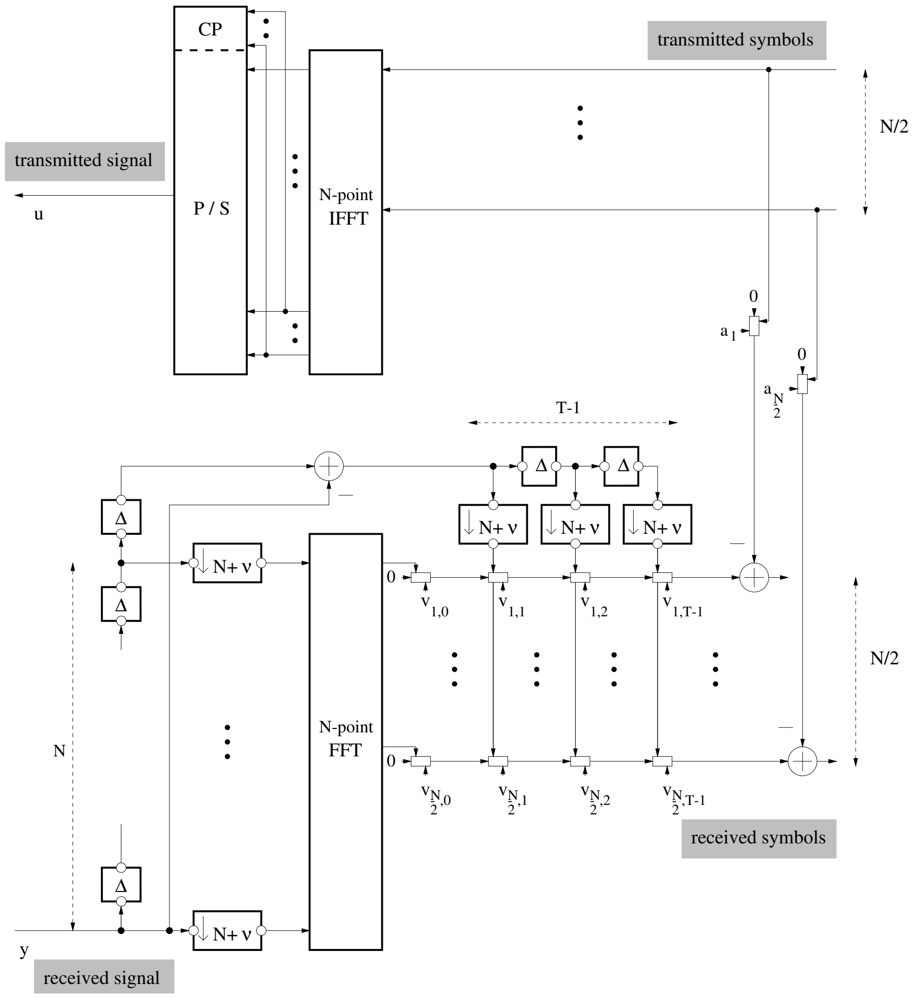

Figure 7.1: Combining PT-EQ with 1-taps PT-EC for the duplexed tones.

$$
\begin{aligned}
J(\mathbf{v}_i, a_i) &= \mathcal{E}\left\{\left|\bar{\mathbf{v}}_i^{\mathrm{T}}\mathbf{F}_i(\mathbf{H}\hat{\mathbf{x}} + \overbrace{\mathbf{H}_E\hat{\mathbf{u}}}^{\text{echo signal}} + \mathbf{n}) - \overbrace{a_i\mathbf{e}_i^{(k)}\hat{\mathbf{u}}}^{\text{echo cancellation}} - \mathbf{e}_i^{(k)}\hat{\mathbf{x}}\right|^2\right\} \\
&= \mathcal{E}\left\{\left|\begin{bmatrix}\bar{\mathbf{v}}_i^{\mathrm{T}} & a_i\end{bmatrix}\left(\begin{bmatrix}\mathbf{F}_i\mathbf{H} \\ \mathbf{0}\end{bmatrix}\hat{\mathbf{x}} + \begin{bmatrix}\mathbf{F}_i\mathbf{H}_E \\ -\mathbf{e}_i^{(k)}\end{bmatrix}\hat{\mathbf{u}} + \begin{bmatrix}\mathbf{F}_i \\ \mathbf{0}\end{bmatrix}\mathbf{n}\right) - \mathbf{e}_i^{(k)}\hat{\mathbf{x}}\right|^2\right\} \\
&= \left\|\left[\begin{array}{c|c}\mathbf{R}_{\hat{\mathbf{x}}}^{1/2}\mathbf{H}^{\mathrm{H}}\mathbf{F}_i^{\mathrm{H}} & \mathbf{O} \\ \mathbf{R}_{\hat{\mathbf{u}}}^{1/2}\mathbf{H}_E^{\mathrm{H}}\mathbf{F}_i^{\mathrm{H}} & -\mathbf{e}_i^{(k)\mathrm{H}} \\ \mathbf{R}_{\mathbf{n}}^{1/2}\mathbf{F}_i^{\mathrm{H}} & \mathbf{O}\end{array}\right]\begin{bmatrix}\bar{\mathbf{v}}_i^* \\ a_i^*\end{bmatrix} - \begin{bmatrix}\mathbf{R}_{\hat{\mathbf{x}}}^{1/2}\mathbf{e}_i^{(k)\mathrm{H}} \\ \mathbf{0} \\ \mathbf{0}\end{bmatrix}\right\|_2^2
\end{aligned}
\tag{7.6}
$$

For a non-duplexed tone a_i is set to zero. The resulting signal, ISI-ICI, residual echo and noise energy for tone i can be computed respectively as

$$S_i = \left|(\mathbf{R}_{\hat{\mathbf{x}}}^{1/2}\mathbf{H}^{\mathrm{H}}\mathbf{F}_i^{\mathrm{H}})_{(N+i,:)}\bar{\mathbf{v}}_i^*\right|^2 \tag{7.7}$$

$$I_i = \left\|\mathbf{R}_{\hat{\mathbf{x}}}^{1/2}\mathbf{H}^{\mathrm{H}}\mathbf{F}_i^{\mathrm{H}}\bar{\mathbf{v}}_i^*\right\|^2 - S_i \tag{7.8}$$

$$E_i = \left\|\left[\begin{array}{c|c} \mathbf{R}_{\hat{\mathbf{u}}}^{1/2}\mathbf{H}_E^{\mathrm{H}}\mathbf{F}_i^{\mathrm{H}} & -\mathbf{e}_i^{(k)\mathrm{H}} \end{array}\right]\begin{bmatrix}\bar{\mathbf{v}}_i^* \\ a_i^*\end{bmatrix}\right\|^2 \tag{7.9}$$

$$N_i = \left\|\mathbf{R}_{\mathbf{n}}^{1/2}\mathbf{F}_i^{\mathrm{H}}\bar{\mathbf{v}}_i^*\right\|^2 \tag{7.10}$$

and $SNR_i = \frac{S_i}{I_i+E_i+N_i}$.

Formula (7.6) optimizes the SNR per tone given a receiver structure consisting of a T-taps PT-EQ and a 1-taps PT-EC. However we know that if the modem works in frame-asynchronous mode or if the 'shortened' echo impulse response is longer than $\nu+1$, a 1-taps PT-EC is not sufficient to cancel the echo. Moreover, a perfect shortening of the echo impulse response to fit in the cyclic prefix is not feasible. The echo interference structure that arises is similar to the interference in case of a far end signal with channel impulse response larger than $\nu+1$, see section 2.1. A received subsymbol $Z_{i_1}^{(k_1)}$ on tone i_1 during symbol period k_1, will experience echo from subsymbols transmitted on tones $i_2 \neq i_1$ during the same symbol period, $U_{i_2}^{(k_1)}$, *i.e.* ICI of type 1, and during other symbol periods $k_2 \neq k_1$, $U_{i_2}^{(k_2)}$, *i.e.* ICI of type 2. There will also be echo from subsymbols transmitted on tone i_1 during other symbol periods, $U_{i_1}^{(k_2)}$, *i.e.* ISI.

Capacity would increase if one could also cancel this ISI-ICI in the echo signal. One solution is to add more EC coefficients as follows. One could cancel ICI1 originating from a range of neighboring tones with taps $[a_{i,-R}\cdots a_{i,0}\cdots a_{i,R}]$ where $a_{i,0}$ cancels the echo from tone i on tone i, *i.e.* the a_i previously discussed, and $a_{i,r}$ cancels the echo from tone $(i+r)$ on tone i, R is the so-called ICI-range. To take into account ISI and ICI2, one could cancel these subsymbols for a range of symbol periods k with $-S \leq k \leq S$, where S is the so-called ISI range. A frequency domain EC based on this principle is proposed by Bogucka *et al* in [18].

Alternatively, one could also cancel the echo by an approach similar to per tone equalization, *i.e.* with a multitaps echo filter per tone. This is explained in detail in the next section.

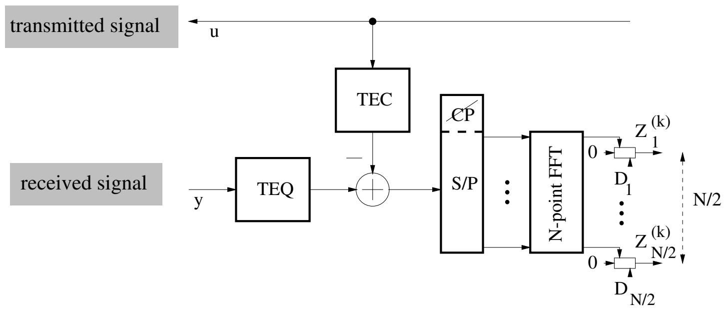

Figure 7.2: Transceiver with T-taps TEQ and T_E-taps TEC.

7.2 Per tone equalization and per tone echo cancellation

In general, the transmitted and received signals may be frame-asynchronous and the modem may have an echo impulse response longer than $\nu+1$. We solve this general echo cancellation problem by means of a transceiver based on a per tone approach. Analogous to per tone equalization, presented in chapter 4, we move the (real) time domain echo canceller (TEC) to the frequency domain to result in a (complex) per tone echo canceller (PT-EC) for each tone separately. By minimizing an extended MMSE problem, with respect to formula (7.6), we are able to optimize the SNR per tone by means of a linear optimization problem, given an equalizer length T and an echo canceller length T_E.

7.2.1 Combination of EQ and EC in a DMT receiver

To describe the algorithm, we use the data model of formula (2.17), which assumes a symmetric rate set-up, *i.e.* all appearing FFTs and IFFTs have size N. The initial transceiver with TEQ and TEC is shown in **Fig. 7.2**. For each tone i, it is based on the following operation

$$Z_i^{(k)} = D_i \cdot \mathrm{row}_i \overbrace{(\mathcal{F}_N) \cdot (\mathbf{Y} \cdot \mathbf{w} - \mathbf{U} \cdot \mathbf{w}_E)}^{1 \text{ FFT}} \tag{7.11}$$

where $\mathbf{w} = [w_0\, w_1 \ldots w_{T-1}]^{\mathrm{T}}$ is the (real) T-taps TEQ, and $\mathbf{Y}$ an $N \times T$ Toeplitz matrix of received samples. Similarly, $\mathbf{w}_E$ is the (real) T_E-taps TEC and $\mathbf{U}$ an $N \times T_E$ Toeplitz matrix of samples of the echo reference signal. Note that $\mathbf{Y}$ and $\mathbf{U}$ contain the same samples as vector $\mathbf{y}$ in formula (2.17) and $\mathbf{u}$ in formula (2.18) respectively.

Formula (7.11) may be rewritten as follows

$$\begin{aligned} Z_i^{(k)} &= \mathrm{row}_i\,(\mathcal{F}_N)\cdot(\mathbf{Y}\cdot\mathbf{w}\cdot D_i-\mathbf{U}\cdot\mathbf{w}_E\cdot D_i) \\ &= \mathrm{row}_i\,\underbrace{(\mathcal{F}_N\cdot\mathbf{Y})}_{T\text{ FFTs}}\cdot\mathbf{w}_i-\mathrm{row}_i\,\underbrace{(\mathcal{F}_N\cdot\mathbf{U})}_{T_E\text{ FFTs}}\cdot\mathbf{w}_{E,i} \end{aligned} \tag{7.12}$$

By putting D_i to the right one obtains a complex T-taps PT-EQ $\mathbf{w}_i$ and a complex T_E-taps PT-EC $\mathbf{w}_{E,i}$ for each tone separately. As demonstrated in chapter 4, T respectively T_E successive FFTs can be calculated efficiently by means of a sliding FFT. A per tone filter needs only one 'full' FFT and the other FFTs can be derived as a complex linear combination of this FFT and $T-1$ respectively T_E-1 real difference terms. The final modem set-up has one FFT operation for the received signal and one FFT operation for the reference echo signal together with equalization/echo filters mainly acting upon difference terms. The FFTs have as their inputs the elements in the first column of $\mathbf{Y}$ and $\mathbf{U}$ respectively. Remark that, if the modem works frame-synchronously, the only FFT needed in the PT-EC, reproduces the transmitted echo symbol $U_{1:N}^{(k)}=\mathcal{F}_N\cdot\mathbf{U}(:,1)$. Hence, in that case, the FFT in the echo branch becomes superfluous. Furthermore, in frame-synchronous mode, the first $\nu+1$ columns of $\mathbf{U}$ are equal up to a rotation, so the first ν difference terms are zero.

In **Fig. 7.3** a per tone filter (PTF) block is defined, including an N-point FFT operation and T-taps per tone filters $\mathbf{v}_i$ for all used tones. The notation $\mathbf{v}$ instead of $\mathbf{w}$ is adopted for the PTFs because we work here with the efficient implementation of these filters, *i.e.* their inputs are one FFT-output and $T-1$ difference terms. A complete DMT-receiver with PT-EQ and PT-EC is then shown in **Fig. 7.4**.

We will also study the performance of two-fold oversampled PT-EQ combined with PT-EC. The appropriate datamodel is given in formula (2.19) where the received signal is sampled at twice the original sample rate. The TEQ can then be rewritten by means of its polyphase components which results in an even (e) and odd (o) TEQ at the sample rate. When transforming such a receiver structure to a per tone structure, one obtains the receiver shown in **Fig. 7.5**.

7.2.2 Joint initialization of PT-EQ and PT-EC

In the sequel, we immediately treat the oversampled PT-EQ, which is more general. In case of sampling at the original sample rate, all 'odd' parts in the following formulas can be set to zero.

To initialize jointly the PTFs for each tone i, one minimizes the following cost function

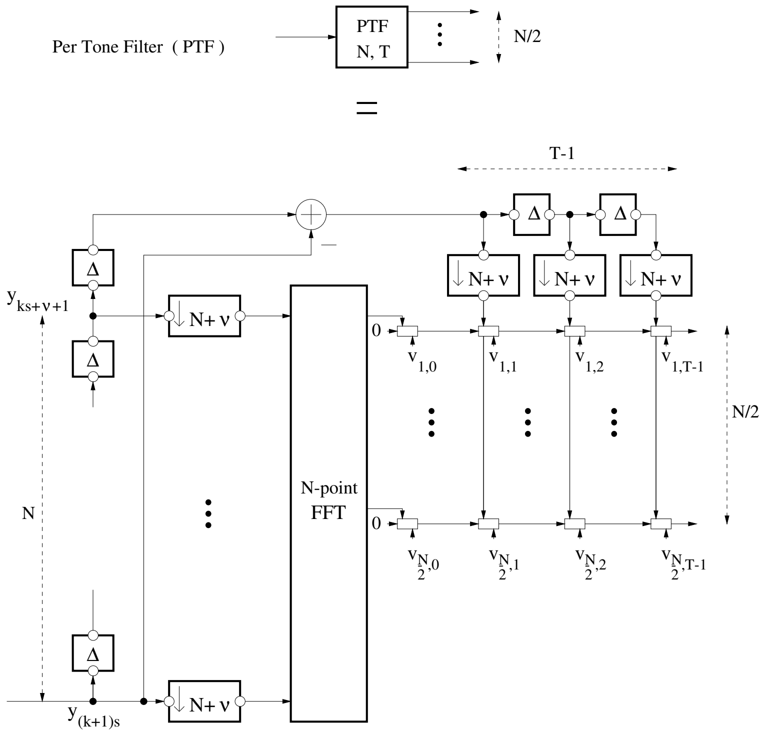

Figure 7.3: An (N,T)-PTF block includes one N-point FFT operation and T-taps per tone filters $\mathbf{v}_i$ for all used tones.

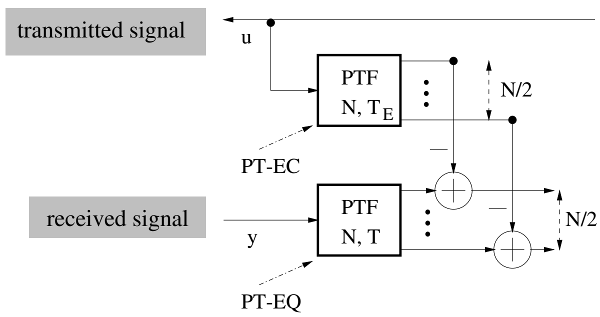

Figure 7.4: Transceiver with T-taps PT-EQ and T_E-taps PT-EC.

$$J(\mathbf{v}_{i,e}, \mathbf{v}_{i,o}, \mathbf{v}_{E,i}) = \mathcal{E}\left\{ \left| \begin{bmatrix} \bar{\mathbf{v}}_{i,e}^{\mathrm{T}} & \bar{\mathbf{v}}_{i,o}^{\mathrm{T}} \end{bmatrix} \cdot \begin{bmatrix} \mathbf{F}_{i,T} & \mathbf{O} \\ \mathbf{O} & \mathbf{F}_{i,T} \end{bmatrix} \cdot \begin{bmatrix} \mathbf{y}_e \\ \mathbf{y}_o \end{bmatrix} \right.\right.$$
$$\left.\left. \underbrace{- \bar{\mathbf{v}}_{E,i}^{\mathrm{T}} \cdot \mathbf{F}_{i,T_E} \cdot \mathbf{u}}_{\text{echo cancellation}} - X_i^{(k)} \right|^2 \right\} \quad (7.13)$$

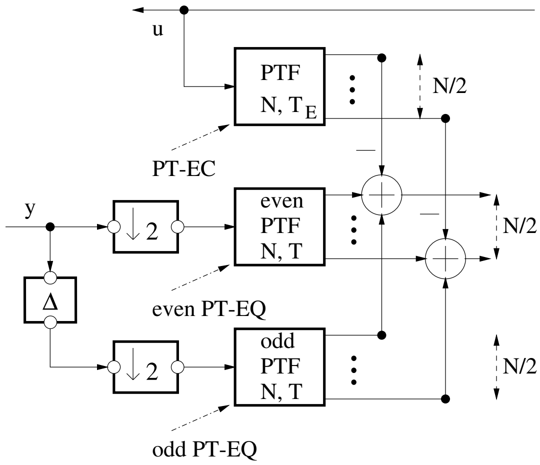

Figure 7.5: Transceiver with 2 times oversampled $2T$-taps PT-EQ and T_E-taps PT-EC.

with $\mathbf{F}_{i,T}$ equal to $\left[\begin{array}{c|c|c} \mathbf{I}_{T-1} & \mathbf{O} & -\mathbf{I}_{T-1} \\ \hline \mathbf{O} & \multicolumn{2}{c}{\mathcal{F}_N(i,:)} \end{array}\right]$. $\mathbf{v}_{i,e}$ and $\mathbf{v}_{i,o}$ are respectively the even and the odd PT-EQ for tone i. $\mathbf{v}_{E,i}$ is the PT-EC for tone i. Formula (7.13) can be rewritten by incorporating the oversampled data model

$$
\begin{aligned}
&J(\mathbf{v}_{i,e}, \mathbf{v}_{i,o}, \mathbf{v}_{E,i}) \\
&= \mathcal{E}\Bigg\{ \Bigg| \begin{bmatrix} \bar{\mathbf{v}}_{i,e}^{\mathrm{T}} & \bar{\mathbf{v}}_{i,o}^{\mathrm{T}} \end{bmatrix} \cdot \begin{bmatrix} \mathbf{F}_{i,T} & \mathbf{O} \\ \mathbf{O} & \mathbf{F}_{i,T} \end{bmatrix} \cdot \begin{bmatrix} \mathbf{H}_e\hat{\mathbf{x}} + \mathbf{H}_{E,e}\hat{\mathbf{u}} + \mathbf{n}_e \\ \mathbf{H}_o\hat{\mathbf{x}} + \mathbf{H}_{E,o}\hat{\mathbf{u}} + \mathbf{n}_o \end{bmatrix} \\
&\qquad\qquad - \bar{\mathbf{v}}_{E,i}^{\mathrm{T}} \mathbf{F}_{i,T_E}(\mathbf{H}_r\hat{\mathbf{u}}) - \mathbf{e}_i^{(k)}\hat{\mathbf{x}} \Bigg|^2 \Bigg\} \\
&= \Bigg\| \left[\begin{array}{cc|c} \mathbf{R}_{\hat{\mathbf{x}}}^{1/2}\mathbf{H}_e^{\mathrm{H}}\mathbf{F}_{i,T}^{\mathrm{H}} & \mathbf{R}_{\hat{\mathbf{x}}}^{1/2}\mathbf{H}_o^{\mathrm{H}}\mathbf{F}_{i,T}^{\mathrm{H}} & \mathbf{O} \\ \mathbf{R}_{\hat{\mathbf{u}}}^{1/2}\mathbf{H}_{E,e}^{\mathrm{H}}\mathbf{F}_{i,T}^{\mathrm{H}} & \mathbf{R}_{\hat{\mathbf{u}}}^{1/2}\mathbf{H}_{E,o}^{\mathrm{H}}\mathbf{F}_{i,T}^{\mathrm{H}} & -\mathbf{R}_{\hat{\mathbf{u}}}^{1/2}\mathbf{H}_r^{\mathrm{H}}\mathbf{F}_{i,T_E}^{\mathrm{H}} \\ \multicolumn{2}{c|}{\mathbf{R}_{\mathbf{n}}^{1/2}\begin{bmatrix} \mathbf{F}_{i,T}^{\mathrm{H}} & \mathbf{O} \\ \mathbf{O} & \mathbf{F}_{i,T}^{\mathrm{H}} \end{bmatrix}} & \mathbf{O} \end{array}\right] \begin{bmatrix} \bar{\mathbf{v}}_{i,e}^{*} \\ \bar{\mathbf{v}}_{i,o}^{*} \\ \bar{\mathbf{v}}_{E,i}^{*} \end{bmatrix} \\
&\qquad\qquad - \begin{bmatrix} \mathbf{R}_{\hat{\mathbf{x}}}^{1/2}\mathbf{e}_i^{(k)\mathrm{H}} \\ \mathbf{0} \\ \mathbf{0} \end{bmatrix} \Bigg\|_2^2
\end{aligned}
\tag{7.14}
$$

with $\mathbf{R}_{\hat{\mathbf{x}}} = \mathcal{E}\{\hat{\mathbf{x}}\hat{\mathbf{x}}^{\mathrm{H}}\}$ and $\mathbf{R}_{\hat{\mathbf{u}}} = \mathcal{E}\{\hat{\mathbf{u}}\hat{\mathbf{u}}^{\mathrm{H}}\}$ the autocorrelation matrices of vectors $\hat{\mathbf{x}}$ and $\hat{\mathbf{u}}$ respectively. $\mathbf{R}_{\mathbf{n}} = \mathcal{E}\{\mathbf{n}\mathbf{n}^{\mathrm{H}}\}$ is the autocorrelation of vector $\mathbf{n} = \begin{bmatrix} \mathbf{n}_e \\ \mathbf{n}_o \end{bmatrix}$. This set of equations has a particular structure. The first block row is constructed with the far end impulse responses and the second block row with the echo impulse responses. The third block row consists of noise data. The first and second block column corresponds to the even and the odd PT-EQ respectively. The third block column corresponds to the PT-EC, so it consists of the echo reference signal.

It is seen that the set-up with 1-taps PT-ECs of section 7.1 is a special case of the current set-up with the T_E-taps PT-ECs. Let us consider the echo cancellation for $T_E = 1$ in frame-synchronous mode

$$\bar{\mathbf{v}}_{E,i}^{\mathrm{T}} \cdot \mathbf{F}_{i,T_E} \cdot \mathbf{u} = a_i \cdot \mathcal{F}_N(i,:) \cdot \begin{bmatrix} u_1^k \\ \vdots \\ u_N^k \end{bmatrix} = a_i \cdot U_i^{(k)} \tag{7.15}$$

the only FFT operation that appears, will produce as output symbol $U_{1:N}^{(k)}$. This is exactly the transmitted echo symbol at time k, so the only FFT becomes superfluous, as already mentioned.

Cost function (7.14) corresponds to MMSE optimal equalizer and echo filter design, and hence incorporates optimal *per tone joint shortening* for the general case of a T-taps equalizer and a T_E-taps echo canceller. The per tone joint shortening improves upon the original time domain joint shortening [3, 80, 136] because it maximizes the SNR for each tone separately.

7.2.3 Interpolated echo cancellation at RT

In the previous sections, it is assumed that the transmit IFFT and receive FFT both have size N. However, when the transmit IFFT is γ times smaller (as is typically the case in an ADSL remote terminal), one can show that there exist an even more efficient implementation.

Assume an RT with $\frac{N}{\gamma}$-point IFFT and N-point FFT. The echo cancellation on tone i at time k corresponds to the second term in formula (7.12)

$$C_i^{(k)} = \mathrm{row}_i \underbrace{(\mathcal{F}_N \cdot \mathbf{U})}_{T_E \text{ FFTs}} \cdot \mathbf{w}_{E,i} \quad \text{for} \quad i = 1 \ldots \frac{N}{2} + 1 \tag{7.16}$$

The $\frac{N}{\gamma}$-point IFFT is followed by a prefix insertion, a γ-fold upsampling and interpolation filtering. The filters are part of the echo path, hence the echo reference signal is the upsampled IFFT output signal (with prefix) and so $\mathbf{U}$ is an $N \times T_E$ Toeplitz matrix with in each column $\gamma - 1$ zeros in between every 2 non-zero entries. This also means that γ successive FFTs, *i.e.* γ FFTs of successive columns of $\mathbf{U}$, are equal up to a phase shift.

Let us first assume an alignment of the echo symbols such that the FFTs of the first γ columns in matrix $\mathbf{U}$ are equal up to a phase shift (the same property holds for the following groups of γ columns). Hence, the FFT of all the columns of $\mathbf{U}$ can be obtained by computing the FFT of a selection of columns, namely $\mathbf{U}(:, 1:\gamma:\mathrm{end})$ and then multiplying these FFTs with the appropriate phase shifts, namely $\boldsymbol{\alpha} = \begin{bmatrix} 1 & \alpha^{i-1} & \dots & \alpha^{(i-1)(\gamma-1)} \end{bmatrix}$. If T_E is not divisible by γ, then the last columns of $\mathbf{U}(:, 1:\gamma:\mathrm{end})$ will only be multiplied with a subvector of $\boldsymbol{\alpha}$. A T_E-taps EC can then be represented as shrunk into an equivalent $\lceil\frac{T_E}{\gamma}\rceil$-taps EC

$$
\begin{aligned}
C_i^{(k)} &= \mathrm{row}_i \underbrace{(\mathcal{F}_N \cdot \mathbf{U}(:, 1:\gamma:\mathrm{end}))}_{\lceil\frac{T_E}{\gamma}\rceil \text{ FFTs}} \cdot \underbrace{\begin{bmatrix} \boldsymbol{\alpha} & \mathbf{0} & \dots \\ & \ddots & \\ \dots & \mathbf{0} & \boldsymbol{\alpha} \end{bmatrix} \cdot \mathbf{w}_{E,i}}_{\tilde{\mathbf{w}}_{E,i}} \\
\boldsymbol{\alpha} &= \begin{bmatrix} 1 & \alpha^{i-1} & \dots & \alpha^{(i-1)(\gamma-1)} \end{bmatrix}
\end{aligned}
\tag{7.17}
$$

where $\tilde{\mathbf{w}}_{E,i}$ is a $\lceil\frac{T_E}{\gamma}\rceil$-taps PT-EC for tone i. Remark that, when T_E is not divisible by γ, the phase matrix has an additional diagonal element in the lower right corner, which is a subvector of $\boldsymbol{\alpha}$.

Second, if the alignment of the echo symbols is such that only the first $\acute{\gamma}$ columns of $\mathbf{U}$ have their FFTs equal up to a phase shift, with $\acute{\gamma} < \gamma$, a formula similar to (7.17) can be obtained. Depending on the alignment of the echo symbols, the echo filter $\tilde{\mathbf{w}}_{E,i}$ may have $\lceil\frac{T_E}{\gamma}\rceil + 1$ taps and the phase matrix may have additional diagonal elements in left upper and the right lower corner.

The N-point FFTs in formula (7.17), can be written as γ times repeated $\frac{N}{\gamma}$-point FFTs because of the zero-structure in each column of $\mathbf{U}$. For every tone i, the echo cancellation is then

$$
\begin{aligned}
C_i^{(k)} &= \mathrm{row}_i \left(\mathbf{R} \cdot \mathcal{F}_{N/\gamma} \cdot \overbrace{\mathbf{U}(1:\gamma:N, 1:\gamma:\mathrm{end})}^{\tilde{\mathbf{U}}} \right) \cdot \tilde{\mathbf{w}}_{E,i} \\
&= \mathrm{row}_{\mathrm{mod}(\frac{i-1}{N/\gamma})+1} \underbrace{\left(\mathcal{F}_{N/\gamma} \cdot \tilde{\mathbf{U}} \right)}_{\lceil\frac{T_E}{\gamma}\rceil \text{ FFTs}} \cdot \tilde{\mathbf{w}}_{E,i}
\end{aligned}
\tag{7.18}
$$

with $\mathbf{R} = [\mathbf{I}_{N/\gamma} \dots \mathbf{I}_{N/\gamma}]^{\mathrm{T}}$, $\tilde{\mathbf{U}}$ an $\frac{N}{\gamma} \times \lceil\frac{T_E}{\gamma}\rceil$ Toeplitz matrix with the $\frac{N}{\gamma}$-point IFFT output samples (with prefix) and 'mod' the remainder after division. Note that, if $\acute{\gamma} < \gamma$, a similar formula can be obtained. A SFG of the interpolated (N, T, γ)-PTF is shown in **Fig. 7.6**, where the notation $\mathbf{v}_i$ instead of $\mathbf{w}_i$ is adopted because we work with the efficient implementation of these filters. Remark that a derivation of the interpolated PT-EC can also be given as a function of the filter $\mathbf{v}_i$.

Overall, it is seen that roughly a γ-fold complexity reduction is obtained in the EC part.

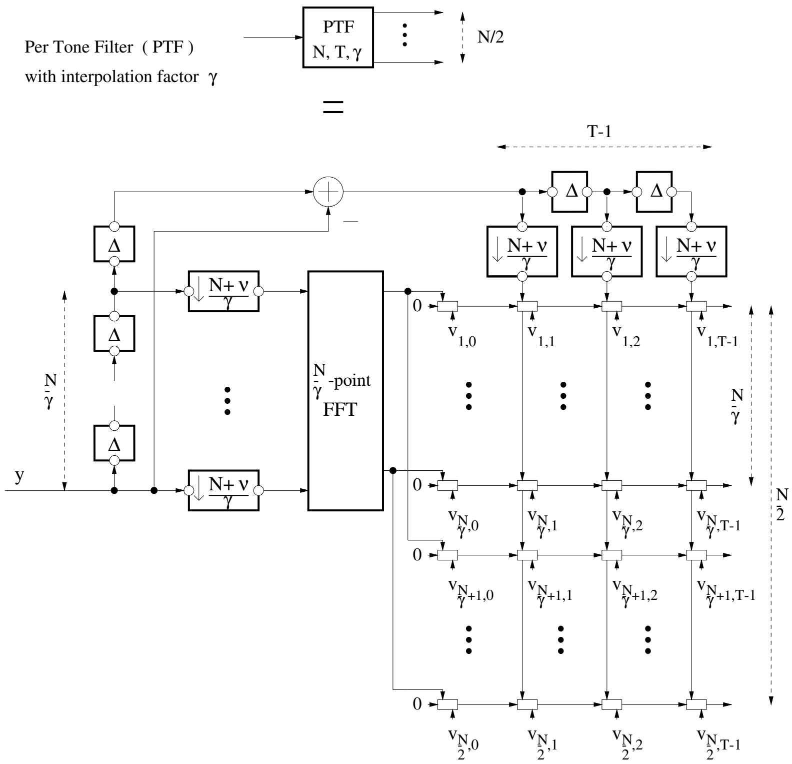

Figure 7.6: An interpolated (N, T, γ)-PTF block includes one $\frac{N}{\gamma}$-point FFT operation and T-taps per tone filters.

7.2.4 Decimated echo cancellation at CO

In this section, we consider a transceiver with N-point IFFT and $\frac{N}{\gamma}$-point FFT (as is typically the case in an ADSL central office). Similar to equation (7.16), on may write the echo cancellation on tone i as

$$C_i^{(k)} = \text{row}_i \underbrace{\left(\mathcal{F}_{N/\gamma} \cdot \mathbf{U}(1\!:\!\gamma\!:\!N,:)\right)}_{T_E \text{ FFTs}} \cdot \mathbf{w}_{E,i} \quad \text{for} \quad i = 1 \ldots \frac{N}{2\gamma} + 1 \tag{7.19}$$

with $\mathbf{U}$ an $N \times T_E$ Toeplitz matrix. The echo canceller has T_E taps at high rate but there are less tones now, which will result in a similar γ-fold complexity reduction as in the interpolated case.

To derive the cost effective PT implementation, we consider $\mathbf{U}(1\!:\!\gamma\!:\!N,:)$

$$\mathbf{U}(1\!:\!\gamma\!:\!N,:) = \begin{bmatrix} u_{\nu+1} & u_{\nu} & u_{\nu-1} & \dots & u_{\nu-\gamma+1} & \dots & u_{\nu-T_E+2} \\ u_{\nu+\gamma+1} & u_{\nu+\gamma} & u_{\nu+\gamma-1} & \dots & u_{\nu+1} & \dots & u_{\nu+\gamma-T_E+2} \\ \vdots & \vdots & \vdots & & \vdots & & \vdots \\ u_{\nu+N-\gamma+1} & u_{\nu+N-\gamma} & u_{\nu+N-\gamma-1} & \dots & u_{\nu+N-2\gamma+1} & \dots & \end{bmatrix} \quad (7.20)$$

where u_l is the echo reference signal with l the sample index. The echo reference data model is given in formula (2.18). The terms $k{\cdot}s$ and δ_3 are omitted in the sample index for the sake of a compact notation. The first γ columns of $\mathbf{U}(1\!:\!\gamma\!:\!N,:)$ do not have any samples in common. The $(\gamma+1)$st column is obtained by downshifting the first column, adding a sample at the beginning and deleting one at the end. Or stated in other words, columns $1, \gamma+1, 2\gamma+1, \dots$ form a Toeplitz matrix, *i.e.* $\mathbf{U}(1:\gamma:N, 1:\gamma:\text{end})$, and the same holds for matrices $\mathbf{U}(1:\gamma:N, 2:\gamma:\text{end}), \dots, \mathbf{U}(1:\gamma:N, \gamma:\gamma:\text{end})$. If T_E is a multiple of γ, these matrices have $\frac{T_E}{\gamma}$ columns. Otherwise the last $\text{mod}(\frac{T_E}{\gamma})$ columns of $\mathbf{U}(1\!:\!\gamma\!:\!N,:)$ are added to the appropriate Toeplitz matrices.

As a result, one may mathematically split the T_E-taps PTF in γ $\frac{T_E}{\gamma}$-taps PTFs: $\mathbf{w}_{E,i}(1\!:\!\gamma\!:\!\text{end}), \dots, \mathbf{w}_{E,i}(\gamma\!:\!\gamma\!:\!\text{end})$ and add their outputs for each tone i. The latter filters each individually can be implemented cost effectively by means of difference terms. A SFG of the decimated $(N, T, \frac{1}{\gamma})$-PTF is shown in **Fig. 7.7**, where we adopt again the notation $\mathbf{v}_i$ instead of $\mathbf{w}_i$ because we work here with the efficient implementation of these filters. The SFG consists of γ parallel $(\frac{N}{\gamma}, \frac{T}{\gamma}, 1)$-PTFs which correspond to the so-called polyphase components of $\mathbf{w}_{E,i}$. Roughly this again corresponds to a γ-fold complexity reduction.

7.2.5 Complexity during data transmission

We compute the complexity during data transmission for the TEC and PT-EC by counting the number of real multiplications and additions. By 'complexity during data transmission', we mean the filtering operation itself. Hence, adopted to echo cancellation, 'complexity during data transmission' is similar to 'echo emulation'. We do not consider the filter adaptation here.

The complexity for the two-fold oversampled TEQ and PT-EQ can be derived from the complexity figures given in section 4.3.

Symmetric rate set-up

It is shown in section 4.3 that the complexity during data transmission for a T-taps TEQ is roughly the same as for $\frac{N}{2}$ T-taps PT-EQs. When not all the

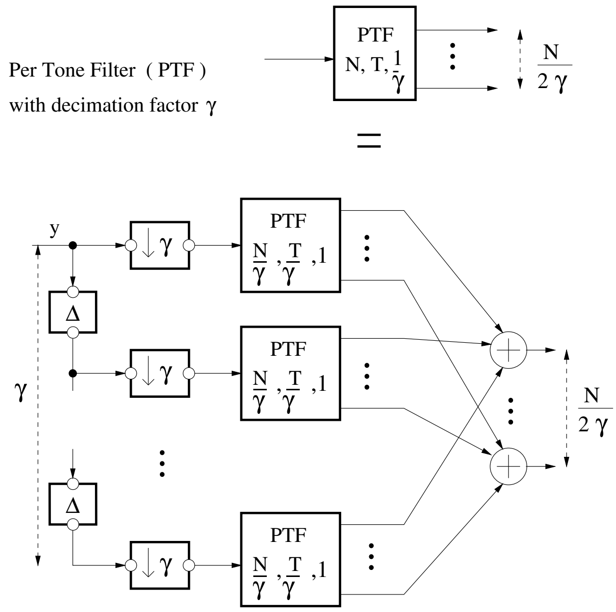

Figure 7.7: A decimated $(N, T, \frac{1}{\gamma})$-PTF block includes γ $(\frac{N}{\gamma}, \frac{T}{\gamma}, 1)$-PTF blocks each having one $\frac{N}{\gamma}$-point FFT operation and $\frac{T}{\gamma}$-taps per tone filters.

	# multiplications	# additions
TEC	$F_s T_E$	$F_s(T_E - 1)$

Table 7.1: Complexity of TEC (in operations/s)

tones are used or when a smaller equalizer size is sufficient for some tones, complexity of the PT method can be reduced even further.

The complexity of the TEC consists only of the T_E taps in the time domain, as presented in **Table 7.1**. There is neither an FFT nor 1-taps PT-EQs involved in this EC.

The PT-EC has the same complexity as the PT-EQ but now with the number of taps equal to T_E. This complexity is shown in **Table 7.2** where it is assumed that the number of echo cancelled tones is $\frac{N}{2}$ and the symbol duration $\frac{N+\nu}{F_s} \approx \frac{N}{F_s}$. It is seen that the number of multiplications and additions for PT-EC remains more or less the same as for TEC when all tones are echo cancelled. However in reality not all tones are echo cancelled and for these tones the number of taps can be set to zero which corresponds to an extra complexity

	# multiplications	# additions
FFT	$\frac{F_s}{N+\nu}\mathcal{O}(N \cdot \log(N))$	$\frac{F_s}{N+\nu}\mathcal{O}(N \cdot \log(N))$
PT-EC	$F_s(T_E+1)$	$F_sT_E + \frac{F_s}{N}(T_E-1)$

Table 7.2: Approximated complexity of PT-EC (in operations/s)

	# multiplications	# additions
TEC	$F_s\lceil\frac{T_E}{\gamma}\rceil$	$F_s(\lceil\frac{T_E}{\gamma}\rceil-1)$
FFT	$\frac{F_s}{N+\nu}\mathcal{O}(\frac{N}{\gamma} \cdot \log(\frac{N}{\gamma}))$	$\frac{F_s}{N+\nu}\mathcal{O}(\frac{N}{\gamma} \cdot \log(\frac{N}{\gamma}))$
PT-EC	$F_s(\lceil\frac{T_E}{\gamma}\rceil+1)$	$F_s\lceil\frac{T_E}{\gamma}\rceil + \frac{F_s}{N}(\lceil\frac{T_E}{\gamma}\rceil-1)$

Table 7.3: Complexity comparison of TEC with PT-EC (in operations/s) for interpolated echo cancellation (in RT with $\frac{N}{\gamma}$-point IFFT and N-point FFT)

saving. Additional complexity however is introduced by the extra FFT in the PT-EC-scheme. This complexity can be decreased if the modem has an asymmetric rate set-up, as shown in the next subsections.

Interpolated echo cancellation at RT

The complexity of TEC versus PT-EC is shown in **Table 7.3**. Note that F_s is the high rate sample frequency, *i.e.* according to N. In comparison with the set-up with an IFFT of size N, the number of multiplications and additions for the TEC and PT-EC is roughly divided by γ, and only one $\frac{N}{\gamma}$-point FFT is needed in the PT implementation.

Decimated echo cancellation at CO

The complexity during data transmission can be found by multiplying by γ the complexity of an $(\frac{N}{\gamma}, \frac{T}{\gamma}, 1)$-PTF. In the assumption that $\frac{N}{2\gamma}$ tones are used and that $\mathrm{mod}(\frac{T_E}{\gamma}) = 0$, the complexity is given in **Table 7.4**, with F_s the high rate sample frequency. In comparison with the interpolated EC, one needs γ $\frac{N}{\gamma}$-point FFTs instead of 1 $\frac{N}{\gamma}$-point FFT and γ times more difference terms, but in this case the number of tones that have to be demodulated is significantly smaller.

	# multiplications	# additions
TEC	$\frac{F_s}{\gamma}T_E$	$\frac{F_s}{\gamma}(T_E-1)$
FFT	$\gamma\frac{F_s}{N+\nu}\mathcal{O}(\frac{N}{\gamma}\cdot\log(\frac{N}{\gamma}))$	$\gamma\frac{F_s}{N+\nu}\mathcal{O}(\frac{N}{\gamma}\cdot\log(\frac{N}{\gamma}))$
PT-EC	$\gamma\frac{F_s}{\gamma}(\frac{T_E}{\gamma}+1)$	$\gamma\frac{F_s}{\gamma}\frac{T_E}{\gamma}+\gamma\frac{F_s}{N}(\frac{T_E}{\gamma}-1)$

Table 7.4: Complexity comparison of TEC with PT-EC (in operations/s) for decimated echo cancellation (in CO with N-point IFFT and $\frac{N}{\gamma}$-point FFT)

7.3 Comparison of echo emulation in t/f domain EC and PT-EC

In t/f domain EC, see chapter 6, a Toeplitz matrix of echo reference samples is written as the sum of a circulant matrix and a matrix with difference terms, *i.e.* $\boldsymbol{\chi}$. Only the circulant part is transformed to the frequency domain, while the difference terms form a time domain correction. This leads to a low complexity EC which uses the echo filter taps in the time domain as well as their Fourier transform in the frequency domain.

In PT-EC, we start from the same Toeplitz matrix (if the same alignment applies), *i.e.* $\mathbf{U}$ in formula (7.11). We then move the TEC $\mathbf{w}_E$ to the frequency domain resulting in the PT-EC $\mathbf{w}_{E,i}$. The latter echo filter is cost effectively implemented by means of $\mathbf{v}_{E,i}$. The cost effective implementation is derived in appendix 4.B. In formula (4.31), the Toeplitz matrix is also written as the sum of a circulant matrix and a matrix with difference terms. The circulant part is then 'transformed' to the frequency domain resulting in a term which is the product of the FFT output for tone i times $v_{i,0}$, the first tap of the modified per tone filter $\mathbf{v}_i$. This tap is equal to the ith component of the Fourier transform of the zero padded original per tone filter $\mathbf{w}_i$.

$$v_{i,0} = \mathcal{F}_N(i,:)\cdot\begin{bmatrix}\mathbf{w}_i\\ \mathbf{0}\end{bmatrix} \tag{7.21}$$

Stated in other words, if the per tone filter would be real and the same for all tones, $\mathbf{w}_i=\mathbf{w}$, then the vector $[v_{1,0}\dots v_{\frac{N}{2}+1,0}]^{\mathrm{T}}$ would define its Fourier transform.

Let us now apply this property to the echo filters. In case of a TEC or a t/f domain EC, there is only one echo filter $\mathbf{w}_E$. This filter can be considered as a 'PT-EC which is the same for all used tones'. The FFT of $\mathbf{w}_E$ is the frequency domain part of the t/f domain EC and thus corresponds to vector $[v_{1,0}\dots v_{\frac{N}{2}+1,0}]^{\mathrm{T}}$.

In the per tone based transceiver, the PT-ECs are complex and different for different tones because the echo path for tone i includes the PT-EQ for tone i which in turn is tone dependent. Hence, vector $[v_{1,0} \ldots v_{\frac{N}{2}+1,0}]^{\mathrm{T}}$ does not represent the FFT of one real echo filter anymore.

The second term of formula (4.31) in appendix 4.B includes the upper triangular matrix with difference terms. We compute the complexity of this term in number of multiplications. If the modem has a real echo filter which is common to all tones, then the product of the upper triangular matrix and the echo filter only costs approximately $(T-1)^2/2$ multiplications. This operation is similar to the time domain part of the t/f domain EC.

However, in the PT-EC, we have a separate complex echo filter per tone. The product of the upper triangular matrix with all the complex per tone filters costs approximately $2N_u(T-1)^2/2$ multiplications. Therefore it is more efficient to implement the per tone filters $\mathbf{w}_{E,i}$ with the difference terms as their inputs and introduce new taps as in $\mathbf{v}_{E,i}$. The latter implementation costs $2N_u(T-1)$ multiplications.

Comparing complexity of the echo emulation (in number of multiplications/s) for both methods and TEC, for symmetric synchronous operation, we obtain **Table 7.5**. The echo emulation complexity is split in two complexity parts. The real input part corresponds to

- the time domain correction $\boldsymbol{\chi}$ in the t/f domain EC,
- the full echo emulation in the TEC,
- and the multiplication with the difference terms in PT-EC.

The complex input part corresponds to

- the frequency domain EC in the t/f domain EC
- and the multiplication with the FFT output in PT-EC

(we apply polar and cartesian representation respectively). T/f domain EC needs one FFT to transform the echo filter taps from frequency to time domain, however this FFT is in fact part of the filter adaptation, and therefore its complexity is denoted between square brackets. In synchronous mode, PT-EC does not need an FFT and the first ν difference terms are zero. The complexity comparison for symmetric asynchronous operation is shown in **Table 7.6**. These complexities can easily be generalized to the asymmetric rate set-ups.

Example 7.3.1. A numerical example of echo emulation complexity in a symmetric rate set-up is given for the following parameters. The symbol size is $N = 512$, the prefix length is $\nu = 32$, the echo filter length is $T_E = 300$ and the sample rate $F_s = 2.208$ MHz. In the asymmetric rate set-ups we

	T/F-EC	TEC	PT-EC
real input	$\frac{F_s}{N+\nu}\frac{(T_E-\nu-1)^2}{2\cdot 2}$	$\frac{F_s}{N+\nu}NT_E$	$\frac{F_s}{N+\nu}N_u 2(T_E-\nu-1)$
complex input	$\frac{F_s}{N+\nu}N_u$		$\frac{F_s}{N+\nu}N_u 4$
FFT	$\left[\frac{F_s}{N+\nu}\mathcal{O}(N\cdot\log(N))\right]$		

Table 7.5: Echo emulation complexity (in multiplications/s) of t/f domain EC, TEC and PT-EC for symmetric synchronous operation. The FFT complexity between square brackets corresponds to the transformation of the echo filter taps from frequency to time domain domain.

	T/F-EC	TEC	PT-EC
real input	$\frac{F_s}{N+\nu}\frac{(T_E-1)^2}{2\cdot 2}$	$\frac{F_s}{N+\nu}NT_E$	$\frac{F_s}{N+\nu}N_u 2(T_E-1)$
complex input	$\frac{F_s}{N+\nu}N_u$		$\frac{F_s}{N+\nu}N_u 4$
FFT	$\left[\frac{F_s}{N+\nu}\mathcal{O}(N\cdot\log(N))\right]$ $+2\frac{F_s}{N+\nu}\mathcal{O}(N\cdot\log(N))$		$\frac{F_s}{N+\nu}\mathcal{O}(N\cdot\log(N))$

Table 7.6: Echo emulation complexity (in multiplications/s) of t/f domain EC, TEC and PT-EC for symmetric asynchronous operation.

furthermore take $\gamma = 4$ and assume that N, ν and F_s are the parameters at the high rate side. We also assume that the RT works frame-synchronously and that the number of used tones in downstream is $N_u = 218$. The CO is then frame-asynchronous and we have $N_u = 23$ in upstream. The complexity (in multiplications/s) is given in **Table 7.7**. The number of FFTs is also given. For a constant echo filter length, in the symmetric rate RT, t/f domain EC has the lowest complexity. The complexity of PT-EC is lower than the complexity of TEC because PT-EC is only performed for the used tones. In the symmetric rate CO, PT-EC has lowest complexity because the small number of used tones in upstream can be exploited, in contrast with the other schemes. In the asymmetric, interpolated, RT, the real input part complexity is basically divided by γ for the 3 EC schemes. As a result, the same comparison holds as for the symmetric RT. In the asymmetric, decimated CO, the real input part complexity of t/f domain EC and TEC is divided by γ. In the decimated PT-EC, their is no significant additional gain in the real part complexity, with respect to the symmetric rate set-up, because the complexity gain resulting from less used tones, was already obtained in the symmetric CO. However, the

		T/F-EC	TEC	PT-EC
synchronous symmetric RT	real input	72.3	623	472
	complex input	0.88		3.54
	FFT	[1 N-point]		
asynchronous symmetric CO	real input	90.7	623	55.8
	complex input	0.093		0.37
	FFT	[1] + 2 N-point		1 N-point
synchronous interpolated RT	real input	18.1	156	117
	complex input	0.88		3.54
	FFT	[1 N-point]		
asynchronous decimated CO	real input	22.7	156	55.2
	complex input	0.093		1.49
	FFT	[1 N-point] + 2 $\frac{N}{\gamma}$-point		γ $\frac{N}{\gamma}$-point

Table 7.7: Echo emulation complexity (in M multiplications/s and number of FFT operations) with $N = 512$ and $\gamma = 4$.

one N-point FFT can be replaced by γ $\frac{N}{\gamma}$-point FFTs, but at the cost of γ times more multiplications of an FFT output with the first tap of a PTF, as is also clear from figure 7.7.
Note that, in case of an asynchronous interpolated RT, t/f domain EC needs 2 N-point FFTs whereas PT-EC needs only 1 $\frac{N}{\gamma}$-point FFT. □

We conclude that, for a certain echo filter length, t/f domain EC has the lowest complexity and that the complexity gain of PT-EC with respect to TEC is due to the selection of the used tones. But, on the other hand, PT-EC combined with PT-EQ clearly enables to optimize capacity for given PTF lengths. Moreover, because PT-EQ is performed first, optimal per tone joint shortening is incorporated in the cost function and the PT-EC may have shorter filter lengths for similar performance.

7.4 Combination of PT-EC with pulse shaping and windowing

VDSL relies on a cyclic prefix, a cyclic suffix and synchronization to maintain tone orthogonality. Further, DMT-based VDSL has pulse shaping and windowing, see section 2.1.7. However when transmitting over longer lines, the size of the cyclic extensions is possibly insufficient and orthogonality between tones may be lost. The same happens when synchronization is not perfect. This, in addition, produces a NEXT problem, see section 1.5. In this section, PT-EC is investigated for VDSL in which the tone orthogonality is lost for some reason. PT-EC can be applied directly as for ADSL to cancel the echo, because the reference echo signal is available in the modem. For NEXT cancellation however, reference signals are only available at the central office (CO). There a *per tone NEXT cancellation*, analogous to PT-EC, may be used.

The overal data model is given in section 2.2.6. A scheme of a VDSL-system with pulse shaping, windowing and PT-EC is shown in **Fig. 7.8**. Remark that the windowing operation is part of the echo path. Because windowing with an extra prefix of size μ is equivalent with a $(\mu+1)$-taps PT-EQ, see section 4.4, the echo impulse response is lengthened by μ. There is no TEQ in VDSL, hence in the equivalent PT-EQs T is set to 1. Remark that if T would be different from 1 and there is windowing in the time domain, we have to compute the T successive FFTs explicitly, as explained in section 4.4. A received VDSL symbol with prefix and suffix contains $N+2\nu$ samples. As a result, the downsamplers in the PTF blocks in figure 7.8, downsample the input signal with a factor $N+2\nu$. Extension of this SFG to two-fold oversampled PT-EQs is straightforward.

For each tone i, the PT-EQ and PT-EC are initialized by minimizing the cost function

$$J(\mathbf{w}_{i,e},\mathbf{w}_{i,o},\mathbf{v}_{E,i}) = \mathcal{E}\left\{ \left| \begin{bmatrix}\bar{\mathbf{w}}_{i,e}^{\mathrm{T}} & \bar{\mathbf{w}}_{i,o}^{\mathrm{T}}\end{bmatrix} \cdot \begin{bmatrix}\mathbf{F}_{win,i,T} & \mathbf{O} \\ \mathbf{O} & \mathbf{F}_{win,i,T}\end{bmatrix} \cdot \begin{bmatrix}\mathbf{y}_e \\ \mathbf{y}_o\end{bmatrix} - \bar{\mathbf{v}}_{E,i}^{\mathrm{T}} \cdot \mathbf{F}_{i,T_E} \cdot \mathbf{u} - X_i^{(k)} \right|^2 \right\} \tag{7.22}$$

with

$$\mathbf{F}_{win,i,T} = \begin{bmatrix} \boxed{\mathcal{F}_{win}(i,:)} & 0 & \cdots \\ & \ddots & \ddots \\ 0 & \cdots & \boxed{\mathcal{F}_{win}(i,:)} \end{bmatrix} \tag{7.23}$$

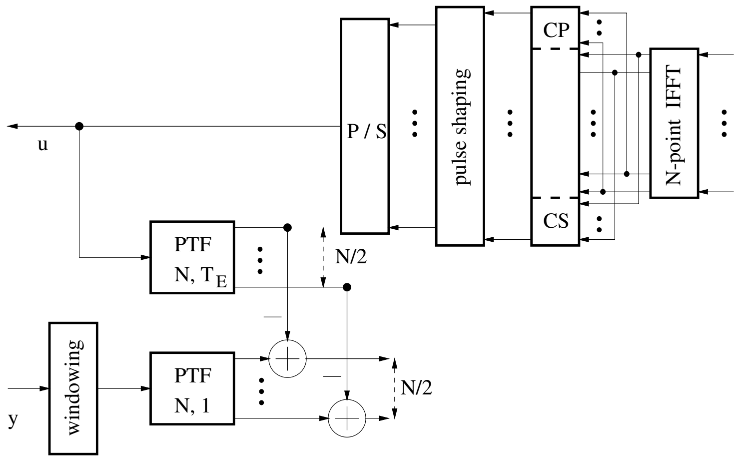

Figure 7.8: A VDSL-system with pulse shaping, windowing, PT-EQ and PT-EC.

and

$$\mathcal{F}_{win} = \mathcal{F}_N \cdot \begin{bmatrix} \mathbf{0} & \mathbf{D}_1 & \mathbf{0} & \mathbf{0} & \mathbf{D}_3 \\ \mathbf{0} & \mathbf{0} & \mathbf{I}_{N-\mu} & \mathbf{0} & \mathbf{0} \\ \mathbf{D}_4 & \mathbf{0} & \mathbf{0} & \mathbf{D}_2 & \mathbf{0} \end{bmatrix} \tag{7.24}$$

where $\mathbf{F}_{win,i,T}$ has T rows and the $(\mathbf{D}_i)_{\frac{\mu}{2}\times\frac{\mu}{2}}$ are diagonal matrices with the windowing coefficients. $\mathbf{w}_{i,e}$ and $\mathbf{w}_{i,o}$ are respectively the even and the odd PT-EQ for tone i. Remark that notation $\mathbf{w}$ instead of $\mathbf{v}$ is used here for the PT-EQ because T successive FFTs are computed explicitly if $T > 1$.

7.5 Simulation results

7.5.1 Per tone echo cancellation in ADSL

Simulation results are presented for a 4km 26 AWG downstream and upstream channel with white noise of -140dBm/Hz. For downstream, the IFFT and FFT have size $N = 512$. For upstream, the IFFT and FFT have size $N = 128$. Hence, the interpolation factor (in RT) and the decimation factor (in CO) are equal to $\gamma = 4$. The corresponding cyclic prefix lengths are $\nu = 32$ and $\nu/\gamma = 8$. An FDM set-up for the used tones is adopted. The upstream tones are tones 8 till 30 and the downstream tones are 39 till 256. Due to relaxed transmit and receive filter order specifications, downstream symbols experience echo from upstream symbols and vice versa. Downstream and upstream PSD on the used tones are -40dBm/Hz and -38dBm/Hz respectively.

The zero reference delay of the far end and the echo impulse response is determined by the interval (with length equal to the prefix length plus one) with highest energy in the far end and the echo impulse response respectively. Bit rates are computed for relative delays $\delta_1 = 0$ and $\delta_2 = \delta_3 = 20$ at both RT and CO.

Fig. 7.9 shows the downstream bit rate as a function of the number of taps T_E of the PT-EC. We compare 32-taps PT-EQ (at original sample rate F_s=2.208 MHz) with 2 times 16-taps PT-EQ (hence, with 2-fold oversampling). The upper bounds are the bit rates for both set-ups when no echo is present. They are 2.89 Mbits/s and 3.23 Mbits/s respectively. For T_E equal to 150, the upper bounds are reached. Remark that, as far as complexity is concerned, the number of EC taps can effectively be divided by $\gamma = 4$ (see section 7.2.3). To compare these bit rates with bit rates obtained by T_E-taps TEC, we have simulated 'ideal' TEC performance by zeroing T_E successive elements with highest energy in the echo impulse response. A 400-taps TEC is then needed to obtain the upper bound bit rates.

Fig. 7.10 shows analogous simulation results for upstream. The upper bounds for the bit rates are 1.12 Mbits/s for 32-taps PT-EQ and 1.11 Mbits/s for 2 times 16-taps PT-EQ. In this case the the sample rate set-up has slightly better performance compared to the oversampled set-up. As far as complexity is concerned, each T_E-taps PT-EC may effectively be replaced by $\gamma = 4$ $\frac{T_E}{\gamma}$-taps PT-ECs (see section 7.2.4). TEC performance has also been simulated by zeroing T_E successive elements in the echo impulse response. A 400-taps TEC is then needed to obtain 1.10 Mbits/s with 32-taps PT-EQ and a 500-taps TEC is needed to obtain 1.10 Mbits/s with 2 times 16-taps PT-EQ.

7.5.2 Per tone echo cancellation in VDSL

Simulation results are presented for the standard VDSL4 line [11] of 500m, this line contains 2 bridged taps. All IFFTs and FFTs have size $N = 4096$. The carrier spacing is the same as in ADSL, *i.e.* 4.3125kHz. The total bandwidth is 8.832MHz, hence the sampling rate F_s is 17.664MHz. The adopted spectral plan for up and downstream tones is as follows:

- band 1: ADSL upstream
- band 2: ADSL downstream
- band 3: downstream: tones 255-347
- band 4: upstream: tones 348-417
- band 5: downstream: tones 464-718
- band 6: upstream: tones 719-812

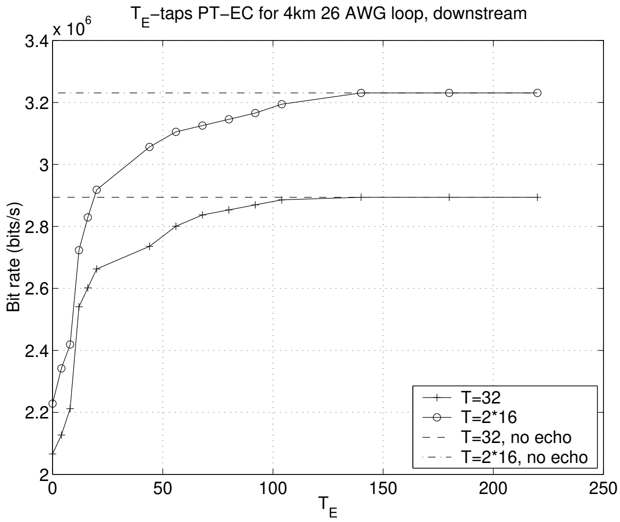

Figure 7.9: Bit rate as a function of the number of taps T_E of the PT-EC for a 4km 26 AWG downstream loop for 32-taps PT-EQ (at original sample rate) and 2 times 16-taps PT-EQ (hence, with 2-fold oversampling). The upper bound is computed without echo.

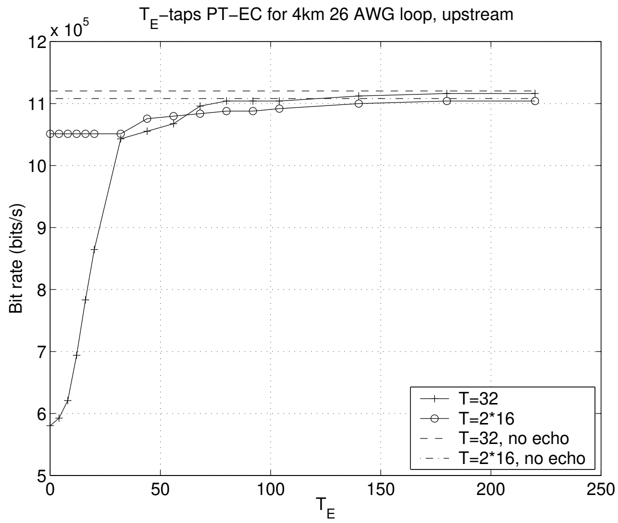

Figure 7.10: Bit rate as a function of the number of taps T_E of the PT-EC for a 4km 26 AWG upstream loop.

- band 7: upstream: tones 927-1229
- band 8: downstream: tones 1230-1623
- band 9: downstream: tones 1646-2048

The cyclic prefix and suffix are both equal to $\nu = 160$. Pulse shaping is defined by $\beta = 140$ and windowing by $\mu = 70$. The zero reference delays correspond to $\nu + 1$ successive samples of the impulse responses, with highest energy. The relative delay of the far end signal is $\delta_1 = 0$ and the relative delay of the echo signal is taken $\delta_2 = \delta_3 = 200$ or $\delta_2 = \delta_3 = 300$ to simulate misalignment of echo with respect to far end. The external noise consists of additive white gaussian noise of -140dBm/Hz. In **Fig. 7.11** the SNR is plotted as a function of the number of echo canceller taps T_E for tone 340 and relative delays $\delta_2 = \delta_3 = 200$ and $\delta_2 = \delta_3 = 300$. Four transceiver set-ups are compared

- without oversampling and with PT-EC (solid line with '+')
- with oversampling and with PT-EC (solid line with 'o')
- without oversampling and no echo (dashed line)
- with oversampling and no echo (dashed-dotted line)

PT-EQ is adopted with $T = 1$ or $T = 2 * 1$ in the non-oversampled and oversampled set-up respectively. Oversampling only, *i.e.* with $T_E = 0$, does not increase the SNR sufficiently because only one tap is used for even and odd channel. By PT-EC, the SNR increases as a function of echo filter length T_E, but the required number of echo canceller taps is rather large. The echo impulse response is about 60 taps at sample rate but the windowing lengthens the echo impulse response by μ. **Fig. 7.12** shows the SNR for all the downstream tones with $\delta_2 = \delta_3 = 200$ for the same channel. Four transceiver set-ups are compared

- without oversampling and 20-taps PT-EC (solid line)
- with oversampling and 20-taps PT-EC (dotted line)
- without oversampling and no PT-EC (dashed line)
- with oversampling and no PT-EC (dashed-dotted line)

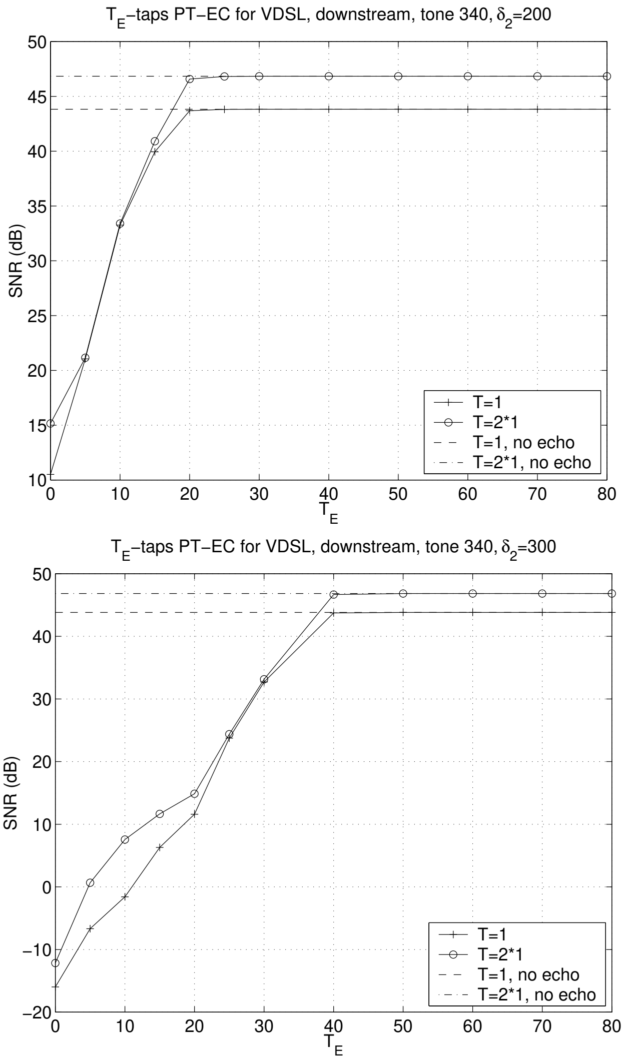

Figure 7.11: SNR as a function of the number of echo canceller taps T_E for tone 340 and relative delays $\delta_2 = 200$ and $\delta_2 = 300$ for standard channel VDSL4 of 500m.

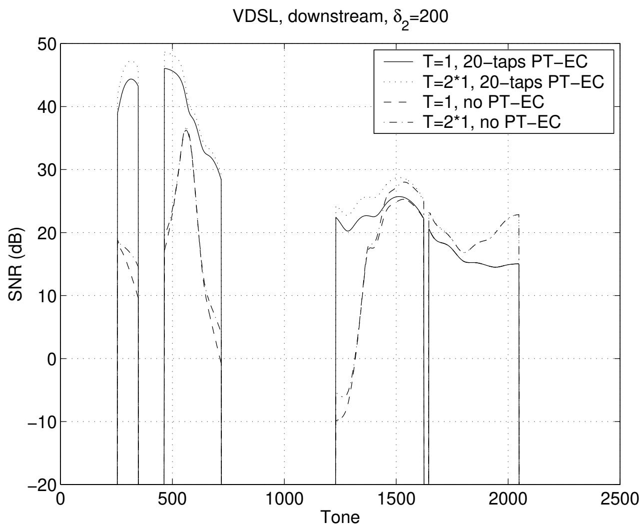

Figure 7.12: SNR as a function of the used downstream tones with $\delta_2 = 200$ for the same channel for four different set-ups.

7.6 Conclusions

We have developed per tone echo cancellation as an extension of per tone equalization. The advantage, with respect to TEC and t/f domain EC, is that this structure allows optimization of the SNR per tone given a certain number of taps for the equalizer and the echo canceller. Moreover, joint shortening is incorporated in the extended per tone cost function.

Slightly modified per tone echo cancellation structures have been derived for the interpolated and decimated rate set-ups, which has resulted in decreased complexity 'during data transmission', or, in other words 'for the echo emulation'. Further, the echo emulation complexity has been compared with the t/f domain echo emulation. It has been shown that t/f domain echo emulation has lowest complexity for a given echo filter length. But, on the other hand, because per tone echo cancellation optimizes capacity, shorter filter lengths may be used for similar performance.

Chapter 8

Conclusions and further research

We formulate the main conclusions of this thesis in section 8.1 and give some suggestions for further research in section 8.2.

8.1 Conclusions

In **part I**, we have studied equalization in DMT-based systems. If the channel impulse response is longer than the cyclic prefix, as is the case in ADSL, a TEQ is usually inserted before demodulation to shorten the channel impulse response. A well-known algorithm to initialize the TEQ coefficients is based on MMSE channel shortening. The squared error between the TEQ output and the target impulse response output is then minimized. To avoid the zero solution, different constraints (unit norm, unit tap, unit energy) can be imposed. We have shown that a unit energy constraint on the received signal of interest and/or on the total received signal leads to the same solution for the TEQ, up to a scaling factor, and hence, leads to the same bit rate.

The main disadvantage of MMSE channel shortening algorithm is that the cost function does not correspond to bit rate optimization. Further, the obtained bit rate is a non-smooth function of the decision delay. As a result, the delay of the received signal is critical. An additional disadvantage is that all tones are equalized with the same filter, which limits the performance of the DMT-system. We aimed at improving upon the classical MMSE channel shortening algorithm.

In a first attempt, we have maintained the TEQ-based receiver structure. We have modified the classical MMSE algorithm by the introduction of weight matrices in the cost function as well as in the constraint, to explicitly disregard the unused tones. Simplified formulas for the correlation matrices in case of white signal of interest and noise have been derived. A significant performance increase has been obtained in upstream. However, the proposed algorithm still does not correspond to bit rate optimization.

In a second attempt, we have changed the receiver structure. Each tone then has its own (complex) TEQ after demodulation, *i.e.* per tone equalization. By minimizing an MSE problem per tone (*i.e.* direct initialization), we are able to optimize the bit rate per tone, which is the main advantage of PT-EQ. The PT-EQ bit rate is an upper bound for the TEQ bit rate and is a very smooth function of the decision delay. An increased performance has been obtained in upstream as well as in downstream. The bit rate 'gap' between the original MMSE channel shortening (with unit norm TIR) and PT-EQ is the largest in upstream (for a given number of equalizer taps). Therefore, it is expected that improved TEQ algorithms can obtain a larger bit rate gain in upstream than in downstream.

The complexity during data transmission is similar for TEQ and PT-EQ if all tones are used. This results from the fact that the T FFTs (per symbol), needed as inputs for a T-taps PT-EQ, can be implemented efficiently by means of 1 FFT operation and $T-1$ (real) difference terms. Furthermore, PT-EQ allows optimization of the number of taps per tone, and one can set the number of taps to zero for the unused tones. On the other hand, the PT-EQ-based receiver needs more memory than the TEQ-based receiver to store more equalizer taps.

The combination of PT-EQ and windowing has been studied. (Time domain) windowing in a DMT-based receiver has been proposed in literature to decrease the sensitivity to RFI, by lowering the sidelobes associated with a DFT filter bank. The efficient PT-EQ structure, *i.e.* by means of difference terms, can not be combined with (time domain) windowing. However, it has been shown that a (time domain) window is equivalent to a certain set of PT-EQs. As a result, windowing can be implemented after demodulation, as a part of the PT-EQs. By optimizing the overall PT-EQ, the window is implicitly optimized per tone.

As an upper bound to per tone equalization, we have performed simulations on SIMO equalization. In the latter structure, there is no demodulating FFT, but the received signal is immediately fed to a (lengthened) equalizer per tone. Hence, an $(N+T-1)$-taps SIMO-equalizer replaces the convolution of the N-point FFT filter for a certain tone with the original T-taps PT-EQ for that tone. SIMO equalization has been shown to perform only a slight bit rate increase for a large complexity increase.

Direct initialization, by means of an MMSE problem per tone, has a high computational cost. Therefore, recursive initialization based on training sequences has been proposed. Because the autocorrelation matrix of the filter input has a large eigenvalue spread, LMS-based initialization is very slow. RLS, on the other hand, has optimal convergence properties and achieves good performance with an acceptable number of training symbols. We have adopted RLS with inverse updating to PT-EQ. Although the RLS complexity is quadratic in the number of filter taps, complexity has been saved considerably. By processing first the real difference terms, which are common for all used tones, the quadratic part of the algorithm is real and common for all used tones. Then a linear, complex part of the algorithm is performed for each tone separately.

To further reduce initialization complexity, tone grouping has been proposed. The optimal PT-EQ is computed only for the center tones (by direct or recursive initialization). Then these equalizers are reused for the other tones in the same group. After tone grouping, a 1-taps FEQ is needed for the non-center tones, similar to the 1-taps FEQ in the TEQ-based modem. Tone grouping can be seen as an intermediate solution between TEQ and PT-EQ. While the TEQ-based modem has one equalizer for all tones, tone grouping has one equalizer per group of tones. With a well-chosen group size, the bit rate decreases only slightly, while the per tone complexity part of the initialization is divided by the group size.

In **part II**, we have studied echo cancellation for DMT-based systems. We have first reviewed time/frequency domain echo cancellation, which is a cost efficient algorithm to cancel echo in DMT-based systems. Mostly, the TEQ is applied before the echo cancellation to enable joint channel shortening, which in turn may lead to a shorter echo cancellation filter. However, joint channel shortening has the same disadvantage as far end channel shortening only, namely that there is no correspondence to bit rate optimization.

When the TEQ is designed to shorten the far end impulse response only, it will in general lengthen the echo impulse response. To avoid the lengthening of the echo path by the TEQ, we have shown that we can apply first time/frequency domain echo cancellation and then TEQ. This set-up is merely considered as an intermediate scheme to apply finally first time/frequency domain echo cancellation and then PT-EQ. The latter scheme allows bit rate optimization for a given echo cancellation filter. The complexities of 'First-TEQ-then-echo' and 'First-echo-then-PT-EQ' are comparable.

Per tone echo cancellation has been proposed as an alternative echo cancellation scheme for DMT-based systems. In a similar way as we have moved the TEQ after the demodulating FFT to result in a set of PT-EQs, we have moved the TEC after the demodulating FFT to result in a set of PT-ECs. The advantage of this scheme is that it allows SNR optimization per tone by an extended MMSE problem, for given filter lengths. The extended cost function incorporates optimal per tone joint shortening.

Adapted PT-EC schemes have been presented for asymmetric-rate set-ups. This has led to decreased complexity for the echo emulation. The echo emulation complexity of PT-EC has been compared with the echo emulation complexity of time/frequency domain EC. For a given filter length, time/frequency domain EC has lowest complexity. But because PT-EC optimizes the bit rate, shorter filter lengths may be used for similar performance.

8.2 Further research

Direct initialization of the PT-ECs requires the solution of an extended MMSE problem, which is rather complex. Note that the set of equations is larger than for direct initialization of PT-EQ only. Again, cost efficient initialization schemes are desirable. As a first scheme, one could extend the RLS scheme with inverse updating. The quadratic part then has $T + T_E - 2$ inputs with T and T_E the number of equalizer and echo canceller taps respectively. There are 2 complex inputs per tone, 1 for the equalizer and 1 for the echo canceller (or even 1 more if two-fold oversampling is adopted). So, the per tone initialization part complexity increases.

The filter adaptation in time/frequency domain EC requires only a 1-taps LMS algorithm per tone. Furthermore, while the filter adaptation is performed in the frequency domain, the complexity is independent of the echo canceller length (in the time domain). Remark that the 1-taps LMS algorithms have to be performed for all tones (not the used tones only) because after frequency domain adaptation, an FFT transforms the frequency domain filter taps to the time domain.

In comparison to time/frequency domain EC, there is need for a simplified algorithm for the joint PT-EQ and PT-EC initialization. Complexity savings can also be obtained by smaller per tone filter lengths because PT-EC includes optimal joint shortening. Hence, an optimization of the required number of per tone filter taps is needed.

When efficient echo cancellation algorithms are available, one can redesign the modem to allow a higher overall bit rate. A first aspect is the re-allocation of tones to up- and downstream. Echo cancellation makes (partly) overlapping up- and downstream bands feasible. Or, one can adopt adjacent FDD, where tones from both transmission directions are adjacent in frequency, and hence, without highly selective transmit and receive filters to separate both directions. A related aspect is the design of the analog and digital transmit and receive filters. Furthermore, the echo signal increases the dynamic range of the received signal which influences the number of bits needed in the receiver's A/D converter.

Interfering up- and downstream tones not only cause an echo problem but also a Near End Crosstalk (NEXT) problem. Note that the NEXT originating from the same type of xDSL service, is called self-NEXT. NEXT cancellation can be simplified if the receiver disposes of reference signals, because then the NEXT cancellation problem is similar to the echo cancellation problem. At CO, such NEXT reference signals may be available and exploited in the design of, for instance, a per tone NEXT canceller, similar to a per tone echo canceller. When no reference signals are available, as is the case at RT, the NEXT cancellation becomes more difficult. One then has to extract the signal of interest from the received signal that can be corrupted by several crosstalkers.

A second crosstalk cancellation problem is the cancellation of Far End Crosstalk (FEXT). FEXT always exists between xDSL services of the same type in the same binder, *i.e.* self-FEXT, because signals transmitted in the same direction by similar xDSL services, occupy the same bandwidth.

VDSL promises higher bit rates than ADSL by utilizing more bandwidth. Since crosstalk increases with frequency, NEXT and FEXT are expected to be more severe for VDSL. Current VDSL proposals mitigate NEXT by an FDD set-up, pulse shaping and synchronization. Pulse shaping lowers the sidelobes at the transmitter. With sufficient synchronization, the leakage from upstream signals into downstream and vice versa can be alleviated. However, FEXT remains in the system and turns out to be a major noise source. Hence, efficient FEXT cancellation schemes are an interesting research subject with application in VDSL.

Crosstalk arising from another type of signals is called alien crosstalk. Home Phoneline Networking Alliance (HPNA) based home LAN forms a significant source of alien crosstalk into VDSL [40]. HPNA uses the existing indoor telephone wiring to provide a local area network for connecting PCs. The HPNA systems occupy high frequencies in the range of the VDSL spectrum. No isolation between the indoor telephone wiring and the telephone access network is foreseen in HPNA installation. As a result, HPNA signals are launched to the access network where they couple into neighboring pairs in the same binder and form a severe crosstalk for VDSL operating on these pairs. A number of schemes to mitigate HPNA have been presented, but turn out to be rather complex. Hence, there is need for efficient HPNA cancellation schemes.

One can furthermore compare TEQ and per tone equalization in other applications such as the HIgh PErformance Radio Local Area Network type 2 (HIPERLAN/2) [43]. HIPERLAN/2 adopts OFDM as modulation technique. The symbol and cyclic prefix length are respectively 64 and 16 samples at 20 MHz. When the channel impulse response becomes longer than the cyclic prefix, interferences arise and equalization can enable higher bit rate.

Bibliography

[1] A. N. Akansu, P. Duhamel, X. Lin, and M. De Courville. Orthogonal Transmultiplexers in Communication: A Review. *IEEE Trans. on Signal Processing*, 46(4):979–995, April 1998.

[2] A. N. Akansu and X. Lin. A Comparitive Performance Evaluation of DMT (OFDM) and DWMT (DSBMT) Based DSL Communications Systems for Single and Multitone Interference. In *Proc. Intern. Conf. on Acoust., Speech and Signal Processing (ICASSP)*, pages 3269–3272, Seattle, Washington, May 1998.

[3] N. Al-Dhahir. Joint Channel and Echo Impulse Response Shortening on Digital Subscriber Lines. *IEEE Signal Processing Letters*, 3(10):280–282, Oct. 1996.

[4] N. Al-Dhahir and J. Cioffi. A Low-Complexity Pole-Zero MMSE Equalizer for ML Receivers. In *Proc. Allerton Conf. on Commun., Control and Computing*, pages 623–632, Sep. 1994.

[5] N. Al-Dhahir and J. M. Cioffi. Fast Computation of Channel-Estimate Based Equalizers in Packet Data Transmission. *IEEE Trans. on Signal Processing*, 43(11):2462–2473, Nov. 1995.

[6] N. Al-Dhahir and J. M. Cioffi. Efficient Computation of the Delay-Optimized Finite-Length MMSE-DFE. *IEEE Trans. on Signal Processing*, 44(5):1288–1292, May 1996.

[7] N. Al-Dhahir and J. M. Cioffi. Efficiently Computed Reduced-Parameter Input-Aided MMSE Equalizers for ML Detection: A Unified Approach. *Trans. on Information Theory*, 42(3):903–915, May 1996.

[8] N. Al-Dhahir and J. M. Cioffi. Optimum Finite-Length Equalization for Multicarrier Transceivers. *IEEE Trans. on Commun.*, 44(1):56–64, Jan. 1996.

[9] N. Al-Dhahir and J. M. Cioffi. A Bandwidth-Optimized Reduced-Complexity Equalized Multicarrier Transceiver. *IEEE Trans. on Commun.*, 45(8):948–956, August 1997.

[10] Network and Customer Installation Interfaces - ADSL Metallic Interface. Tech. Report T1E1.4/98-007R5, ANSI, Plano, Texas, Nov. 1998.

[11] VDSL - system requirements. Tech. Report T1E1.4/98-043R8, ANSI, Plano, Texas, Nov. 1998.

[12] R. Baldemair. Suppression of Narrow Frequency Bands in Multicarrier Transmission Systems. In *Proc. European Signal Processing Conf. (Eusipco)*, Tampere, Finland, Sep. 2000.

[13] M. Barton, L. Chang, and T. R. Hsing. Performance Study of High-Speed Asymmetric Digital Subscriber Lines Technology. *IEEE Trans. on Commun.*, 44(2):156–157, Feb. 1996.

[14] D. Bengtsson, P. Deutgen, N. Grip, M. Isaksson, L. Olsson, F. Sjöberg, and H. Öhman. Zipper Performance when Mixing ADSL and VDSL in Terms of Reach and Capacity. Tech. Report T1E1.4/97-138, ANSI, Clearwater Beach, Florida, May 1997.

[15] J. A. C. Bingham. Multicarrier Modulation for Data Transmission: An Idea Whose Time Has Come. *IEEE Commun. Mag.*, 28(5):5–14, May 1990.

[16] J. A. C. Bingham. *ADSL, VDSL, and Multicarrier Modulation.* Wiley Interscience, 2000.

[17] H. Bogucka and K. Wesolowski. *Echo Cancellation in the Multicarrier Modulation Data Transmission Systems*, pages 1637–1640. In Vandewalle et al. [131], 1992.

[18] H. Bogucka and K. Wesolowski. Frequency-Domain Echo Cancellation in Digital Multicarrier Modulation Systems. *IEEE Trans. on Commun.*, 48(2):333–342, Feb. 2000.

[19] R. W. Chang. Synthesis of Band-limited Orthogonal Signals for Multichannel Data Transmission. *Bell System Tech. J.*, 45:1775–1796, Dec. 1966.

[20] W. Y. Chen. Broadcast Digital Subscriber Lines. *IEEE J. on Select. Areas in Commun.*, 13(9):1550–1557, Dec. 1995.

[21] W. Y. Chen. *DSL, Simulation Techniques and Standards Development for Digital Subscriber Line Systems.* Macmillan Technical Publishing, 1998.

[22] W. Y. Chen. The Development and Standardization of Asymmetrical Digital Subscriber Line. *IEEE Commun. Mag.*, 37(5):68–72, May 1999.

[23] W. Y. Chen, J. L. Dixon, and D. L. Waring. High Bit Rate Digital Subscriber Line Echo Cancellation. *IEEE J. on Select. Areas in Commun.*, 9(6):848–860, August 1991.

[24] G. Cherubini, E. Eleftheriou, and S. Ölçer. Filtered Multitone Modulation for VDSL. In *Proc. IEEE Global Telecommun. Conf. (GLOBECOM)*, Rio de Janeiro, Brazil, Dec. 1999.

[25] G. Cherubini, E. Eleftheriou, S. Ölçer, and J. M. Cioffi. Filter Bank Modulation Techniques for Very High-Speed Digital Subscriber Lines. *IEEE Commun. Mag.*, 38(5):98–104, May 2000.

[26] J. S. Chow and J. M. Cioffi. A Cost-Effective Maximum Likelihood Receiver for Multicarrier Systems. In *Proc. Intern. Conf. on Commun. (ICC)*, pages 948–952, Chicago, June 1992.

[27] J. S. Chow, J. M. Cioffi, and J. A. C. Bingham. Equalizer Training Algorithms for Multicarrier Modulation Systems. In *Proc. Intern. Conf. on Commun. (ICC)*, pages 761–765, Geneva, May 1993.

[28] J. S. Chow, J. C. Tu, and J. M. Cioffi. A Discrete Multitone Transceiver System for HDSL Applications. *IEEE J. on Select. Areas in Commun.*, 9(6):895–908, August 1991.

[29] P. S. Chow, J. M. Cioffi, and J. A. C. Bingham. A Practical Discrete Multitone Transceiver Loading Algorithm for Data Transmission over Spectrally Shaped Channels. *IEEE Trans. on Commun.*, 43(2/3/4):773–775, Feb./March/April 1995.

[30] P. S. Chow, J. C. Tu, and J. M. Cioffi. Performance Evaluation of a Multichannel Transceiver System for ADSL and VHDSL Services. *IEEE J. on Select. Areas in Commun.*, 9(6):909–919, August 1991.

[31] J. M. Cioffi. A Fast Echo Canceller Initialization Method for the CCITT V32 Modem. In *Proc. IEEE Global Telecommun. Conf. (GLOBECOM)*, pages 1950–1954, Tokyo, Japan, Nov. 1987.

[32] J. M. Cioffi. *Asymmetric Digital Subscriber Lines*, chapter 34, pages 450–479. In Gibson [47], 1997.

[33] J. M. Cioffi and J. A. C. Bingham. A Data-Driven Multitone Echo Canceller. In *Proc. IEEE Global Telecommun. Conf. (GLOBECOM)*, pages 57–61, Phoenix, AZ, Dec. 1991.

[34] J. M. Cioffi and J. A. C. Bingham. A Data-Driven Multitone Echo Canceller. *IEEE Trans. on Commun.*, 42(10):2853–2869, Oct. 1994.

[35] J. M Cioffi, V. Oksman, J.-J. Werner, T. Pollet, P. M. P. Spruyt, J. S. Chow, and K. S. Jacobsen. Very-High-Speed Digital Subscriber Lines. *IEEE Commun. Mag.*, 37(4):72–79, April 1999.

[36] C. Conroy, B. Kim, and J. Cioffi. Some Implementation Issues Relevant to VDSL A/D Converters for Digital Duplexing. Tech. Report T1E1.4/99-272, ANSI, June 1999.

[37] J. W. Cook, R. H. Kirkby, M. G. Booth, K. T. Foster, D. E. A. Clarke, and G. Young. The Noise and Crosstalk Environment for ADSL and VDSL Systems. *IEEE Commun. Mag.*, 37(5):73–78, May 1999.

[38] B. Daneshrad and H. Samueli. A 1.6 Mbps Digital-QAM System for DSL Transmission. *IEEE J. on Select. Areas in Commun.*, 13(9):1600–1610, Dec. 1995.

[39] B. De Moor and J. Vandewalle. A Unifying Theorem for Linear and Total Linear Least Squares. *IEEE Trans. on Autom. Control*, 35(5):563–566, May 1990.

[40] R. Dearnaley, D. Thorne, and J. Cook. Practical Measurements on the Effect of HPNA Systems on VDSL Reach. Tech. Report T1E1.4/99-265, ANSI, Ottawa, Canada, June 1999.

[41] O. Edfors, M. Sandell, J. J. van de Beek, D. Landström, and F. Sjöberg. An Introduction to Orthogonal Frequency-Division Multiplexing. Research Report 1996:16, Division of Signal Processing, Luleå University of Technology, 1996.

[42] Transmission and Multiplexing; Access transmission systems on metallic access cables; VDSL; Part 1: functional Requirements. Tech. Report TS 101 270-1 V1.1.6, ETSI, August 1999.

[43] Broadband Radio Access Networks; HIPERLAN Type 2; Physical Layer. Tech. Report TS 101 475 V1.1.1, ETSI, 2000.

[44] D. D. Falconer and F. R. Magee. Adaptive Channel Memory Truncation for Maximum Likelihood Sequence Estimation. *Bell System Tech. J.*, 52(9):1541–1562, Nov. 1973.

[45] B. Farhang-Boroujeny and Y. C. Lim. A Comment on the Computational Complexity of Sliding FFT. *IEEE Trans. on Circuits and Systems*, 39(12):875–876, Dec. 1992.

[46] G. D. Forney and M. V. Eyuboğlu. Combined Equalization and Coding Using Precoding. *IEEE Commun. Mag.*, 29(12):25–34, Dec. 1991.

[47] J. D. Gibson, editor. *The Communications Handbook*. CRC Press Inc., 1997.

[48] G. H. Golub and C. F. Van Loan. *Matrix Computations*. Johns Hopkins University Press, second edition, 1989.

[49] W. Goralski. xDSL Loop Qualification and Testing. *IEEE Commun. Mag.*, 37(5):79–83, May 1999.

[50] S. Haykin. *Adaptive Filter Theory*. Prentice-Hall Inc., Englewood Cliffs, N.J., second edition, 1991.

[51] B. Hirosaki. An Analysis of Automatic Equalizers for Orthogonally Multiplexed QAM Systems. *IEEE Trans. on Commun.*, 28(1):73–83, Jan. 1980.

[52] B. Hirosaki. An Orthogonally Multiplexed QAM System Using the Discrete Fourier Transform. *IEEE Trans. on Commun.*, 29(7):982–989, July 1981.

[53] B. Hirosaki, S. Hasegawa, and A. Sabato. Advanced Groupband Data Modem Using Orthogonally Multiplexed QAM Technique. *IEEE Trans. on Commun.*, 34(6):587–592, June 1986.

[54] M. Ho. *Multicarrier Echo Cancellation and Multichannel Equalization*. PhD thesis, Stanford University, 1995.

[55] M. Ho, J. M. Cioffi, and J. A. C. Bingham. Discrete Multitone Echo Cancellation. *IEEE Trans. on Commun.*, 44(7):817–825, July 1996.

[56] M. L. Honig. Echo Cancellation of Voiceband Data Signals Using Recursive Least Squares and Stoachastic Gradient Algorithms. *IEEE Trans. on Commun.*, 33(1):65–73, Jan. 1985.

[57] R. A. Horn and C. R. Johnson. *Matrix Analysis*. Cambridge University Press, 1999.

[58] G. H. Im, C. K. Un, and J. C. Lee. Performance of a Class of Adaptive Data-Driven Echo Cancellers. *IEEE Trans. on Commun.*, 37(12):1254–1263, Dec. 1989.

[59] G.-H. Im and J.-J. Werner. Bandwidth-Efficient Digital Transmission over Unshielded Twisted-Pair Wiring. *IEEE J. on Select. Areas in Commun.*, 13(9):1643–1655, Dec. 1995.

[60] M. Isaksson, D. Bengtsson, P. Deutgen, N. Grip, F. Sjöberg, L. Olsson, P. Ödling, and H. Öhman. Zipper - a Duplex Scheme Proposal for VDSL Based on DMT. Tech. Report T1E1.4/97-137, ANSI, Clearwater Beach, Florida, May 1997.

[61] M. Isaksson, D. Bengtsson, P. Deutgen, M. Sandell, F. Sjöberg, P. Ödling, and H. Öhman. Zipper - a Duplex Scheme for VDSL Based on DMT. Tech. Report T1E1.4/97-016, ANSI, Austin, Texas, Feb. 1997.

[62] M. Isaksson, P. Deutgen, F. Sjöberg, S. K. Wilson, P. Ödling, and P. O. Börjesson. Zipper - a Flexible Duplex Method for VDSL. In *Proc. International Workshop on Copper Wire Access Systems*, pages 95–99, Budapest, Hungary, Oct. 1997.

[63] M. Isaksson and D. Mestdagh. Asynchronous Zipper Mode. Tech. Report 982t16, ETSI STC TM6, Antwerpen, Belgium, April 1998.

[64] M. Isaksson and D. Mestdagh. Pulse Shaping & Windowing in Zipper: Reduction of Out-of-Band Power and Spectral Compatibility. Tech. Report 982t15, ETSI STC TM6, Antwerpen, Belgium, April 1998.

[65] M. Isaksson, F. Sjöberg, R. Nillson, P. Ödling, D. Bengtsson, and D. Mestdagh. Pulse Shaping with Zipper - Spectral Compatibility and Asynchrony. Tech. Report T1E1.4/98-041, ANSI, Austin, Texas, March 1998.

[66] Draft New Recommendation G.992.1: ADSL Transceivers. Tech. Report G.992.1, International Telecommunication Union, July 1999.

[67] D. C. Jones. Frequency Domain Echo Cancellation for Discrete Multitone Asymmetric Digital Subscriber Line Transceivers. *IEEE Trans. on Commun.*, 43(2/3/4):1663–1672, Feb./March/April 1995.

[68] I. Kalet. The Multitone Channel. *IEEE Trans. on Commun.*, 37(2):119–124, Feb. 1989.

[69] I. Kalet and S. Shamai. On the Capacity of a Twisted-Wire Pair: Gaussian Model. *IEEE Trans. on Commun.*, 38(3):379–383, March 1990.

[70] K. J. Kerpez and K. Sistanizadeh. High Bit Rate Asymmetric Digital Communications Over Telephone Loops. *IEEE Trans. on Commun.*, 43(6):2038–2049, June 1995.

[71] T. C. Kwok. Residential Broadband Architecture over ADSL and G.Lite (G.992.2): PPP over ATM. *IEEE Commun. Mag.*, 37(5):84–89, May 1999.

[72] P. J. Kyees, R. C. McConnell, and K. Sistanizadeh. ADSL: A New Twisted-Pair Access to the Information Highway. *IEEE Commun. Mag.*, 33(4):52–60, April 1995.

[73] J. W. Lechleider. High Bit Rate Digital Subscriber Lines: A Review of HDSL Progress. *IEEE J. on Select. Areas in Commun.*, 9(6):769–784, August 1991.

[74] E. A. Lee and D. G. Messerschmitt. *Digital Communication*. Kluwer Academic Publishers, second edition, 1998.

[75] I. Lee, J. S. Chow, and J. M. Cioffi. Performance Evaluation of a Fast Computation Algorithm for the DMT in High-Speed Subscriber Loop. *IEEE J. on Select. Areas in Commun.*, 13(9):1564–1570, Dec. 1995.

[76] I. Lee and J. M. Cioffi. A Fast Computation Algorithm for the Decision Feedback Equalizer. *IEEE Trans. on Commun.*, 43(11):2742–2749, Nov. 1995.

[77] A. Leke and J. M. Cioffi. A Maximum Rate Loading Algorithm for Discrete Multitone Modulation Systems. In *Proc. IEEE Global Telecommun. Conf. (GLOBECOM)*, pages 1514–1518, Phoenix, Arizona, Nov. 1997.

[78] A. Leke and J. M. Cioffi. Transmit Optimization for Time-Invariant Wireless Channels Utilizing a Discrete Multitone Approach. In *Proc. Intern. Conf. on Commun. (ICC)*, pages 954–958, Montreal, Canada, June 1997.

[79] K. Maxwell. Asymmetric Digital Subscriber Line: Interim Technology for the Next Forty Years. *IEEE Commun. Mag.*, 34(10):100–106, Oct. 1996.

[80] P. J. W. Melsa, R. C. Younce, and C. E. Rohrs. Impulse Response Shortening for Discrete Multitone Transceivers. *IEEE Trans. on Commun.*, 44(12):1662–1672, Dec. 1996.

[81] D. J. G. Mestdagh, M. R. Isaksson, and P. Ödling. Zipper VDSL: A Solution for Robust Duplex Communication over Telephone Lines. *IEEE Commun. Mag.*, 38(5):90–96, May 2000.

[82] M. Milisavljević and E. I. Verriest. Fixed Point Algorithm for Bit Rate Optimal Equalization in Multicarrier Systems. In *Proc. Intern. Conf. on Acoust., Speech and Signal Processing (ICASSP)*, Phoenix, Arizona, March 1999.

[83] K. Murano, S. Unagami, and F. Amano. Echo Cancellation and Applications. *IEEE Commun. Mag.*, 28(1):49–55, Jan. 1990.

[84] M. Nafie and A. Gatherer. Time-Domain Equalizer Training for ADSL. In *Proc. Intern. Conf. on Commun. (ICC)*, pages 1085–1089, Montreal, Canada, June 1997.

[85] K. Narumiya. A Consideration of ADSL Service under NTT's Network. *IEEE Commun. Mag.*, 37(5):98–101, May 1999.

[86] R. Nilsson, F. Sjöberg, and S. K. Wilson. Combating Impulse Noise in DMT-based VDSL Systems. In *Proc. Radioveten. Konf. (RVK)*, pages 384–388, Karlskrona, Sweden, June 1999.

[87] V. Oksman and J.-J. Werner. Single-Carrier Modulation Technology for Very High-Speed Digital Subscriber Line. *IEEE Commun. Mag.*, 38(5):82–89, May 2000.

[88] L. Olsson, M. Isaksson, D. Bengtsson, P. Deutgen, F. Sjöberg, G. Ökvist, H. Öhman, P. Ödling, N. Grip, and P. O. Börjesson. Influence of the Zipper Duplex Scheme on the Receiver Dynamic Range. Tech. Report T1E1.4/97-139, ANSI, Clearwater Beach, Florida, May 1997.

[89] K. Pahlavan and J. L. Holsinger. Voice-Band Data Communication Modems: A Historical Review: 1919-1988. *IEEE Commun. Mag.*, 26(1):16–27, Jan. 1988.

[90] C. T. Pan and R. J. Plemmons. Least Squares Modifications with Inverse Factorization: Parallel Implications. *J. Computational and Applied Mathematics*, 27:109–127, 1989.

[91] Z. Papir and A. Simmonds. Competing for Throughput in the Local Loop. *IEEE Commun. Mag.*, 37(5):61–66, May 1999.

[92] A. Peled and A. Ruiz. Frequency Domain Data Transmission using Reduced Computational Complexity Algorithms. In *Proc. Intern. Conf. on Acoust., Speech and Signal Processing (ICASSP)*, pages 964–967, Denver, CO, April 1980.

[93] T. Pollet, M. Peeters, M. Moonen, and L. Vandendorpe. Equalization for DMT-Based Broadband Modems. *IEEE Commun. Mag.*, 38(5):106–113, May 2000.

[94] T. Pollet, H. Steendam, and M. Moeneclaey. Performance Degradation of Multicarrier Systems caused by an Insufficient Guard Interval. In *Proc. International Workshop on Copper Wire Access Systems*, pages 265–270, Budapest, Hungary, Oct. 1997.

[95] B. R. Saltzberg. Performance of an Efficient Parallel Data Transmission System. *IEEE Trans. on Communication Technology*, 15(6):805–811, Dec. 1967.

[96] B. R. Saltzberg. Comparison of Single-Carrier and Multitone Digital Modulation for ADSL Applications. *IEEE Commun. Mag.*, 36(11):114–121, Nov. 1998.

[97] S. D. Sandberg and M. A. Tzannes. Overlapped Discrete Multitone Modulation for High Speed Copper Wire Communications. *IEEE J. on Select. Areas in Commun.*, 13(9):1571–1585, Dec. 1995.

[98] M. Schenk, D. Schmücking, A. Wörner, and I. Ruge. VDSL - die 3. Generation der Digitalen Teilnehmeranschlußleitung. *Telekom Praxis*, (6):10–19, June 1996.

[99] D. Schmücking, M. Schenk, A. Wörner, R. Hasholzner, and I. Ruge. Ein Model für den VHDSL-Kanal. *NTZ*, (2):20–27, Feb. 1996.

[100] D. Schmücking and A. Wörner. Transmission Capacity and Design of a VHDSL-System. In *Proc. Intern. Conf. on Commun. (ICC)*, pages 1426–1431, Dallas, TX, June 1996.

[101] A. Sendonaris, V. V. Veeravalli, and B. Aazhang. Joint Signaling Strategies for Approching the Capacity of Twisted-Pair Channels. *IEEE Trans. on Commun.*, 46(5):673–685, May 1998.

[102] J. L. Seoane, S. K. Wilson, and S. Gelfand. Analysis of Intertone and Interblock Interference in OFDM when the Length of the Cyclic Prefix is shorter than the Length of the Impulse Response of the Channel. In *Proc. IEEE Global Telecommun. Conf. (GLOBECOM)*, pages 32–36, Phoenix, Arizona, Nov. 1997.

[103] F. Sjöberg. A VDSL Tutorial. Research Report 2000:02, Division of Signal Processing, Luleå University of Technology, April 2000.

[104] F. Sjöberg, M. Isaksson, R. Nilsson, P. Ödling, S. K. Wilson, and P.O. Börjesson. Zipper: A Duplex Method for VDSL Based on DMT. *IEEE Trans. on Commun.*, 47(8):1245–1252, August 1999.

[105] F. Sjöberg, R. Nilsson, P. O. Börjesson, P. Ödling, B. Wiese, and J. A. C. Bingham. Digital RFI Suppression in DMT-based VDSL Systems. Submitted to IEEE Trans. on Commun., Jan. 1999.

[106] F. Sjöberg, R. Nilsson, N. Grip, P. O. Börjesson, S. K. Wilson, and P. Ödling. Digital RFI Suppression in DMT-based VDSL Systems. In *Proc. International Conference on Telecommunications*, pages 189–193, Chalkidiki, Greece, June 1998.

[107] F. Sjöberg, R. Nilsson, M. Isaksson, P. Ödling, and P. O. Börjesson. Asynchronous Zipper. In *Proc. Intern. Conf. on Commun. (ICC)*, pages 231–235, Vancouver, Canada, June 1999.

[108] F. Sjöberg, S. K. Wilson, and M. Isaksson. Multi-Rate Power Back-off in the Upstream of VDSL. Submitted to IEEE Trans. on Commun., Nov. 1999.

[109] P. Spruyt, P. Reusens, and S. Braet. Performance of Improved DMT Transceiver for VDSL. Tech. Report T1E1.4/96-104, ANSI, Colorado Springs, Colorado, April 1996.

[110] K. Van Acker, G. Leus, M. Moonen, S. Claes, and O. van de Wiel. An Improved Optimization Algorithm for Time Domain Equalizer Design in ADSL Modems. In *Proc. International Workshop on Copper Wire Access Systems*, pages 117–123, Budapest, Hungary, Oct. 1997.

[111] K. Van Acker, G. Leus, M. Moonen, S. Claes, and O. van de Wiel. Improved Time Domain Equalization for ADSL. In *Proc. ProRISC Workshop on Circuits, Systems and Signal Processing*, pages 615–620, Mierlo, The Netherlands, Nov. 1997.

[112] K. Van Acker, G. Leus, M. Moonen, and T. Pollet. Frequency Domain Equalization with Tone Grouping in DMT/ADSL Receivers. In *Proc. Asilomar Conf. on Signals, Systems and Computers*, pages 1067–1070, Pacific Grove, California, Oct. 1999.

[113] K. Van Acker, G. Leus, M. Moonen, and T. Pollet. Combination of Echo Cancellation and Equalization in DMT-based ADSL modems. Internal Report 00-32, ESAT-SISTA, K.U.Leuven (Leuven, Belgium), submitted to IEEE Trans. on Commun., 2000.

[114] K. Van Acker, G. Leus, M. Moonen, and T. Pollet. RLS-based Initialization for Per Tone Equalizers in DMT-Receivers. In *Proc. European Signal Processing Conf. (Eusipco)*, Tampere, Finland, Sep. 2000.

[115] K. Van Acker, G. Leus, M. Moonen, and T. Pollet. RLS-based Initialization for Per Tone Equalizers in DMT-Receivers. Internal Report 00-12b, ESAT-SISTA, K.U.Leuven (Leuven, Belgium), submitted to IEEE Trans. on Commun., 2000.

[116] K. Van Acker, G. Leus, M. Moonen, O. van de Wiel, and T. Pollet. Per Tone Equalization for DMT Receivers. In *Proc. IEEE Global Telecommun. Conf. (GLOBECOM)*, pages 2311–2315, Rio de Janeiro, Brazil, Dec. 1999.

[117] K. Van Acker, G. Leus, M. Moonen, O. van de Wiel, and T. Pollet. Per Tone Equalization for DMT-based Systems. Accepted for publication in IEEE Trans. on Commun., 2000.

[118] K. Van Acker, M. Moonen, and T. Pollet. Per Tone Echo Cancellation for DMT-based Systems. Internal Report 00-101, ESAT-SISTA, K.U.Leuven (Leuven, Belgium), submitted to the Intern. Conf. on Acoust., Speech and Signal Processing (ICASSP 2001), 2000.

[119] K. Van Acker, M. Moonen, and T. Pollet. Per Tone Echo Cancellation for DMT-based Systems. Internal Report 00-119, ESAT-SISTA, K.U.Leuven (Leuven, Belgium), submitted to IEEE Trans. on Commun., 2000.

[120] K. Van Acker, T. Pollet, G. Leus, and M. Moonen. Combination of Per Tone Equalization and Windowing in DMT-Receivers. In *Proc. Fifth Bayona Workshop on Emerging Technologies in Telecommunications*, pages 49–53, Bayona, Spain, Sep. 1999.

[121] K. Van Acker, T. Pollet, G. Leus, and M. Moonen. Combination of Per Tone Equalization and Windowing in DMT-Receivers. Internal Report 99-46b, ESAT-SISTA, K.U.Leuven (Leuven, Belgium), submitted to Signal Processing, 1999.

[122] M. Van Bladel and M. Moeneclaey. Performance of Time-Domain Equalized Multicarrier Systems on ADSL Loops. In *Proc. IEEE Third Symposium*

on Communications and Vehicular Technology in the Benelux, pages 198–201, Eindhoven, The Netherlands, Oct. 1995.

[123] M. Van Bladel and M. Moeneclaey. Time-Domain Equalization for Multicarrier Communication. In *Proc. IEEE Global Telecommun. Conf. (GLOBECOM)*, pages 167–171, Singapore, Nov. 1995.

[124] L. Van der Perre, S. Thoen, P. Vandenameele, B. Gyselinckx, and M. Engels. Adaptive Loading Strategy for a High Speed OFDM-based WLAN. In *Proc. IEEE Global Telecommun. Conf. (GLOBECOM)*, Sydney, Australia, Nov. 1998.

[125] J.-F. Van Kerckhove and P. Spruyt. Adapted Optimization Criterion for FDM-Based DMT-ADSL Equalization. In *Proc. Intern. Conf. on Commun. (ICC)*, pages 1328–1334, Dallas, TX, June 1996.

[126] P. Vandenameele, S. Thoen, M. Engels, and H. De Man. A Combined OFDM/SDMA Approach for WLAN. In *Proc. Vehicular Technology Conference*, Houston, Texas, May 1999.

[127] P. Vandenameele, L. Van der Perre, M. Engels, and H. De Man. A Novel Class of Uplink OFDM/SDMA Algorithms for WLAN. In *Proc. IEEE Global Telecommun. Conf. (GLOBECOM)*, pages 6–10, Rio de Janeiro, Brazil, Dec. 1999.

[128] L. Vandendorpe. Fractionally Spaced Linear and DF MIMO Equalizers for Multitone Systems without Guard Time. *Annals of Telecommunications*, 52(1-2):21–30, Jan.-Feb. 1997.

[129] L. Vandendorpe, L. Cuvelier, F. Deryck, J. Louveaux, and O. van de Wiel. Improved Detectors for DMT-based VDSL Transmission. In *Proc. International Workshop on Copper Wire Access Systems*, Budapest, Hungary, Oct. 1997.

[130] L. Vandendorpe, L. Cuvelier, F. Deryck, J. Louveaux, and O. van de Wiel. Fractionally Spaced Linear and Decision-Feedback Detectors for Transmultiplexers. *IEEE Trans. on Signal Processing*, 46(4):996–1011, April 1998.

[131] J. Vandewalle, R. Boite, M. Moonen, and A. Oosterlinck, editors. *Signal Processing VI: Theories and Applications*. Elsevier Science Publishers, 1992.

[132] N. A. M. Verhoeckx, H. C. Van Den Elzen, F. A. M. Snijders, and P. J. Van Gerzen. Digital Echo Cancellation for Baseband Data Transmission. *IEEE Trans. on Acoust., Speech and Signal Processing*, 27(6):768–781, Dec. 1979.

[133] P. Vetter, D. Goderis, L. Verpooten, and A. Granger. Systems Aspects of APON/VDSL Deployment. *IEEE Commun. Mag.*, 38(5):66–72, May 2000.

[134] A. Wang, J.-J. Werner, and S. Kallel. Effect of Bridged Taps on Channel Capacity at VDSL Frequencies. In *Proc. Intern. Conf. on Commun. (ICC)*, pages 236–245, Vancouver, Canada, June 1999.

[135] B. Wang and T. Adali. A Frequency-Domain Eigenfilter Approach for Equalization in Discrete Multitone Systems. In *Proc. Asilomar Conf. on Signals, Systems and Computers*, pages 1058–1062, Pacific Grove, California, Oct. 1999.

[136] B. Wang and T. Adali. Joint Impulse Response Shortening for Discrete Multitone Systems. In *Proc. IEEE Global Telecommun. Conf. (GLOBECOM)*, pages 2508–2512, Rio de Janeiro, Brazil, Dec. 1999.

[137] S. B. Weinstein and P. M. Ebert. Data Transmission by Frequency-Division Multiplexing Using the Discrete Fourier Transform. *IEEE Trans. on Communication Technology*, 19(5):628–634, Oct. 1971.

[138] J.-J. Werner. The HDSL Environment. *IEEE J. on Select. Areas in Commun.*, 9(6):785–800, August 1991.

[139] J. Yang, S. Roy, and N. H. Lewis. Data-Driven Echo Cancellation for a Multitone Modulation System. *IEEE Trans. on Commun.*, 42(5):2134–2144, May 1994.

[140] R. C. Younce and P. J. W. Melsa. Changes to Proposed Text for Section 6.8.2 of ADSL Draft Standard. Tech. Report T1E1.4/93-267, ANSI, Oct. 1993.

[141] R. C. Younce, P. J. W. Melsa, and S. Kapoor. Echo Cancellation for Asymmetrical Digital Subsriber Lines. In *Proc. Intern. Conf. on Commun. (ICC)*, pages 301–306, New Orleans, May 1994.